AD-A085 770 AIR FORCE ACADEMY CO F/G 20/4
AIR FORCE ACADEMY AERONAUTICS DIGEST - FALL 1979.(U)
APR 80 E J JUMPER, M M TOWER, F GUGGISBERG
UNCLASSIFIED USAFA-TR-80-7 NL

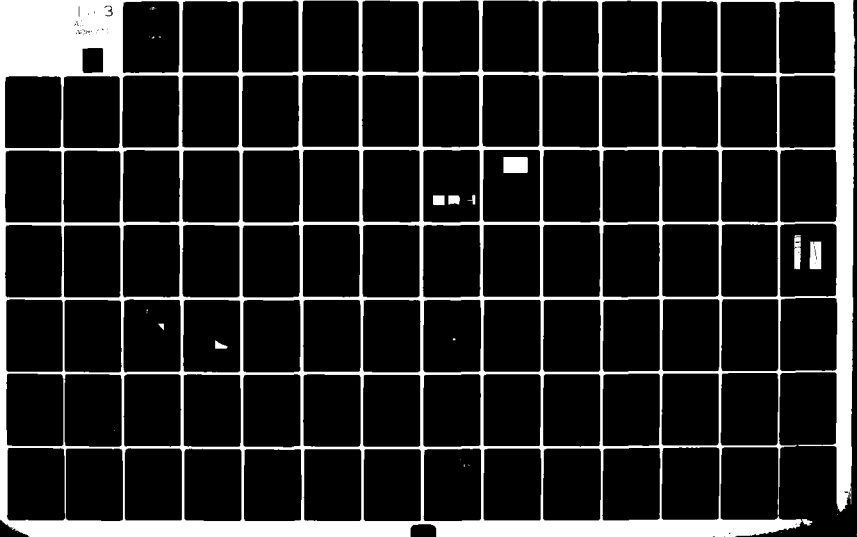

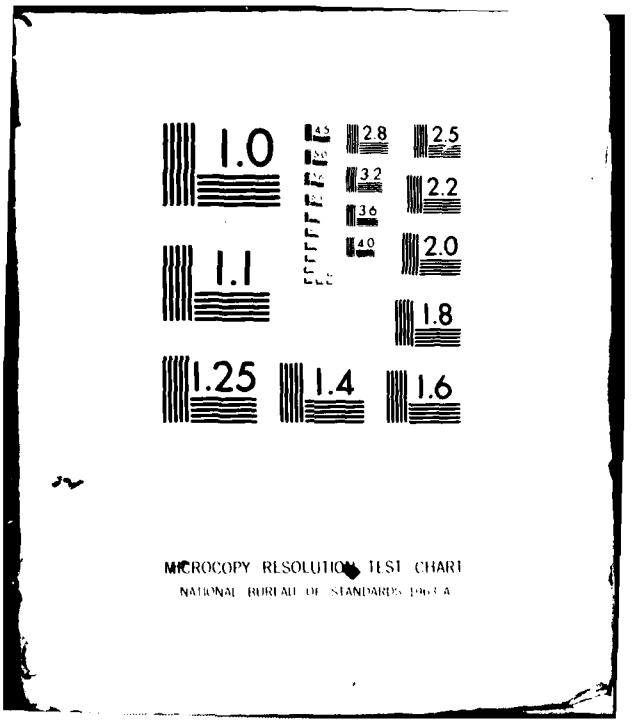
1.0
1.1
1.25
1.4
1.6
1.8
2.0
2.2
2.5
2.8
3.2
3.6
4.0
4.5
MICROCOPY RESOLUTION TEST CHART
NATIONAL BUREAU OF STANDARDS 1963-A

LEVEL II

AD A075419

USAFA-TR-80-7

AD A085770

AIR FORCE ACADEMY AERONAUTICS DIGEST - FALL 1979

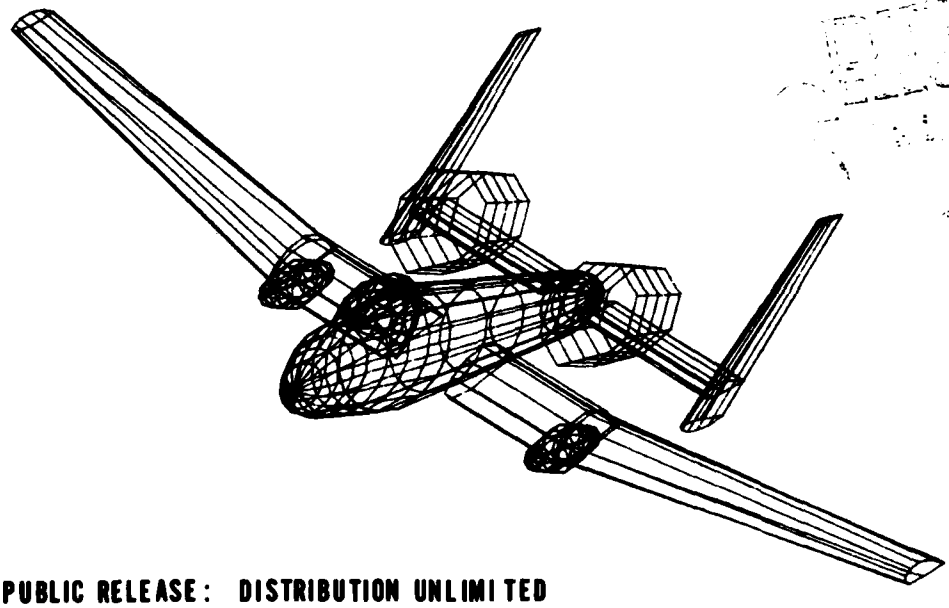

APRIL 1980

FINAL REPORT

APPROVED FOR PUBLIC RELEASE: DISTRIBUTION UNLIMITED

DEPARTMENT OF AERONAUTICS

DEAN OF THE FACULTY

UNITED STATES AIR FORCE ACADEMY

COLORADO 80840

COVER:
Capt Glynn Sisson, DFAN, generated this perspective view of the A-10 on the Air Force Academy's computer graphics system. The students generate similar configurations in their senior aircraft design course using the computer graphics system to aid in their design project. The designs can be illustrated in orthogonal views or rotated into isometric views to give the student designer a better idea of what he has created.

Editorial Review by Capt Fannalou Guggisberg
Department of English
USAF Academy, Colorado 80840

This digest has been reviewed and is approved for publication.

M H Bacon

M. D. BACON, Colonel, USAF
Director of Research and
Continuing Education

UNCLASSIFIED

SECURITY CLASSIFICATION OF THIS PAGE (When Data Entered)

REPORT DOCUMENTATION PAGE	READ INSTRUCTIONS BEFORE COMPLETING FORM
1. REPORT NUMBER: USAFA-TR-80-7 (14)	2. GOVT ACCESSION NO.: AD-A085 770
3. RECIPIENT'S CATALOG NUMBER	
4. TITLE (and Subtitle): Air Force Academy Aeronautics Digest, Fall 1979 (6)	5. TYPE OF REPORT & PERIOD COVERED: Final Report (9)
6. PERFORMING ORG. REPORT NUMBER	
7. AUTHOR(s): Editors: E. J. Jumper, M. M. Tower, F. Guggisberg (10)	8. CONTRACT OR GRANT NUMBER(s): (12) 3.01
9. PERFORMING ORGANIZATION NAME AND ADDRESS: Department of Aeronautics, United States Air Force Academy, CO 80840	10. PROGRAM ELEMENT, PROJECT, TASK AREA & WORK UNIT NUMBERS
11. CONTROLLING OFFICE NAME AND ADDRESS (11)	12. REPORT DATE: Apr 80
	13. NUMBER OF PAGES: 195
14. MONITORING AGENCY NAME & ADDRESS (if different from Controlling Office)	15. SECURITY CLASS. (of this report)
	15a. DECLASSIFICATION/DOWNGRADING SCHEDULE

16. DISTRIBUTION STATEMENT (of this Report)

Approved for Public Release; Distribution Unlimited

17. DISTRIBUTION STATEMENT (of the abstract entered in Block 20, if different from Report)

18. SUPPLEMENTARY NOTES

19. KEY WORDS (Continue on reverse side if necessary and identify by block number)

Aerodynamics, Fluid Mechanics, Thermodynamics, Education, Wind Tunnel, Aeronautical Instrumentation, Aeronautical History

20. ABSTRACT (Continue on reverse side if necessary and identify by block number)

This digest covers unclassified research in aeronautics performed at the United States Air Force Academy during the six months ending 1 January 1980. This report includes individual technical papers in the specific areas of aerodynamics, fluid mechanics, experimental instrumentation, thermodynamics and heat transfer, engineering education and aeronautical history.

DD FORM 1 JAN 73 1473 EDITION OF 1 NOV 65 IS OBSOLETE

UNCLASSIFIED

SECURITY CLASSIFICATION OF THIS PAGE (When Data Entered)

011550

PREFACE

This report is the fourth issue of the Air Force Academy Aeronautics Digest. The articles printed here represent recent scholarly work by students and faculty of the Department of Aeronautics, members of other departments of the Academy and The F. J. Seiler Research Laboratory, researchers directly or indirectly involved with USAFA-sponsored projects, and authors in fields of interest to the USAFA.

In addition to complete papers, the Digest also includes, when appropriate, abstracts of lengthier reports and articles published in other formats. The editors will consider for publication contributions in the general field of Aeronautics, including

-Aeronautical Engineering
  --Flight Mechanics
  --Propulsion
  --Structures
  --Instrumentation
-Fluid Mechanics
-Thermodynamics and Heat Transfer
-Engineering Education
-Aeronautical History

Papers on other topics will be considered on an individual basis. Contributions should be sent to:

Editor, Aeronautics Digest
DFAN
US Air Force Academy, CO 80840

The Aeronautics Digest is presently edited by Major E. J. Jumper, PhD, Captain M. M. Tower, PhD, and Captain F. Guggisberg (Department of English), who provided the final editorial review. Our thanks also to our secretary, Mary Lynne Wright, for her diligent typing and cheerful attitude. Starting next issue Captain A. M. Higgins will be the editor-in-chief of the Digest.

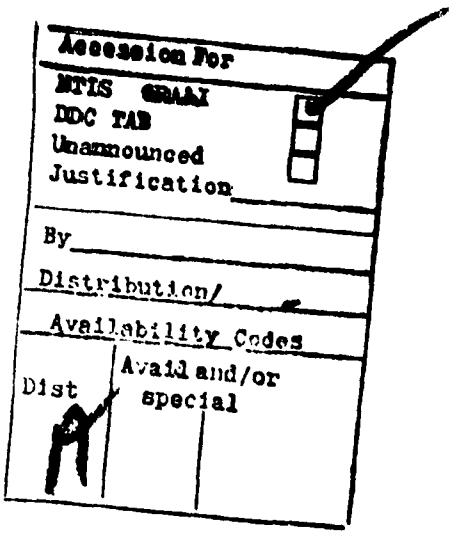

CONTENTS

CONTENTS (cont.)

SECTION I

AERODYNAMICS

COMPARISON OF TOWPLANE PERFORMANCE

J. P. Retelle, Jr.* and P. Jordan**

Abstract

We evaluated the overall aerodynamic performance of five different towplanes during glider aerotows, measuring takeoff time and distance, climb rate, and elapsed time to glider release and to the towplane's return to the takeoff point. All towplanes towed similar trainer sailplanes of the same make, model, and approximate gross weight. Additional data provided a limited insight on the effect of elevated density altitude. While comparing data from the four tow aircraft, we draw no conclusions, since the ultimate selection of a towplane will be based upon safety, cost operational utility, and availability, as well as aerodynamic performance. Our results merely provide a baseline of experimental data to assist in selecting the proper towplane for any glider aerotow operation.

I. Introduction

Selecting the optimum towplane for a glider aerotow operation depends on many factors, such as safety, cost, operational utility, availability, and aerodynamic performance. All too often, cost decides actual towplane selection, since most towplanes presumably have similar aerodynamic performance. The resulting towplane performance, especially during adverse conditions of high winds or high density altitude, often surprises the pilots of both the towplanes and gliders. This report presents data on the aerodynamic performance of five different towplanes, towing similar trainer sailplanes of the same approximate weight. These results should provide soaring operations personnel with the information they need to consider this aspect properly when selecting tow aircraft.

The environment under which we conducted the tests is as harsh as any in the United States. The United States Air Force Academy operates an extensive glider program, training several hundred basic glider students per year, as well as numerous private, commercial, and flight instructor candidates. The flying program runs throughout the entire year, but the heavy activity is during the summer months, when glider operations run from dawn to dusk each day. The Academy airfield elevation is 6500 feet MSL, but density altitudes above 9500 feet are not uncommon during the summer. In addition to the two-place trainer sailplanes used in this evaluation, lighter single-place and heavier two-place Schweizer sailplanes must be towed.

The comparison and evaluation of glider tow aircraft is especially difficult, since no airplane has been specifically designed for this purpose. Some of the aircraft tested fell in the so-called "workhorse" category, while we chose others either for their performance characteristics or for abilities in other flight areas, such as aerial spraying. All aircraft were modified with tow hooks at the tail, and several had engine installations different from the production versions of the aircraft.

---

*Major, USAF, Associate Professor of Aeronautics, DFAN
**Captain, USAF, Assistant Chief, Soaring Branch, CWOA

II. Description of Aircraft

The five towplanes evaluated are described below in Table 1. The abbreviated names shown, will be used throughout this report to prevent confusion and do not imply favoritism toward any aircraft. At the start of the test, all towplanes were topped off with fuel, and test personnel observed preflight inspections. We installed high-grade pressure barographs in each towplane, and used new tow ropes of equal length.

Table 1

TOWPLANE CHARACTERISTICS

Towplane	Make	Number	Maximum Gross Weight (lb)	Empty Weight (lb)	Fuel (Gal)	Engine H.P.
Pawnee	Piper	N4867Y	1975	1589	36	260
Rallye	Rallye	N360RA	2272	1650	72	235
Scout	Bellanca	N5042N	2150	1774	36	180
Super Cub	Piper	N3182Z	1415	1039	36	180*
Super Cub	Piper	N5546Z	1469	1103	36	200*

*Modified from production aircraft

The sailplanes used in this test were all Schweizer 2-33A trainers. We arranged crews so that the gross weights were approximately the same. These weight data appear in Table 2.

Table 2

GLIDER GROSS WEIGHT

Glider	Weight (lb)
538	983
93S	990
60S	992
92S	1002
539	990

III. Description of Experiment

The towplane owners provided towplane pilots, with the exception of the Rallye, which was piloted by an experienced member of the Academy Soaring Staff. All towplane pilots were highly experienced in glider towing and were familiar with the Academy flying area. The glider crews each consisted of one cadet student pilot and one Air Force officer who was a qualified glider pilot.

All towplanes flew at least fifteen flights. The first flight for each aircraft was a practice flight, but in all cases the data from these practice flights were of high quality and were included as valid results. One later flight of the Rallye had to be repeated because of a towplane traffic conflict in the pattern, so it flew sixteen total flights. Wind velocity and direction, as well as density altitude, were noted for each flight.

A ground observer measured takeoff distances for the towplanes (not the gliders) and transmitted this information by radio to the recorder. Distance marking cones placed every fifty feet at the side of the runway facilitated this measurement. To provide uniformity, the towplanes always started their takeoff roll from the same point on the runway. The towrope was stretched taut by pulling the sailplane back just prior to the aerotow.

The principal source of data for each towplane was a ground observer using a stopwatch with lap-time capability. We assigned one airborne observer to each sailplane. He recorded the elapsed time from towplane brake release to lift-off, glider release, and return to the "ready line" on the runway. Radio calls from the takeoff point monitor and the towplane pilots assured that all times were noted accurately.

The glider flight crews collected additional timing data to measure specifically the rate of climb. They recorded the elapsed time between each 500-foot altitude interval while on tow, from the lift-off point to the release point. These separate measurements did not need to be correlated with the ground measurements. The glider flight crews terminated all tows at 8500 feet MSL (2000 feet AGL).

IV. Results and Discussion

The graphs shown in this section present a time or distance comparison between the five towplanes. Results shown represent averages over the fifteen flights by each towplane. The measured data for each flight of each towplane appear in Appendix A. The only corrections applied to recorded data were for the effect of wind velocity on takeoff distance, and are thoroughly described below.

The elapsed-time data are presented in Figure 1. The symbols represent the average values and the vertical bars represent plus and minus one standard deviation of the experimental data. The data on the left side are the average elapsed times from brake

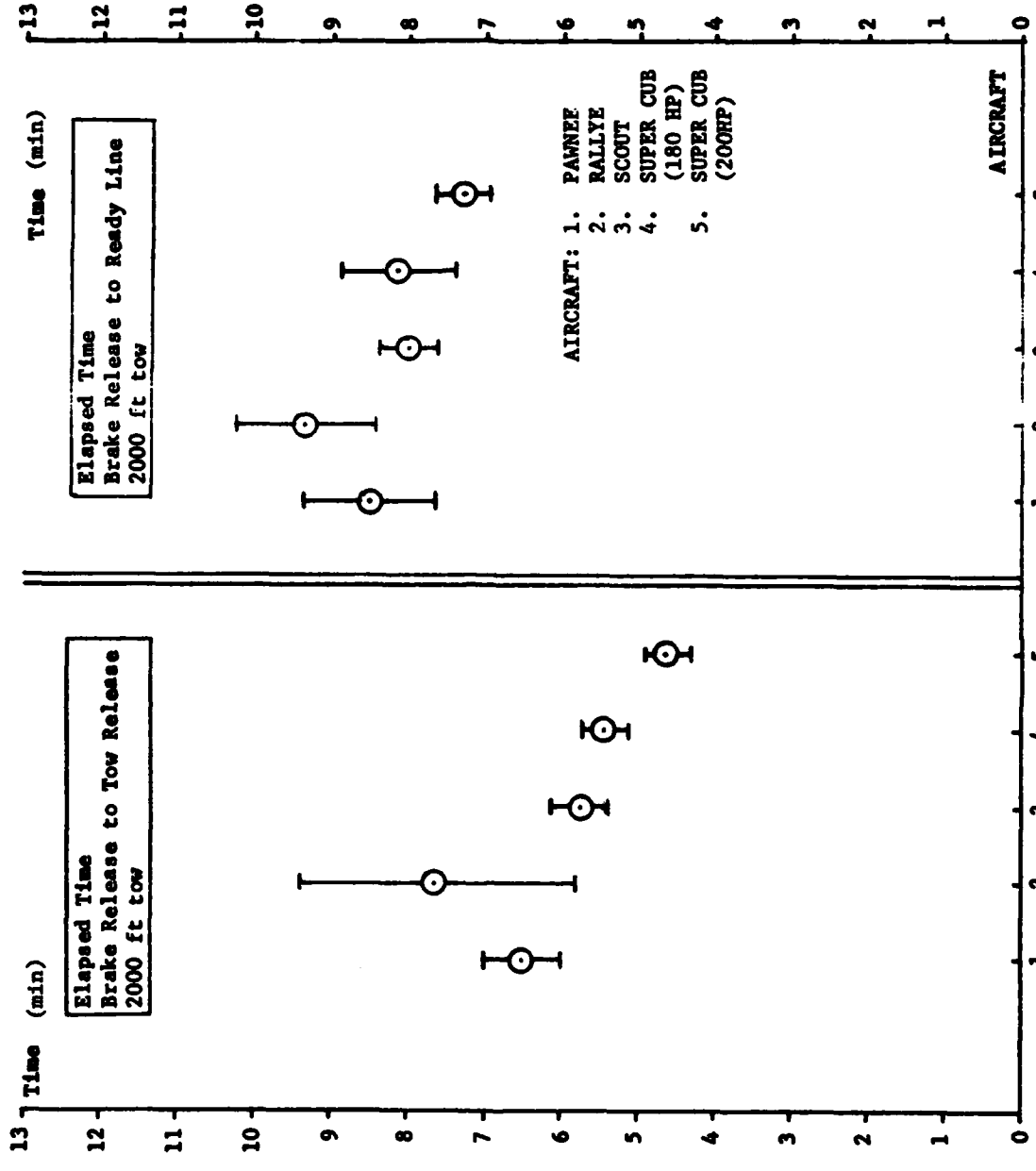

Figure 1. Elapsed Time Data

release on the runway to glider release at 8500 feet MSL. The times vary between a maximum value of 7 minutes 42 seconds to a minimum of 4 minutes 40 seconds. The time difference of 3 minutes shows a 38 percent decrease for the tow time of the second towplane.

The data on the right side of Figure 1 are the average elapsed times from towplane brake release on the runway to the return of the towplane to the "ready line" (approximately 200 feet downwind of the brake-release line) following the tow. The data vary between a maximum of 9 minutes 33 seconds to a minimum of 7 minutes 18 seconds, a 22 percent difference. The larger scatter in these results could be due to differences in the piloting technique used following glider release. All towplane pilots were instructed not to exceed 105 mph while returning to the field, and were to use "normal" procedures consistent with engine cooling, constant-speed propeller operation, and flight safety. Because of these potentials for variance, despite the dissimilarity in aircraft, we feel that much of the data scatter is due to pilot inputs.

The tow-per-hour calculations appear in Figure 2. The numbers on the left side show the data with no allowances for fuel endurance, refueling time, or hook-up time. The possible number of tows varies between a maximum of 8.2 tows per hour to a minimum of 6.4 tows per hour. The calculations on the right side yield the number of tows that could be expected during a 12-hour towing day, allowing a half hour for refueling and ignoring hook-up time. The estimated fuel flow rate of each towplane while towing is indicated. As a sample calculation, consider the Pawnee. It has 36 gallons of fuel and an estimated fuel flow rate of 14 gallons per hour, giving an endurance of 2.57 hours. Thus, a 12-hour towing day would allow for 4 tanks of fuel and 3 refuelings. This would theoretically permit 72.5 tows per day, using 144 gallons of fuel. If the last refueling took the total towing day past 12 hours (as in the example described above), the last refueling was ignored. The calculated total number of gallons of fuel used per day is shown in parentheses next to the data point for each aircraft.

A similar time-related calculation is the time-fraction, shown in Figure 3. The total-time fraction is the total time for one tow divided by the towplane endurance. The airborne-time fraction is the elapsed time from brake release to glider release divided by the towplane endurance. The results then give a non-dimensional number which accounts for towplane endurance, due to either a large fuel load or a low fuel flow rate. The results for the total-time fraction show the Rallye with the lowest, or best, time fraction due to its large fuel load, and the Pawnee with the highest time fraction due to its high fuel flow rate. The results for the airborne-time fraction show that the faster rates of climb of the three high-wing aircraft overshadowed any shortcomings due to their lower endurance times. The towplane pilot must also be considered, due to

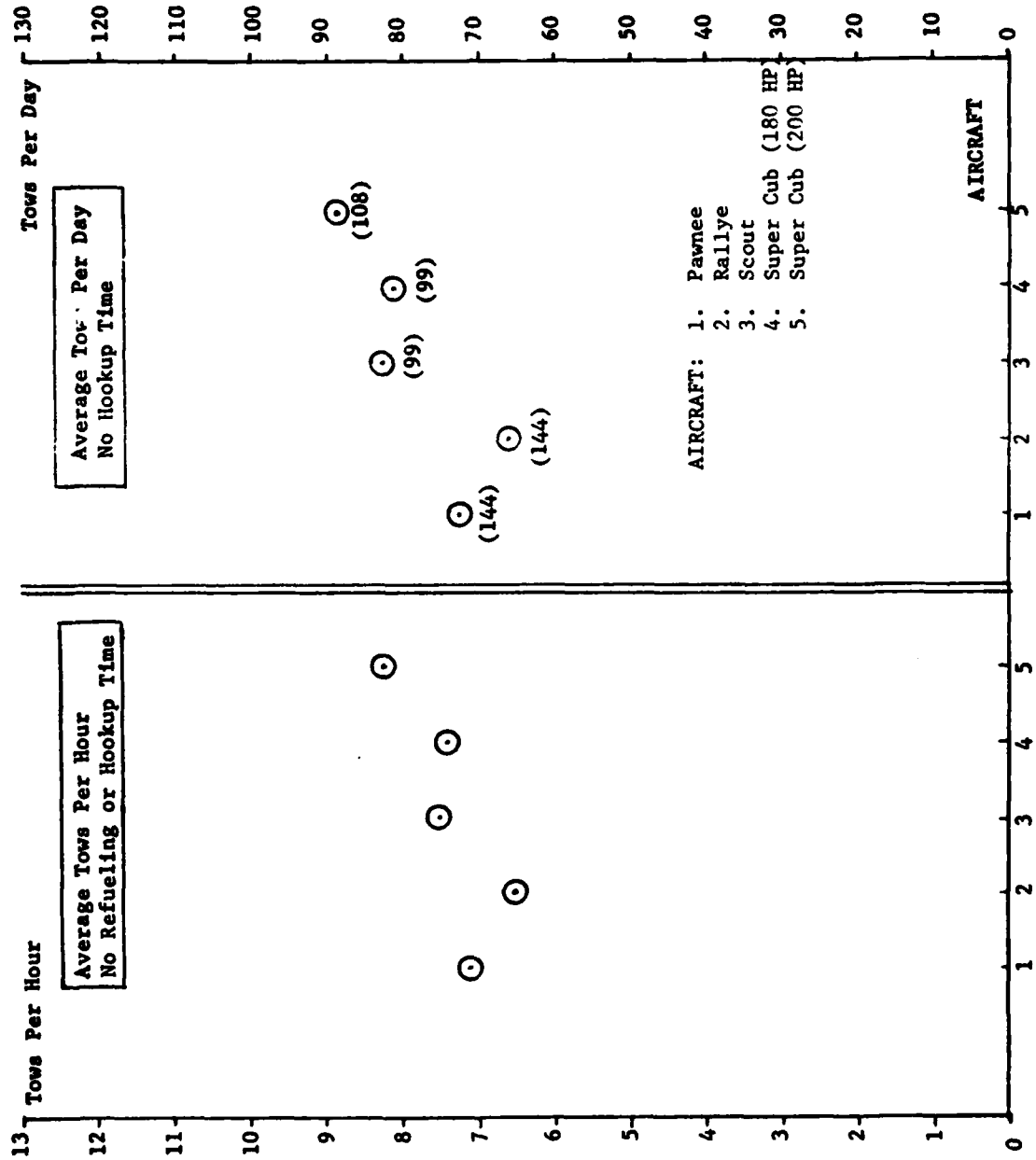

Figure 2. Tows per Hour/Day

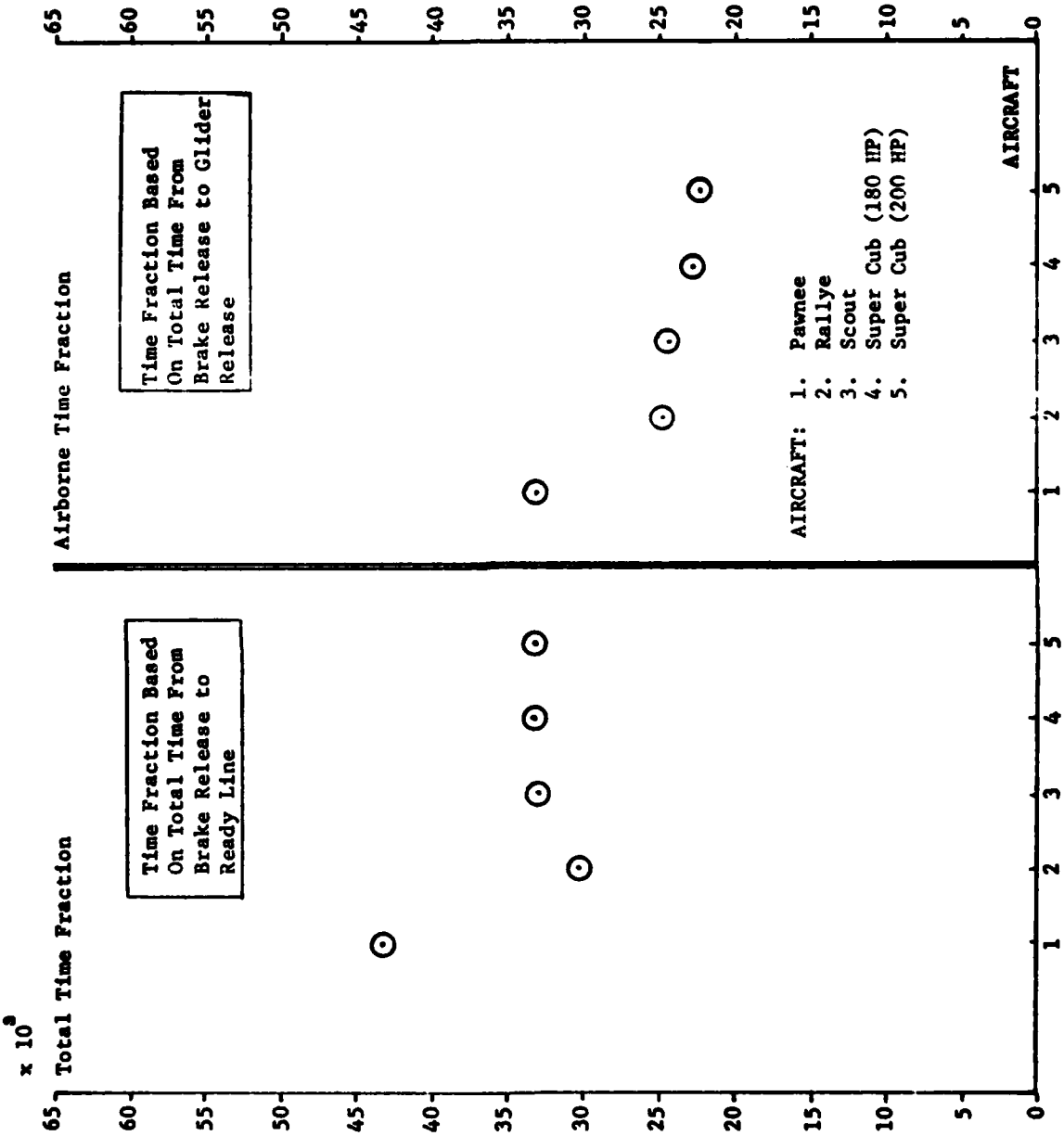

Figure 3. Time Fractions

the demanding nature of this type of flying. The limiting factor could very well be the endurance of the towplane pilot, rather than of the plane itself.

Figure 4 displays the average rate of climb calculated for the 2000-foot tow from the elapsed-time data. The left side shows a rate of climb based on the total elapsed time from towplane brake release to the return to the ready line. Here the high-wing (lighter) aircraft are obviously superior, with the higher horsepower of the 200 HP Cub providing an apparent advantage. More realistic results appear on the right side, with rate of climb calculations based only on the flight portion of the tow. Nevertheless, the same trend is obvious, with the 200 HP Cub producing a 50 percent increase over the lowest towplane.

Figures 5 through 9 present the average-rate-of-climb data collected by the glider flight crews. The large standard deviations show the considerable influence of winds, turbulence, and thermal heating. It is interesting to note that the two Cub towplanes showed an increase in average rate of climb between the first and second 500-foot segments of the tow. The other three towplanes showed a <u>decrease</u> in rate of climb between the same two segments. The reason for this anomaly is unknown, but we can conjecture that the lower relative rate of climb of the Cubs in the first tow segment could be due to an early lift-off by the towplanes. This result would then be due strictly to piloting technique.

The corrected average takeoff distance measured by the ground observer is presented in Figure 10. The measured distances were corrected to a no-wind condition using the equation below (Ref. 1).

$$(\text{Distance})_{\text{no wind}} = (\text{Distance})_{\text{measured}} \left[1 - \frac{V_w}{V_{to}}\right]^2$$

where V_w is the wind component velocity along the runway heading and V_{to} is the estimated towplane takeoff speed (shown in Appendix A). These corrected data are plotted versus measured density altitude. One can see that, after the early tows when the density altitude was low and the towplanes were heavy with fuel, the takeoff distances became shorter with time. Thus, the decrease in towplane weight apparently was the strongest factor during the early flights. At some point during the day, at density altitudes of about 7500 feet, the takeoff distances started increasing, indicating, perhaps, that elevated density altitude began degrading takeoff performance. The lighter-weight Cub towplanes have an obvious advantage in low takeoff distance, while the heavier Scout and Rallye towplanes have about 30 percent higher takeoff distances. All aircraft show about the same percent degradation with density altitude increases (with the exception

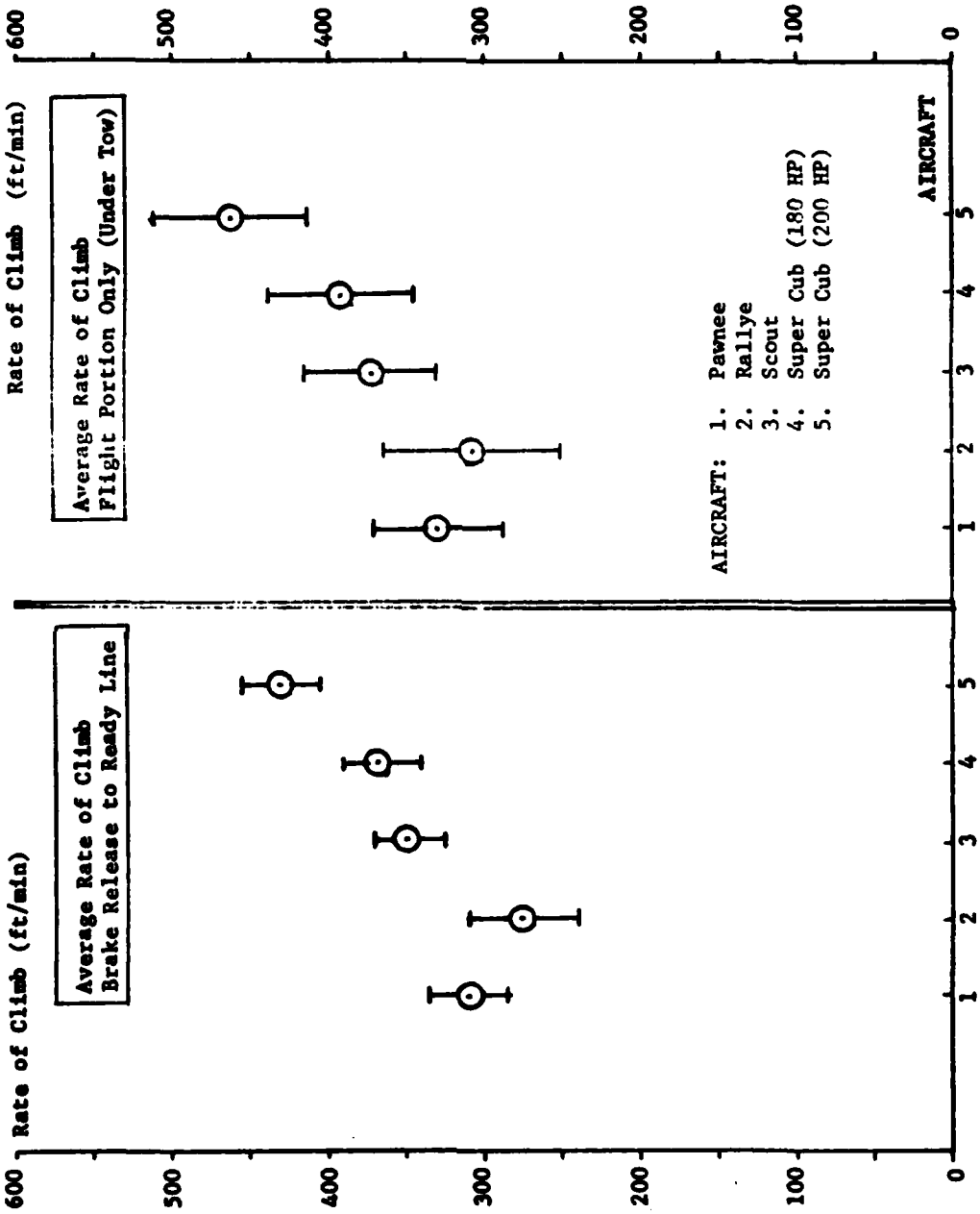

Figure 4, Average Rate of Climb

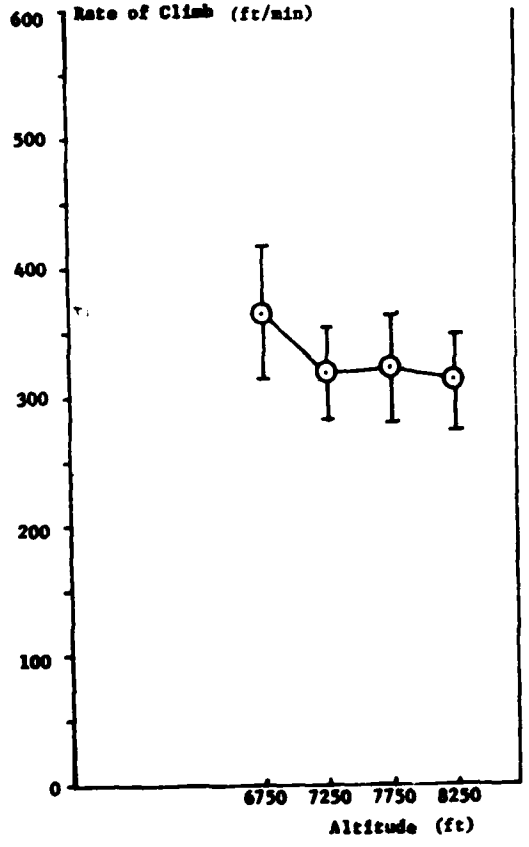

Figure 5. Average Rate of Climb at Altitude Intervals with Standard Deviation--Pawnee

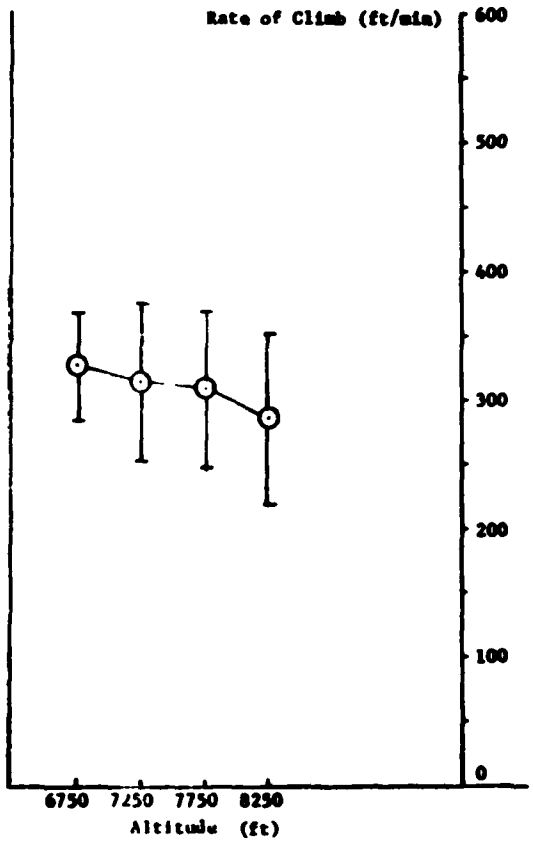

Figure 6. Average Rate of Climb During Aerotow--Ballye

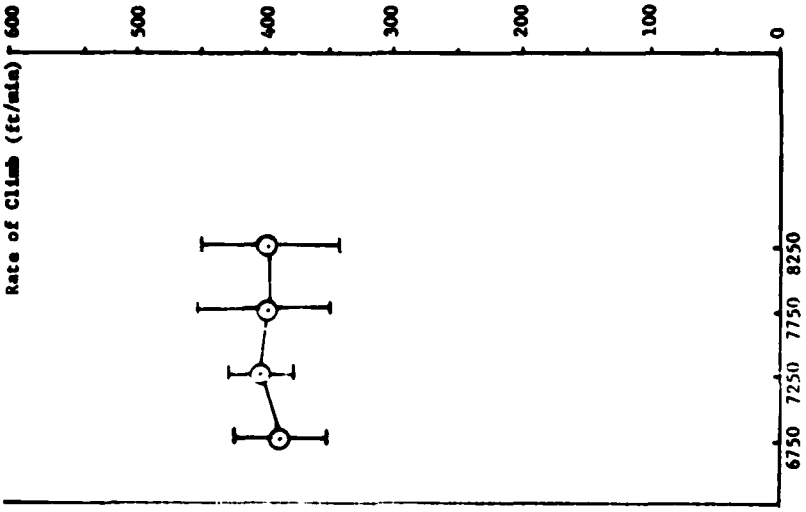

Figure 8. Average Rate of Climb During Aerotow--Super Cub (180 HP)

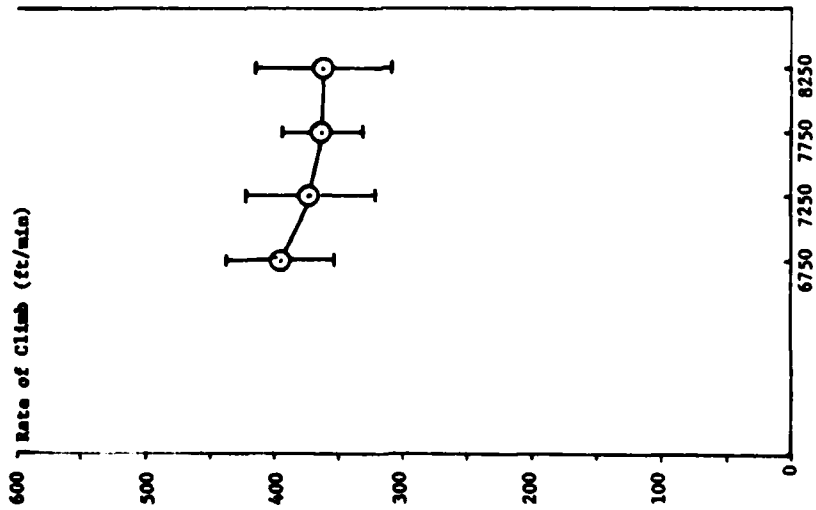

Figure 7. Average Rate of Climb During Aerotow--Scout

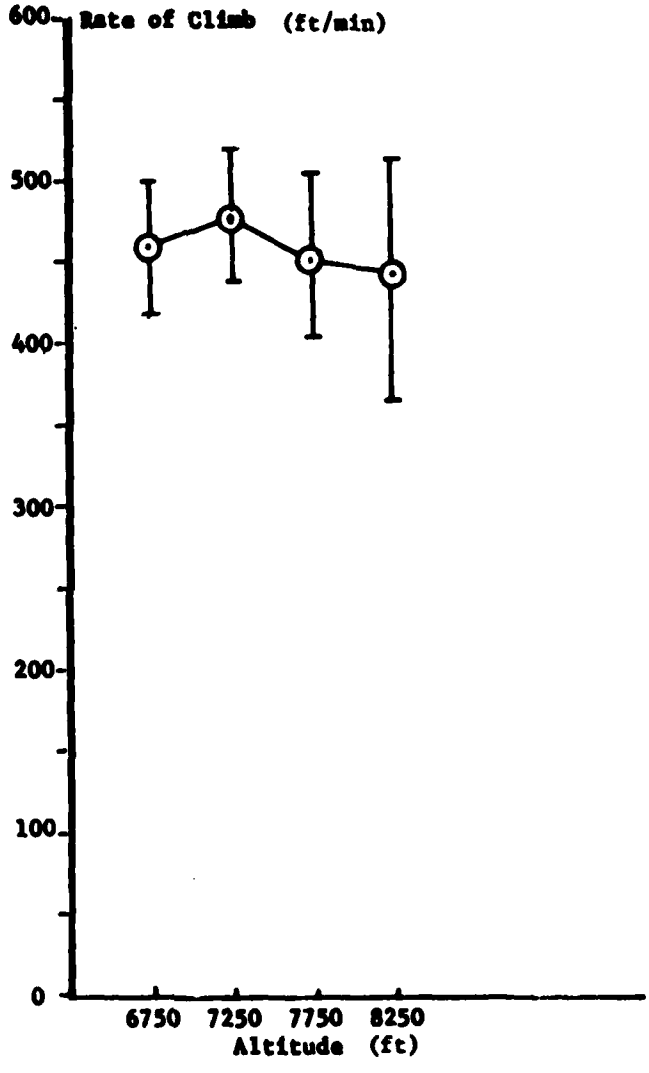

Figure 9. Average Rate of Climb During Aerotow--Super Cub (200 HP)

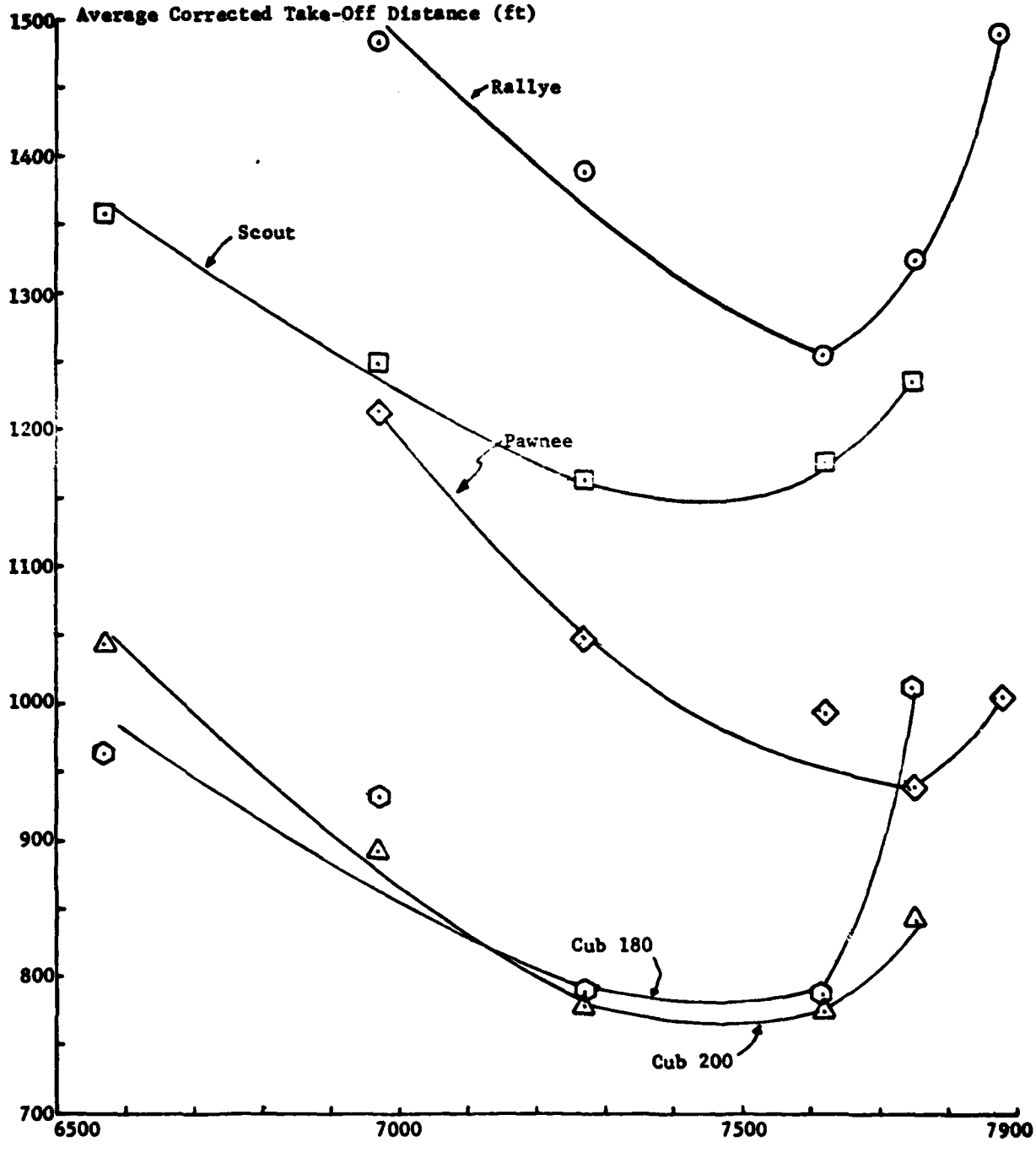

Figure 10. Take-Off Distance (Corrected to No-Wind) Versus Density Altitude

of the 180 HP Cub), but the Scout and Rallye start from higher baseline takeoff distances and increases due to density altitude are especially significant.

We can estimate the effect of elevated density altitude by assuming that the engine power decreases as the ratio of the air density increases. Thus, for example, for a density altitude of 9000 feet MSL, the density ratio when compared to the standard field altitude of 6500 feet is 0.926. The towplane engine power, then, would decrease by about 7.4 percent, and the aircraft climb rate and takeoff distance would degrade by the same order of magnitude.

V. Summary

We compared the five towplanes which participated in this test with respect to elapsed time for tows, tows per hour, tows per day, rates of climb, and takeoff distance. The results provide baseline performance data that can be used along with other considerations for the selection of an optimum towplane. These results do not show effects due to towing heavier sailplanes; the influences of very high density altitudes, strong winds, and high turbulence; or the performance during high-altitude tows into wave conditions. While further testing should be done for these cases, the data presented herein should be helpful in evaluating normal soaring operations in Colorado.

Acknowledgements

The authors wish to thank Major James Jacobs, Captain Vernon McGraw, and SMSgt John Monteith of the Cadet Airmanship Division for their assistance in organizing and conducting this test program. We are indebted to SSgt Dunajski, who assisted in the measurements, as well as to the numerous cadets and officers who flew the sailplanes and collected the data.

Reference

1. Flight Test Engineering Handbook. AF TR-6273. AF Flight Test Center, Edwards AFB, CA, January 1966.

Appendix A

DATA

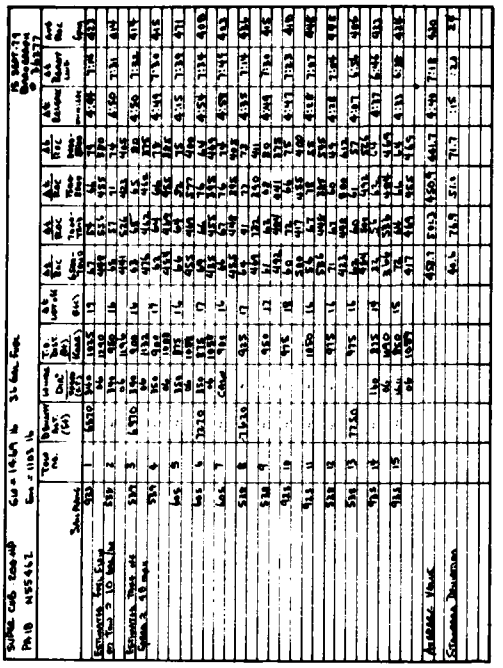

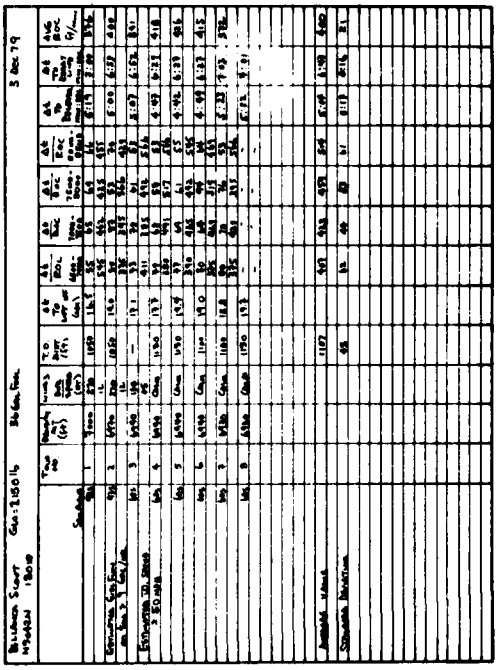

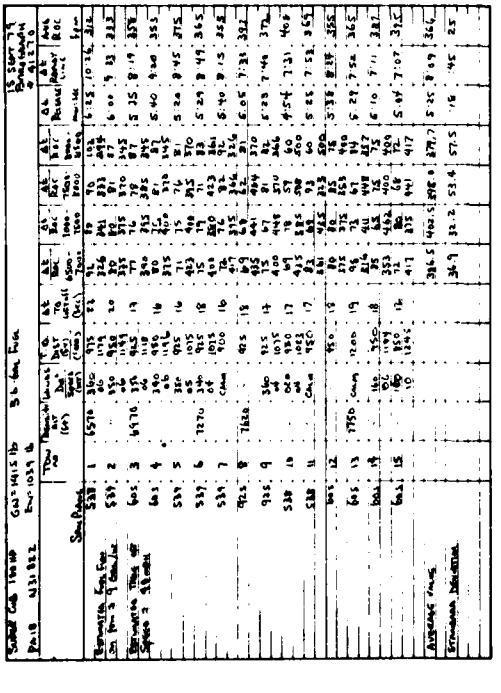

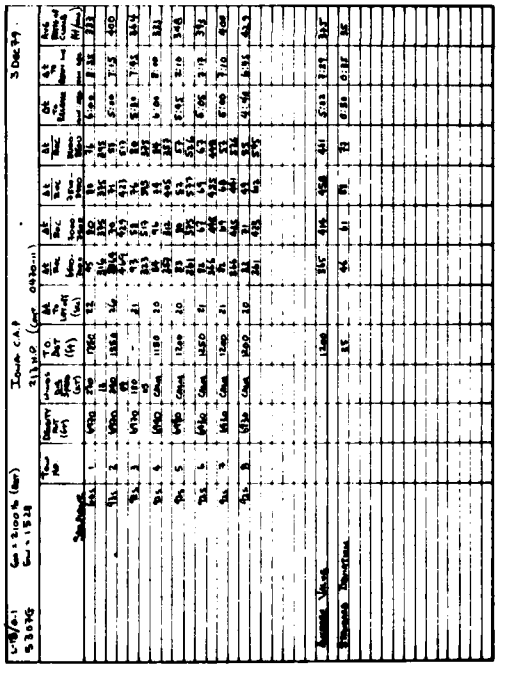

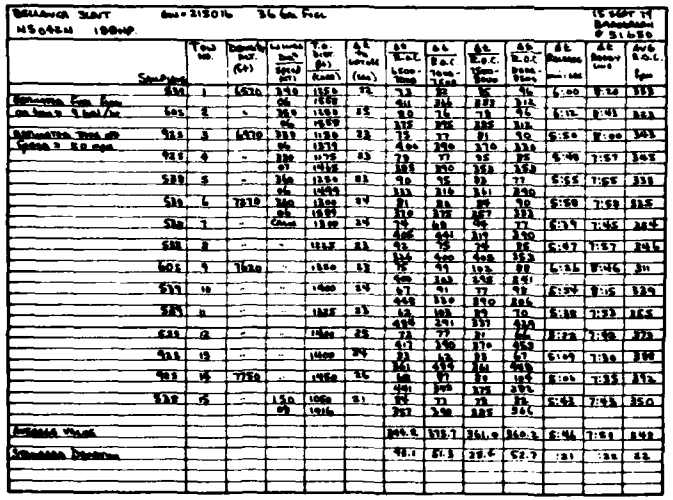

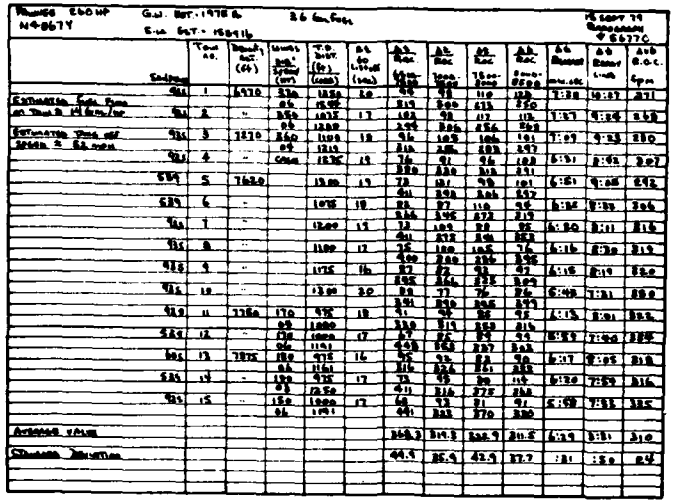

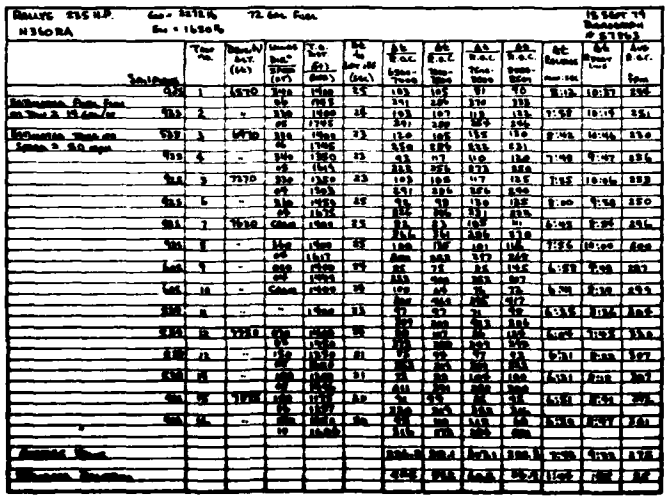

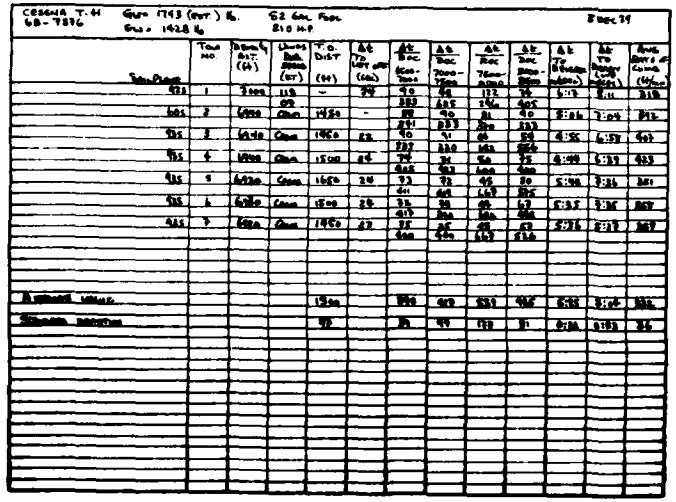

ADDITIONAL TOWPLANE FLIGHT TESTS

We tested two additional tow aircraft on 3 December 1979. Despite the late date, we tested these aircraft to provide a broader data base and to include two light aircraft available through Air Force channels. The aircraft were the 0-1 and the T-41 and their specifications are included on the following data sheets. In order to provide a comparison, we retested the Scout used in previous tests, and conducted this test exactly like the previous series, using gliders and flight crews of approximately the same weights. Data shown on the following figures present average values of the data, and the indicated error bands represent one standard deviation. Results show the 0-1 and T-41 to be very similar in most performance areas tested. The elapsed-time data in Figure B1 show that these two aircraft used approximately 10 percent more time during tows than the Scout. Rate of climb data in Figure B2 show 10-12 percent lower values for the two aircraft when compared to the Scout. Takeoff data on Figure B3 show significantly greater distances for the T-41. This could be due to the tricycle landing gear and level ground attitude of this aircraft. Rate of climb data for 500-foot altitude intervals are shown in Figures B4-B6. The wide dispersion of data for the T-41, as well as the lower rates of climb at higher altitudes, is probably due to pilot technique.

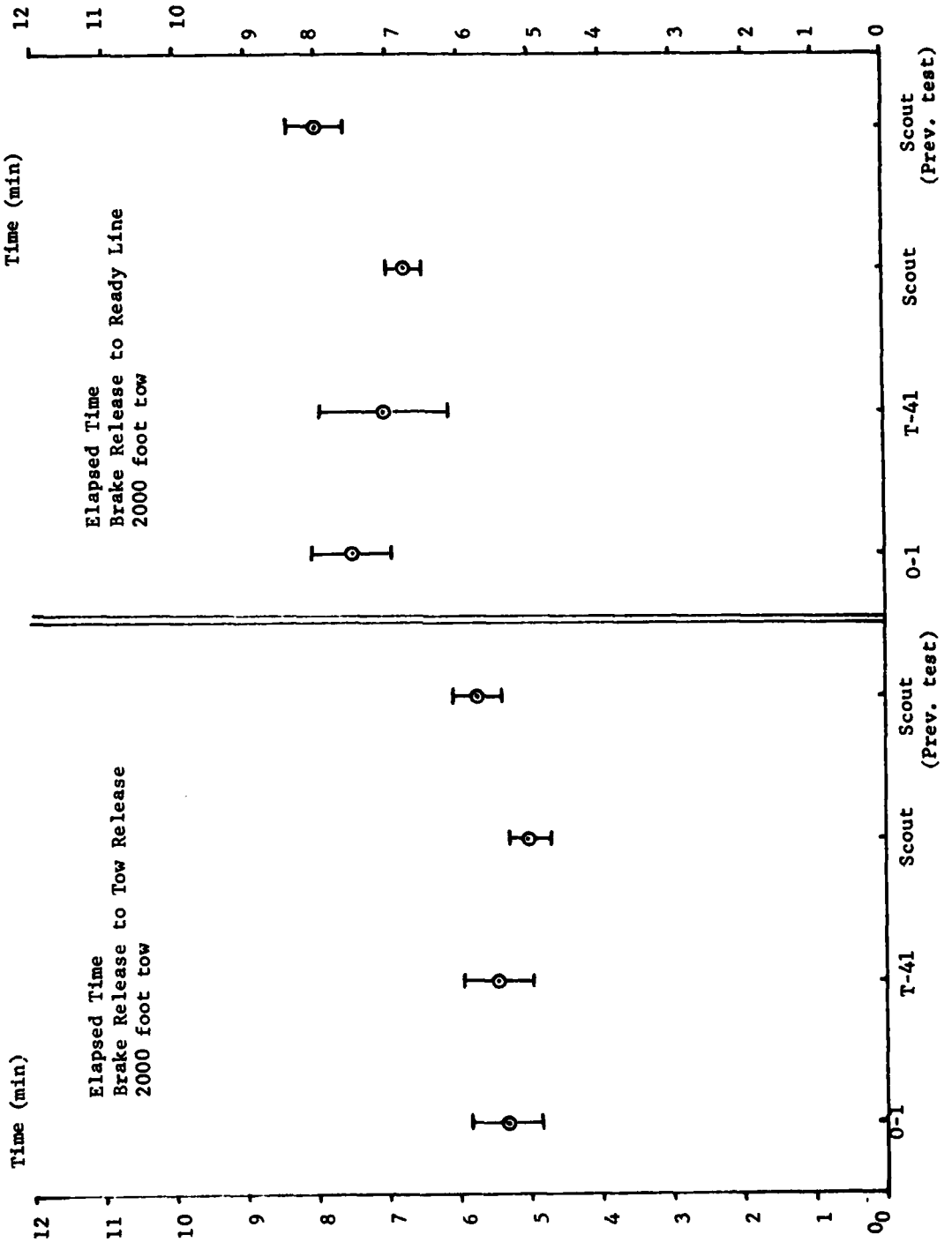

Figure B1. Elapsed Time Data

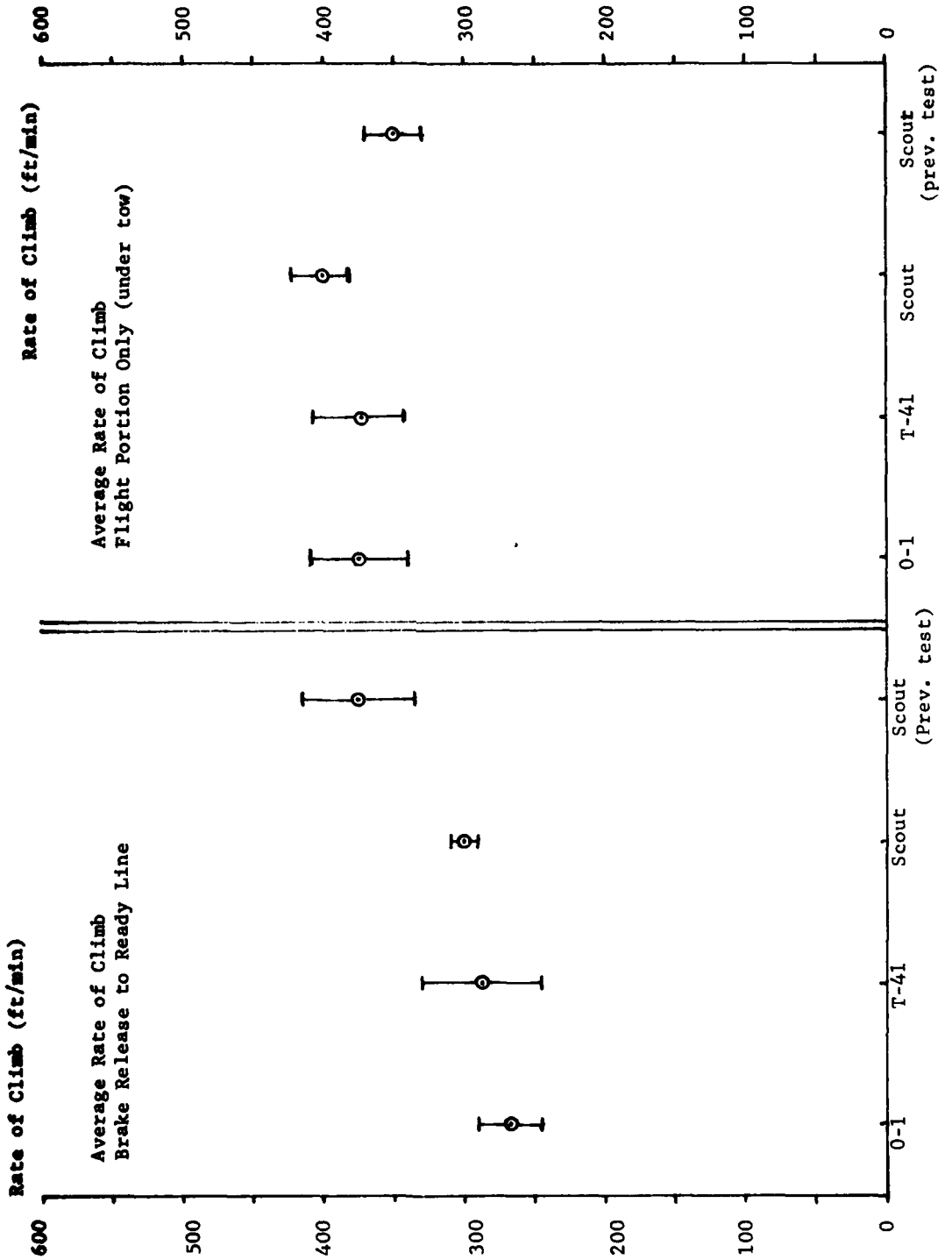

Figure B2. Rate of Climb Data

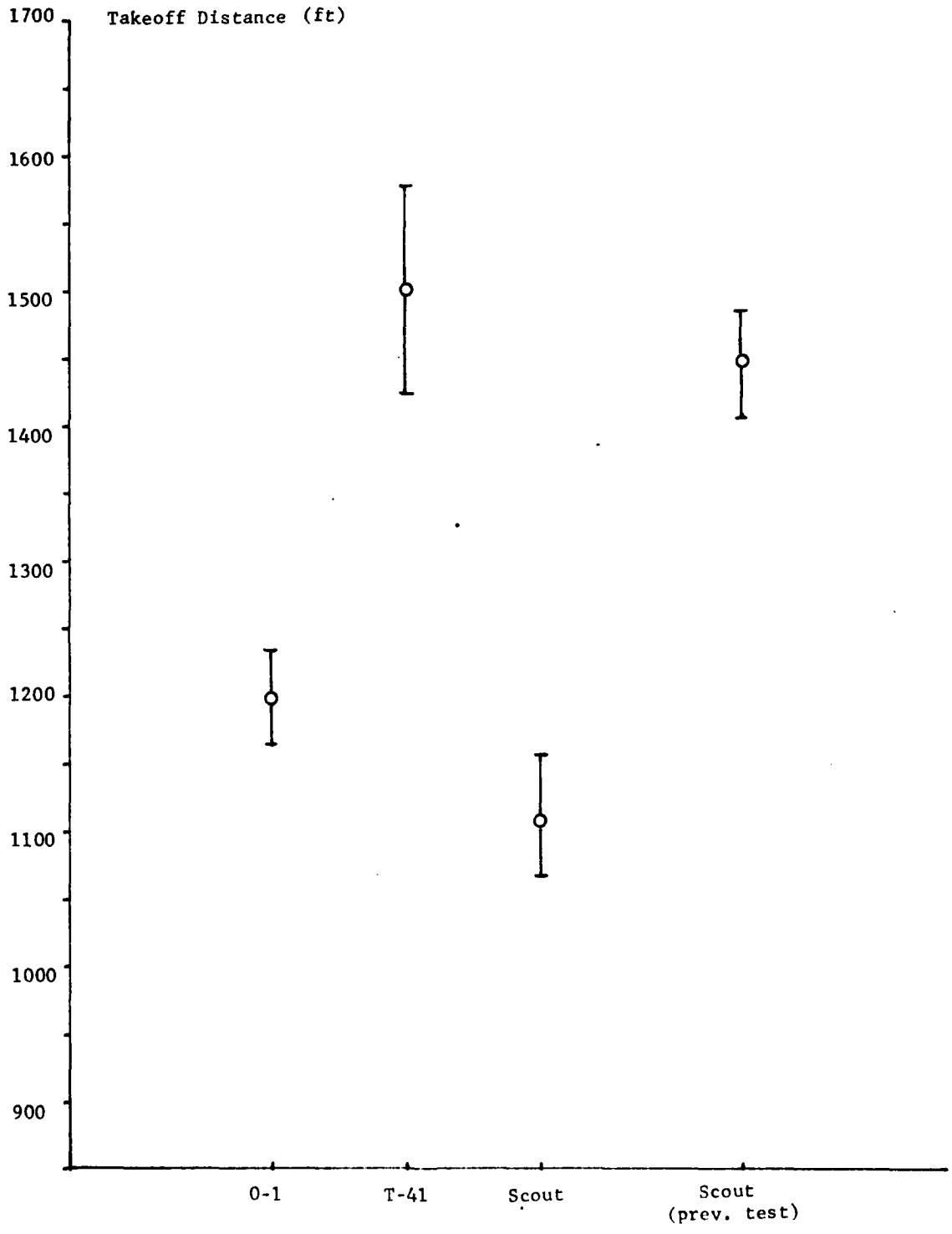

Figure B3. Takeoff Distance Data

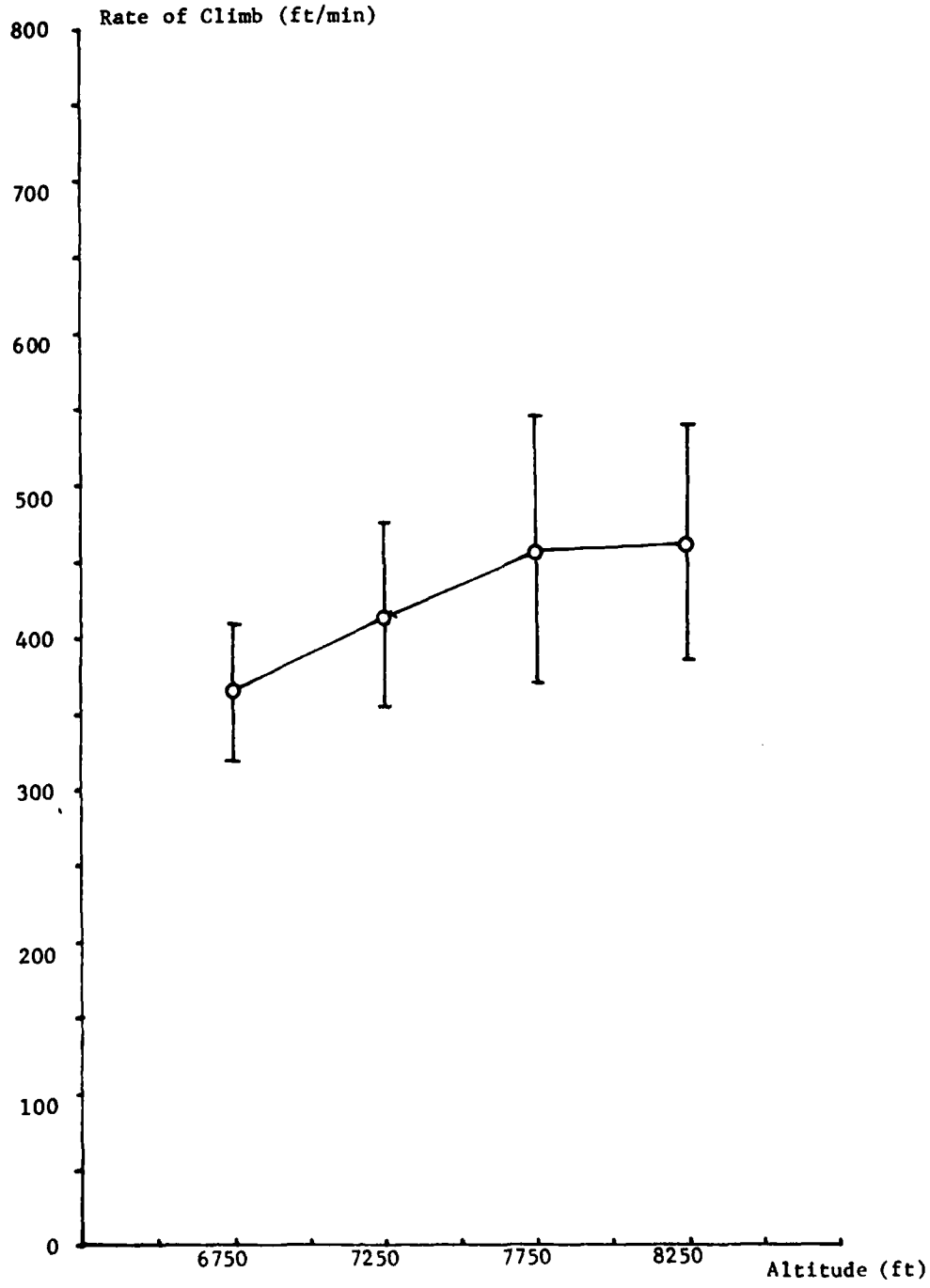

Figure B4. O-1 Average Rate of Climb

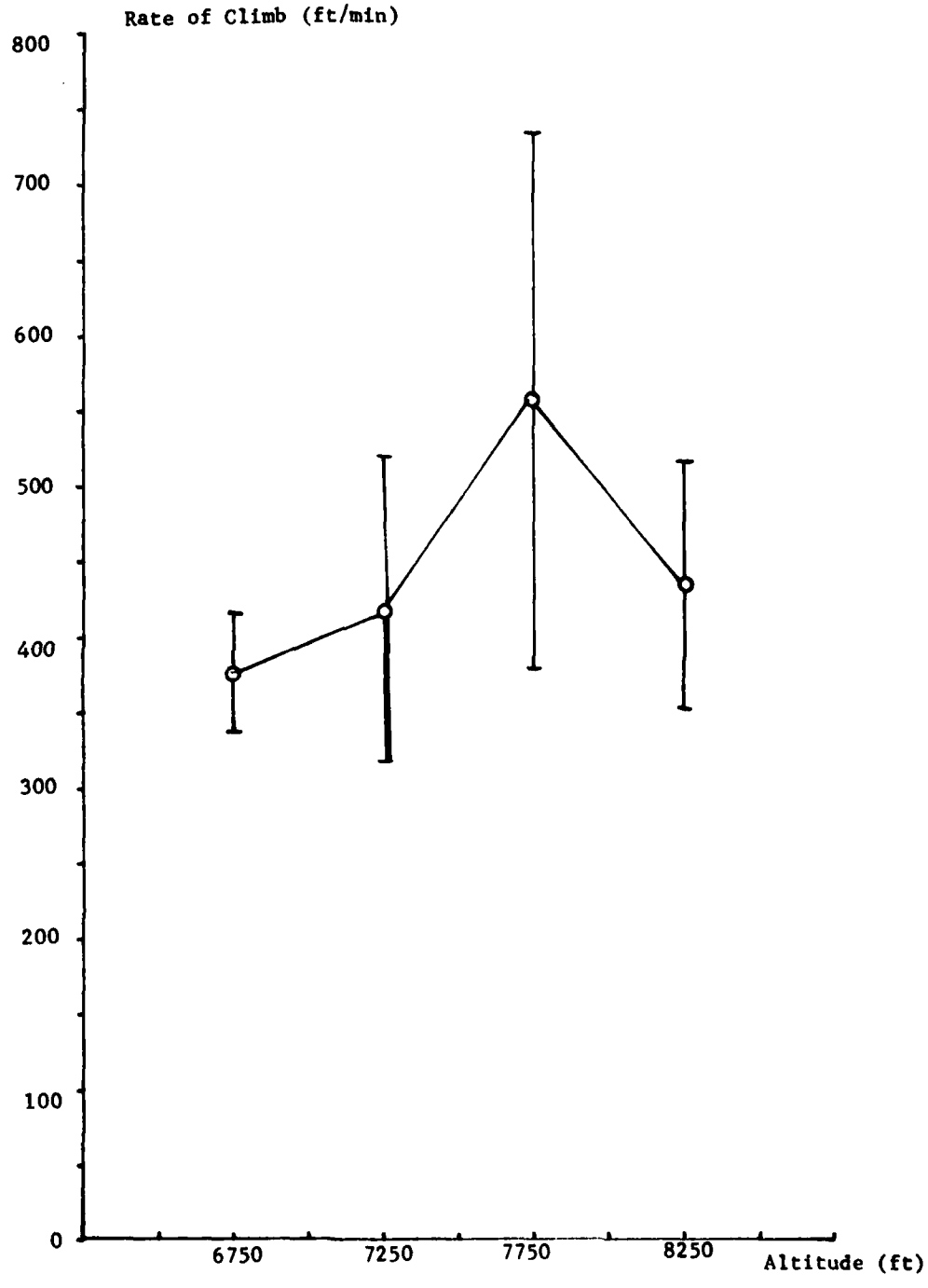

Figure B5. T-41 Average Rate of Climb

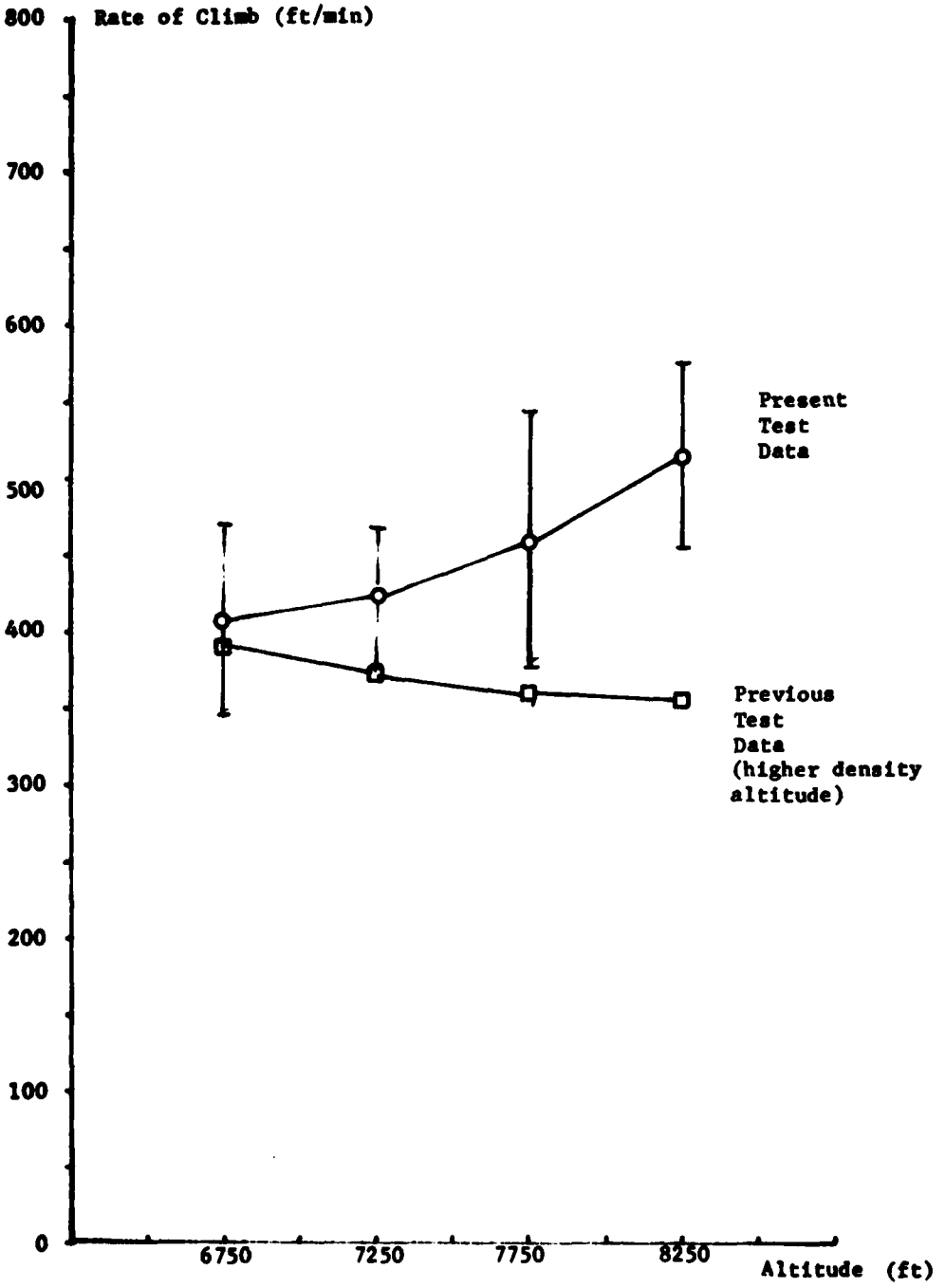

Figure B6. Scout Average Rate of Climb

COMPUTERIZED WAVE DRAG PREDICTION USING A MODIFIED SUPERSONIC AREA RULE

Gary N. Harris*

Abstract

This report examines a computer program which predicts the wave drag of an aircraft using only the Mach one equivalent body shape. The program accepts the body shape in tabular form. The program is then validated by wind tunnel testing at the USAFA Trisonic Wind Tunnel and compared to actual F-15 data. The results indicate this program is able to predict the qualitative wave drag changes due to adding protuberances to an aircraft.

I. Introduction

This paper is a continuation of Schlotterbeck's work on supersonic wave drag prediction (Ref. 1). Schlotterbeck developed a computer program which predicts the wave drag of slender bodies of revolution in supersonic flow using a modified form of Von Karmen's area rule. Schlotterbeck did not validate his program with wind tunnel tests but he did examine a theoretical body for program sensitivity.

This report describes a modification to Schlotterbeck's program. His program requires the equivalent body description to be input as an equation, and the modification allows these data to be input in tabular form. This report also describes a validation study of the program and an application of the program to an F-15 with a comparison to actual F-15 data (Ref. 2).

II. Program Modification

Schlotterbeck found the area distribution (first and second derivatives of the area distribution) at a given Mach number through an iteration process. He first determined the actual radius value (r) at an increment (I) away from the point he was examining (point A) by placing this new axial value (point B) in his radius equation (see Figure 1). He then found the perpendicular distance (d) from the body center line to the Mach angle plane through the body. He compared these two values and readjusted his axial increment to converge the two values. He repeated this process in an iterative fashion until the difference between the two points was sufficiently small (10^{-6} inches). This process was repeated at one degree increments around the body at each axial location to achieve an area rule for that Mach number. He then determined the first and second derivatives of the area distribution and numerically integrated his modified supersonic area rule.

---

*2/Lt, USAF, Research Assistant, DFAN

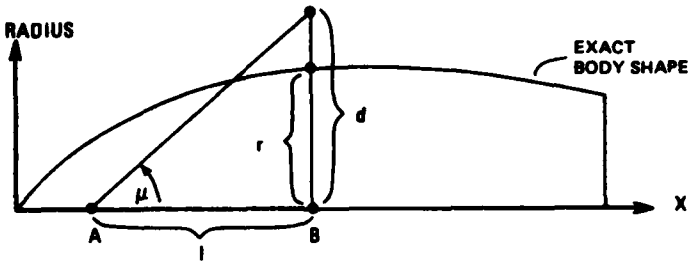

Figure 1. Schlotterbeck's Convergence Technique

Using this method, one confronts a problem if the basic body is irregular or if protuberances are added to a basic body. The problem is that it can become very difficult to describe an irregular body by an equation. We corrected the problem by changing the program to accept a body shape in tabular form. This tabular approach uses a linear interpolation between the discrete data points (points C and D in Figure 2, for example) and a convergence routine like Schlotterbeck's, to achieve a new radius value at each angle and axial location.

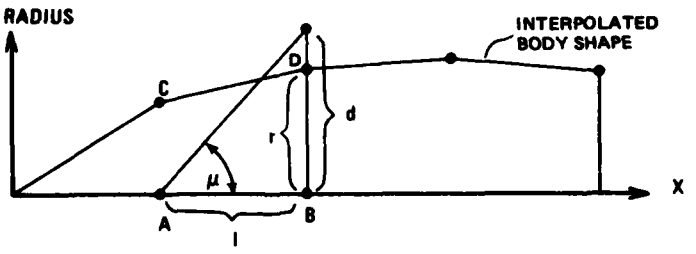

Figure 2. Tabular Convergence Technique

A separate problem arises when deciding how many data points are needed to achieve a sufficiently accurate picture of the equivalent body. For a smooth body (parabolic shape) the results showed that data given every 2% of the length (50 values) resulted in C_{d_w} errors up to 8 or 9% compared to Schlotterbeck's program. However, data given every 1% of the length (100 values) reduced the error to less than .2% (Figure 3). For highly irregular shapes, more data should probably be used, but computer time limitations may determine a practical limit to the number of data points actually used. Table 1 shows the relationship between number of points and computer processor time for the Burroughs B6700 computer.

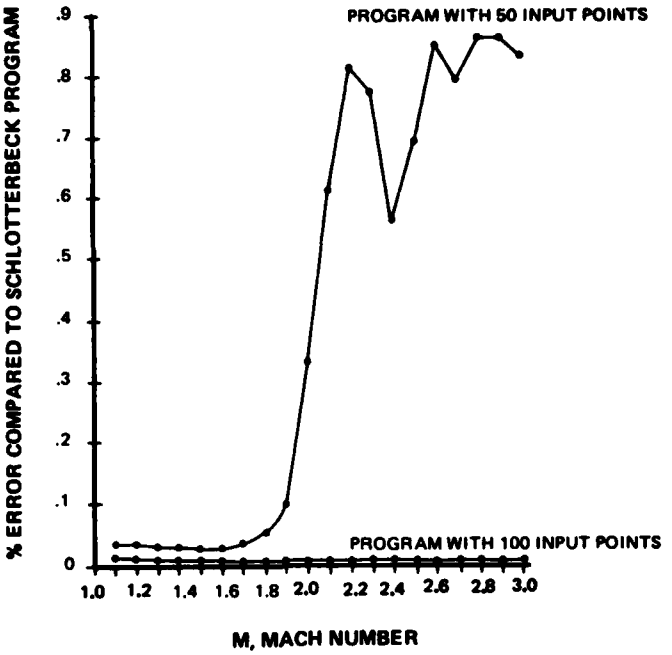

Figure 3. Error Analysis for Tabular Technique

Table 1

COMPUTER TIME REQUIREMENTS

Number of Input Points	Approximate CPU Time Required
50	1.5 minutes
100	3.5 minutes
200	12.0 minutes

III. Wind Tunnel Validation

The initial step in program validation involved checking the data presented by Schlotterbeck. In his paper he examined a baseline body of revolution and the effect of adding a given axially symmetric perturbation to the baseline body in two different locations. His program predicted variations in C_{d_w}, depending on where the perturbations were located, even though the perturbation size was not changed. The perturbation located in the rear resulted in higher C_{d_w} than when it was located in the front (Figure 4).

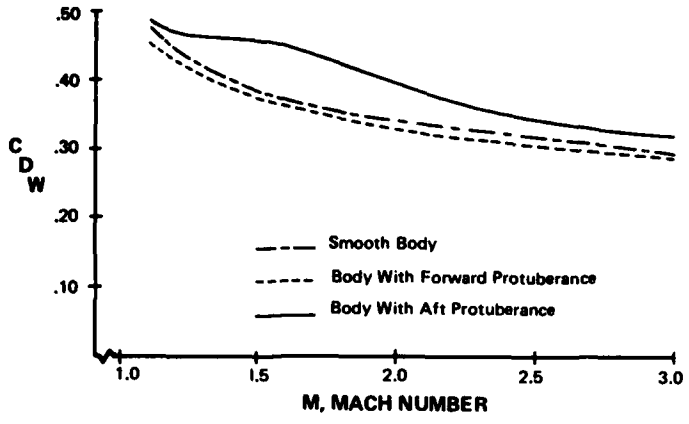

Figure 4. Schlotterbeck's Results (Ref. 1)

Unfortunately, when these bodies of revolution were built, the size of the perturbations was so small they only contributed a bump on the order of .004 inches. The combination of fabrication inaccuracy and noise in the data acquisition and reduction system masked any discernible drag differences. However, for the baseline body, the C_{d_w} values Schlotterbeck found (.3 to .5) were approximately the same as the wind tunnel C_d values (.2 to .4), and both had the trend of decreasing C_d as Mach increased. These results lend credence to Schlotterbeck's analysis, but are not conclusive enough to give full confidence in its use. Therefore, new bodies of revolution with larger perturbation additions were designed, built, and wind-tunnel tested in the USAFA Trisonic Wind Tunnel. These new wind tunnel bodies are shown below (Figures 5, 6, 7, and 8).

Figure 5. Baseline Body

Figure 6. Body with Front Bump

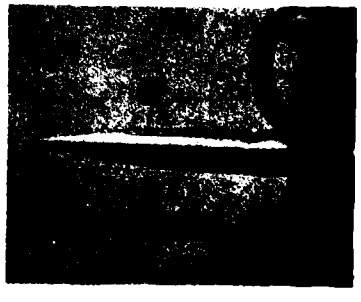

Figure 7. Body with Rear Bump

Figure 8. Model Design with Interchangeable Parts

Figures 9, 10, and 11 present the wind tunnel test results. It is interesting to note that while the baseline body differs somewhat from wind tunnel data (characteristic of the area-rule method of drag prediction), the program more closely predicts the difference in wave drag, ΔC_{d_w}, produced by adding protuberances. This result is most encouraging since it is the ΔC_{d_w} which is of interest to this study.

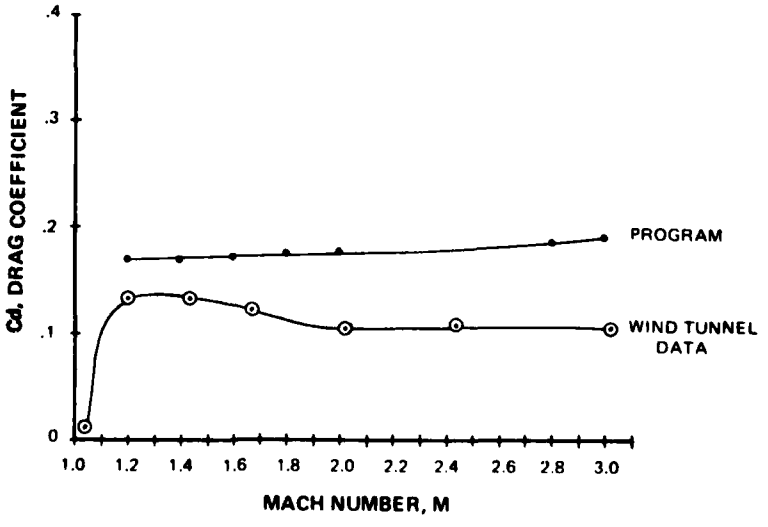

Figure 9. Drag for Baseline Body

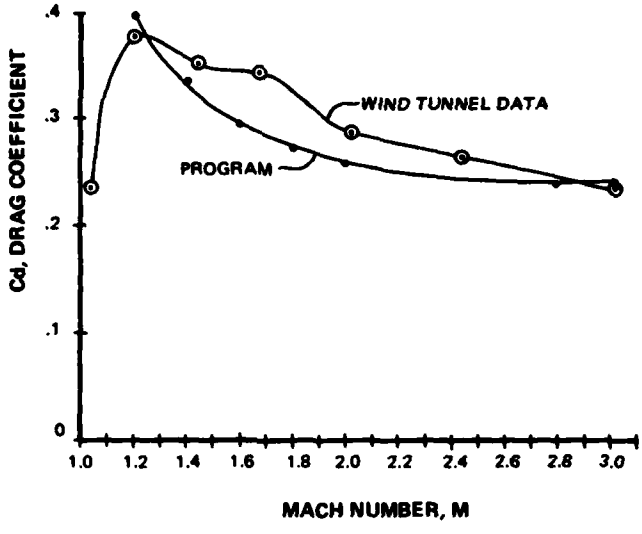

Figure 10. Drag for Body with Front Bump

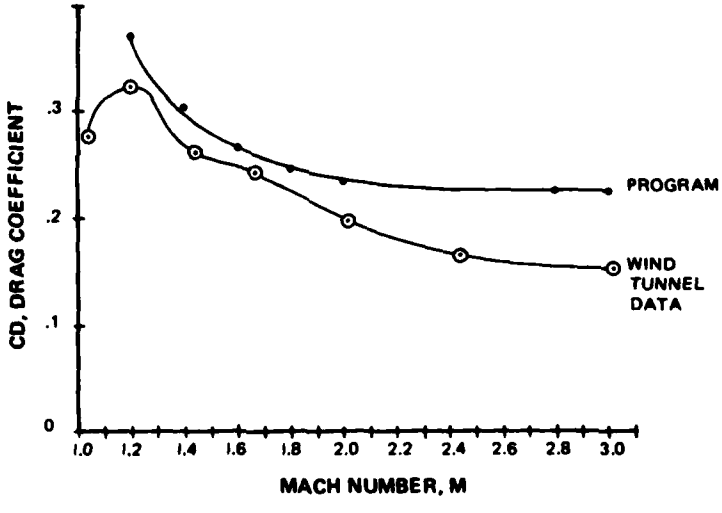

Figure 11. Drag for Body with Rear Bump

Examining the curves more closely (see Figures 12 and 13), we find that the trends in C_{d_w} are correct and the actual C_{d_w} values are close (especially at $M < 2.0$, the Mach number range of interest to this project). The most important comparison, however, shows which protuberance location results in the highest drag.

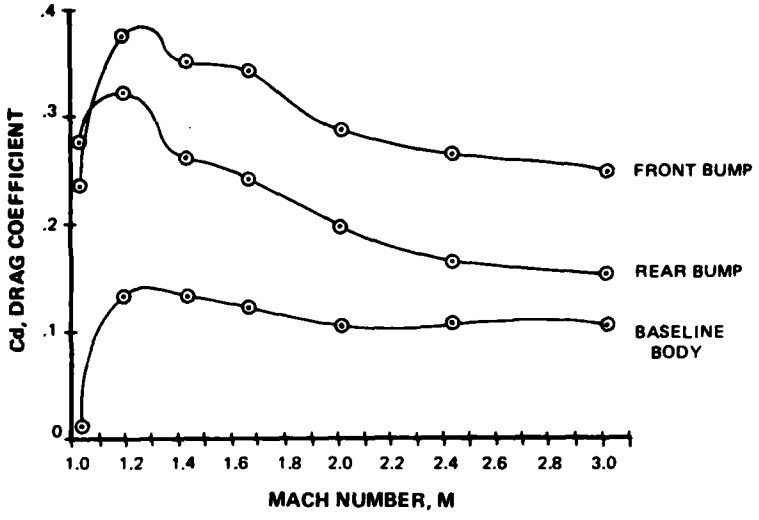

Figure 12. Wind Tunnel Drag Data

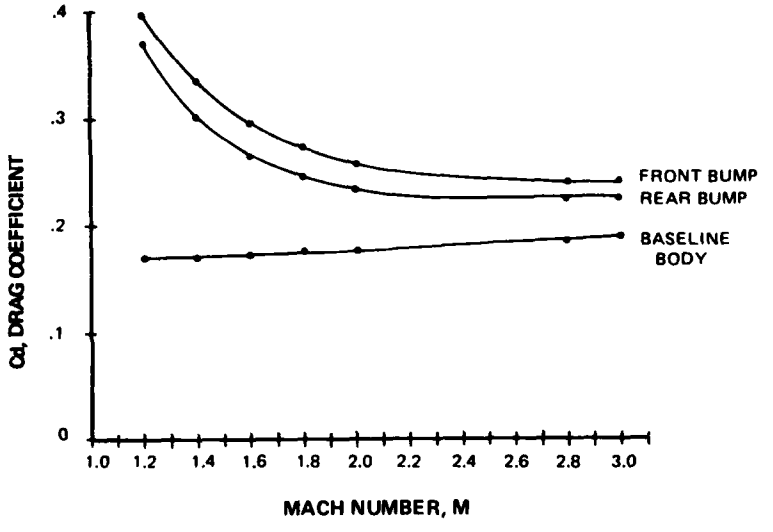

Figure 13. Predicted Drag

From the testing and analysis of the new wind tunnel bodies, we feel confident that the program closely models bodies of revolution. Up to this point we have not made mention of the program being applied to an actual aircraft. This final step in program validation is discussed in the next section.

IV. Simplified Area Rule Application

Our simplified area rule makes use of the Mach one equivalent body to determine the area distributions at all other Mach numbers. In this regard we numerically produced

an equivalent body of revolution which had the same area distribution as an F-15. The McDonnell Aircraft Company provided the area data for the F-15 (Ref. 4). The tabular modification to Schlotterbeck's program made it possible to input the F-15 data easily without converting it into equation form.

In addition to the basic F-15, the effects of adding a pallet store and 3 turrets were examined, for which drag data are available (Ref. 2). The area distributions of these perturbations were needed to modify the basic F-15 area distribution, and were obtained from scale drawings (Figures 14, 15, 16, and 17) (Ref. 2).

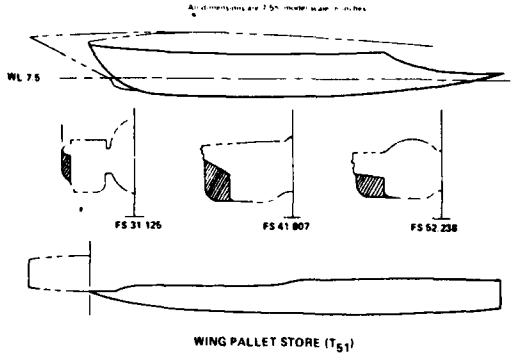

Figure 14. Wing Pallet Store

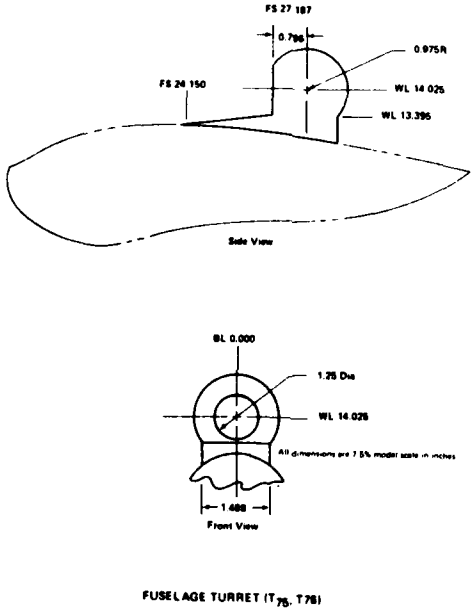

Figure 15. Fuselage Turret

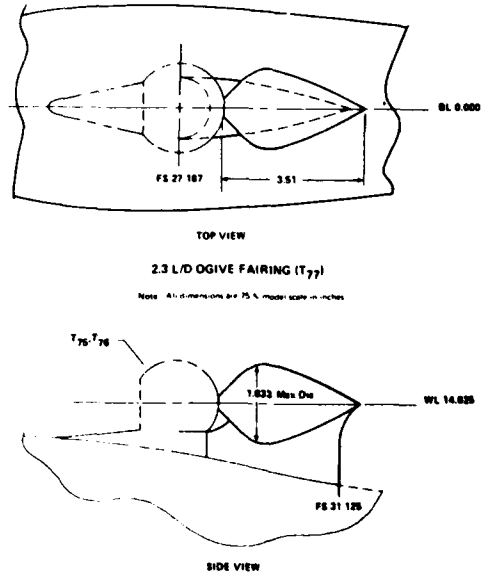

Figure 16. Turret with 2.3 L/D Ogive Fairing

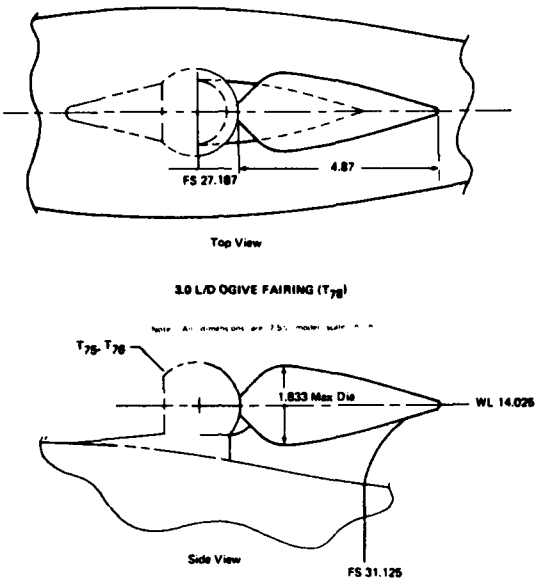

Figure 17. Turret with 3.0 L/D Ogive Fairing

The results indicate that the ΔC_d values for adding the pallet to the basic F-15 were quite accurate (Figures 18 and 19). This was expected because the pallet contributed little pressure drag, which the program was not designed to handle (i.e., the major drag effect was due to wave drag, which was predicted by the program).

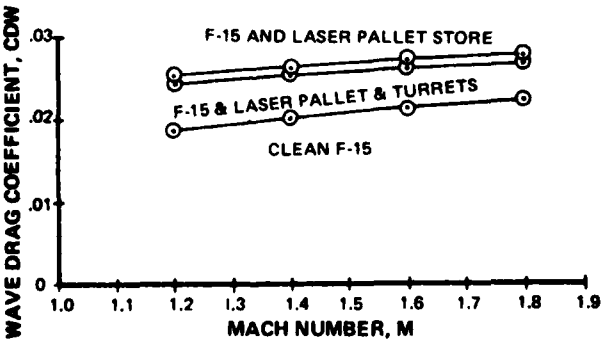

Figure 18. Computer-Predicted F-15 Drag

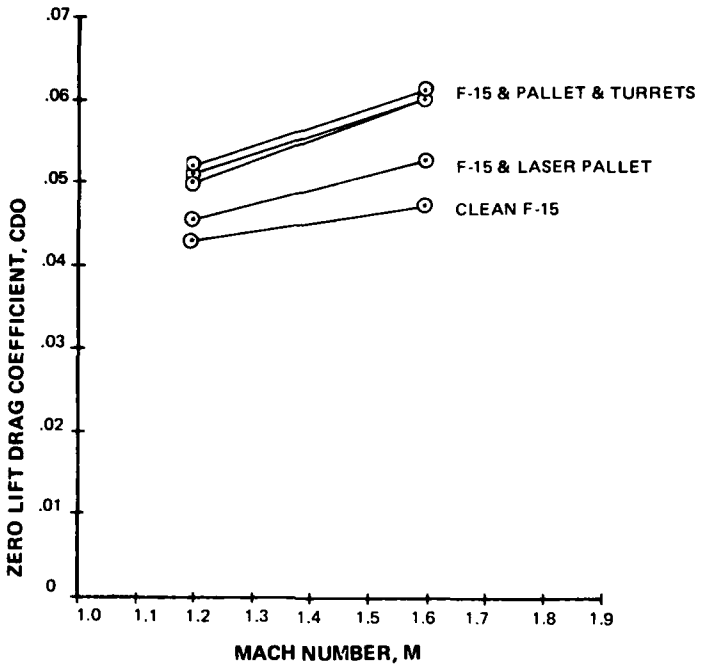

Figure 19. F-15 Wind Tunnel Drag Data

However, the large-scale effects of adding the turrets to the F-15 and pallet are inaccurate. The program predicted a C_{d_w} decrease (from the C_{d_w} of the F-15 and pallet), while the actual wind tunnel results show a C_d increase (Figures 18 and 19).

Referring to the turret drawings, we clearly can expect a great deal of pressure drag (base separation and relief) from the turrets (Ref. 3). Examination of the basic turret (to which the 2.3 ogive and 3.0 ogive fairings have been added) was omitted because of the large amount of separation that occurs behind it.

The turrets with fairings were designed to reduce this pressure drag by reducing the base pressure due to separation. As a result, these turret designs have much lower pressure drag than the basic turret, but because their designs are so similar, their pressure drag is approximately equal (Ref. 3). Therefore, any differences in drag between these two turrets would probably be due to wave drag rather than pressure drag, and examination of these two turrets would help in establishing the validity of the program.

In examining the ΔC_{d_w} for these turrets, we find the effects matched the F-15 data. The program correctly predicted that the C_d of the 3.0 ogive fairing began lower than the C_d of the 2.3 ogive fairing (at M = 1.2) and then converged to the same value at higher Mach numbers (Figures 20 and 21).

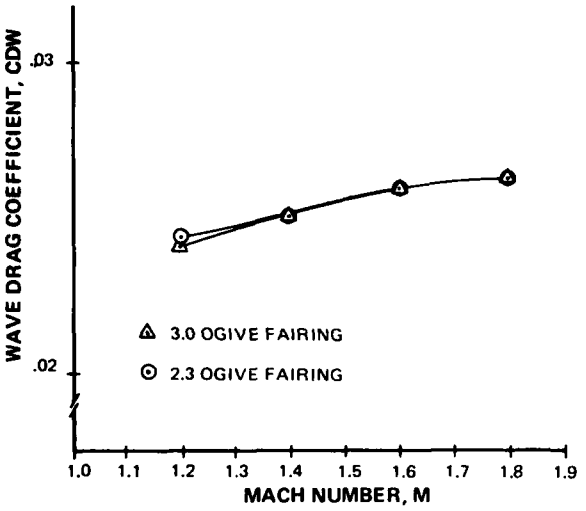

Figure 20. Computer-Predicted Turret Drag

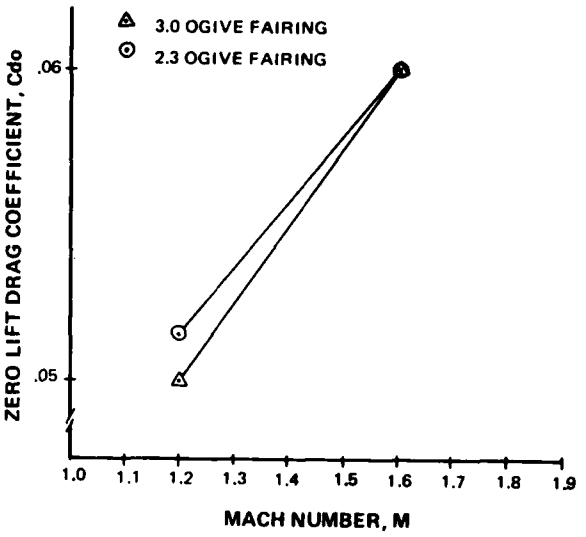

Figure 21. Turret Wind Tunnel Drag Data

The program again resulted in accurate ΔC_d values and trends when the effects of pressure drag were minimal. For this reason also, we can infer that the program correctly analyzes C_{d_w}.

V. Conclusions

The results show that the tabular input data for area modification to Schlotterbeck's program result in the same accuracy as the original program if at least 100 input points are used. Further, the program is very accurate at predicting ΔC_d effect of adding protuberances to both bodies of revolution and actual aircraft shapes when pressure drag contribution is not considered.

We believe this program, coupled with our simplified area rule theory, represents a new concept in wave drag prediction. The practice of using only the Mach one equivalent body of an aircraft to predict the wave drag at higher Mach numbers has not been found in any other publications. This method is much easier to use than prior methods, and the results provide a good qualitative look at the C_{d_w}. The program is especially useful in predicting the ΔC_{d_w} effect of adding protuberances to an aircraft. This program provides the designer or engineer with a fast qualitative look at the effect of adding protuberances to aircraft.

References

1. Schlotterbeck, Glen R. Wave Drag Predictions on Slender Bodies of Revolution Using the Supersonic Area Rule. USAFA TR-79-1, 1979.

2. Littlepage, H. S. Aerodynamic Study of Turrets on Fighter Aircraft. AFWL-TR-74-45, Vol. II, 1974.

3. Jumper, Eric J. Private Communication. Aeronautics Department, USAF Academy, Colorado 80840.

4. Niedling, L. G. Private Communication. McDonnell Aircraft Company, St. Louis, Missouri.

THE EFFECT OF WIND ON AIRCRAFT CLIMB ANGLE

Michael M. Tower* and Richard F. Felton**

Abstract

This paper presents an academic exercise on the effect of atmospheric winds on an aircraft's climb angle relative to the ground. An analytic equation is derived for climb angle which includes terms that are the result of head or tail winds. Then a hodograph plot is used to show that the same results can be obtained graphically.

I. Introduction

The question that this paper addresses is, what effect do surface winds have on an aircraft's climb angle? When an aircraft is in a steady climb as depicted in Figure 1, a climb angle, γ, is established which is the angle between the flight path and the horizontal. The angle can be related to the four forces (lift, drag, thrust, and weight)

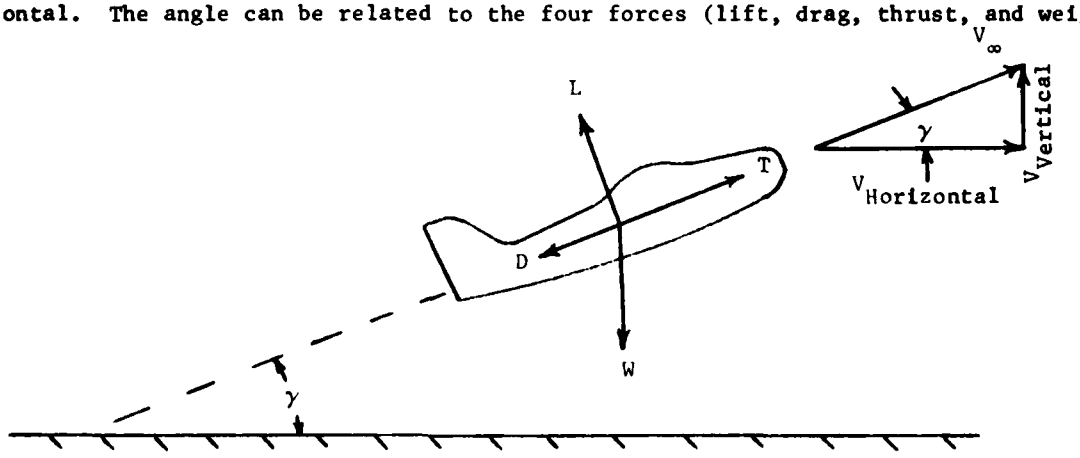

Figure 1. Climb Angle and Aircraft Forces

acting on the aircraft by the summation of forces. Summing the forces in the direction of the flight path, we can obtain the following equation:

$$\pm \sum F_{V_\infty} = T - D - W \sin\gamma = 0 \quad ,$$

or

$$\gamma = \sin^{-1} \frac{(T - D)}{W} \quad . \qquad (1)$$

Considering this equation, we find no apparent effect on the climb angle with respect to the air mass as a result of natural winds. However, this is misleading and is erroneous when considering the climb angle with respect to the ground. From intuition one would expect a surface wind to change the climb angle as shown in Figure 2.

---

*Captain, USAF, Associate Professor of Aeronautics, DFAN
**Lt Col, USAF, Tenure Associate Professor of Aeronautics, DFAN

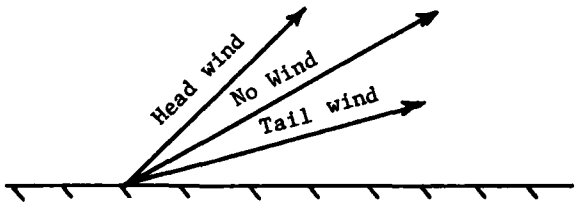

Figure 2. Intuitive Concept of the Wind's Effect on Climb Angle

The effect of wind direction becomes important when the pilot is interested in clearing an obstacle at the end of the runway. In general, climb angle is important when clearing a ground obstacle, so we are concerned with the most altitude gained for the horizontal (ground) distance covered, and not our climb angle relative to the air mass.

To show the wind effect on climb angle, we will derive a climb angle equation for a head and tail wind, then demonstrate the effect graphically with a hodograph plot for an arbitrary aircraft.

II. Analytical Wind Effect

A. Head wind case

For the effect of a head wind on climb angle consider the vector sketch in Figure 3.

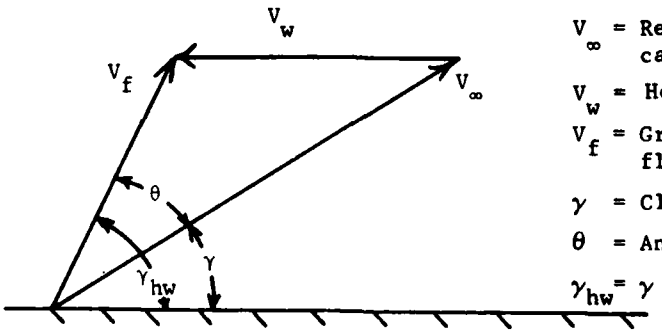

V_∞ = Relative wind velocity on a calm day (true airspeed).

V_w = Head wind velocity

V_f = Ground reference resultant flight path velocity.

γ = Climb angle on a calm day

θ = Angle between V_∞ and V_f

$\gamma_{hw} = \gamma + \theta$

Figure 3. Velocity Vector Definitions

We would like to determine the resultant climb angle, γ_{hw}, due to a head wind which can be obtained from the following trigonometry. From the law of sines,

$$\frac{V_w}{\sin \theta} = \frac{V_f}{\sin \gamma} \quad ,$$

rewriting

$$\sin\theta = \frac{V_w}{V_f} \sin\gamma \quad ,$$

but from Eqn (1)

$$\sin\gamma = \left(\frac{T - D}{W}\right) \quad ,$$

and substituting

$$\sin\theta = \frac{V_w}{V_f} \left(\frac{T - D}{W}\right) \quad . \tag{2}$$

To eliminate V_f we must introduce the law of cosines:

$$V_f^2 = V_w^2 + V_\infty^2 - 2 V_w V_\infty \cos\gamma$$

and the identity

$$\cos\gamma = \sqrt{1 - \sin^2\gamma}$$

or

$$\cos\gamma = \sqrt{1 - \left(\frac{T - D}{W}\right)^2} = \frac{1}{W}\sqrt{W^2 - (T - D)^2} \quad ,$$

so that now

$$V_f^2 = V_w^2 + V_\infty^2 - 2 V_w V_\infty \frac{1}{W} \sqrt{W^2 - (T - D)^2} \quad . \tag{3}$$

The resultant flight path velocity, V_f, may now be substituted into Eqn (2):

$$\theta = \sin^{-1}\left\{\frac{V_w (T - D)}{W} \left[\frac{1}{V_w^2 + V_\infty^2 - \frac{2V_w V_\infty}{W}\sqrt{W^2 - (T - D)^2}}\right]^{\frac{1}{2}}\right\}$$

and finally the resultant climb angle may be found from

$$\gamma_{hw} = \gamma + \theta = \sin^{-1}\left\{\frac{T - D}{W}\right\} + \sin^{-1}\left\{\frac{V_w (T - D)}{W} \left[\frac{1}{V_w^2 + V_\infty^2 - \frac{2V_w V_\infty}{W}\sqrt{W^2 - (T - D)^2}}\right]^{\frac{1}{2}}\right\} \quad . \tag{4}$$

As expected in a no-wind condition when $V_w = 0$, the equation reduces to the no-wind climb angle, Eqn (1).

B. Tail wind case

Similarly, the same derivation may be made for a tail wind, resulting in

$$\gamma_{tw} = \sin^{-1}\left\{\frac{T - D}{W}\right\} - \sin^{-1}\left\{\frac{V_w (T - D)}{W}\left[\frac{1}{V_w^2 + V_\infty^2 + \frac{2V_w V_\infty}{W}\sqrt{W^2 - (T - D)^2}}\right]^{\frac{1}{2}}\right\} \quad . \quad (5)$$

III. Graphical Wind Effect

The same results as the analytical method may be obtained from a graphical method. Using a hodograph* plot, a pilot can quickly see the effect of wind on the aircraft climb angle. A hodograph without wind is shown in Figure 4. Two maximum performance points can be read directly from the graph, namely maximum rate of climb, point A, and maximum climb angle, point B.

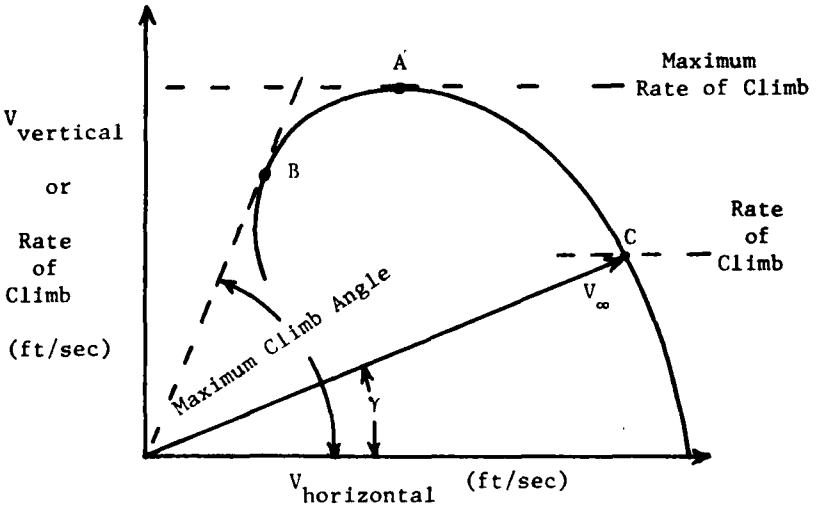

Figure 4. Typical Hodograph

Any other point, for example, C, described by the velocity vector, V_∞, yields a smaller rate of climb and associated climb angle.

The effect of wind can be incorporated into the hodograph by displacing the origin left for a tail wind and right for a head wind, as shown in Figure 5.

*A hodograph is a path made by the extremity of a moving linear velocity vector drawn from an origin. The velocity vector represents the linear velocity of the moving object. The graph's coordinates are the vertical and horizontal components of the velocity vector.

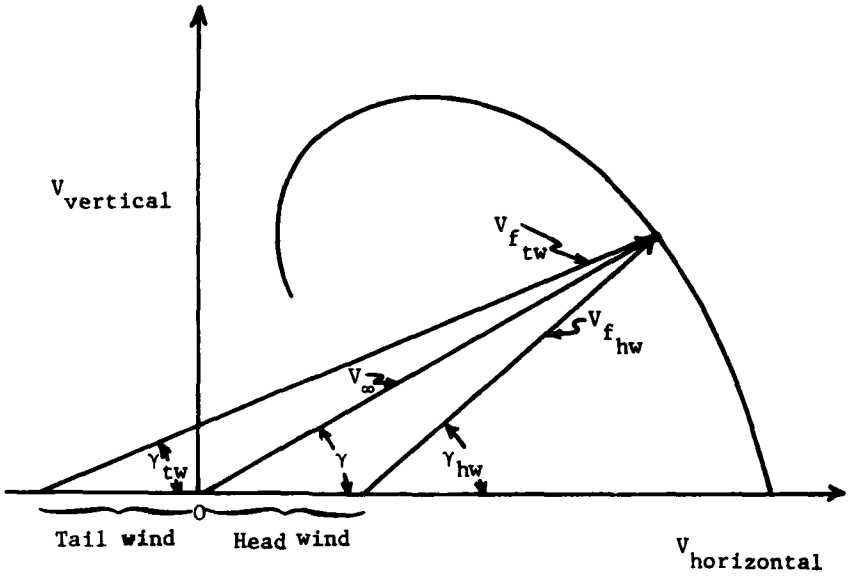

Figure 5. Wind Effect on Climb Angle

Notice that the rate of climb does not change in the presence of winds, which is to be expected. The new climb angle can be quickly and accurately obtained from the plot by the use of a protractor. Further, the hodograph plot predicts the same results as Eqn (4) and (5).

SECTION II

FLUID MECHANICS

A FRACTIONAL DERIVATIVE RELATIONSHIP IN NEWTONIAN FLUIDS

R. L. Bagley* and J. R. Shea, III**

Abstract

This paper presents a relationship between shear stress and fluid velocity in Newtonian viscous fluid. The interesting aspect of the relationship is that the shear stress is expressed as real order, fractional derivative of the velocity profile in the fluid.

Recent work in the dynamics of viscoelastic materials suggests that empirical, stress-strain constitutive relationships can be expressed as relations of fractional order time derivatives of stress fields to fractional order time derivatives of strain fields (Ref. 1 and 2). The primary advantages of these relationships are that they require relatively few empirical constants to model mechanical properties over wide frequency ranges for some materials, and that the mathematical expressions remain linear. The primary disadvantage of these relationships is their empirical nature. Thus, when this approach is used, important physical insights may be overlooked.

The fluid dynamics problem of an initially stationary fluid with a plate at one boundary commencing transverse motion presents a simple example in which a solution to a well-posed equation of motion can be expressed directly in terms of shear stress as a fractional order time derivative of the fluid velocity without resort to empiricism. Figure 1 schematically shows this problem.

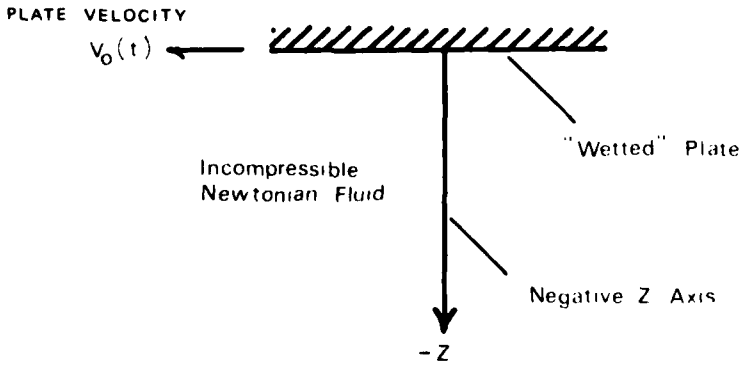

Figure 1. Schematic of Half-Space of Newtonian Fluid Bounded by a "Wetted" Plate

---

*Captain, USAF, Instructor of Engineering Mechanics, DFEM
**Research Staff Member, Institute for Defense Analysis, Arlington, Virginia

Stokes was the first to study this problem in 1851 when he investigated the motion of the fluid resulting from in-plane sinusoidal motion of the plate (Ref. 3). However, the fractional time derivative relationship is applicable for more general motion of the plate and the fluid.

To demonstrate this, we will briefly sketch the derivation of the motion of the viscous fluid which begins with the equation of motion,

$$\rho \frac{\partial v}{\partial t} = \mu \frac{\partial^2 v}{\partial z^2} \quad , \tag{1}$$

where ρ is the fluid density, μ is the viscosity, and v is the velocity profile of the fluid which changes with time, t, and distance from the "wetted" plane, z. By taking the Laplace transform of the equation, we reduce it to an ordinary differential equation,

$$\rho \left[s\, \bar{v}(s,z) - v(o,z) \right] = \mu \frac{d^2\, \bar{v}(s,z)}{dz^2} \quad , \tag{2}$$

where

$$\bar{v}(s,z) = \int_o^\infty e^{-st}\, v(t,z)dt = \mathcal{L}[v(t,z)] \tag{3}$$

and v(o,z) is the initial velocity profile in the fluid. The initial velocity of the fluid is zero, which further simplifies Eqn (2) to

$$\rho\, s\, \bar{v}(s,z) = \mu \frac{d^2\, \bar{v}(s,z)}{dz^2} \quad . \tag{4}$$

The general solution to Eqn (4) is

$$\bar{v}(s,z) = A(s)\, e^{\sqrt{\frac{\rho s}{\mu}}\, z} + B(s)\, e^{-\sqrt{\frac{\rho s}{\mu}}\, z} \quad . \tag{5}$$

Applying the boundary conditions that the velocity of the fluid at the "wetted" plate must match the velocity of the plate and that the velocity of the fluid in the half-space must be bounded produces

$$\bar{v}(s,z) = \bar{v}_o(s)\, e^{\sqrt{\frac{\rho s}{\mu}}\, z} \quad , \tag{6}$$

where $v_o(s)$ is the transform of the motion of the plate.

Having obtained the transform of the velocity profile in the fluid, Eqn (6), we can find the transform of the stress in the fluid, $\bar{\sigma}$ (s, z), using the standard shear stress relationship for the Newtonian fluid,

$$\bar{\sigma}(s,z) = \mu \frac{d\bar{v}(s,z)}{dz} \quad . \tag{7}$$

The transform of the stress is

$$\bar{\sigma}(s,z) = \sqrt{\mu \rho} \ \sqrt{s} \ \bar{v}(s,z) \quad . \tag{8}$$

We can bring this transform back to the time domain by observing that the transform is the product of the transforms of two known functions of time.

$$\bar{\sigma}(s,z) = \sqrt{\mu \rho} \ \frac{1}{\sqrt{s}} \cdot s \ \bar{v}(s,z) \tag{9}$$

$$\bar{\sigma}(s,z) = \sqrt{\mu \rho} \mathcal{L}\left[\frac{1}{\Gamma(1/2)t^{1/2}}\right] \cdot \mathcal{L}\left[\frac{\partial v}{\partial t}\right] \tag{10}$$

Thus, the stress is the convolution of the two functions of time.

$$\sigma(t,z) = \frac{\sqrt{\mu \rho}}{\Gamma(1/2)} \int_0^t \frac{\frac{\partial v}{\partial \tau}(\tau,z)}{(t-\tau)^{1/2}} \, d\tau \tag{11}$$

Since the initial velocity profile, v(o,z), is zero, Eqn (11) is equivalent to

$$\sigma(t,z) = \left[\frac{1}{\Gamma(1/2)} \frac{\partial}{\partial t} \int_0^t \frac{v(\tau,z)}{(t-\tau)^{1/2}} \, d\tau\right] \sqrt{\mu \rho} \quad . \tag{12}$$

The expression in brackets is precisely in the form of a derivative of fractional order* with respect to time, defined as

$$D^{\alpha}[x(t)] = \frac{1}{\Gamma(1-\alpha)} \frac{d}{dt} \int_0^t \frac{x(\tau)}{(t-\tau)^{\alpha}} \, d\tau \quad . \tag{13}$$

In the stress-velocity relationship, Eqn (12), the order of differentiation is seen to be 1/2 and the partial derivative term is present because the convolution integral is a function of t and z. In operator format, Eqn (12) becomes

$$\sigma(t,z) = \sqrt{\mu \rho} \ D^{1/2}_{(t)} \left[v(t,z)\right] \quad , \tag{14}$$

where the subscript, t, in parentheses denotes that the fractional differentiation is with respect to time. The form of this solution is similar to that found by Donaldson (Ref. 5) in presenting general solutions to the diffusion equation using fractional calculus.**

*The fractional derivative is the inverse operation of fraction integration as defined by Riemann and Liouville (Ref. 4).

**The original differential equation of motion, Eqn (1), is in the form of the one-dimensional diffusion equation.

Eqn (14) is, of course, precisely equivalent to the general shear stress expression for a Newtonian fluid,

$$\sigma = \mu \frac{\partial v}{\partial z} \quad ,$$

given the initial condition and boundary conditions of the problem under consideration. Insofar as a viscous fluid may be viewed as a limiting case of a viscoelastic material, it is interesting to observe that viscous fluids spawn a stress-strain rate constitutive relationship containing time derivatives of fractional order without resort to empiricism. This observation suggests that the empirical viscoelastic constitutive relationships, based on fractional differentiation, might not be entirely arbitrary constructions.

References

1. Bagley, R. L. and P. J. Torvik. "A Generalized Derivative for an Elastomer Damper." The Shock and Vibration Bulletin, No. 49, Part 2 (1979), 135-143.

2. Bagley, R. L. Applications of Generalized Derivatives to Viscoelasticity. Ph.D. Dissertation, AFIT/DD/AA/79S-2, Air Force Institute of Technology, 1979.

3. Stokes, G. G. "On the Effect of the Internal Friction of Fluids on the Motion of Pendulums." Cambridge Philosophical Transactions, Vol. 9 (1851), 8.

4. Ross, B. "A Brief History and Exposition of the Fundamental Theory of Fractional Calculus." Lecture Notes in Mathematics. Vol. 457, 1-36. New York: Springer-Verlag, 1975.

5. Donaldson, J. A. "A Family of Integral Representations for the Solution of the Diffusion Equation." Lecture Notes in Mathematics. Vol. 457, 146-150. New York: Springer-Verlag, 1975.

USAFA-TR-80-7

INTENSE LASER-SOLID INTERACTIONS

Philip E. Nielsen* and John P. Jackson**

Abstract

Solid matter responds both thermally and mechanically to intense laser radiation. The type of response, however, depends not only on the intensity of the laser, but also on the atmospheric conditions in which the surface is situated. This paper gives an overview on the physics of combustion and shockwaves produced at a target when irradiated by a laser beam.

I. Introduction

During the 20 years since the laser was first invented, it has undergone rapid development. Originally a tool useful in the study of optics or atomic physics, it has now reached the point where many engineering applications are either envisioned or in being. In many of these engineering applications, such as welding or drilling materials, the role of the laser is to place large amounts of energy on a surface; monochromaticity and coherence, features unique to laser light, are relatively unimportant. In support of such applications, a large body of literature has grown up in an area called "laser effects," having to do with what happens when an intense light source is incident upon a solid surface. The need for work in this area is clear, since in many high-power laser-surface interactions the effects observed differ considerably from those intended. This is particularly true for those interactions which take place in the presence of the atmosphere. Glowing plasmas are often seen to form where the laser strikes the surface, detach from it, and travel in the direction of the light source (Figure 1) (Ref. 1). It is clear in a case like this that most of the available energy is being used to maintain and propagate the plasma, and that little is being deposited on the target. Clearly, such effects must be accounted for in establishing the practicality of various potential laser applications.

The purpose of this article is to discuss the theory of "laser effects," with particular emphasis upon the influence of plasma ignition upon intense laser-solid interactions. Broadly speaking, we find that laser effects fall into two categories, thermal and mechanical. In the former case, what is sought is the heating of a surface, hereafter referred to as the "target," for some specific purpose. This is probably the most obvious of laser effects, and such applications as welding and "drilling" holes are already in industrial use. In the latter case, it is desired to create stresses within the target through the generation of high pressures on its surface. These can result, for example, from the momentum transferred as vaporized target material leaves the surface. In view of the higher power densities required for mechanical effects of this

*Major, USAF, Associate Professor, Dept of Physics, Air Force Institute of Technology, Wright-Patterson AFB, OH 45433
**Captain, USAF, Associate Professor of Physics, DFP

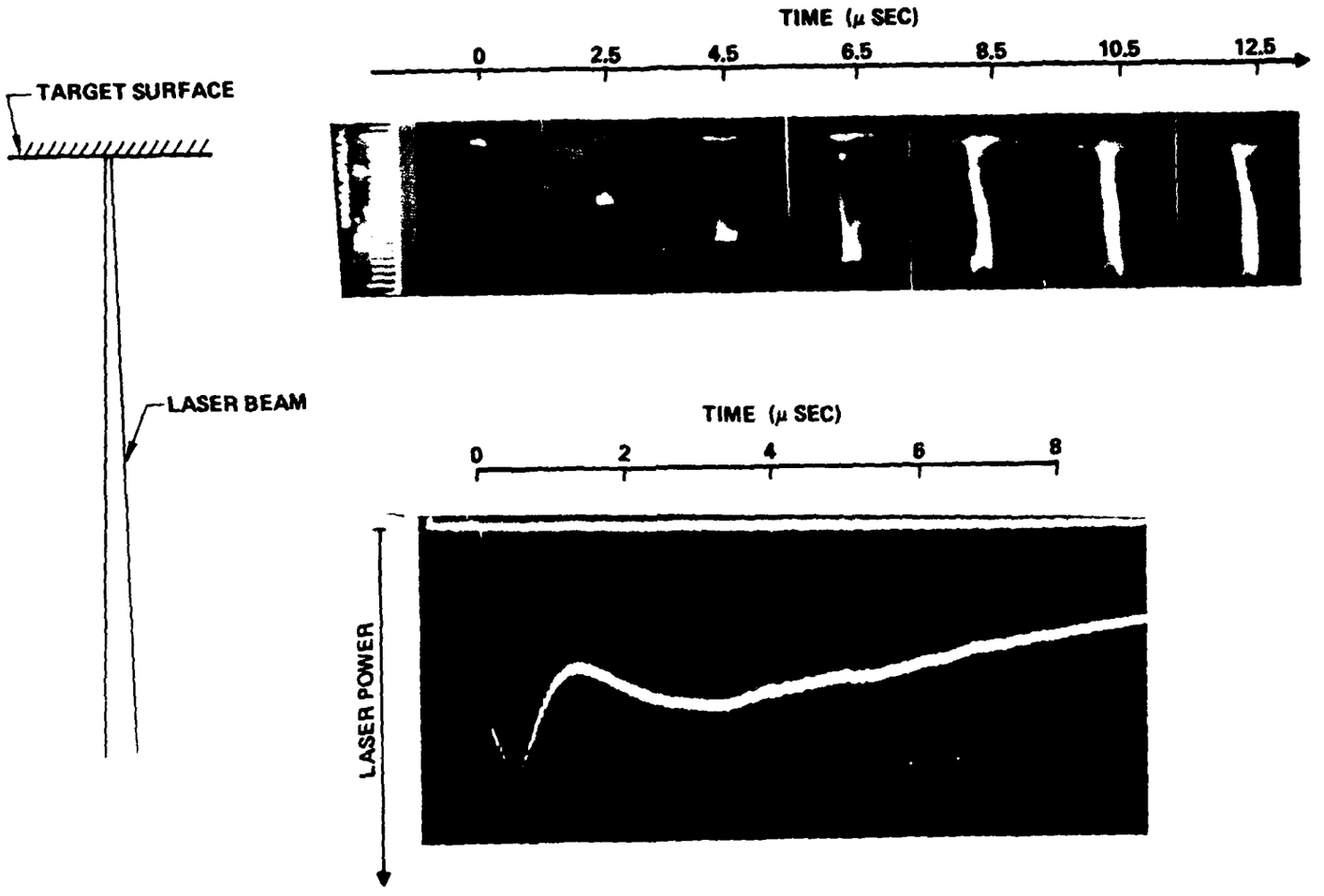

Figure 1. A Traveling Plasma Formed When an Intense Laser Strikes a Solid Surface. Note That as the Laser Power Weakens, the Propagation Velocity of the Plasma Decreases, and the Depth to Which the Light Penetrates Increases. The Initial Velocity is Over Ten Times the Speed of Sound.

type, few practical applications exist at present. Among the most notable of the projected applications is the compression of small pellets of deuterium and tritium in a laser-fusion reactor. It has also been suggested that momentum transfer from a laser-target interaction could be used industrially to shock-harden metals and alloys.

We will discuss first thermal, and then mechanical effects. As both effects are strongly influenced by whether the interaction is in vacuum or air, these two possibilities are considered for each type of effect. We present the measures commonly used to judge the effectiveness of a laser-target interaction, and show that the variety of possible phenomena is so great that no one parameter can adequately characterize them all.

II. Thermal Effects

At laser frequencies, a large fraction (~95%) of the light is reflected from a metallic target and the remainder is deposited within an extremely short penetration depth (10^{-7} - 10^{-8} cm). For a nonmetallic target, the majority of the light is absorbed over a length which can vary over a wide range of values, but which is typically of order 10^{-4} cm. Reflection coefficients and absorption lengths are generally estimated using simple concepts of solid-state physics. For metals, this involves the use of the Drude model, in which the metal is considered to be a gas of free electrons interacting with a background lattice of ions. For insulators, use is made of the energy-band structure of the material in question; while laser light is strongly absorbed at frequencies whose energy connects allowed energy levels of the solid, it is otherwise largely unattenuated. Though this principle is simple and quite adequate for making estimates of laser absorption, difficulty is often encountered in making detailed comparisons between theory and experiment, since real targets are in many ways unlike theoretical ones. In particular, practical surfaces are covered with impurity sites, defect sites, and other sites at which laser light may be more effectively absorbed than by the bulk material. Further, even pure materials may not be adequately treated by simple models.

In view of this difficulty in theoretically characterizing the deposition of energy within a target, it has become common to characterize the thermal response of a target by an experimentally determined "thermal coupling coefficient." This parameter is simply defined as the ratio of laser energy transferred to the target during irradiation to the amount of energy contained in the beam. Thus, the coupling coefficient is a measure of the efficiency by which laser energy is converted into thermal energy in the target, and is used as a "figure of merit" for thermal effects. A low value of the coupling coefficient indicates a poor return for the total energy invested into the beam, whereas a value near unity indicates efficient laser-target coupling.

The coupling coefficient is clearly related to the absorption coefficient of the sample for the laser radiation, but is not exactly the same for a number of reasons.

First, the coupling coefficient is an average quantity evaluated over the entire laser pulse, while the absorption coefficient is in general temperature dependent, and will vary during the interaction. Second, losses of energy from the sample by radiation or conduction may cause the experimentally measured coupling coefficient to depart from the fraction of energy actually absorbed by the sample. Finally, as we shall see later, air plasmas and target vapor formed at the target surface may serve to absorb laser energy and transfer it to the target differently than the surface could itself absorb laser radiation. Thus, the coupling coefficient is an ill-defined quantity, and depends upon the material irradiated, the characteristics of the laser and surrounding environments, and the means by which the energy transferred to the target is measured experimentally. At best, it can only serve as an indication of how effectively various materials respond thermally under various circumstances.

Temperature rise alone is not a significant laser effect for many applications. As the laser intensity and pulse width are increased, it soon becomes energetically possible to melt or vaporize the target material, thus ablating the surface and raising the possibility of sample penetration by the beam. To see at what point such effects become possible, we consider the thermal wave which propagates into the target as laser energy is deposited on its surface (Figure 2).

In a given time interval, thermal energy propagates into the sample a distance which depends on how well the sample conducts heat. If this heated region is to melt or vaporize, the energy density within it must exceed that required to reach the melting or vaporization temperature, respectively. Thus, there is competition between thermal conduction, which in carrying energy away lowers the energy density, and laser energy deposition, which raises it. As a result, there is, for a given laser pulse width, a threshold intensity, illustrated in Figure 3 for one-dimensional heat flow, below which phase changes cannot occur.

Once melting or vaporization become energetically possible, theoretical analysis becomes somewhat difficult. Problems arise because the energy balance within the sample must now account for heats of melt and vaporization, and the degree to which molten material must be vaporized for removal from the target is unclear. If all molten material is immediately removed from the sample, as through gravity or the flushing effect of a cross-wind, then a simple energy balance shows that the sample surface recedes at a velocity proportional to the laser flux as shown in Figure 4. On the other hand, if all molten material is retained and vaporized, the surface recedes at the slower velocity shown in Figure 4. As the heat of vaporization is typically an order of magnitude greater than the heat of fusion or melting, we see from Figure 4 that for the same laser intensity sample penetration would take about ten times longer if all molten material were vaporized than if it were simply removed. An additional

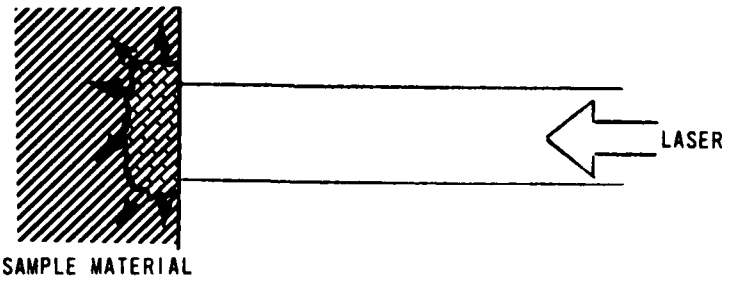

Figure 2. Absorbed Laser Energy is Transported into the Sample by Thermal Conduction. If the Surface is to Melt, Laser Energy Must be Deposited Faster than Thermal Conduction can Carry it Away.

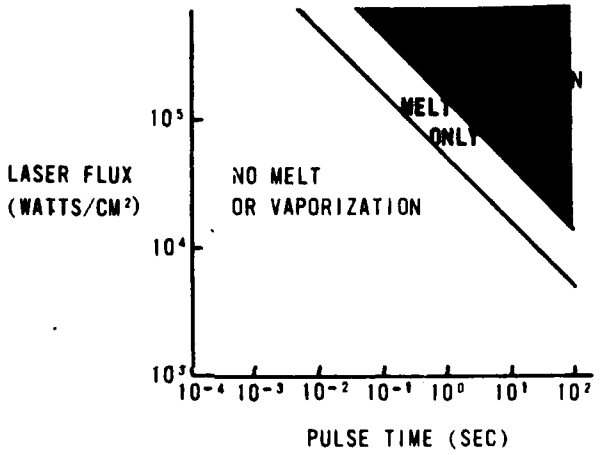

Figure 3. Thresholds for Surface Melting and Vaporization, Assuming One-Dimensional Heat Flow.

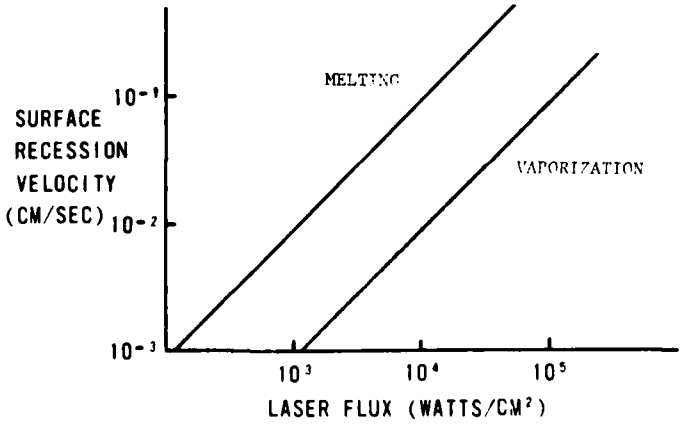

Figure 4. Calculated Surface Recession Velocities as a Function of Laser Intensity for Melting and Vaporization.

complication is caused by the fact that in its molten or vapor state, the target material may absorb laser radiation at a rate much different than in the solid state. Thus, the surface absorptivity affecting the recession velocity may be altered during irradiation.

There exist many theoretical studies on the sensitivity of penetration times to the fraction of molten material retained, and on how that fraction is altered via gravity, expulsion of droplets, and so forth. These are then used in interpreting experimental data. At very high intensities ($>10^4$ watts/cm^2), surface material is generally vaporized before it has a chance to flow or be eliminated by other means. At lower power densities ($<10^3$ watts/cm^2), sample penetration generally occurs by melting.

The considerations outlined above are sufficient to analyze thermal effects when the laser strikes the target in a vacuum, but when air is present, the interaction is complicated by the possibility that plasmas may be ignited in the air above the target. As an example, Figure 5 shows the effective thermal coupling coefficient for 10.6μ laser pulses of width 10^{-5} sec with aluminum (Ref. 2). We see that for the higher energy pulses, where plasmas are seen to form, the coupling is considerably enhanced above the 3% value obtained at lower intensities. The implication is that energy may be more efficiently delivered to a target by a train of high-energy pulses than by a continuously operating low-power laser delivering the same total energy.

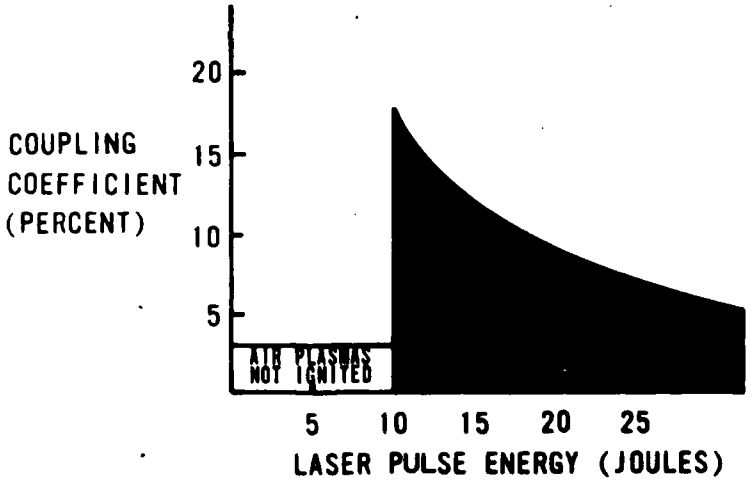

Figure 5. Thermal Coupling Coefficient for 10.6μ, 10^{-5} sec Laser Pulses with Aluminum.

It is generally acknowledged that this phenomenon arises because the plasmas created at the target absorb laser radiation much more efficiently than the metal surface, thus affecting the transfer of energy to the target. The effect of plasma formation on thermal coupling can also be unfavorable, since for long pulse interactions,

the plasma can travel along the path of the laser beam and away from the target as a "Laser Absorption Wave" (LAW), effectively decoupling the laser radiation from the target. Thus, a complete understanding of laser-target interactions in air requires knowledge of the mechanisms for plasma ignition and LAW propagation.

In order to see how a LAW might propagate, we consider a high-temperature region in the air which is being irradiated from one side by a high-intensity laser. If this region has a temperature less than that at which it will be highly ionized (~10,000°K), it will transfer its thermal energy to cooler surrounding regions faster than energy can be supplied by the incident laser radiation, and will cool. However, if the initial temperature is greater than 10,000°K, the air, now a plasma, will be ionized to such a degree that free electrons can very efficiently absorb the laser radiation. The result is that the high-temperature region will be heated fast enough by collisions with energetic electrons to replace the energy lost by cooling. Since laser deposition occurs mainly on the side of the air plasma exposed to the radiation, a nonuniform heating occurs, which results in propagation of the air plasma (or LAW) towards the source of light.

This phenomenon is more easily understood if we consider the above-mentioned processes one at a time, realizing, of course, that all are really acting simultaneously. Shown in Figure 6a is an initial high-temperature plasma. If we assume this region to be created so fast that the air has no time to flow, it has the same density as the rest of the air, and will be at higher than ambient pressure. The resulting pressure gradients will cause the plasma to expand to the new configuration of Figure 6b by doing work against its surroundings, a process which reduces the thermal content of the expanding volume. In addition, as shown in Figure 6c, energy will "leak out" of the volume through heat conduction and radiation. Both of these energy-exchange processes will further decrease the thermal energy of the plasma volume but will, to a certain degree, heat surrounding cooler layers. The processes of expansion and heat transport would continue until all of the initial energy of the plasma were lost, were it not for the replacement of energy losses by the laser. As long as the plasma is at a temperature high enough to remain ionized (>10,000°K), and the laser is sufficiently intense (>10,000 w/cm^2 for a 10.6μ CO_2 laser), the plasma will be able to maintain itself by absorbing laser radiation. As portrayed in Figure 6d, the absorption of laser energy occurs in that part of the plasma which is exposed to the incident laser radiation. Parts behind this region receive comparatively little radiation since they are shielded by the front layer. The result is a replenishment of energy only on the side of the plasma facing the source of light, and therefore a net displacement occurs towards the laser, a direction commonly referred to as "up the beam."

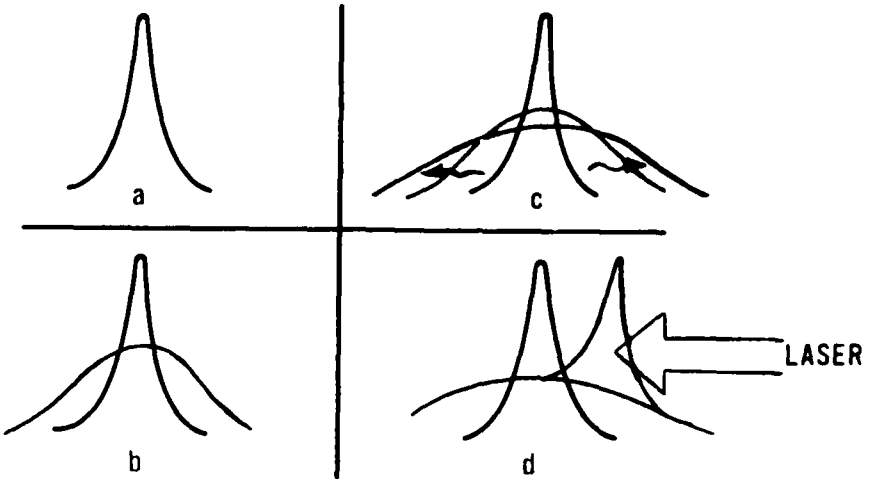

Figure 6. Mechanisms Leading to the Propagation of a Laser Absorption Wave. (a) Initial Temperature Profile Created by Target Vapor, Target Electrons, or Electric Discharge in Beam. (b) Temperature Profile after Hydrodynamic Expansion. (c) Temperature Profile After Energy is Transported by Thermal Conduction and Radiation is Absorbed. The Net Effect is Propagation of the Plasma up the Laser Beam as Discussed in the Text.

As might be expected, the degree to which the pressure in the plasma exceeds the ambient pressure (overpressure) depends upon how much laser energy is absorbed per unit-volume before that energy can be spread out by hydrodynamic expansion. Laser energy is absorbed by the LAW over a distance which for CO_2 laser radiation at 10.6 micron wavelength varies from one cm at one atmosphere to 10^{-4} cm at 10^{2} atmosphere. Over this distance, thermal energy can be built up without a significant change in gas density until expansion waves traveling at the local speed of sound can propagate across the absorption length or the beam radius (whichever is smaller). The pressure, being proportional to the energy per volume, will build above ambient until that time is reached. For CO_2 laser intensities less than about 10^{5} watts/cm^2, the overpressure is considerably less than ambient, while for intensities around 10^{6} watts/cm^2 the overpressure becomes comparable to the ambient pressure. When the laser intensity is around 10^{7} watts/cm^2, enough energy can be absorbed to drive a powerful shock wave whose amplitude is many times atmospheric pressure. Such a wave is called a Laser Supported Detonation (LSD) Wave, whereas those at lower fluxes are called Laser Supported Combustion (LSC) Waves. This terminology arises because of the strong analogy between LAW phenomena and the detonation (explosion) or combustion (burning) of chemical mixtures. Gaseous mixtures which undergo exothermic chemical reactions are normally stable at room temperature, and are ignited only as the temperature approaches some critical value or "flash point." Once the mixture has been ignited at one point, the release of energy associated with the reaction serves to heat surrounding areas to the flash point, and so the reaction proceeds throughout the mixture. If the reaction

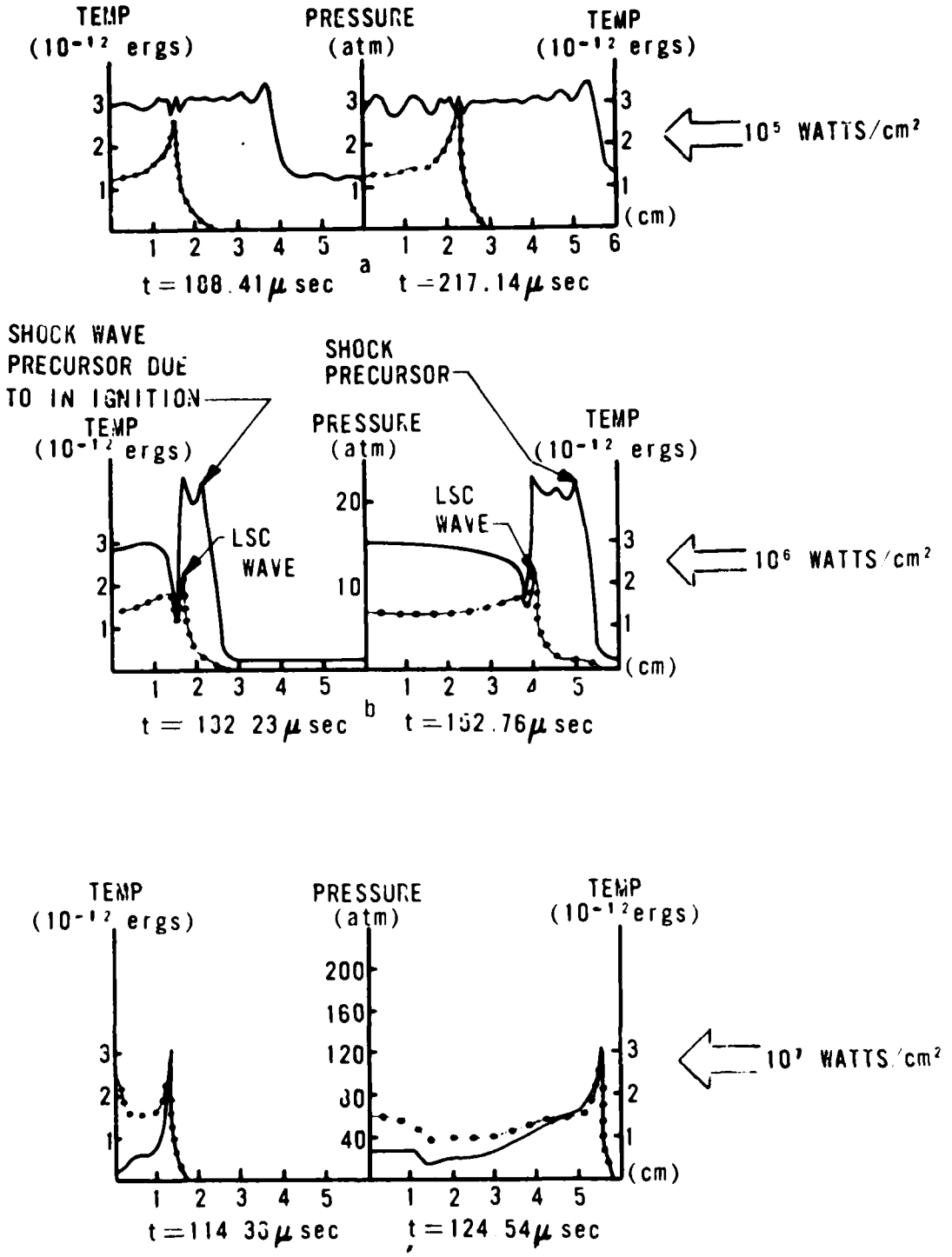

Figure 7. Temperature and Pressure Profiles for LAW's Maintained by Various Laser Intensities. As the Temperature and Pressure Profiles Come Together, the Laser-Supported Combustion Wave Becomes a Laser-Supported Detonation Wave.

proceeds so rapidly that pressures build up, it propagates supersonically as a detonation, in which adjacent areas of the gas are shock-heated to the flash point. If the reaction proceeds more slowly, it propagates subsonically as a combustion, in which thermal conduction heats adjacent areas to the flash point. In the case of a LAW, the mean ionization potential of the air plays the role of the flash point; as the temperature approaches the ionization potential, the air becomes ionized and energy is released into the air as it absorbs the laser radiation. This energy release serves to propagate the plasma either supersonically as an LSD or subsonically as an LSC. In Figure 7, we show temperature and pressure profiles for LAW's maintained by three laser intensities, based on detailed computer calculations made by the authors. The transition from an LSC, in which the high temperature absorption zone lies far behind the overpressure front, to an LSD, in which they are coincident, is clear. In Figure 8, we show the temperature, pressure, and velocity fields from a computer-simulated LAW forming at a target surface and subsequently propagating up the beam.

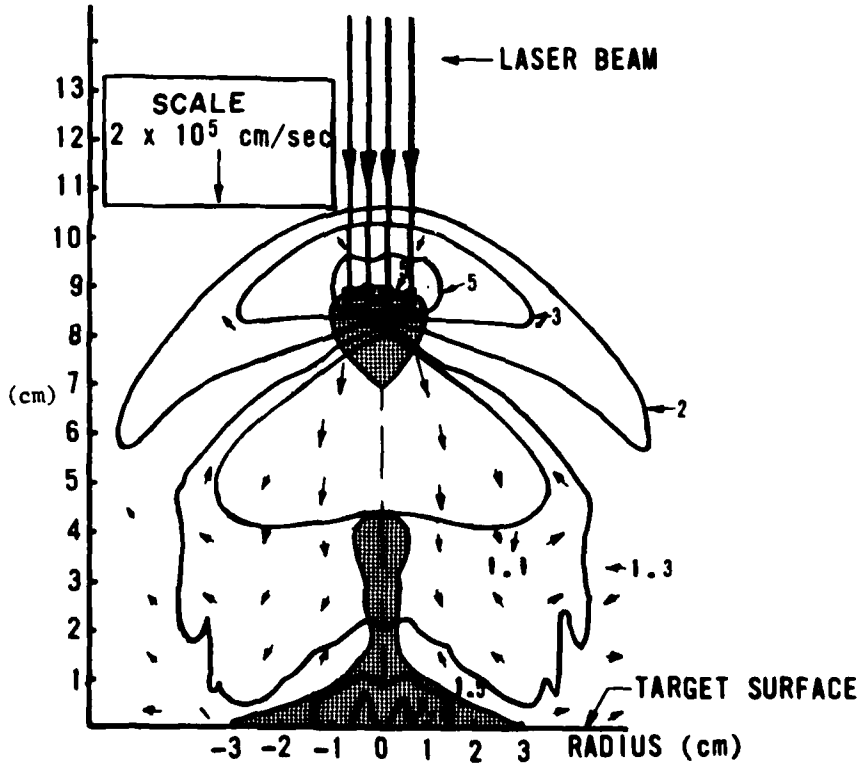

Figure 8. Temperature, Pressure, and Velocity Distributions in a Typical LAW. Lines Show Pressure Contours in Atmospheres, Arrows Show the Flow Field with Arrow Length Proportional to Velocity in Upper Left Corner, and Shaded Area Shows Region Where the Temperature Exceeds 8000°K. The Laser Intensity is 10^6 W/cm^2 at $\lambda = 10.6\mu$.

At the lower intensities for which the primary target response is thermal, the LSC wave is the plasma phenomenon most likely to affect that response. Whenever an LSC wave is ignited, energy transfer to the target may no longer be interpreted solely in terms of beam absorption at the target surface. As it forms, the LSC wave will allow most of the beam to pass through it, but as it develops further (becoming more and more opaque to laser radiation), beam degradation becomes more and more severe. This will tend to decrease the coupling coefficient. But while the LSC wave is near the target (before it has a chance to propagate up the beam), it can transfer some of its thermal energy to the surface via radiation, thermal conduction, and perhaps other mechanisms. This will tend to increase the coupling coefficient. Thus, the thermal response of the target is the result of competing factors whose magnitudes are similar and whose signs differ. Consequently, a theoretical analysis on the "back of an envelope" becomes difficult, if not impossible. Our calculations indicate that thermal conduction plays a more important role than radiative transfer in the "enhanced thermal coupling" seen in Figure 5. This is because the LSC is largely transparent to its own radiation, so that the intensity of radiation from it is proportional to its volume. During its formative stage, the LSC is quite thin and thus radiates very little energy. As the LSC grows up the beam, the energy radiated becomes more substantial, but by this time it has decoupled from the surface, so that the fraction of the radiation which intercepts the target is relatively small.

Another possibility which we have considered is that as an LSC is ignited at a surface, hydrodynamic expansion may drive target vapor back towards the surface, where the vapor may condense back into liquid and solid phases, returning energy to surface and thus "enhancing" the temperature rise and measured coupling coefficient. An interesting point is that to the extent that this mechanism is operable, the enhancement seen in Figure 5 may not mean that the laser is more efficiently absorbed, only that the partitioning of the absorbed energy between bulk temperature rise and small-scale vaporization may be altered.

From all of these considerations, it is clear that the "coupling coefficient" may mean completely different things under different circumstances, even though its value may not differ by much. Accordingly, the thermal effects expected in any given case cannot adequately be predicted by specifying this one parameter alone.

III. Mechanical Effects

Significant mechanical effects begin at the threshold for vaporization, for then the recoil pressure of the blowoff vapor begins to transfer momentum to the surface. As we saw earlier, vaporization occurs when the rate of energy deposition from the laser exceeds the rate at which the energy is carried into the interior of the sample through thermal conduction, so that the heated zone can reach the vaporization temperature

If one is interested in mechanical effects, the thermal coupling coefficient is no longer a useful figure of merit. Indeed, momentum transfer would be maximized if all the energy in the laser pulse were invested in target ejecta, in which case no energy would reside in the target and the "coupling coefficient" of section II would vanish! Consequently the effectiveness of mechanical coupling between a laser and a surface is commonly expressed in terms of the so-called "specific impulse" or ratio of momentum transferred to energy in the laser pulse. This quantity is therefore not dimensionless, and is commonly expressed as dyne-sec/joule, since it tends to have values of order 1-10 when so expressed. Figure 9 shows the specific impulse for titanium as a function of laser intensity for irradiation both in vacuum and in air (Ref. 3). We see that the interaction is altered by the presence of a surrounding atmosphere just as it was in the case of thermal effects. Consequently, as in the previous section, we discuss these two cases separately.

Following the onset of vaporization, the vapor blowoff produces a reaction pressure over the irradiated area. This pressure is roughly proportional to the temperature and density of the evolving vapor. The density of the vapor is in turn determined by the rate with which the laser is eating its way into the target, and is seen from Figure 4 to be roughly linear with the laser intensity. For a finite length laser pulse, the impulse delivered is simply the pressure times the pulse length and the irradiated area, while the beam energy is the intensity multiplied by the same factors. Thus, it would be reasonable to expect that above the threshold for vaporization, the specific impulse will be essentially independent of the laser intensity. That this is not the case, even in a vacuum, is evident from Figure 9.

Since the specific impulse in Figure 9 falls off with increasing intensity, it follows that there are effects not accounted for in the simple analysis above, since higher intensity lasers are less efficient in delivering impulses. The problem is that at the higher intensities the beam is sufficiently powerful to induce breakdown in, and thus ionize, the emerging vapor. Once this occurs, the vapor may absorb a portion of the incoming beam, and a self-regulating absorption rate develops as indicated schematically in Figure 10.

If the vapor absorbs the beam too strongly, the target ablation rate declines. The vapor, which is no longer replenished, disperses and allows increased target interaction. On the other hand, if the vapor is not strongly absorbing, increased deposition of laser energy on the target will enhance the vapor density and thus its absorptivity. Under these circumstances, the vapor density must remain more or less constant as laser intensity increases, while its temperature rises owing to the deposition of beam energy. A simple, one-dimensional fluid-mechanical calculation shows that the vapor temperatures

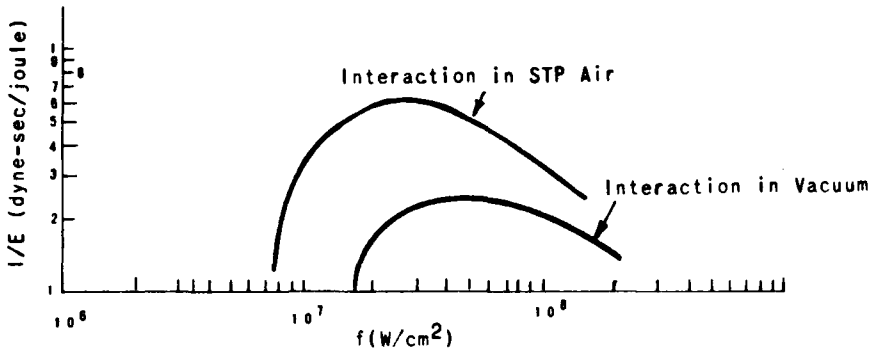

Figure 9. Momentum Transfer to Titanium as a Function of Laser Intensity for a Nd:Glass Laser ($\lambda = 1.06\mu$) with a Pulse Width of Approximately 1.1 sec, Focused to an Area of 0.67 cm^2 on Targets 5/8 in Diameter. Vacuum Data Were Taken at a Background Pressure of 25 microns.

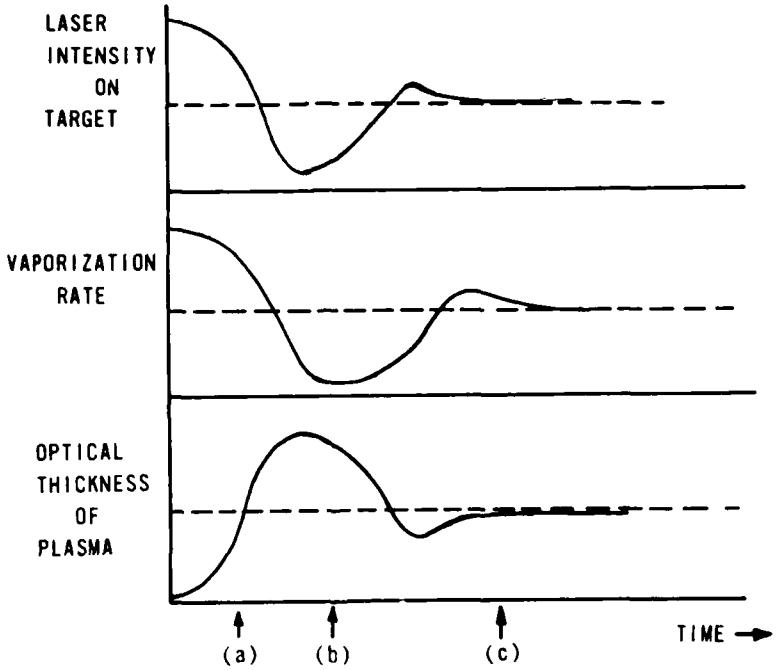

Figure 10. Self-Regulating Vacuum Vaporization in the Presence of a Plasma: (a) If the Plasma is Optically Thin, a Lot of Light Reaches the Surface and Vaporization Augments the Plasma, (b) If the Plasma is Optically Thick, Vaporization Ceases and the Plasma Disperses, (c) Steady State, Where the Ablation Rate Maintains a Constant Plasma Thickness.

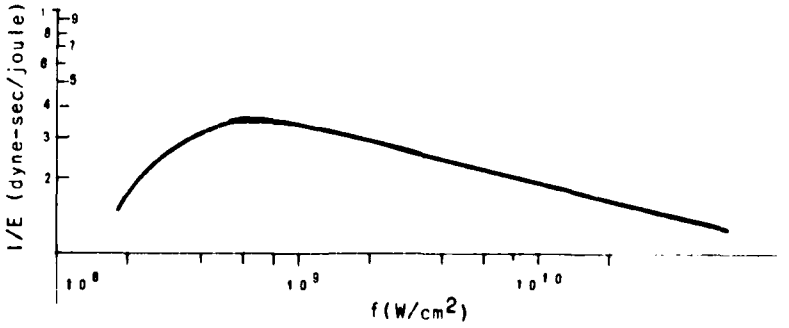

Figure 11. Momentum Transfer to Beryllium as a Function of Laser Intensity for a Ruby Laser ($\lambda = 6943$Å) with a Pulse Width of Approximately 10 nanoseconds, Focused to Areas ranging from 3×10^{-3} to 3×10^{-2} cm^2.

should rise as the 2/3 power of the laser intensity, as should also the pressure on the target. Thus, the specific impulse should vary inversely as the 1/3 power of the laser intensity. This behavior is evident in the experimental data of Figure 11 and serves to confirm our understanding of the physics involved (Ref. 4).

Why should these results be different if the experiment is performed in the atmosphere instead of in a vacuum? The answer lies in the fact that once the vapor becomes an ionized plasma, air breakdown can be initiated and the plasma, no longer confined to regions near the target surface, can propagate up the beam and away from the target as a LAW. No longer will the cessation of target vaporization mean the end of material to sustain the beam-absorbing plasma; the air, as discussed previously, now becomes the medium within which the plasma propagates.

It might at first be supposed that when a LAW forms, vaporization and the transfer of momentum to the target would cease simultaneously, thus leading to specific impulses far below those seen in a vacuum interaction. That this is not the case is clear from Figure 9. Figure 12 reveals the even more interesting fact that with a constant irradiated area in air, the impulse delivered depends upon the area of the sample, while in vacuum it does not (Ref. 3). The latter result is not surprising, in view of the fact that the area over which momentum is transferred in a vacuum interaction is that area which is irradiated, and not that of the target; the former result suggests that the mechanism of impulse delivery in air must differ significantly from that in a vacuum.

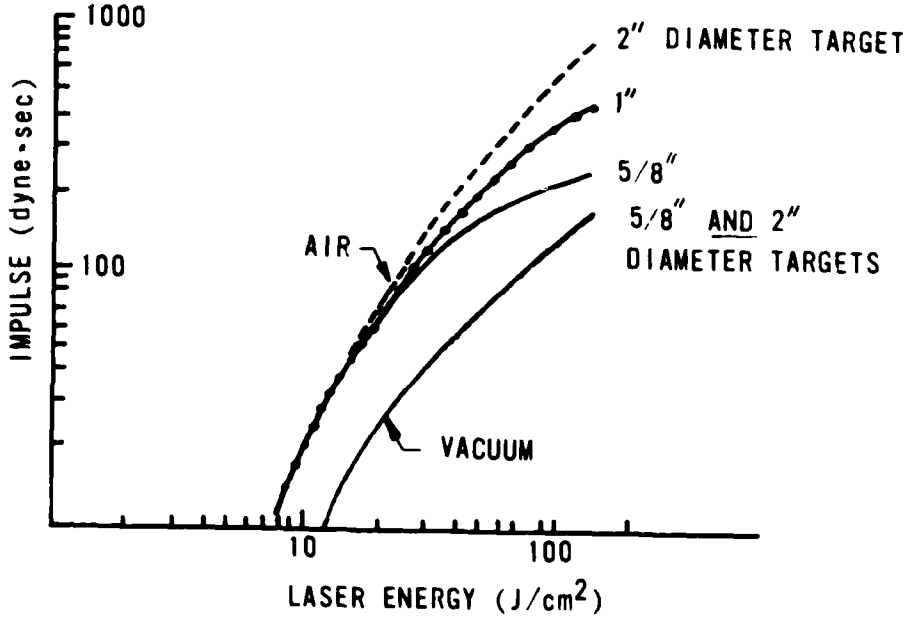

Figure 12. Momentum Transfer to Titanium Targets of Various Sizes for a Nd:Glass Laser ($\lambda = 1.06\,\mu$), 1.1 sec Pulse Width, Irradiated Area is 0.67 cm^2.

The key to understanding Figure 12 lies in recognizing that at the intensities where mechanical interaction is possible, any LAW's formed will propagate as LSD waves. Since an LSD wave propagates at supersonic velocities, it leaves behind hot, high pressure gases which must expand to a pressure balance. As they do so, they exert pressure on the target, delivering impulse to it. It is thus clear why impulse delivered can depend on target size; when the expanding gases reach the target edge they relax around it, and impulse delivery ceases. This sequence of events is illustrated in Figure 13.

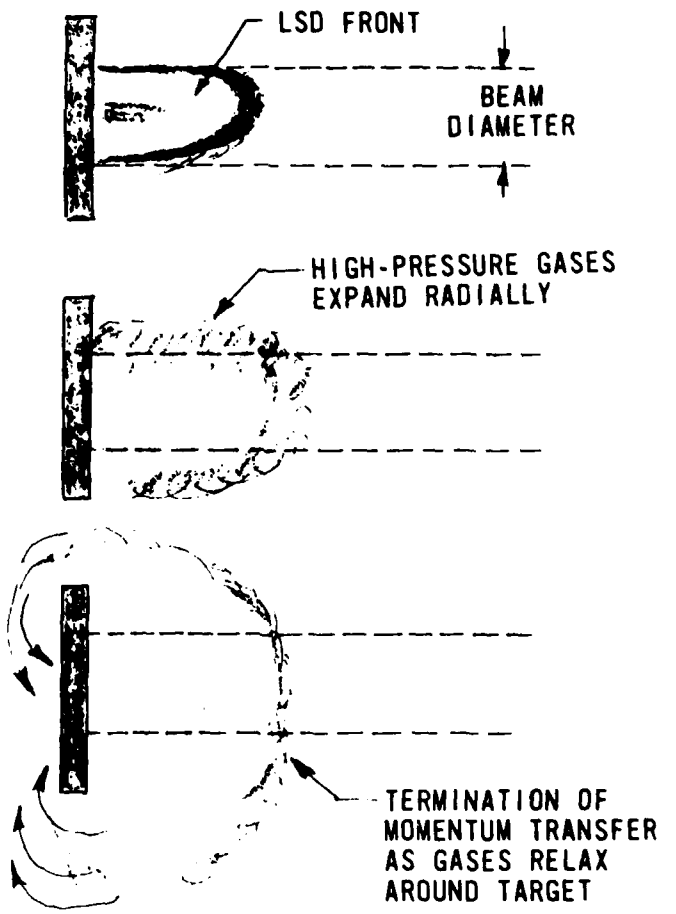

Figure 13. Relaxation of High-Pressure Gases Around Target to Terminate Impulse Delivery.

Owing to the supersonic propagation of the LSD wave up the laser beam, a long, cylindrical column of high energy density is formed from the target surface on very short time scales. This column, whose initial properties are established by the incident laser intensity, evolves in time to a first approximation as a cylindrical "blast wave," a phenomenon well known in gas dynamics. The pressure decreases as the square of the radius of the expanding wave, thus reflecting the redistribution of energy over a

greater and greater area. At the same time, the expansion velocity varies as the square root of the pressure, and hence inversely with the radius. The authors have used this model quite successfully to correlate data on the momentum transferred to targets in the presence of LSD waves (Ref. 5). Figure 14 shows the results of detailed numerical calculations of the fluid flow in a propagating LSD wave. It should be noted that behind the LSD wave front, the flow does indeed become essentially cylindrical in nature. It is thus not surprising that the detailed calculations agree well with the predictions of a simple blast wave analysis. One interesting aspect of this analysis is that, while the impulses delivered to targets in the presence of LSD waves are as large as, and in many cases greater than, those delivered in a vacuum interaction, the physical mechanism is completely different. In the vacuum case, a high impulse results from a large pressure over the relatively small irradiated area. In the air case, it results from a low pressure over a fairly large area.

Of course, the impulse delivered to a surface does not increase without limit as the sample surface area increases. A natural limit is reached when the surface area exceeds the area over which the LSD wave gases must expand to reach pressure balance. For areas beyond this limit, the impulse delivered remains constant.

For very short laser pulses (less than 10^{-7} sec) there is not sufficient time for an LSD wave to form and propagate, and in this case the results for air and vacuum interactions should approach one another.

IV. Conclusions

We have seen that the interaction of a laser with a target and the subsequent production of the various "laser effects" summarized in Figure 15 are an extremely complex affair. Easily measurable "figures of merit" such as the coupling coefficient and specific impulse are difficult to interpret, particularly at higher intensities, and are at best an ambiguous guide to the utility of a laser in accomplishing various tasks. We do believe, however, that the physics necessary to understand laser effects is well in hand, at least for the intensity ranges considered here. Problems arise only when we try to apply what is in principle understood to various cases of interest. Finding the most useful means for employing lasers in practical applications will undoubtedly occupy the attention of many able scientists and engineers for years to come.

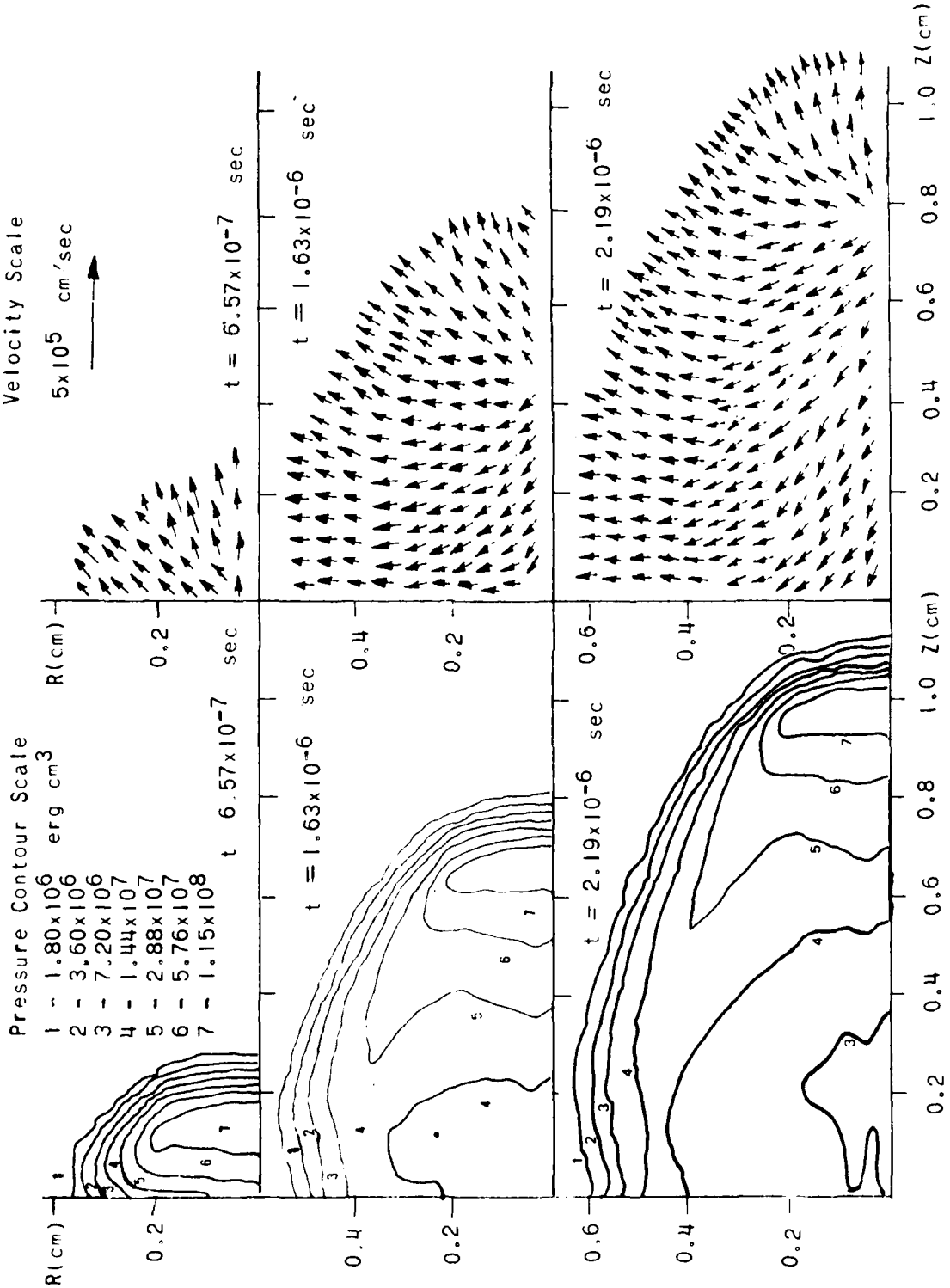

Figure 14. Calculated Pressure Contours and Velocity Fields at Several Times for an LSD Ignited by a 10^7 W/cm^2, 0.22 cm radius Laser Beam Incident on Aluminum.

References

1. Hall, R. B. Private Communication. The Boeing Aerospace Corporation, Seattle, WA.

2. Stamm, M. R. and P. E. Nielsen. "Thermal and Radiative Coupling of a CO_2-Laser Pulse with an Aluminum Target." Bulletin of the American Physical Society, Vol. 19, No. 9 (1974), 855.

3. Rudder, R. R. Private Communication. Air Force Weapons Laboratory, NM 87117.

4. Gregg, D. W. and S. J. Thomas. "Momentum Transfer Produced by Focused Laser Giant Pulse." Journal of Applied Physics, Vol. 37 (June 1966), 2787-2789.

5. Nielsen, P. E. "Hydrodynamic Calculations of Surface Response in the Presence of Laser-Supported Detonation Waves." Journal of Applied Physics, Vol. 46 (October 1975), 4501-4505.

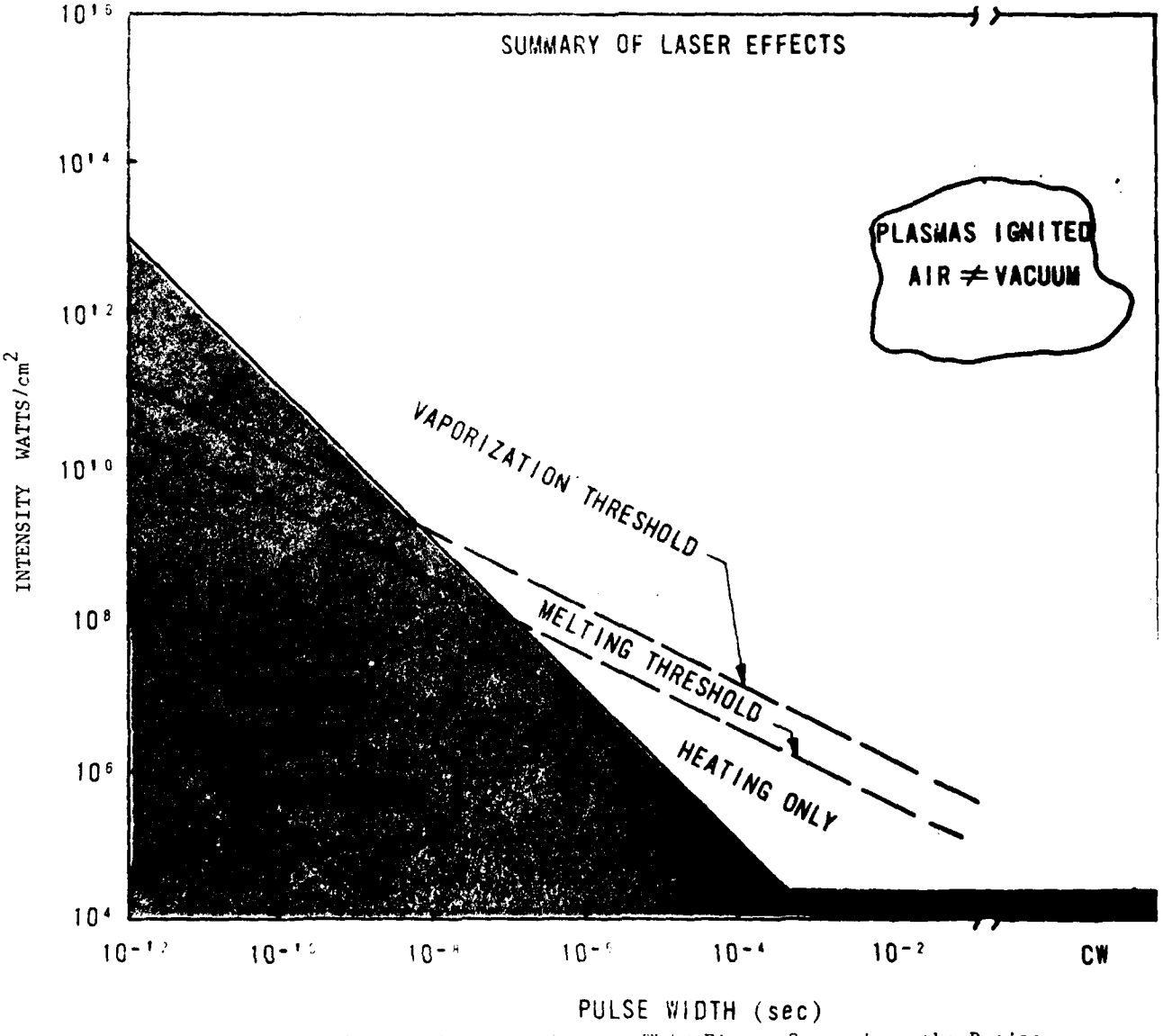

Figure 15. Summary of Laser-Target Effects. This Figure Summarizes the Region Where (for 10.6μ Radiation) Various Effects Occur. The Dashed Lines are Thresholds for Melting and Vaporization, Respectively. The Unshaded Region Shows Where a Plasma May be Ignited in Air and Progagated as a LAW.

SECTION III

THERMODYNAMICS AND HEAT TRANSFER

THE SOLAR RANKINE CYCLE AND THE ENERGY CRISIS

R. C. Oliver* and G. A. DuFresne**

Abstract

This paper discusses the analysis of a Rankine solar system for application to family dwellings and remote site energy production. The analysis considers a system combining a simple inexpensive tracking solar collector with a Rankine cycle electrical generator. Unlike previous analyses of similar systems this analysis includes the use of energy usually considered waste as a source of low-quality energy for space heating. Some discussion of working fluids for Rankine cycles is also included.

I. Introduction

The Rankine cycle has been in use for a number of years and is by far the largest converter of fossil fuel into electrical or mechanical energy. Rankine cycles are also used to convert the heat from a nuclear reaction to usable energy. It is feasible to use solar energy as the heat source and produce mechanical or electrical energy.

Because of the complexity and technically advanced components, the Rankine cycle has not been widely advanced for solar energy conversion. Solar Rankine cycles are technically feasible now; it is the economics which are still in question. The dwindling fossil fuel supplies and the use of energy as a tool of national policy make a solution to the energy crisis imperative. The system proposed herein will not meet all of the nation's needs, but it could release a significant amount of high-quality energy for more optimal uses.

II. The Rankine Cycle

The Rankine cycle is a vapor power system which employs rotating rather than the reciprocating machinery used by its predecessor, the steam engine. It is important to note at the outset that the Rankine cycle is not limited to steam or water, but can employ a wide variety of working fluids. Although numerous modifications to the basic cycle are possible (reheat, regeneration, and economizers, for example), this discussion will be limited to the basic (closed) Rankine cycle. This cycle, depicted in Figure 1, consists of a pump, which pressurizes liquid; a boiler, which adds heat converting the liquid to a vapor; a turbine, which extracts work from the high temperature; high pressure vapor; and a condenser, which reduces the turbine backpressure by removing heat and condensing the working fluid to a liquid. The specific working fluid and its pressure/temperature regime dictate specific performance. The heat source may vary considerably and the working fluid must be usable at reasonable pressures in the temperature range between the boiler and condenser. A number of criteria for working fluids have been proposed (Ref. 1 and 2).

---

*Major, USAF, Associate Professor of Aeronautics, DFAN

**C1C, USAF Academy

Figure 2 indicates the thermodynamic states of the cycle for a general unspecified fluid. The turbine shaft work would be used directly to do work, or, more likely, would be used to generate electricity, putting the energy into the most common denominator.

III. The Solar Rankine Cycle

For the solar Rankine cycle, the energy source is solar insolation and a working fluid must be chosen with workable pressure ranges and meaningful efficiencies. The application considered (either a remote site or a dwelling) requires both heat and electrical energy. Two schemes would be possible, depending on the system efficiencies and the relative importance of heating versus electrical energy. In the first (see Figure 3), the solar energy from the collector is input directly to the boiler of the Rankine system. A portion of this energy is converted to electrical energy while the majority of the input energy must be removed from the condenser as heat. This condenser heat can be used directly for space heating or stored and used as required.

In the second case, the collected energy goes directly into storage and can be used as heat or Rankine cycle input, as required by the user. In this case, the boiler input temperature will be somewhat reduced (transport and storage losses), but the condenser temperature can be lower as this heat would be used for heating or rejected directly to the environment. In Case I we would want to store the condenser heat at as high a temperature as possible in order to use it most efficiently.

If the Rankine cycle is considered only as a generator of electricity and the major effect (providing heat) is neglected, the analysis is incomplete and the energy use far from optimum.

IV. Additional Considerations

The Rankine cycle is a heat engine and as such its efficiency increases with the difference between the boiler and condenser temperature. Our analysis must include a consideration of the type of solar collector. The flat plate collector outlet temperature is about 200°F, the concentrator about 350°F, and the tracking concentrator about 600°F. Each of these collectors has its own efficiency of collection as a function of output temperature. Additionally, the cost increases with the complexity.

One must, of course, consider the combined system. Barber (Ref. 3) analyzed the Rankine cycle using the three temperatures given above and concluded that the flat plate collector is not competitive with the higher temperature units. Barber found that the Rankine cycle power output was approximately 10 percent of the energy incident on the collector for the higher temperature systems. His analysis indicated the depressing result that two thirds of the solar Rankine system cost is attributable to the collector system. This figure is particularly distressing when you consider the Rankine cycle possesses by far the most technically advanced apparatus. Barber's conclusion was

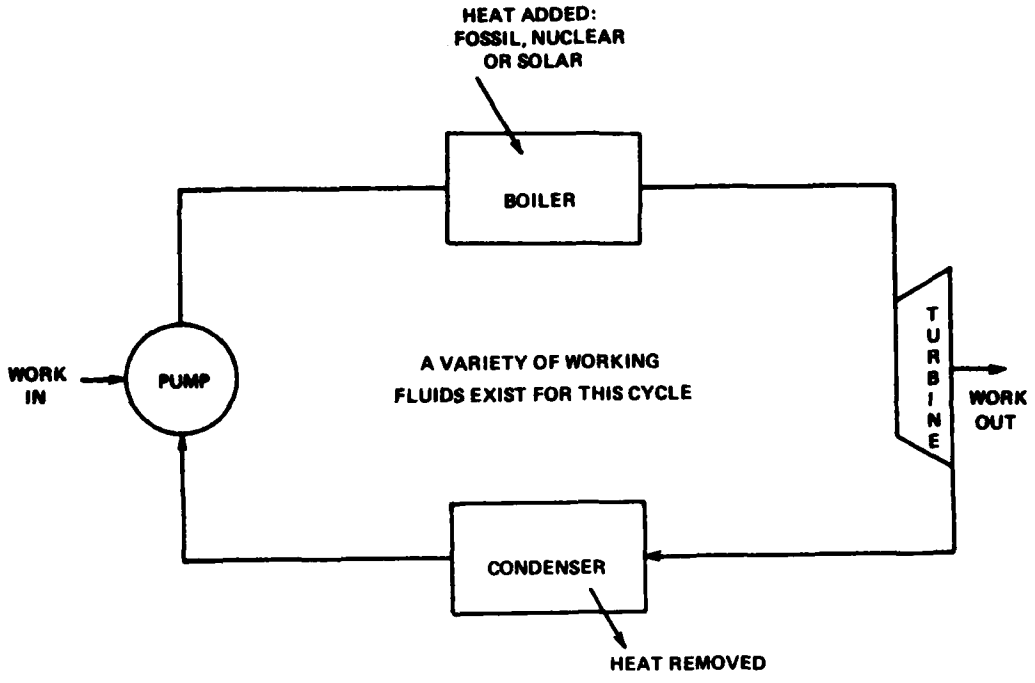

Figure 1. Typical Closed Rankine Cycle

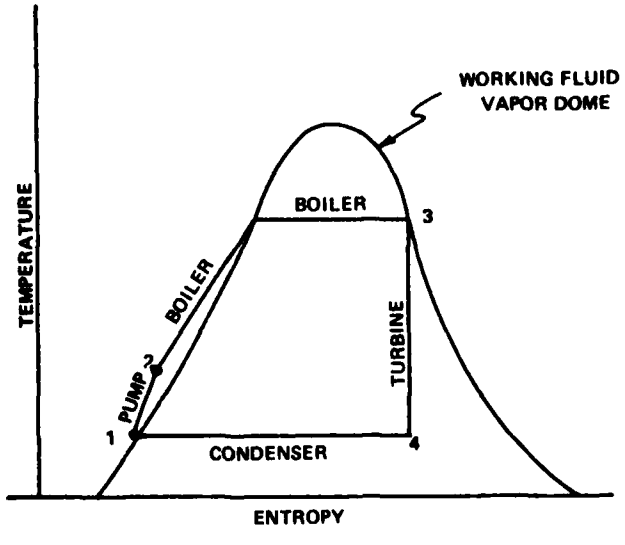

Figure 2. Typical Closed Rankine Cycle Shown on Temperature-Entropy Process Diagram

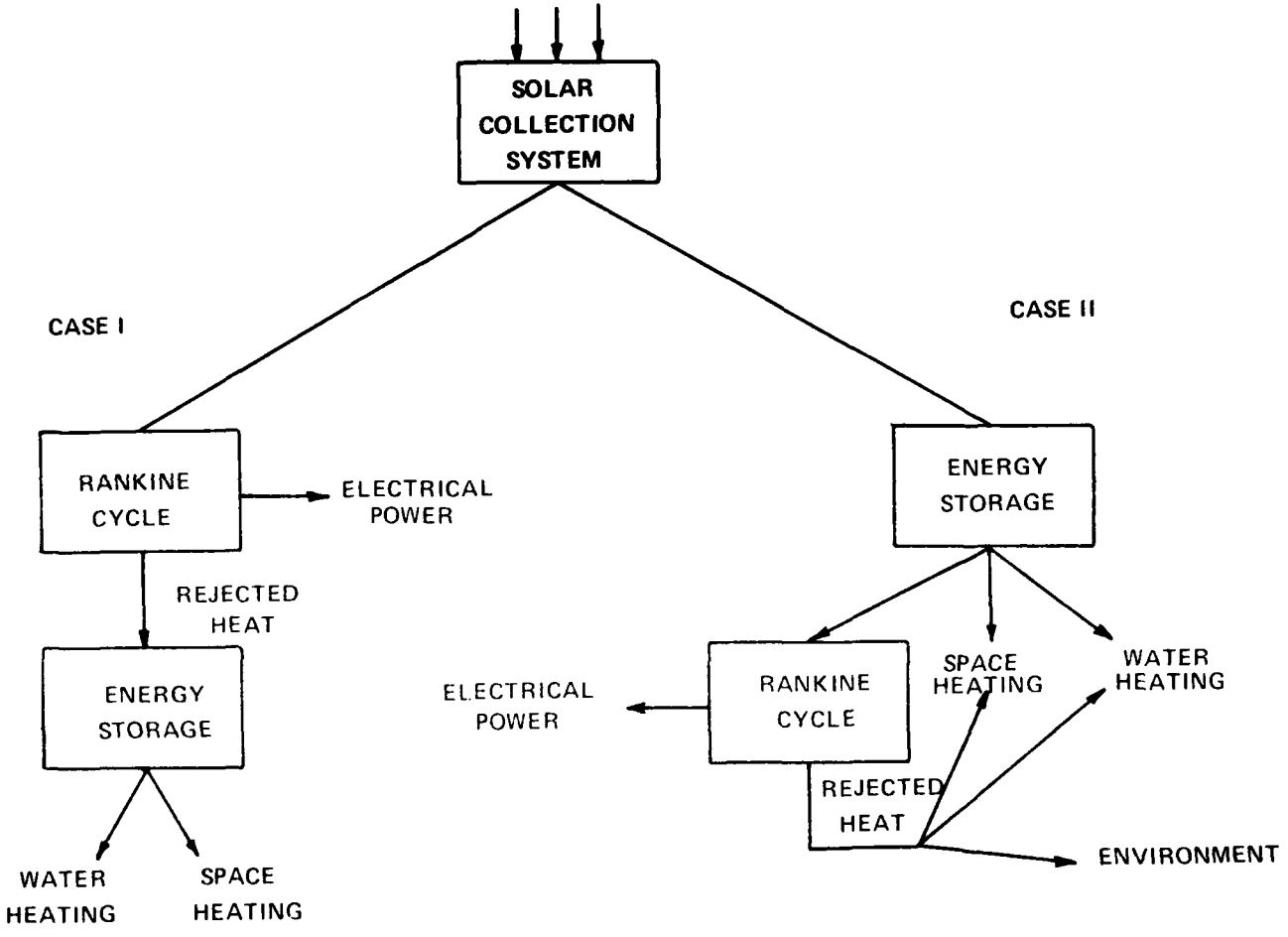

Figure 3. Variations of Combined Solar Heating/Electrical Generation System

that such systems would not be competitive until the cost of electrical power increased about threefold. Note, however, that he did not include any heating benefits which would alter the economic analysis. Also left pending was the thought that a cheaper concentrating or tracking collector was needed. Independent work by Charles Curnutt (Ref. 4) proposes a simple mirror tracking system which one can construct cheaply. Although Curnutt stopped short of applying this to the Rankine cycle, the idea bears investigation.

V. Propose' System

We propose a system for remote site applications composed of a basic Rankine cycle driving an electrical generator. The heat gathered by a tracking collector is input to the boiler either directly or from storage. The collector is a vertical pole which tracks the sun in two directions. Simple electronics (described in the appendix) keep the pole oriented at the sun from sunrise to sunset. Atop the pole is the collector. Horizontal arms extend from the base of the pole supporting arrays of mirror tiles after Curnutt (Ref. 4) These tiles are adjusted so that they reflect the incident sunlight onto the collector. As the entire pole tracks the sun, the mirrors do not need continual adjustment, but reflect the sun's rays to the collector whenever the pole is tracking the sun. The concept is straightforward and much cheaper than tracking collectors referenced by Barber. Pole and mirror array size, however, place an upper limit on the size of the system.

The collector on the top of the pole resembles a boiler and can heat or even vaporize water or any other suitable working fluid. Figure 4 is a sketch of the energy collection system.

The combination of this type of collector with the Rankine cycle provides a system which can heat and power many remote sites. Although the solar collection efficiency is somewhat less than a conventional tracking concentrator, the costs are substantially reduced. We estimate that, rather than 67 percent of the system cost, this type of solar collector would reduce the collector costs to approximately 20 percent of the cost of the Rankine cycle.

Both the substantial reduction in collector costs and the use of the collected energy as space heating in addition to providing electricity result in lower costs and better use of the collected energy.

VI. Fluid Selection

The Rankine cycle working fluid could be heated directly in the solar collector, or a different fluid could be used to gather the solar energy and transport it to a more conventional Rankine cycle boiler. The major fluid concern is the Rankine working fluid.

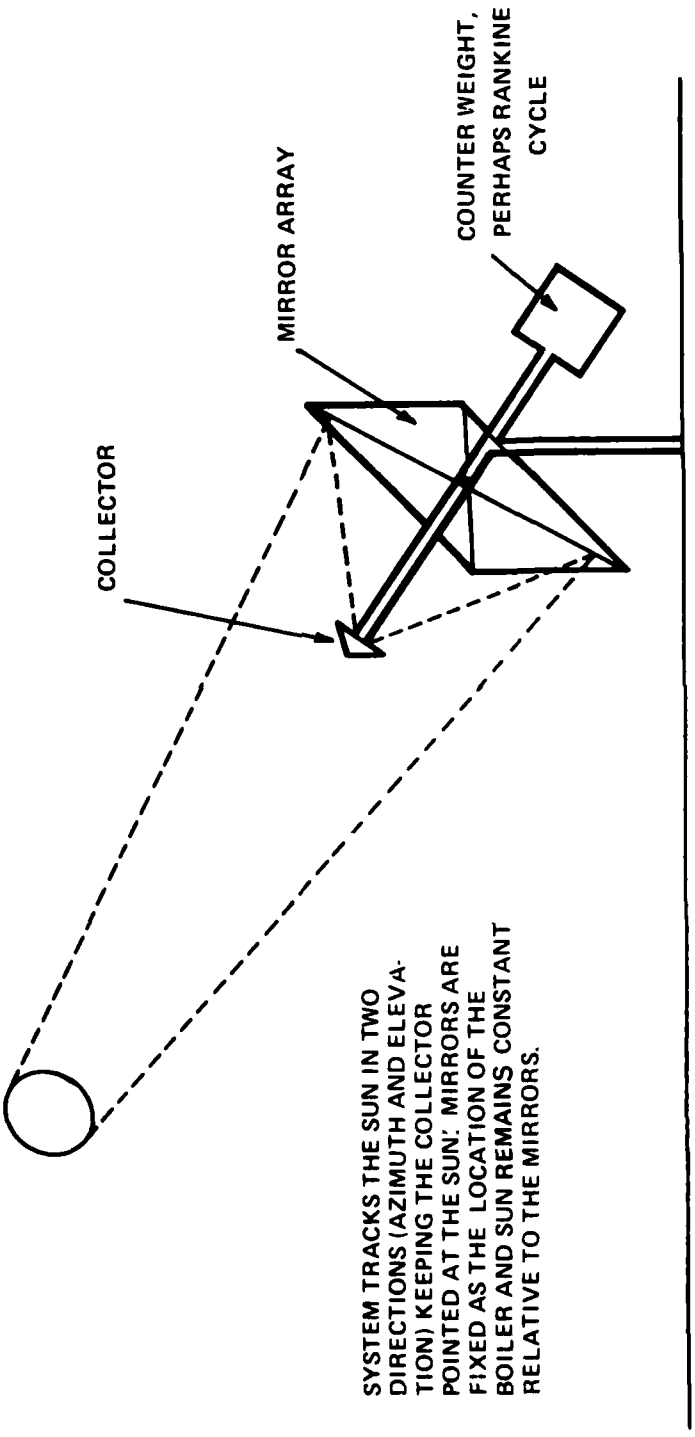

Figure 4. Sketch of Solar Energy Collecting System

A substance that would have reasonable pressure in the boiler and condenser and operate in the temperature range available with no detrimental effect is needed. A search of the ASHRAE Handbook (Ref. 5) indicates that isobutane would operate in the desired range. Several recent papers also considered a similar search and disclosed several additional substances for consideration. Iqbal, et al., suggest cis-2-butane (Ref. 2) while Palmer proposes acetone, Freon 11, methylene chloride, and acetonitile (Ref. 6). All of the substances mentioned are suitable, available, and cheap, and have essentially no detrimental qualities. Once the system design is finalized the temperature can be estimated and one of these substances can be chosen on the basis of best performance.

VII. Residential Application

We estimated the value of the solar energy system described in this paper by using a method illustrated in Kreider and Kreith (Ref. 7). The monthly insolation (tabulated) for Denver, Colorado, was used to calculate the energy collected per month. We then compared this value to the monthly heating requirements and proposed converting the excess energy to electricity. Conservative figures were used throughout. For example, the collector efficiency was set at 30 percent. Further, we considered 75 percent of the incoming radiation to be beam (i.e., direct as opposed to diffuse) and thereby usable in a reflective system. The house considered was sized for a nominal family of three. Table 1 gives some details of the dwelling analyzed.

Table 1

PARAMETERS OF RESIDENCE USED FOR ANALYSIS

Wall Area	2000 ft^2
Roof Area	3000 ft^2
Window Area (single glaze)	1000 ft^2
Standard Construction	
Heat Required (70°F)	36,600 BTU per degree day

Table 2 illustrates the calculations. For the first case, a single 400 ft^2 collector surface provides 41.46 MBTU's for heating and 13.68 MBTU's for converting into electricity.

The cost saved, or the value of the system per year, was computed using the 1975 average residential service cost of 5.05 cents per kw-hr electric (Ref. 8) (this service cost has increased to probably 7 cents per kw-hr). This 5.05 cent service cost yielded a $14.65 per MBTU value. Natural gas is somewhat cheaper, where available, and should be costed accordingly. The energy saved as heat converts directly results in a

savings of $607.60 per year, while the "excess" energy is converted to electrical energy at 20 percent efficiency and results in $40.09 per year, for a total "value" of $647.70 for a 400 ft^2 collector system.

If we expand the system to 1200 ft^2 (3 base units), the value becomes $1,413.57 for heating and $201.90 for the electrical power produced, a total value of $1,615.50 for the year. The values of the insolation used are historical averages, and as such do not match exactly the monthly values used, but over several years no more than a 3 percent error is likely.

We should note that the more electrical power produced, the lower our return per unit area ($1.62 ft^{-2} for 400 ft^2 and $1.35 ft^{-2} for 1200 ft^2). This is due to the energy conversion efficiency of the Rankine cycle. If all collected energy is converted to electrical power, the values would be $161.56 for the 400 ft^2 system and $484.68 for the 1200 ft^2 system. This rate of return is significantly less than if heating is incorporated. A more southerly location would provide greater insolation, greater electrical output, and greater return.

VIII. Summary

The Rankine cycle, long the major energy conversion cycle and, therefore, the most technically advanced, can be used for solar electrical production and heating. When one considers both heating and electrical needs, a solar Rankine system employing the collector described can significantly supplement the energy requirements of a remote site. Such a system also has application to a single-family dwelling in that collected energy could be used for space heating in the winter, electrical power in the summer, and water heating all year long. It is conceivable that a Rankine cycle could be used with existing solar collectors to provide electrical energy whenever the energy is not required for heating. The inclusion of such a system with standard solar collectors would materially change the rate of return and the optimum collector size.

The technology for both the collector and the energy conversion cycle exists today. Although minor developmental problems can be expected, no major obstacles prevent the development of the solar Rankine System. We believe that using the proposed collector will substantially reduce the combined costs for heating and electrical power, approaching commercially available costs. When one considers remote sites, this system appears to excel over other alternate (non-fossil or renewable) energy schemes.

Table 2

ANALYSIS OF DENVER RESIDENTIAL UNIT BASED ON MONTHLY DATA

MONTH	BEAM RADIATION (REF 7) $\frac{BTU}{d\ ft^2}$	DAILY COLLECTED (30%) $\frac{BTU}{d\ ft^2}$	SOLAR MONTHLY TOTAL (MBTU)	UNIT MONTHLY HEATING REQUIREMENTS (WATER & SPACE) (REF 7)	400 ft^2 SOLAR EXCESS OR (DEFICIT)	1200 ft^2 SOLAR EXCESS OR (DEFICIT)
Jan	720	216	2.68	42.32	(39.64)	(34.28)
Feb	953	286	3.20	35.14	(31.94)	(25.54)
Mar	1223	367	4.55	33.35	(28.8)	(24.25)
Apr	1463	439	5.29	21.28	(15.99)	(10.7)
May	1635	490	6.08	11.43	(5.35)	6.81
Jun	1830	549	6.6	3.28	3.32	16.52
Jul	1770	531	6.57	1.11	5.44	18.6
Aug	1650	495	6.14	1.22	4.92	17.2
Sep	1380	414	4.98	5.14	(.16)	9.8
Oct	1058	317	3.93	16.55	(12.62)	(4.76)
Nov	769	230	2.76	30.84	(28.08)	(22.56)
Dec	630	189	2.36	38.77	(36.41)	(31.69)

Solar Summary 400 ft^3 system provides: heating 41.46 MBTU and electrical 13.68 MBTU

1200 ft^3 system provides: heating 96.49 MBTU and electrical 68.93 MBTU

References

1. Reynolds, W. C. and H. C. Perkins. Engineering Thermodynamics. New York: McGraw-Hill, 1977.

2. Iqbal, K. Z., H. H. West, and K. E. Starling. "Hydrocarbon Working Fluid and Operating Conditions Selection for the Conventional Geothermal Binary Cycle." SAE/P-78/75, Society of Automotive Engineers, Inc., 1978.

3. Barber, R. E. "Current Costs of Solar Powered Organic Rankine Cycle Engines." Solar Energy, Vol. 20 (1978), 1-6.

4. Curnutt, C. "Tracking Solar Furnace." Popular Science, October 1978, p. 78.

5. ASHRAE Handbook of Fundamentals. New York: American Society of Heating, Refrigerating, and Air-Conditioning Engineers, Inc., 1976.

6. Palmer, D. A. "Selection of a Rankine Cycle Fluid for Recovery of Work from Heat at a Moderate Temperature." SAE/P-78/75, Society of Automotive Engineers, Inc., 1978.

7. Kreider, J. F. and F. Kreith. Solar Heating and Cooling: Engineering, Practical Design, and Economics. New York: McGraw-Hill, 1975, pp. 116-120.

8. Wind Energy Mission Analysis. Final Report. SAN/1075-1/1, Lockheed-California Co., 1976, pp. 2-24.

Appendix A

DESCRIPTION OF THE CONSTRUCTION AND TESTING OF THE SOLAR TRACKING COMPONENT

The tracking system for the solar collector allows the unit to track the sun during the day, until a west limit switch is closed. The unit then runs in reverse until the east limit switch is opened. The unit then stops and is ready to begin tracking again the next morning with the appearance of the sun.

Figure A-1 shows the circuit configuration of the tracking unit when it is in its normal tracking mode. The route outlined in heavy dashed lines indicates the path of positive current flow. As the sun shines on the photo-transistor, a flow of current across the photo-transistor to the coil of the relay R1 is normally established. R1 is an open relay; therefore, as current flows across the coil the relay is activated and R1 closes allowing current to flow. The current flowing through R1 then reaches the coil of the relay R2, activating it. As seen in the figure, R2 has two relays. These are both normally open and, therefore, both close when the relay is activated. The positive current then flows out of R2 and into the motor as shown.

The second relay of R2 provides a route for negative current flow, or ground, to follow. The heavy black lines in the figure illustrate the negative path. As seen in the figure, the negative flow also passes through one of the relays of R3. This particular relay is normally closed; therefore, since R3 is not activated, the relay stays closed and the negative path is complete.

The circuit will remain in this configuration while sunlight strikes the photo-transistor. In this case the sun engages the motor and causes the unit to track the sun. The actual tracking is on-off, in that the collector will move slightly ahead of the sun position and wait until the sun moves slightly ahead of the collector prior to moving again. The unit will continue tracking until the west limit switch is closed. This indicates that the unit is done tracking for the day and ready to reset for the next morning. Once the west limit switch is closed, the sun is no longer a factor in the circuit's working. The motor will run in reverse until the unit has been reset to the morning position, at which time the east limit switch will open, the motor will disengage, and the unit will be ready to track once again when the sun comes up.

Figure A-2 shows the circuit configuration of the tracking unit when it is in its reverse mode. As the figure shows, the positive and negative contacts to the motor have switched, heavy dashed lines again indicating positive, and heavy solid lines, negative. R1 and R2 are both inactivated for this mode, and therefore, interrupt the circuit. R3, however, does become activated due to the positive current flow reaching its coil. Two of the relays of R3 are normally open (no) while the other two are normally closed (nc).

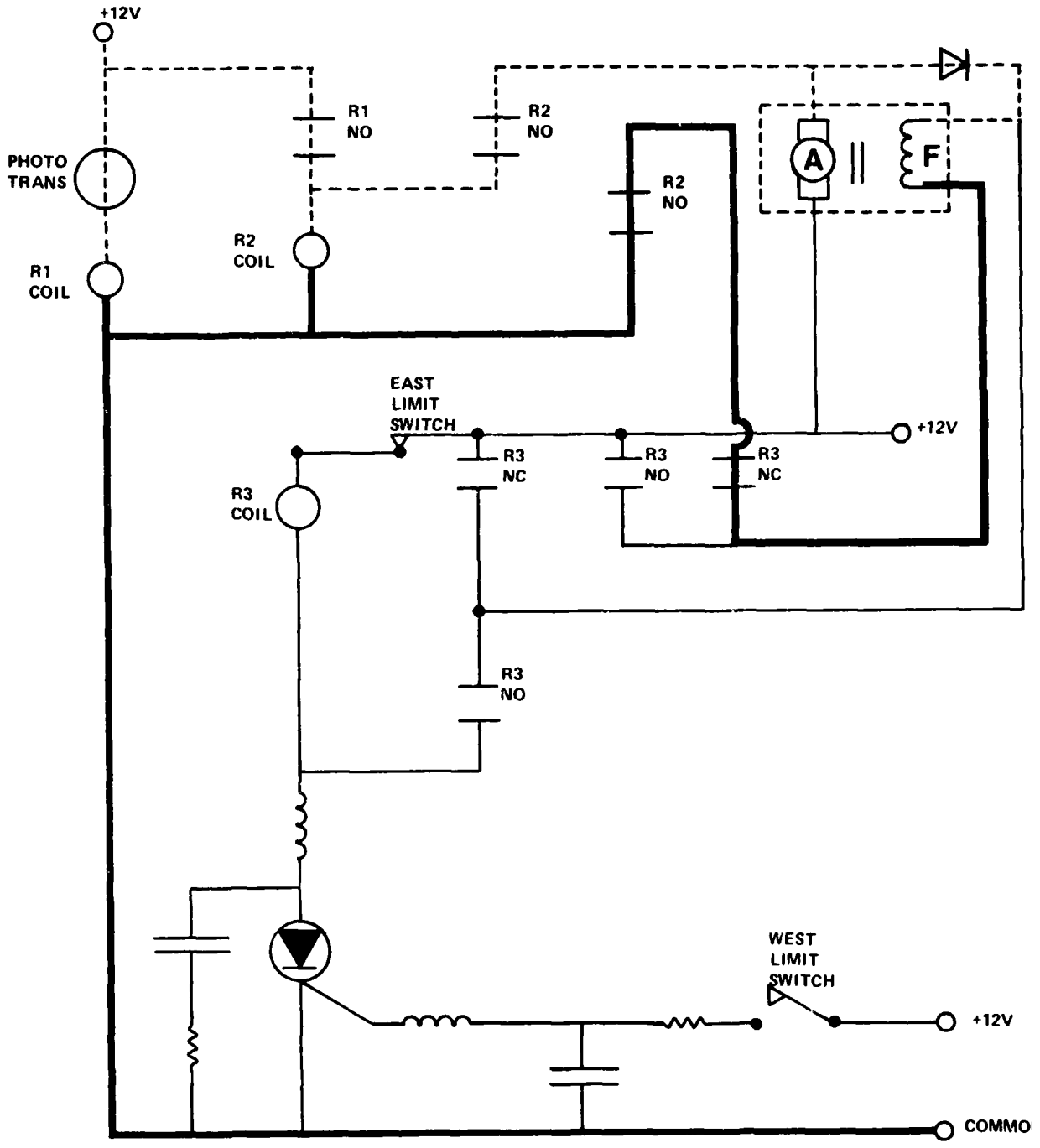

Figure A-1. Solar Tracker Electronic Schematic Illustrating The Sun Tracking (East to West) Mode

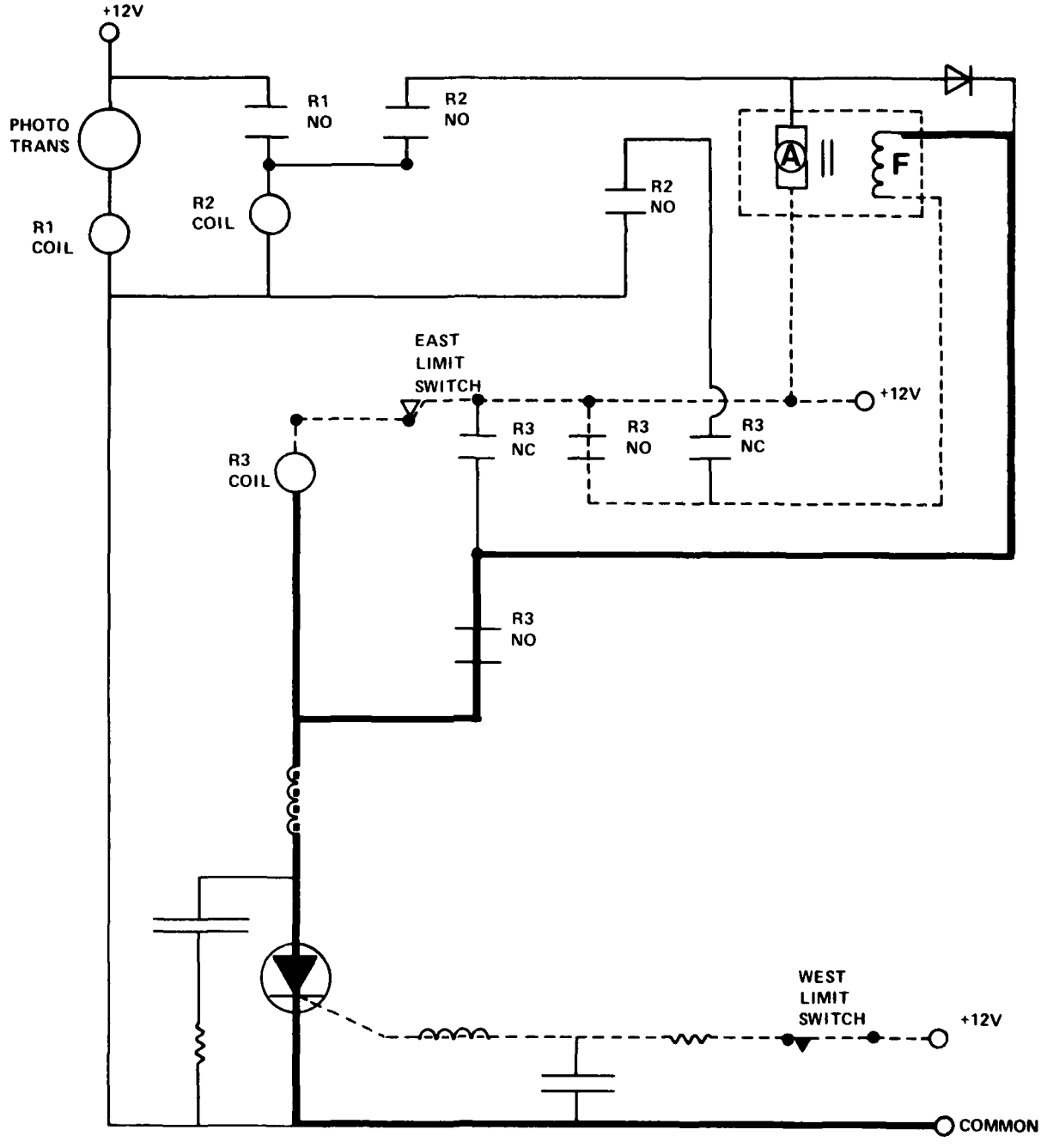

Figure A-2. Solar Tracker Electronic Schematic Illustrating The Reset or End of Day Mode

Therefore, once R3 is activated, the two normally closed relays interrupt the circuit while the other two close and allow the negative and positive flows to and from the motor. These two paths are shown in Figure A-2.

Once the unit has been reset, the east limit switch is opened. This terminates the positive current flow to the motor and, therefore, disengages it. The unit is now ready to assume its initial circuit configuration (Figure A-1) with the appearance of the morning sun.

The basic schematic was provided by Mr. C. Curnutt and was described in general terms in Ref. 4. The list of materials provided herein varies slightly from that provided and several modifications have been made to facilitate remote or manual control of the tracker.

The circuit configurations shown in Figures A-1 and A-2 are for the normal, east to west tracking of the sun; however, the system must also compensate for seasonal changes in the path of the sun. This can be done using the same circuit, with one minor alteration. A second photo-transistor will be added near the armature input as shown in Figure A-3. The west limit switch will also be closed permanently. Therefore, when the sun shines on the original photo-transistor, the motor will run in its normal fashion, but when the sun shines on the added photo-transistor, the motor will run in reverse. This new circuit will drive a motor in addition to the one previously mentioned. This will allow the system to track in both directions (east-west and north-south).

Vital to the operation of the tracking system is the placement of the photo-transistors. They must be situated such that no sunlight will reach them when the sun is directly overhead. Any deviations of the sun from this overhead position, however, must cause the proper correction by stimulating one or more of the photo-transistors. The proposed configuration for the three photo-transistors is shown in Figure A-4.

The shaded rectangle in the figure represents a shading device to be placed above the transistors. When the sun is directly overhead, nothing will happen. However, as the sun deviates, one or more photo-transistors will be illuminated and activated, causing the necessary motor to activate, centering the system.

Manual switches will also be incorporated into the tracking system. For the east-west circuit, switches will be wired across the photo-transistor and the west limit switch. Therefore, when the transistor switch is closed, the system will move toward the west; if the other switch is closed, the system will move toward the east.

For the north-south circuit, switches will be placed across both photo-transistors. Therefore, when one switch is closed, the system will move north; when the other switch is closed, the system will move south.

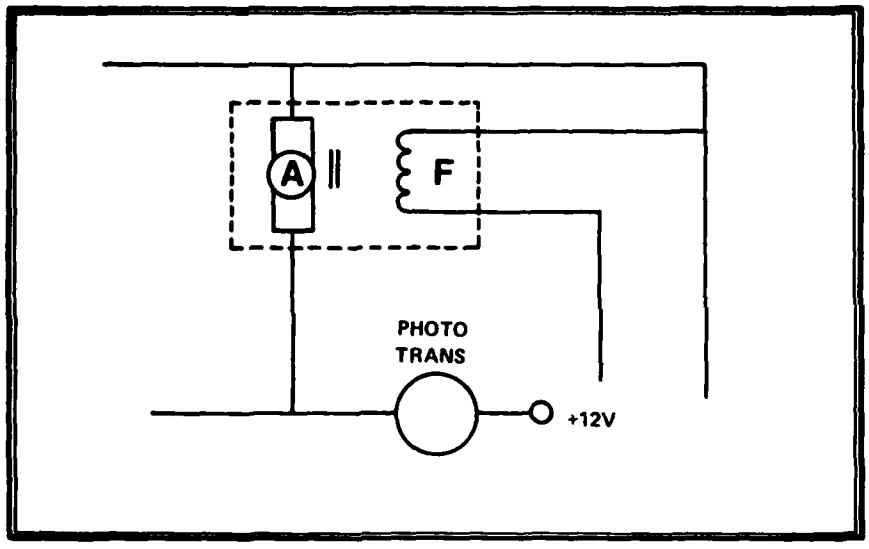

Figure A-3. Electronic Schematic Illustrating Placement of Additional Photo-Transistor For North-South Tracking

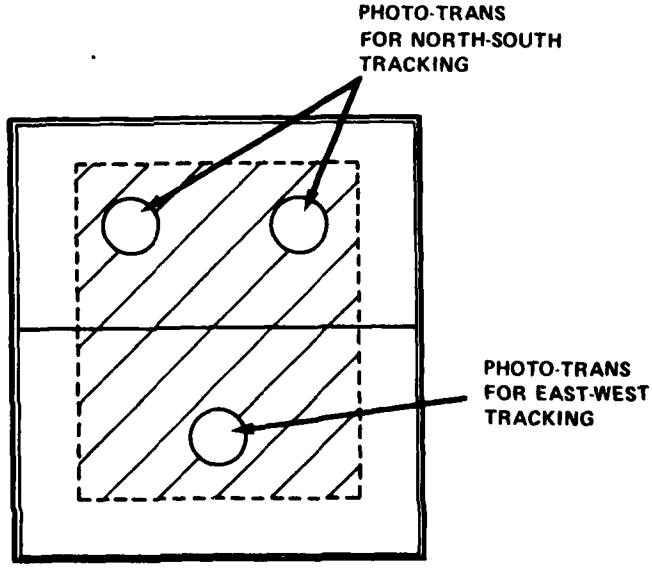

Figure A-4. Illustration of Photo-Transistor Placement For East-West and North-South Tracking

TESTING

The tracking circuit was tested in both its normal and reverse modes. In testing the normal, sun-driven mode, we by-passed the photo-transistor and input the 12 volts directly to the relay R1 to simulate the situation in which the sun would be shining directly on the photo-transistor, allowing the 12 volts to reach the relay R1. The outputs that would be applied to the field and armature of the motor were then tested and found to be 12 volts each, as desired. Thus, the tracking circuit operated correctly in the normal mode of operation.

The reverse mode was next tested. This mode was simulated by applying the 12 volts directly to the west limit switch (with the switch closed) and also to the armature input, as shown in Figure A-2. Again, the outputs from the circuit were tested, and the 12 volts were found to be entering the field and armature in the opposite direction, indicating that the motor would run in reverse for this configuration. Thus, the tracking circuit operated successfully in both modes and can now be applied to the actual motor.

Table A-1

COMPONENT COSTS

(2)	12 VDC DPDT Plug-In Relay	$5.49	
	SPDT Mini Relay	2.99	
(2)	100 uH RF Choke	.99	
(2)	.1 uF PC Capacitor	.79	(pair)
(2)	Subminiature Lever Switch	1.39	
	Silicon Photo-Transistor	.89	
	400 Volt SCR	1.19	
COST		$22.39	

The total cost for all electronic parts used in the tracking circuit is $22.39. Table A-1 shows the itemized component costs. This figure is based on current Radio Shack prices. Two entire tracking circuits will be needed for the final tracking system, resulting in an overall cost of $44.78.

SECTION IV

INSTRUMENTATION AND HARDWARE

CALIBRATED AIRSPEED AND THE "F" FACTOR

Fred H. Porter, III* and Roger D. Hartman**

Abstract

This paper presents the basis for the "F" factor used to convert calibrated airspeed to equivalent airspeed, mentioning the documents that define these quantities. The results of the development appear in functional, tabular, and graphic forms. The equations are in sufficient detail for programming the computation of the "F" factor.

I. Introduction

Many pilots and navigators have used the "F" factor to convert calibrated airspeed to equivalent airspeed in the "ICET" method of airspeed computation. The "F" factor is equally useful for evaluating the dynamic pressure and aerodynamic forces on an aircraft when the calibrated airspeed is known. Perhaps the following discussion will provide some insight into the source and proper use of these quantities.

II. Calibrated Airspeed

Calibrated airspeed, V_c, is a definition. It is related to differential pressure, q_c, according to Eqns (1) and (2). Differential pressure is further defined as the difference between measured total pressure and ambient pressure, $P_t' - P_a$. For $V_c \leq a_{sl}$

$$q_c = P_{a_{sl}} \left[\left(1 + 0.2 \left(\frac{V_c}{a_{sl}} \right)^2 \right)^{7/2} - 1 \right] \tag{1}$$

and for $V_c > a_{sl}$

$$q_c = P_{a_{sl}} \left[\frac{166.92158 \left(\frac{V_c}{a_{sl}} \right)^7}{\left(7 \left(\frac{V_c}{a_{sl}} \right)^2 - 1 \right)^{5/2}} - 1 \right] \tag{2}$$

The sensed locations of P_t' and P_a appear in the following schematic of an ideal aircraft pitot-static system.

---

*Lt Col, USAF, Assistant Professor of Aeronautics, DFAN
**Captain, USAF, Assistant Professor of Aeronautics, DFAN

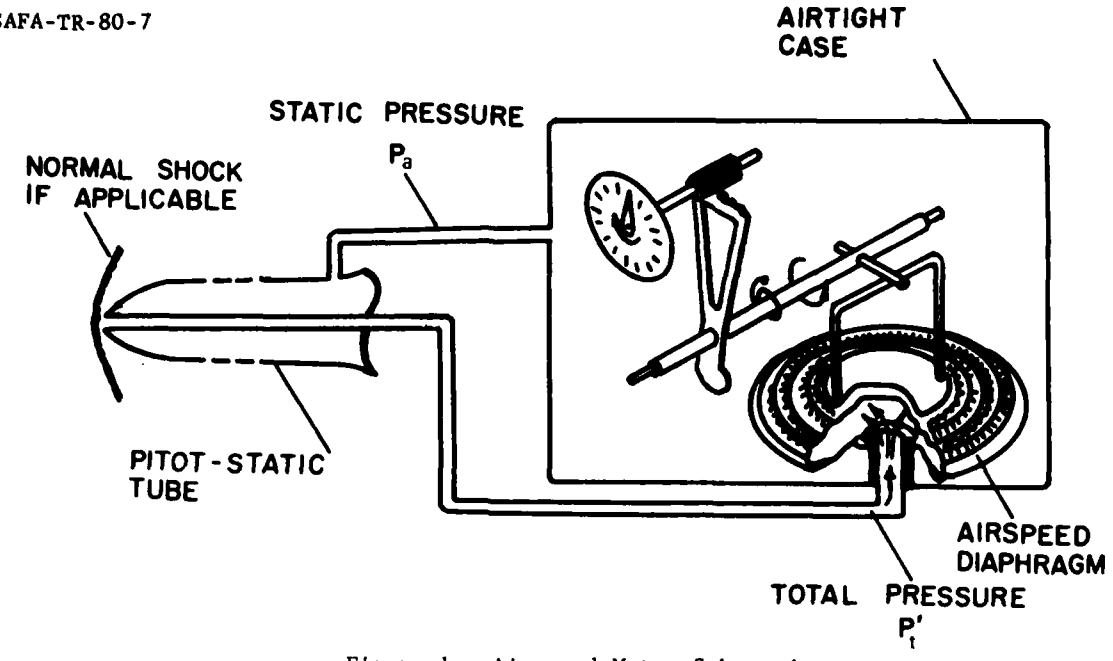

Figure 1. Airspeed Meter Schematic

NASA Technical Note D-822 (Ref. 1) defines calibrated airspeed, and MIL-STD-1524A (Ref. 2) repeats the definition. The relationship between q_c and V_c appears in tabular form such that, given a differential pressure, one can determine a certain airspeed. Instrument manufacturers build airspeed indicators that follow this rule. Important features are

a. The instrument is simple and reliable, and instrument error is typically less than 0.5 knots.

b. Calibrated airspeed is very close to equivalent airspeed in the critical phases of flight.

c. The calibrated airspeed indicator has no way of sensing whether there is a normal shockwave in front of the pitot tube or not. It simply switches from the subsonic rule to the supersonic rule when the needle passes 661.5 knots (the sea level standard day speed of sound).

III. Equivalent Airspeed

Equivalent airspeed is also a definition. It is defined in terms of dynamic pressure, q.

$$q = \tfrac{1}{2}\rho V^2 \tag{3}$$

Equivalent airspeed, V_e, is the speed that would be required to generate the same dynamic pressure if the standard sea level value of density were substituted into Eqn (3).

$$q = \tfrac{1}{2}\rho_{sl} V_e^2$$

Solving for V_e yields

$$V_e = \sqrt{\frac{2q}{\rho_{sl}}} \quad , \tag{4}$$

which illustrates that equivalent airspeed depends only on dynamic pressure. It is a complete indication of aerodynamic loading.

Another formulation of dynamic pressure includes Mach number:

$$q = \tfrac{1}{2} \gamma P_a M^2 \quad . \tag{5}$$

Eqns (4) and (5) can be combined to produce equivalent airspeed at any Mach number, subsonic or supersonic:

$$V_e = \sqrt{\frac{\gamma P_a}{\rho_{sl}}} M \quad . \tag{6}$$

Eqn (6) holds at any Mach number.

Mach number can be expressed using Bernoulli's equation for compressible flow, and in the subsonic case we see that equivalent airspeed depends only on measured total pressure and ambient pressure, since P_t' is free stream total pressure.

$$V_e = \sqrt{\frac{\gamma P_a}{\rho_{sl}}} \sqrt{5\left[\left(\frac{P_t' - P_a}{P_a} + 1\right)^{2/7} - 1\right]} \quad . \tag{7}$$

Clearly a reliable mechanical instrument could not be built to follow this rule, since ambient pressure inputs would be required in three separate places. The supersonic case, which includes the factor for total pressure recovery behind a normal shock, is even worse.

By substituting standard sea level pressure into Eqn (7) in two places, we arrive at the definition of calibrated airspeed for $V_c \leq a_{sl}$, the inverse of Eqn (1).

$$V_c = a_{sl} \sqrt{5\left[\left(\frac{P_t' - P_a}{P_{a_{sl}}} + 1\right)^{2/7} - 1\right]} \tag{8}$$

IV. "F" Factor

The "F" factor is the ratio of equivalent airspeed to calibrated airspeed.

$$F = \frac{V_e}{V_c} \tag{9}$$

From Eqn (6) one might think that the computation of the "F" factor would be straightforward, but it is not. One must first determine whether there is a normal shock in front of the pitot tube, then one may select the appropriate equation to calculate Mach number. (Figure 1 illustrates this problem.) For $M \leq 1.0$,

$$M = \sqrt{5\left[\left(\frac{P_t' - P_a}{P_a} + 1\right)^{2/7} - 1\right]} \quad ; \tag{10}$$

for $M > 1.0$,

$$M = \sqrt{0.7766628\left(\frac{P_t' - P_a}{P_a} + 1\right)\left(1 - \frac{1}{7M^2}\right)^{5/2}} \quad . \tag{11}$$

Notice that in the supersonic case, Mach number is a function of itself and the equation can be solved only by iteration. This method is not practical for hand calculation.

A simple test can determine if there is a normal shock in front of the pitot boom. If one sets Mach number to 1.0 and solves Eqn (10) for the ratio of differential pressure to ambient pressure, then

$$\frac{q_c}{P_a} = \frac{P_t' - P_a}{P_a} = 1.2^{3.5} - 1 = 0.89293 \quad . \tag{12}$$

If the ratio exceeds the value in Eqn (12), use the supersonic equation to calculate Mach number.

Finally, from Eqn (6),

$$F = \frac{\sqrt{\frac{\gamma P_a}{\rho_{sl}}}}{V_c} M \quad , \tag{13}$$

which shows that the "F" factor depends only on measured total pressure and ambient pressure; however, the situation must be treated for the presence of a normal shock.

The relationship between ambient pressure, P_a, and pressure altitude is specified in the U.S. Standard Atmosphere, 1962 (Ref. 3). For altitude at or below the tropopause (36,089 ft),

$$P_a = P_{a_{sl}}\left(1 - 6.8756 \times 10^{-6} H_c\right)^{5.2559} \quad , \tag{14}$$

and for altitudes above the tropopause,

$$P_a = P_{a_{sl}}\left[0.223361\, e^{4.80635 \times 10^{-5}\,(36089 - H_c)}\right] .$$

These equations are correct for pressure altitude in feet and ambient pressure in lbs/ft^2.

V. Finding the "F" Factor

It is handy for aircrews to have a single table relating airspeed to "F" factor. This table on the USAF-issue air navigation computer is repeated below. The pilot enters with calibrated airspeed and altitude.

Table 1

PILOT'S "F" FACTOR

Press Alt (Feet)	Calibrated Airspeed (Knots)							
	200	250	300	350	400	450	500	550
10,000	1.0	1.0	0.99	0.99	0.98	0.98	0.97	0.97
20,000	0.99	0.98	0.97	0.97	0.96	0.95	0.94	0.93
30,000	0.97	0.96	0.95	0.94	0.92	0.91	0.90	0.89
40,000	0.96	0.94	0.92	0.90	0.88	0.87	0.87	0.86
50,000	0.93	0.90	0.87	0.86	0.84	0.84	0.84	0.84

The solution to this problem can also be shown graphically, eliminating the need for many tables (see Figure 2). Actually this figure is more useful than the table because equivalent and calibrated velocities are related directly, which means one can obtain a calibrated airspeed given an equivalent airspeed or vice versa.

Symbols

a_{sl}	Standard Sea Level Speed of Sound
F	V_e/V_c
H_c	Pressure Altitude
M	Mach Number
P_a	Ambient Atmospheric Pressure
$P_{a_{sl}}$	Standard Sea Level Atmospheric Pressure
P_t'	Measured Total Pressure (Behind Normal Shock if Applicable)
q	Dynamic Pressure
q_c	Differential Pressure = $P_t' - P_a$
V	True Airspeed
V_c	Calibrated Airspeed
V_e	Equivalent Airspeed
ρ	Ambient Atmospheric Density
ρ_{sl}	Standard Sea Level Atmospheric Density
γ	Ratio of Specific Heats

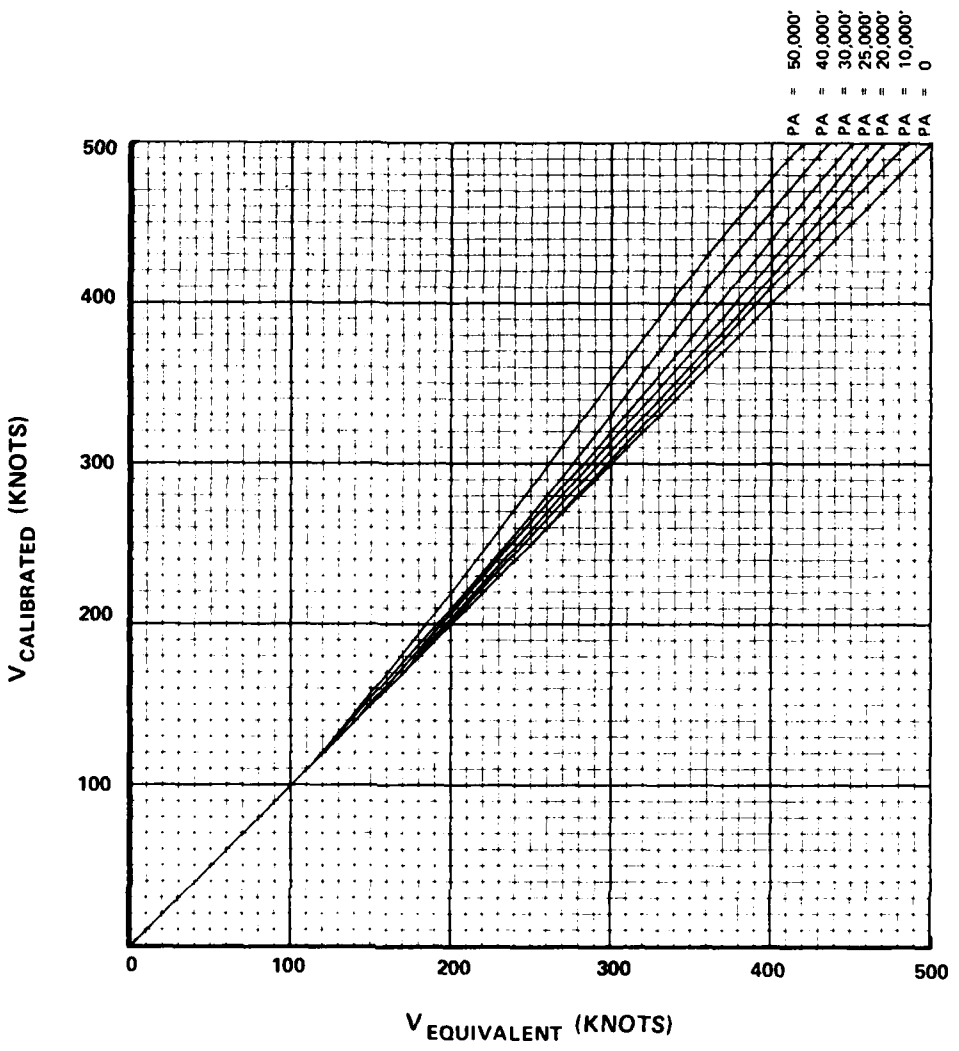

Figure 2. $V_{calibrated}$ vs $V_{equivalent}$ for Pressure Altitudes Between Sea Level and 50,000 Feet

References

1. Livingston, S. P. and W. Gracey. Tables of Airspeed, Altitude, and Mach Number Based on Latest International Values for Atmospheric Properties and Physical Constants. NASA TN D-822, August 1961.

2. Military Standard, MIL-STD-1524A. Table of Differential Pressure in Relation to Calibrated Airspeed. ASD/ENESS Wright Patterson AFB, Ohio, 31 July 1972.

3. U.S. Standard Atmosphere, 1962. National Aeronautics and Space Administration, United States Air Force, United States Weather Bureau, December 1962.

CALIBRATION OF A PITOT-STATIC AIRSPEED METER

Daniel H. Daley*

Abstract

This paper presents an explanation of the relationship between calibrated, equivalent, and true airspeed in understandable terms for Air Force pilots and aeronautical engineering students. It explains the correction factors used in going from one airspeed type to another through examples. The paper also discusses the calibration of low speed (incompressible flow), high subsonic speed (compressible flow) and supersonic airspeed meters.

I. Introduction

A Pitot-static tube used on an airplane for airspeed measurements senses the static pressure of the surrounding free stream air and a pressure obtained by bringing the air approaching the Pitot tube to a rest condition. This latter pressure is called total pressure. We shall use the symbols p for free stream static pressure, and p_o for free stream total pressure.

The static pressure and the total pressure sensed by the Pitot-static tube are fed to opposite sides of a thin metallic diaphragm in a sealed case as shown schematically in Figure 1. The diaphragm movement resulting from different pressures acting on the opposite sides of the diaphragm is measured by a pointer and dial gauge as shown. Since the pointer movement depends upon the pressure difference sensed by the diaphragm, we can calibrate the dial to read the measured pressure difference, Δp_m, which is equal to $p_o - p$. Thus we show the dial in Figure 1 to read Δp_m. Of course, an airspeed meter should read airspeed, not Δp_m. We need, therefore, to relate the pressure difference measured by an airspeed instrument to the airspeed.

II. Calibration of a Water-Speed Meter

A Pitot-static tube can be used to measure the speed of a motorboat in water. The total pressure sensed by the Pitot tube is, in this incompressible fluid case, the sum of the static pressure and the incompressible dynamic pressure. We find that the incompressible dynamic pressure depends upon the density of the water and the square of the water speed relative to the tube. Thus

$$\text{incompressible dynamic pressure} = \frac{\rho V^2}{2} \quad . \tag{1}$$

where ρ is the density of water and V is the speed of water.

---

*Colonel, USAF, Professor of Aeronautics, DFAN

Editor's Note: This paper was first written in 1970 to explain the different airspeeds to Academy Instructors; subsequently it was improved upon and presented to the Air Training Command Aerodynamics Workshop on 17-20 July 1979. It was also used as a student handout for core aero during the Fall 1979 Semester.

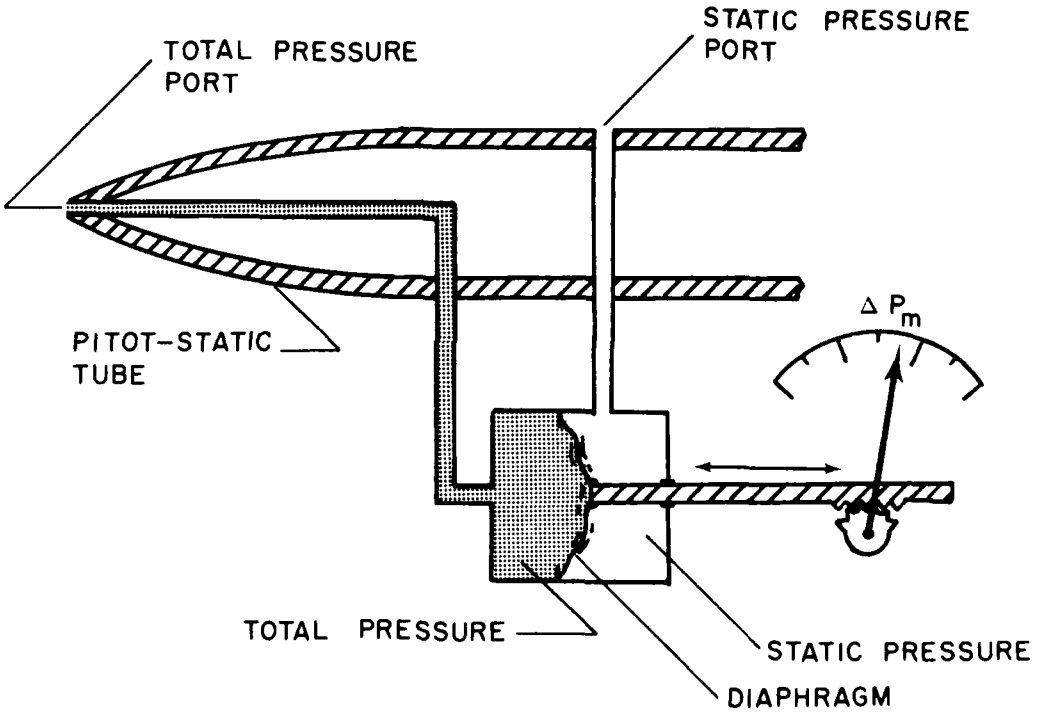

Figure 1. Airspeed Meter Schematic

AD-A085 770 AIR FORCE ACADEMY CO F/G 20/4
AIR FORCE ACADEMY AERONAUTICS DIGEST - FALL 1979.(U)
APR 80 E J JUMPER, M M TOWER, F GUGGISBERG
UNCLASSIFIED USAFA-TR-80-7 NL

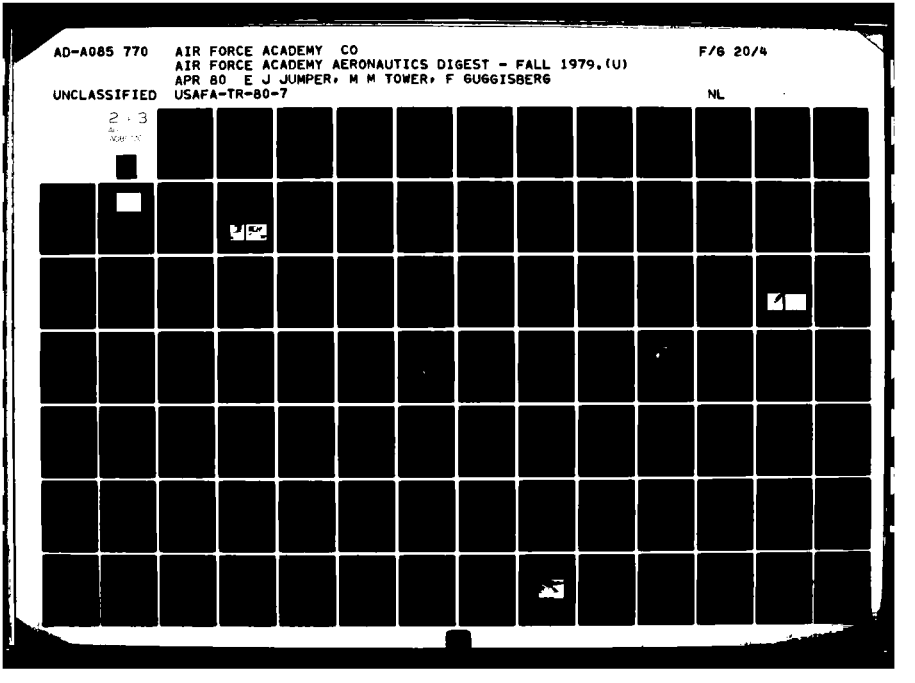

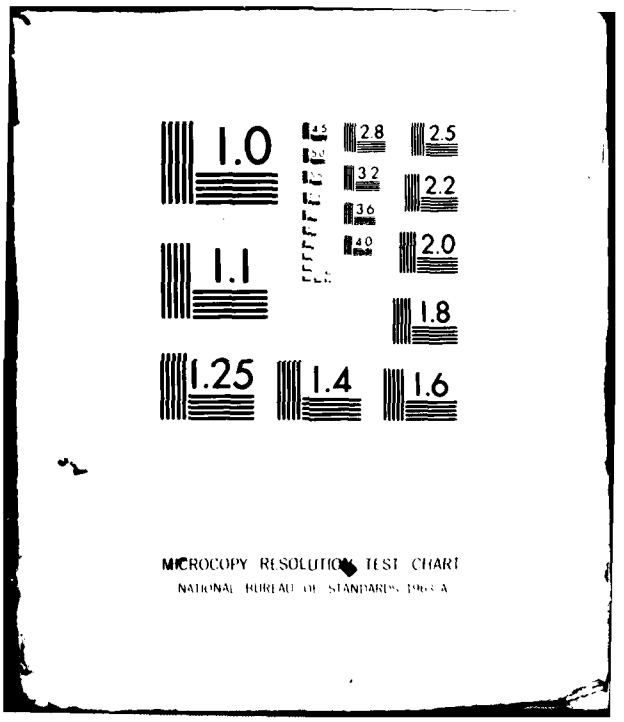
1.0
1.1
1.25
2.8
3.2
3.6
4.0
2.5
2.2
2.0
1.8
1.4
1.6
MICROCOPY RESOLUTION TEST CHART
NATIONAL BUREAU OF STANDARDS 1963-A

The total pressure measured by a Pitot-static tube in water is, then, total pressure = static pressure + incompressible dynamic pressure or

$$p_o = p + \frac{\rho V^2}{2} \quad . \tag{2}$$

Since the pressure difference measured by a water-speed gauge is total pressure less static pressure, we have

$$\Delta p_m = p_o - p = \frac{\rho V^2}{2} \quad . \tag{3}$$

Using this relation between Δp_m and V, we can make a calibration table and curve relating a Δp_m reading on the dial in Figure 1 to V; this is done in Table 1 and Figure 2.

Table 1

Δp_m CALIBRATION FOR WATER

Δp_m (psi)	V (kts)
0	0
16	29.2
36	43.8
64	58.4
81	65.7
100	73

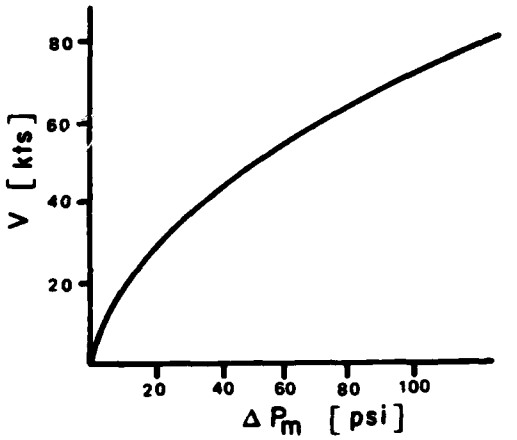

Fig 2. Water Speed Meter Calibration

To make entries in Table 1, we use the density of water for ρ and arrange units so that Δp_m is measured in pounds per square inch and V in knots. Doing this we get

$$V = \frac{1}{\sqrt{\rho}} \sqrt{2\Delta p_m} = 7.3 \sqrt{\Delta p_m} \quad . \tag{4}$$

All of the above is for a constant value of water density. Since water is essentially incompressible, its density is constant.

Even though air is a very compressible substance, its density remains essentially constant in an air flow at flight speeds less than, say, about 300 knots. Therefore, prior to 1925, airspeed meters were calibrated using the relation in Eqn (3). Since 1925 (Ref. 1), however, airspeed meters in the United States have been calibrated

using a relation between Δp_m and V that accounts for the compressibility of air. Since compressibility is taken into account in the calibration of airspeed meters, let us examine the compressible air case.

III. Calibration of a Compressible Gas Airspeed Meter

For an incompressible fluid the total pressure is given by the equation

$$p_o = p + \frac{\rho V^2}{2} \tag{5}$$

or

$$p_o = p\left[1 + \frac{\rho V^2}{2p}\right] \quad . \tag{6}$$

The compressible gas air equation looks similar to Eqn (6) except the number 3.5* appears at two locations. It is

$$p_o = p\left[1 + \frac{1}{3.5}\,\frac{\rho V^2}{2p}\right]^{3.5} \quad . \tag{7}$$

Using Eqn (7) we find the pressure difference measured by an airspeed meter to be

$$\Delta p_m = (p_o - p) = p\left\{\left[1 + \frac{1}{3.5}\,\frac{\rho V^2}{2p}\right]^{3.5} - 1\right\} \quad . \tag{8}$$

Solving this equation for the true airspeed, V_T, we get

$$V_T = \underbrace{\left(\frac{1}{\sqrt{\rho}}\right)}_{A}\ \underbrace{\sqrt{7p\left[\left(\frac{\Delta p_m}{p} + 1\right)^{1/3.5} - 1\right]}}_{B} \tag{9}$$

or

$$V_T = A\,B \quad . \tag{10}$$

Since A depends on the air density and, for a given Δp_m, B depends on the air pressure, we let

A = the density factor

B = the pressure factor.

We calibrate an airspeed meter using standard sea level values of density and pressure in Eqn (10). Therefore, to convert a Δp_m reading on the dial of Figure 1 to calibrated airspeed, V_{cal}, we use standard sea level density to evaluate the density factor, A_{sl}. And we use standard sea level pressure along with the given Δp_m reading to evaluate the pressure factor, B_{sl}. Thus

---

* $\frac{\gamma}{\gamma-1} = 3.5$ for air

$$V_{cal} = A_{sl} B_{sl} \tag{11}$$

For any value of Δp_m, Eqn (11) can be used to find V_{cal}. This was done to obtain the airspeed meter calibration data of Table 2 and Figure 3.

Table 2

Δp_m CALIBRATION FOR AN AIRSPEED METER

Δp_m (psf)	Δp_m ("H_2O)	V_{cal} (kts)
0	0	0
8.3	1.6	50
34.3	6.6	100
77.4	14.9	150
139	26.7	200
220	42.3	250
321	61.8	300
445	85.7	350
594	114.3	400

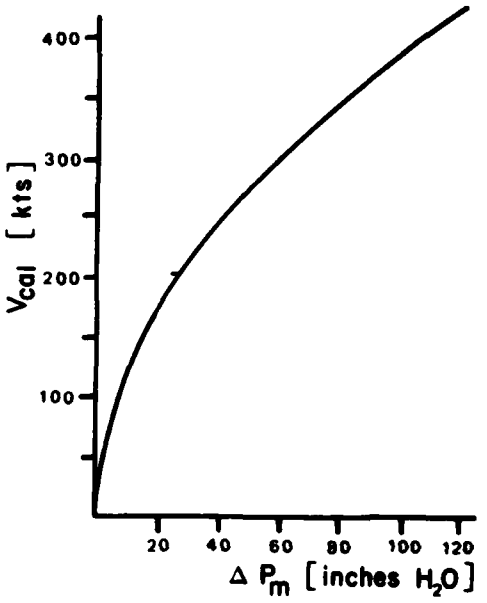

Figure 3. Airspeed Meter Calibration

Under flight conditions at other than the standard sea level values of density and pressure, the calibrated airspeed will not be the true airspeed. In practice a pilot converts a calibrated airspeed meter reading to true airspeed by multiplying V_{cal} by a pressure correction $\left(\frac{B}{B_{sl}}\right)$ and a density correction $\left(\frac{A}{A_{sl}}\right)$ to give

$$V_T = \left[V_{cal}\right] \left(\frac{B}{B_{sl}}\right) \left(\frac{A}{A_{sl}}\right) \quad . \tag{12}$$

That this gives

$$V_T = A\,B \tag{13}$$

can be verified by replacing V_{cal} by

$$V_{cal} = A_{sl}\,B_{sl} \quad . \tag{14}$$

The pressure correction $\left(\frac{B}{B_{sl}}\right)$ corrects V_{cal} to the correct altitude pressure, and the density correction corrects $V_{cal}\left(\frac{B}{B_{sl}}\right)$ to the correct altitude density.

The calibrated airspeed corrected for pressure only is called equivalent airspeed, V_{eq},

$$V_{eq} = V_{cal}\left(\frac{B}{B_{sl}}\right) \quad . \tag{15}$$

The pressure correction $\left(\frac{B}{B_{sl}}\right)$ is called the F-factor on a pilot's airspeed calculator. It is also inappropriately* called the compressibility error or correction.

When V_{eq} is corrected for density, V_T is obtained:

$$V_T = V_{eq}\left(\frac{A}{A_{sl}}\right) \quad . \tag{16}$$

This sequence of corrections gives rise to the easy-to-remember rule ICE-T (Indicated-Calibrated-Equivalent-True) used by pilots.

IV. The Density Correction

Observe in the true airspeed equation preceding Eqn (10) that the density factor A is

$$A = \frac{1}{\sqrt{\rho}} \quad . \tag{17}$$

Therefore

$$\frac{A}{A_{sl}} = \sqrt{\frac{\rho_{sl}}{\rho}} \quad . \tag{18}$$

But the density of air is proportional to the air pressure and is inversely proportional to temperature, T. Therefore,

$$\frac{A}{A_{sl}} = \sqrt{\frac{p_{sl}\,T}{p\,T_{sl}}} = C\sqrt{\frac{T}{p}} \quad , \tag{19}$$

where C is a constant. Hence, to evaluate (A/A_{sl}) the pilot needs to know the temperature and pressure corresponding to his flight altitude. These are the data, in fact, that a pilot's calculator requires as input (in the form of outside air temperature and pressure altitude) to convert V_{eq} to V_T.

---

*It's inappropriate because the compressibility of air is taken into account in the calibration of airspeed meters by using Eqn (10) rather than the incompressible equation, $\Delta p_m = \frac{\rho V^2}{2}$.

V. The Pressure Correction, $F = (B/B_{sl})$

The true airspeed equation preceding Eqn (10) shows that

$$B = \sqrt{7p\left[\left(\frac{\Delta p_m}{p} + 1\right)^{1/3.5} - 1\right]} \quad ; \tag{20}$$

therefore,

$$F = \frac{B}{B_{sl}} = \sqrt{\frac{\cancel{7}p\left[\left(\frac{\Delta p_m}{p} + 1\right)^{1/3.5} - 1\right]}{\cancel{7}p_{sl}\left[\left(\frac{\Delta p_m}{p_{sl}} + 1\right)^{1/3.5} - 1\right]}} \quad . \tag{21}$$

For a known altitude pressure, p, and a given measured pressure difference, Δp_m, the pressure correction, F, can be evaluated by this equation (Ref. 2). Since Δp_m fixes V_{cal} (as shown by the airspeed meter calibration curve of Figure 3), the F-factor can be tabulated versus pressure altitude and V_{cal}. This is the way the F-factor is presented on a pilot's calculator and in Table 3.

Table 3

PRESSURE CORRECTION FOR CALIBRATED AIRSPEED

F-FACTOR

Press. Alt Feet	Calibrated Airspeed Knots							
	200	250	300	350	400	450	500	550
10,000	1.0	1.0	.99	.99	.98	.98	.97	.97
20,000	.99	.98	.97	.97	.96	.95	.94	.93
30,000	.97	.96	.95	.94	.92	.91	.90	.89
40,000	.96	.94	.92	.90	.88	.87	.87	.86
50,000	.93	.90	.87	.86	.84	.84	.84	.84

VI. Airspeed Meter Calibration in Supersonic Flight

In supersonic flight a Pitot tube has a shock wave in front of it as shown in Figure 4. The total pressure, p_o, of the free stream air that impinges upon the nose of the Pitot tube is reduced to p_{o_1}, as the air passes through the shock wave. The airspeed meter senses the total pressure, p_{o_1}, and, by judicious placement of the static pressure port, the free stream static pressure.

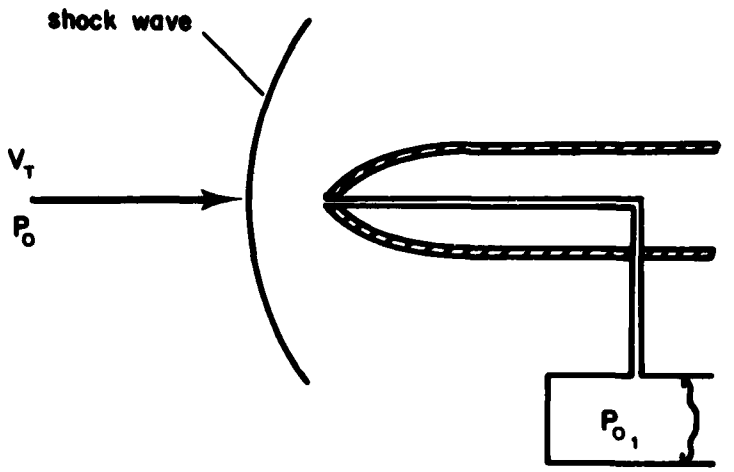

Figure 4. Pitot Tube in Supersonic Flight

The measured pressure difference, Δp_m, in the presence of a shock wave is

$$\Delta p_m = p_{O_1} - p \quad , \tag{22}$$

where

$$p_{O_1} = \left(\frac{p_{O_1}}{p_O}\right)\left(\frac{p_O}{p}\right) p \quad . \tag{23}$$

The ratio $\left(p_{O_1}/p_O\right)$ is the total pressure ratio (less than one) across a normal shock. The ratio (p_O/p) is, as in the subsonic case,

$$\frac{p_O}{p} = \left[1 + \frac{1}{3.5}\,\frac{\rho V^2}{2p}\right]^{3.5} \quad . \tag{24}$$

The pressure difference measured across the diaphragm of an airspeed meter in supersonic flight is, therefore,

$$\Delta p_m = \left[\left(\frac{p_{O_1}}{p_O}\right)\left(1 + \frac{1}{3.5}\,\frac{\rho V^2}{2p}\right)^{3.5} - 1\right] p \quad . \tag{25}$$

Solving for the true airspeed, V_T, we obtain

$$V_T = \underbrace{\frac{1}{\sqrt{\rho}}}_{A} \underbrace{\sqrt{7p\left\{\left[\left(\frac{\Delta p_m}{p} + 1\right)\left(\frac{p_o}{p_{o_1}}\right)\right]^{1/3.5} - 1\right\}}}_{B'} \tag{26}$$

or

$$V_T = A\,B' \quad . \tag{27}$$

Since $p_{o_1}/p_o = 1$ in subsonic flight, this reduces to $V_T = A\,B$ as it should.

In supersonic flight, we have

$$F = \frac{B'}{B_{sl}} = \sqrt{\frac{7p\left\{\left[\left(\frac{\Delta p_m}{p} + 1\right)\left(\frac{p_o}{p_{o_1}}\right)\right]^{1/3.5} - 1\right\}}{7p_{sl}\left\{\left[\left(\frac{\Delta p_m}{p_{sl}} + 1\right)\right]^{1/3.5} - 1\right\}}} \quad . \tag{28}$$

To evaluate F we select V_T and a pressure altitude. These fix Mach number; hence, $\left(\frac{p_o}{p_{o_1}}\right)$ and p and ρ. The measured pressure difference, Δp_m, is computed using Eqn (25). Then F is evaluated. Next, with Δp_m known, V_{cal} is found using the equation

$$V_{cal} = A_{sl}\,B_{sl} \tag{29}$$

In this way the F-factor can be determined for supersonic flight speeds* and tabulated against pressure altitude and V_{cal} as on a pilot's calculator.

Acknowledgements

The author thanks Captains M. Tower and R. Hartman for their help in the preparation of this paper.

*In actual practice the airspeed meter does not know when a shock wave is formed. Thus it is calibrated to expect supersonic flight and the associated shock wave at ΔP_m corresponding to a sea-level flight speed of 661 knots (the speed of sound at sea level), and at this point switches from the subsonic pressure correction factor equation, Eqn (25), to the supersonic equation, Eqn (28).

References

1. Beij, K. Hilding. Aircraft Speed Instruments. NACA TR-420, 1932.

2. Schoolfield, W. C. "A Simple Method of Applying the Compressibility Correction in the Determination of True Air Speed." Journal of the Aeronautical Sciences, Vol. 9, No. 12 (October 1942), 457-464.

CALIBRATION OF PRESTON TUBES IN A WATER FLOW CHANNEL OF VARYING AREA*

H. M. Brilliant**

Abstract

This report discusses two techniques for determining the skin friction coefficient from measurements other than direct force measurements. One technique uses velocity profile data and the other uses Preston tubes. Both are based on law-of-the-wall velocity profiles. The velocity profile technique has been used to determine the skin friction coefficient with water flow in a channel of varying area. The skin friction coefficient obtained has been used to calibrate Preston tubes. The results are compared with earlier calibration experiments.

I. Introduction

Viscous forces in the usual sense are significantly large only in a small region near a solid object but can affect the flow indirectly over a large region. Thus, it is important (and also very difficult) to measure the viscous force. In a survey paper, Winter (Ref. 1) reviews a variety of techniques used to measure skin friction forces at a solid surface. Following the lead of Brown and Joubert (Ref. 2) and others, he classified these techniques as shown in Figure 1.

The earliest technique employed to measure skin friction is the direct method. According to Winter, "The first systematic investigations were made over 100 years ago by Froude (in 1872) who measured the drag of a series of planks towed at various speeds along a tank...." To obtain accurate local measurements, small floating elements whose deflection is proportional to the force on them are used. While this may sound simple, the apparatus is actually very complicated and expensive. Winter discusses some of the major problems.

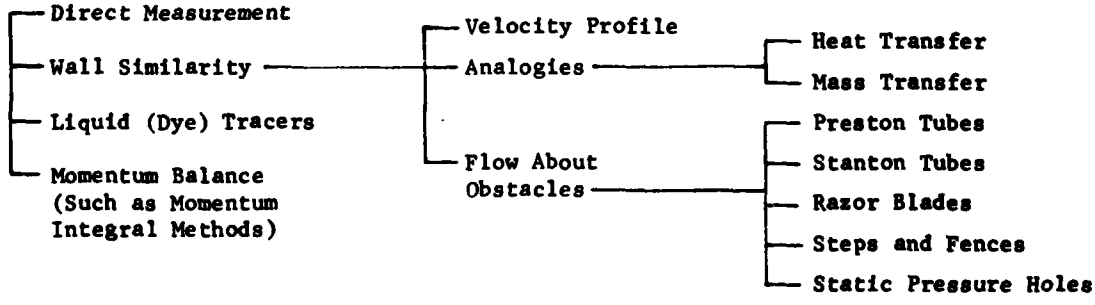

Figure 1. Classification of Skin Friction Measurement Techniques

*This work has been sponsored by the Aero Propulsion Laboratory (TBX) as part of a program to develop shaped block devices to measure skin friction in turbomachinery. Their support is greatly appreciated.

**Captain, USAF, Associate Professor of Aeronautics, DFAN

A more practical method is the velocity profile method. By measuring the velocity at various locations in the boundary layer, we can obtain the skin friction by matching the measured velocity profile with that obtained by similarity solutions. This is the technique used in this experiment.

The Preston tube technique was first presented by Preston (Ref. 3) in 1954. Based on the similarity solution of the velocity profile, Preston realized that, by measuring the velocity at a known distance from the wall, he could calculate the entire velocity profile and, thus, the skin friction coefficient. He used a circular pitot tube lying on the surface and a nearby static pressure to determine the velocity. Patel (Ref. 4) presented a more extensive calibration of the Preston tube, including a study of the effects of pressure gradients on the calibration. Patel and Brown and Joubert, among others, have established limits on the use of Preston tubes.

In this report, the theory behind the velocity profile and Preston tube methods will be discussed first. This will be followed by a discussion of the apparatus and procedure used in this experiment. Finally, the determination of the skin friction coefficient and the calibration of the Preston tubes will be presented.

II. Wall Similarity and Velocity Profile Methods - The Law of The Wall

Over the last 40 years, there has been extensive research into turbulent boundary layers. Through experiments of his own and of others, Clauser (Ref. 5) first realized that turbulent boundary layers have an inner flow composed of three regions: a viscous (linear) sublayer, a transition region, and a logarithmic region. The viscous sublayer, adjacent to the wall, is a region in which laminar viscous forces dominate turbulent forces. The logarithmic region, also called the "law-of-the-wall" region, is the outer of the three regions. In theory, the skin friction coefficient can be determined by measurements in the viscous sublayer; however, in practice, the viscous sublayer is too thin for most instruments, so the logarithmic region is used to determine the skin friction coefficient.

Following Bradshaw (Ref. 6), we can write the velocity profile in the three regions as

$$\text{Viscous Sublayer:}\quad \frac{u}{u_\tau} = \frac{yu_\tau}{\nu} \qquad 0 \le \frac{yu_\tau}{\nu} < 5 \qquad \text{(1a)}$$

$$\text{Transition Region:}\quad \frac{u}{u_\tau} = 5\ln\frac{yu_\tau}{\nu} - 3 \qquad 5 \le \frac{yu_\tau}{\nu} < 30 \qquad \text{(1b)}$$

$$\text{Logarithmic Region:}\quad \frac{u}{u_\tau} = 2.44\ln\frac{yu_\tau}{\nu} + 5 \qquad 30 \le \frac{yu_\tau}{\nu} < 500 \qquad \text{(1c)}$$

Here, u is the velocity at a distance, y, from the wall; ν is the kinematic viscosity, and u_τ is the friction velocity defined by

$$u_\tau = \sqrt{\frac{\tau_w}{\rho}} \quad , \tag{2}$$

with τ_w being the wall shear stress and ρ being the fluid density. Figure 2 shows a plot of the profile given by Eqns (1). The skin friction coefficient, C_f, is defined by

$$C_f \equiv \frac{\tau_w}{\frac{1}{2}\rho u_\infty^2} \quad , \tag{3a}$$

where u_∞ is the freestream velocity. Thus, C_f is related to the friction velocity by

$$C_f = 2\left(\frac{u_\tau}{u_\infty}\right)^2 \quad . \tag{3b}$$

The velocity profile functions can be written with the skin friction coefficient as a parameter. For example, Eqn (1c) becomes

$$\frac{u}{u_\infty} = \sqrt{\frac{C_f}{2}}\left\{2.44\,\ell n\left(\sqrt{\frac{C_f}{2}}\,\frac{yu_\infty}{\nu}\right) + 5\right\} \quad . \tag{4}$$

Plots of Eqn (4) and the two equations corresponding to Eqns (1a) and (1b) are called Clauser charts. Usually, they have u/u_∞ versus $\log_{10}\left(\frac{yu_\infty}{\nu}\right)$ with C_f as a parameter. Examples are shown later in the report (see Figures 9a - d). By measuring the local velocity, u, at a location, y; the freestream velocity, u_∞; and the fluid temperature (to obtain ν), we can obtain the skin friction coefficient, C_f. In practice, these measurements are made at many locations and a more accurate value of C_f can be found using a least square curve fit on the measured versus theoretical u/u_∞. The curve fit method used in this project is discussed by Huffman, et al. (Ref. 7).

Since Eqns (1) are valid only if $yu_\tau/\nu < 500$, this method could be applied only to a limited number of data points. The problem could be eliminated if the inner flow given by Clauser is blended with an outer or wake region to form a complete boundary layer profile. Following Thompson (Ref. 8), we introduce the intermittency function, γ_s, as the weight between the inner solution and the outer (freestream) solutions. The value of the intermittency function depends on the location of the data point in the boundary layer as indicated by Figure 3. The combined solution is

$$\frac{u}{u_\infty} = \gamma_s \left[\frac{u}{u_\infty}\right]_{\text{inner}} + (1 - \gamma_s) \quad , \tag{5}$$

where $\left[\frac{u}{u_\infty}\right]_{\text{inner}}$ is obtained from Eqns (1) via the method used to obtain Eqn (4).

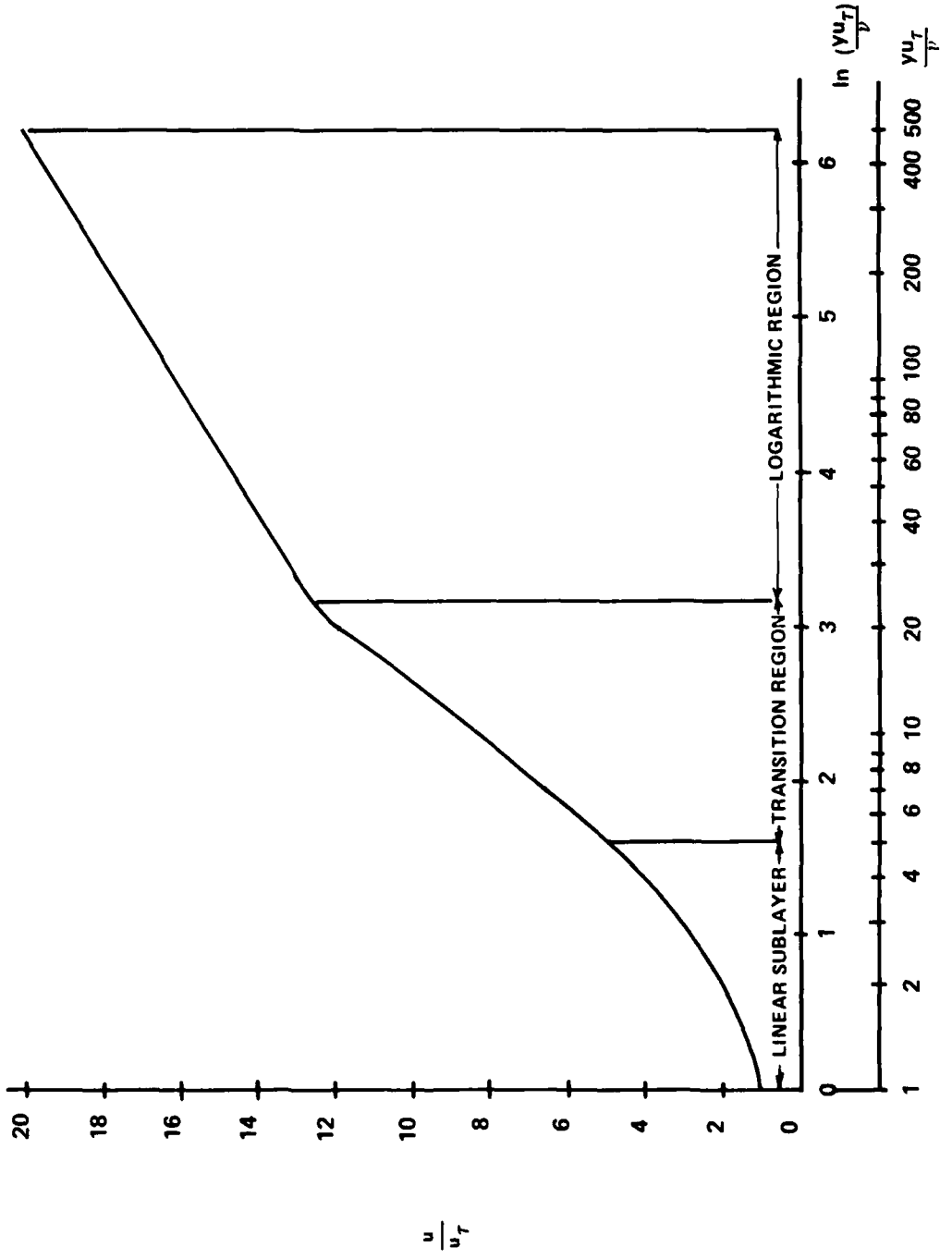

Figure 2. Velocity Profile in the Inner Region of a Turbulent Boundary Layer

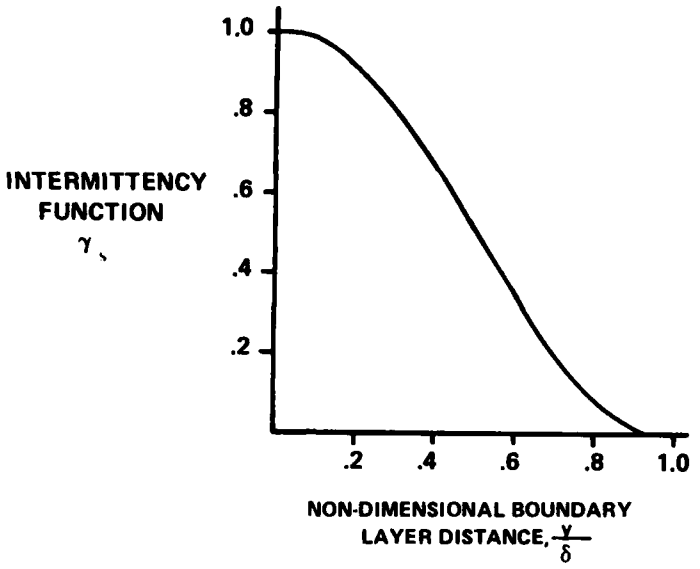

Figure 3. The Intermittency Function (Adopted from Ref. 9)

Wall similarity is applicable as long as either Eqn (1) or (5) is valid. Flows with strong adverse or favorable pressure gradients may affect the validity of the law of the wall. Winter indicates that as long as a logarithmic region can be observed, the method should be valid and that the lack of this region should be obvious from the data.

III. Application of Wall Similarity to Preston Tubes

As indicated during the discussion of Eqn (4), measurement of u at one point in the boundary layer should be sufficient to determine the skin friction coefficient. Preston developed a device to do this. He measured the total pressure by putting a Pitot tube along the wall and measured the static pressure near the Pitot tube inlet, as shown in Figure 4. The difference between the total and static pressure, Δp, is related to the mean velocity of the flow over the Pitot inlet. Preston proposed the following non-dimensional relationship between Δp and τ_w:

$$\frac{\tau_w d^2}{4\rho\nu^2} = \text{fn}\left(\frac{\Delta p d^2}{4\rho\nu^2}\right) \qquad (6)$$

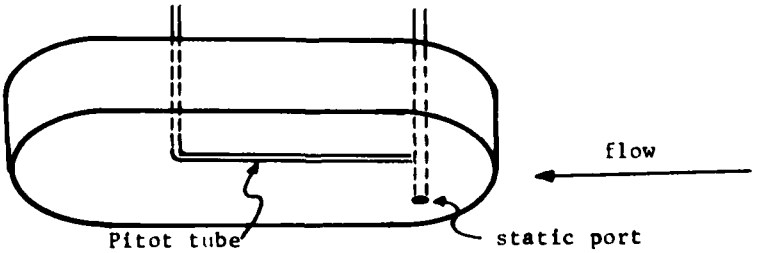

Figure 4.a. Schematic of a Preston Tube

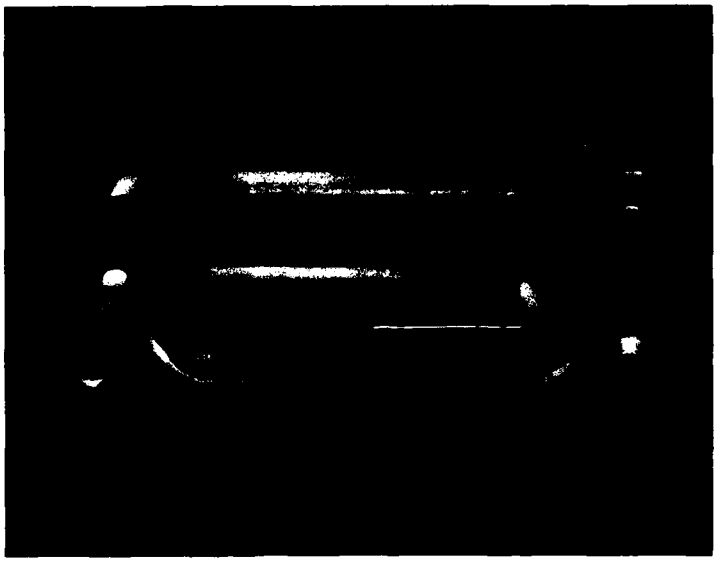

Figure 4.b. Photograph of Preston Tube Used in This Experiment

where d is the Pitot tube diameter.† If a Preston tube is tested at a location where τ_w (or C_f) is known, the function of Eqn (6) can be obtained. Patel proposed the following curve fits for that function:

$$y^* = 0.8287 - 0.1381\, x^* + 0.1437\, x^{*2} - 0.0060\, x^{*3} \quad (2.9 < x < 5.6) \tag{7a}$$

$$y^* + 2 \log_{10} (1.95\, y^* + 4.10) = x^* \quad (5.6 \leq x \leq 7.6) \tag{7b}$$

where

$$x^* = \log_{10} \left(\frac{\Delta p d^2}{4\nu^2} \right) \quad \text{and} \quad y^* = \log_{10} \left(\frac{\tau_w d^2}{4\rho\nu^2} \right) . \tag{7c}$$

For $x^* = 4.8$ (the lowest value tested in this experiment), Eqn (7b) produces less than a 0.7% error in y^* and a 1.5% error in τ_w or C_f from the value predicted by Eqn (7a). Thus, Eqn (7b) will be used in this report for comparison with test results. Note that both Preston and Patel did their tests with air as the fluid.

Pressure gradient limits are extremely important in Preston tube calibrations since the failure of the law of the wall invalidates the assumptions used to obtain Eqn (6).

†Note that $\frac{d}{2}$ is the radius of the tube and, thus, the mean height above the surface; thus, the factor of 4 is included in the functional relationship.

In the velocity profile method, the lack of a logarithmic region should be obvious and place limits on the pressure gradient; however, since only one velocity is measured by the Preston tube, the lack of such a region is not obvious. Patel, Brown and Joubert, and others have suggested limits for the use of Preston tubes. They base the limits on the non-dimensional parameter, $\Delta = \frac{\nu}{\rho u_\tau^3} \frac{dp}{dx}$, where $\frac{dp}{dx}$ is the pressure gradient (positive or negative) at the axial station where τ_w is to be determined. Patel suggested the following limits for a 3% [6%] error in τ_w:

adverse pressure gradient: $0 < \Delta < 0.01\ [0.015],\ \frac{u_\tau d}{\nu} \leq 200\ [250]$

favorable pressure gradient: $0 > \Delta > -0.005\ [-0.007],\ \frac{u_\tau d}{\nu} \leq 200\ [200],\ \frac{d\Delta}{dx} < 0$

The limits suggested by Brown and Joubert are a more complicated function relating a maximum value of Δ to $\frac{u_\tau d}{\nu}$ for a given percent error. These limits should be valid for any law-of-the-wall application.

IV. Apparatus and Procedure

The calibration tests were conducted in the water flow channel shown in Figure 5. Water from the reservoir was pumped to the head tank. The velocity of the flow in the channel was controlled jointly by the water level in the head tank and the position of the tailgate. Instrumentation was installed on the flat wall shown in the photograph. The other side of the channel was curved to produce a converging-diverging channel.

The instrumentation included thirty-one static pressures, a Pitot pressure probe which could traverse the boundary layer at nine locations, Preston tubes of various designs, and a mercury thermometer to measure water temperature. The static pressures were measured via the vertical manometers shown in Figure 5b. They were located both upstream and downstream of the channel throat. Of the nine total pressure ports, two were far upstream of the channel throat and were not useful because the boundary layer was too thin. One of the ports was moved slightly when the Preston tube ports were installed. The Pitot tube had an outer diameter of 0.030 inches. The total pressure and the corresponding static pressure were measured via inclined manometers located on the far side of the water channel. Only one port could be used at a time. The Preston tubes were used at the same locations as the total pressure measurements, and the pressures on the Preston tube were also measured on the incline manometers.

The first tests were to determine the skin friction coefficient at various locations along the flow. The Pitot tube was moved outward from the wall to the freestream in increments from 0.015 to 0.050 inches, with the smaller steps near the wall. When the

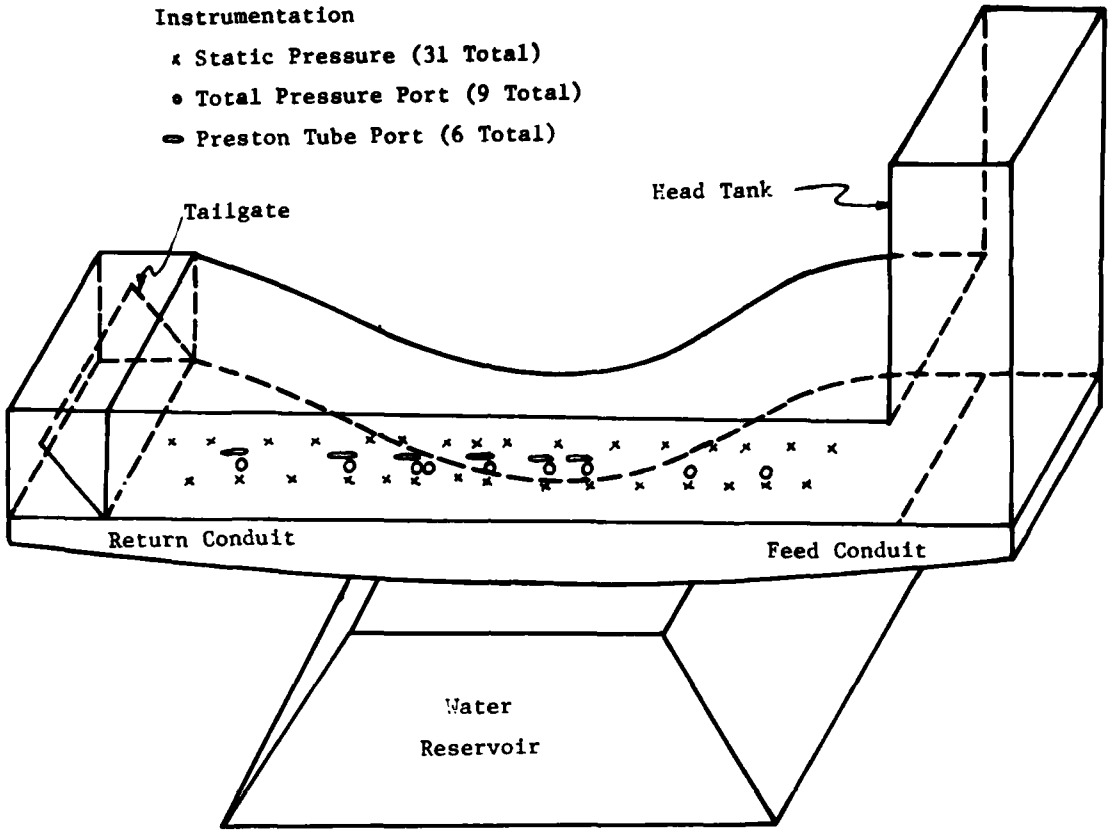

Figure 5.a. Schematic of the Water Flow Channel

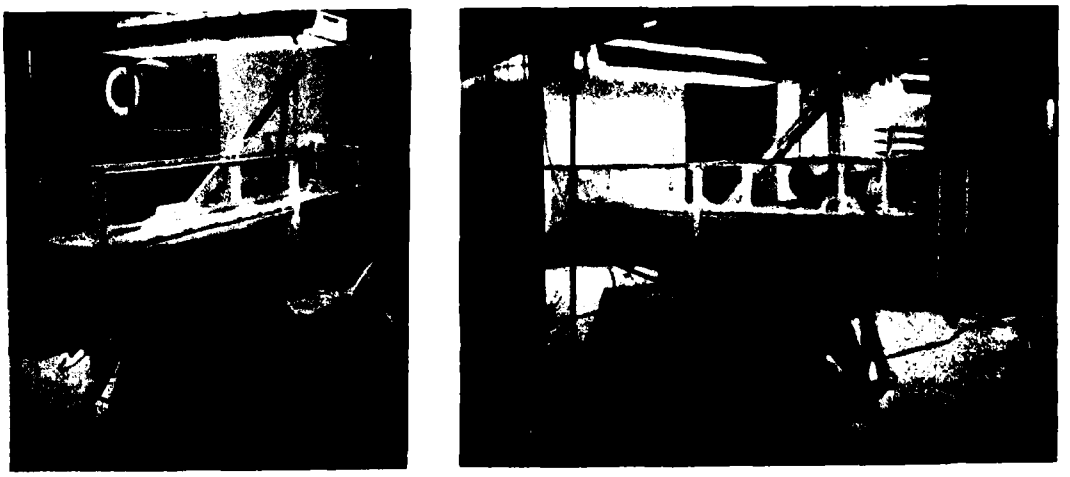

Figure 5.b. Photograph of the Water Flow Channel

total pressure started to decrease, indicating the edge of the boundary layer, measurements were continued only one or two more increments for a check. In the forward locations, where the boundary layer was thin, less than ten increments were needed for a complete boundary layer transverse. At the last station, as many as thirty-five measurements were needed. A computer program, incorporating the curve fit technique discussed earlier (Ref. 7), was used to find C_f and other boundary layer and flow properties.

Based on the data obtained by the velocity profile measurements, the Preston tubes were calibrated. Various designs were tested at each of the six stations. Several were repeated, including using water at different temperatures to change x* and y* via a change in the kinematic viscosity. Again, a computer program was used to reduce the data. It incorporated corrections to C_f due to changes in the Reynolds number based on the momentum thickness, i.e., cnanges in $Re_\theta = \frac{\theta u_\infty}{\nu}$ where θ is the momentum thickness.

V. Results

A. Channel Flow Variation

Figures 6 through 8 show the results of the thirty-one static pressure measurements. The static pressure in Figure 6 is a typical profile along the flow. The figure also indicates the stations where the total pressures were measured. The minimum channel cross-section (the throat) occurs in a 6-inch constant-area section from just downstream of station 2 to just upstream of station 4. Note that the pressure continues to drop in the throat indicating that the boundary layer is growing fast enough to affect the effective flow area.

The velocity distribution shown in Figure 7 is calculated using Bernoulli's equation:

$$p_o = p + \tfrac{1}{2}\rho u_\infty^2 \quad , \tag{8}$$

with p_o assumed equal to the static pressure at the first static pressure tap where the area is very large. Measurements of the total pressure indicate that p_o decreases a little due to friction. This decrease is incorporated into the boundary layer calculations, but not into Figure 7.

Two non-dimensional pressure gradients are shown in Figure 8. They are

$$\Delta' = \frac{\nu}{\rho u_\infty^3}\frac{dp}{dx} \tag{9a}$$

$$\Delta = \frac{\nu}{\rho u_\tau^3}\frac{dp}{dx} \quad . \tag{9b}$$

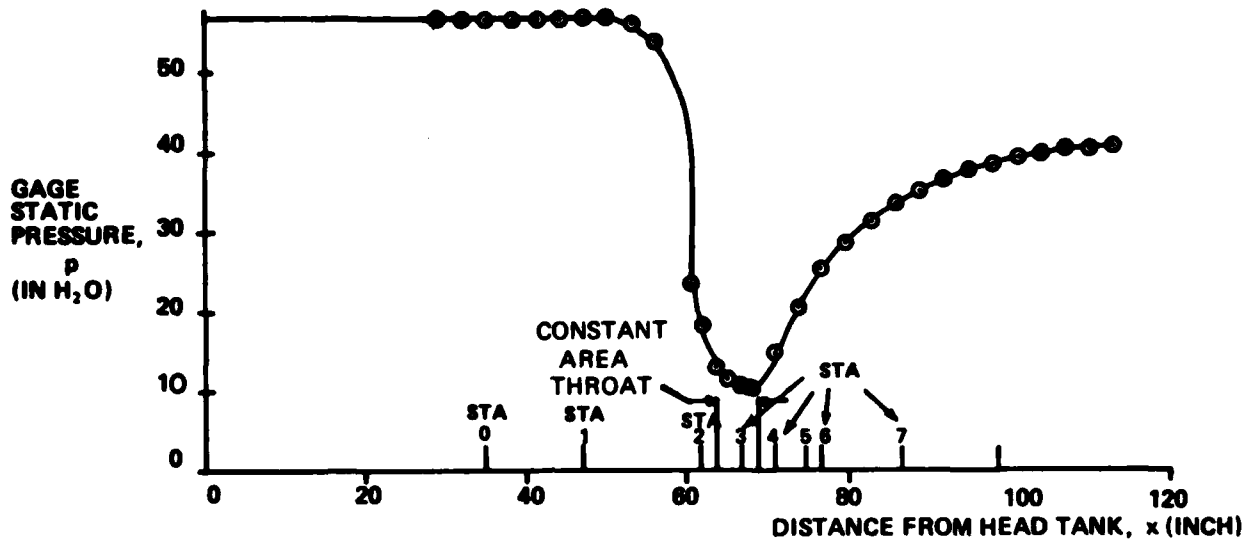

Figure 6. Channel Static Pressure Distribution

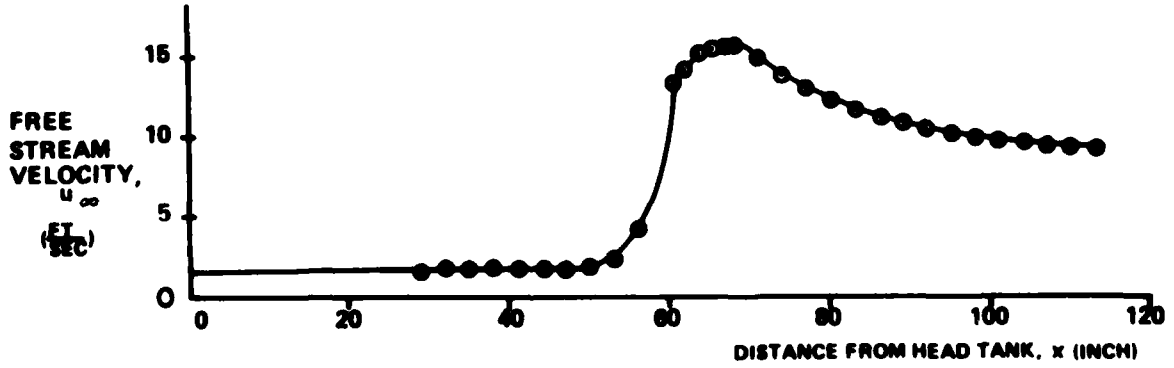

Figure 7. Channel Velocity Distribution

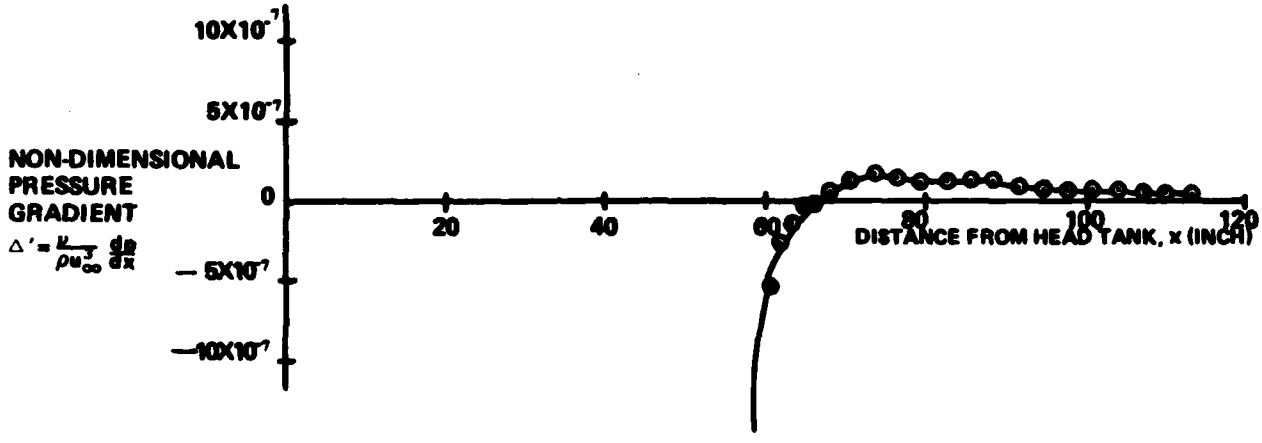

a. PRESSURE GRADIENT BASED ON FREE STREAM VELOCITY

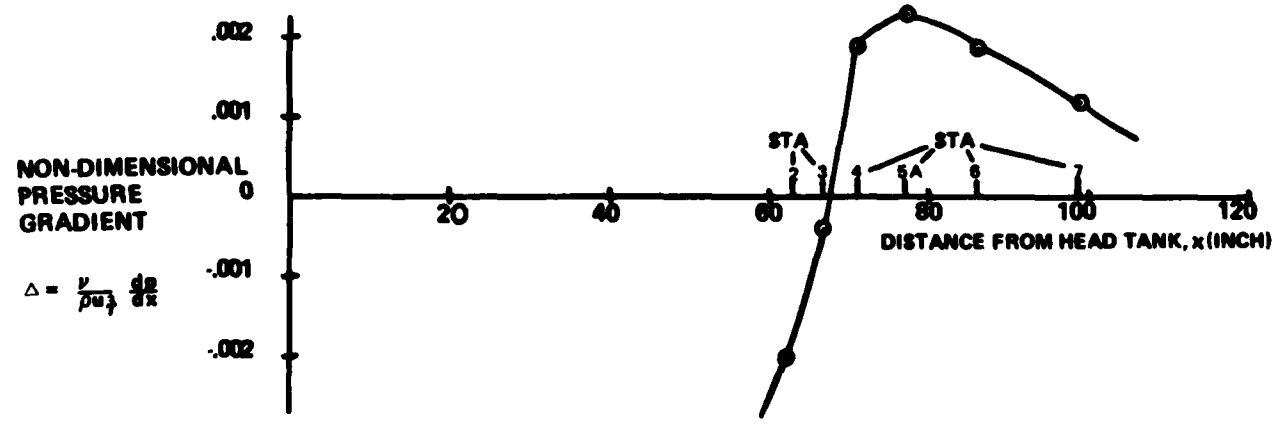

b. PATEL'S PRESSURE GRADIENT PARAMETER

Figure 8. Non-Dimensional Pressure Gradient Distribution

Eqn (9b) is that proposed by Patel as a limit to the validity of Preston tube calibrations. Since u_τ is available only where boundary layer profiles were measured, the second non-dimensional pressure gradient, Eqn (9a), is introduced here for a more complete picture of the pressure gradient. Note the difference in magnitude of the two pressure gradient terms. Also, note that Δ never exceeds Patel's limits during the entire flow.

B. Boundary Layer Characteristics

1. Velocity Profiles

Figures 9a-d show the measured velocity profile on a Clauser chart. Note that while the Clauser chart is based on Eqn (4), the measured profile is curve-fitted based on Eqn (5). Thus, the C_f value indicated on the figures may not agree exactly with what the eye would estimate from the Clauser chart.

At station 2 (Figure 9a), there is no obvious logarithmic region. This could occur because the pressure gradient here is too strong or because the boundary layer is too thin and the Pitot tube too thick to get very deep into the boundary layer. In either case, the results at this station are questionable. They are included only for completeness. The value for C_f for the three runs varied by almost 20%, even though only one data point is significantly different. A mean value of C_f was used in the Preston tube calibration.

Starting at station 3 (Figure 9b), there is an obvious logarithmic region. This region grows at the later stations (Figures 9c and 9d). The difference in profiles for different runs at stations 5/5A and 7 cannot be explained. The profile data indicate that separation did not occur at any station even where there is an adverse pressure gradient. This is confirmed by visual observations.*

2. Boundary Layer Thickness and Reynolds Number

Figure 10 shows the boundary layer thickness, δ, and the momentum thickness, θ, along the plate. As expected, the boundary layer grows. After the throat, this growth is aided by the adverse pressure gradient. The boundary layer thickness is effectively zero at station 1 and no useful data could be obtained at that point.** The momentum thickness is very small at station 2 and grows rapidly after that point.

---

*Separation did not occur on the curved wall either.

**Because of this, station 0 was never used.

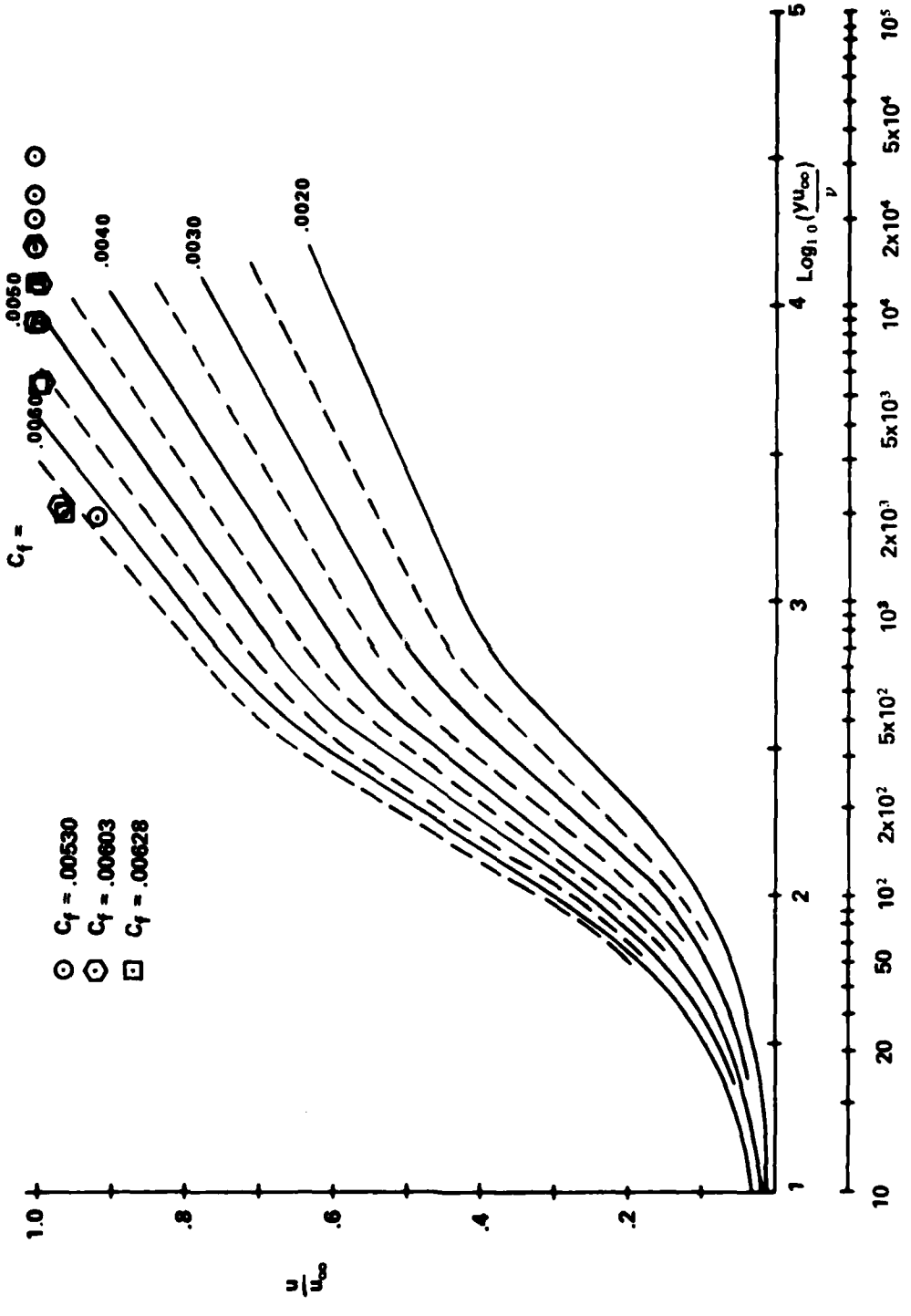

a. STATION 2 (THREE DIFFERENT RUNS)

Figure 9. Clauser Chart and Measured Velocity Distribution

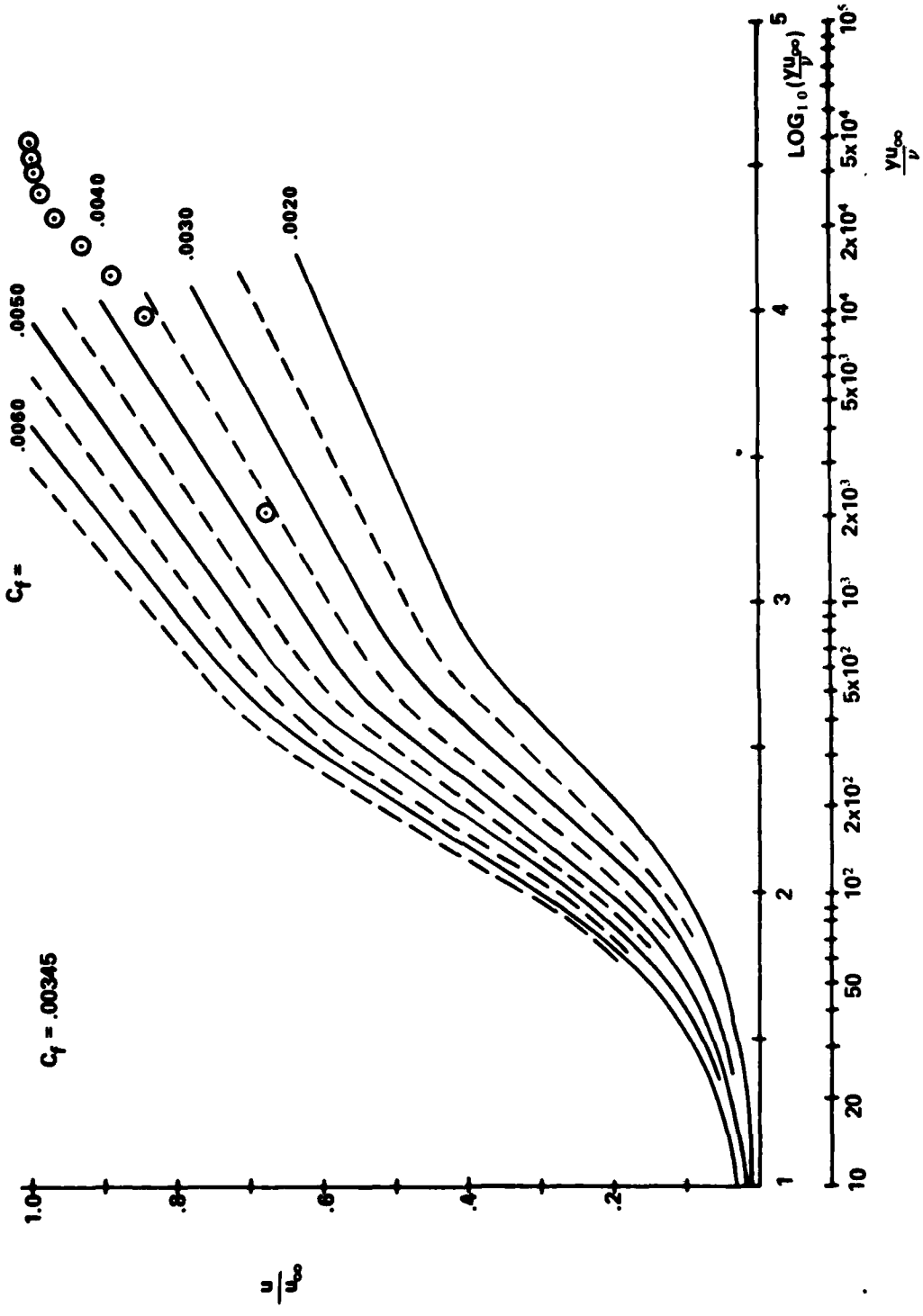

b. STATION 3 (ONE RUN)

Figure 9. Continued

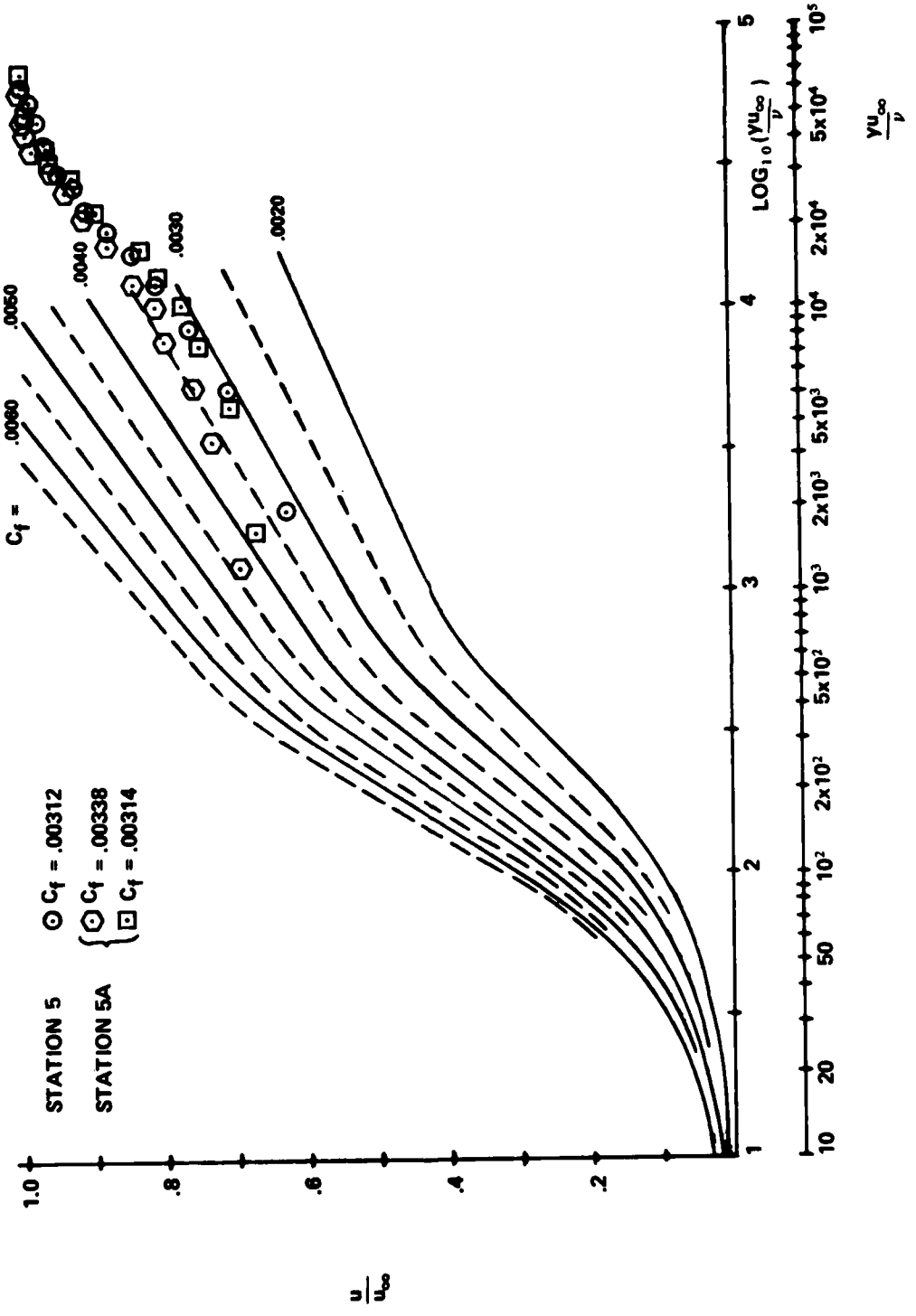

c. STATION 5 (ONE RUN) AND STATION 5A (TWO RUNS)

Figure 9. Continued

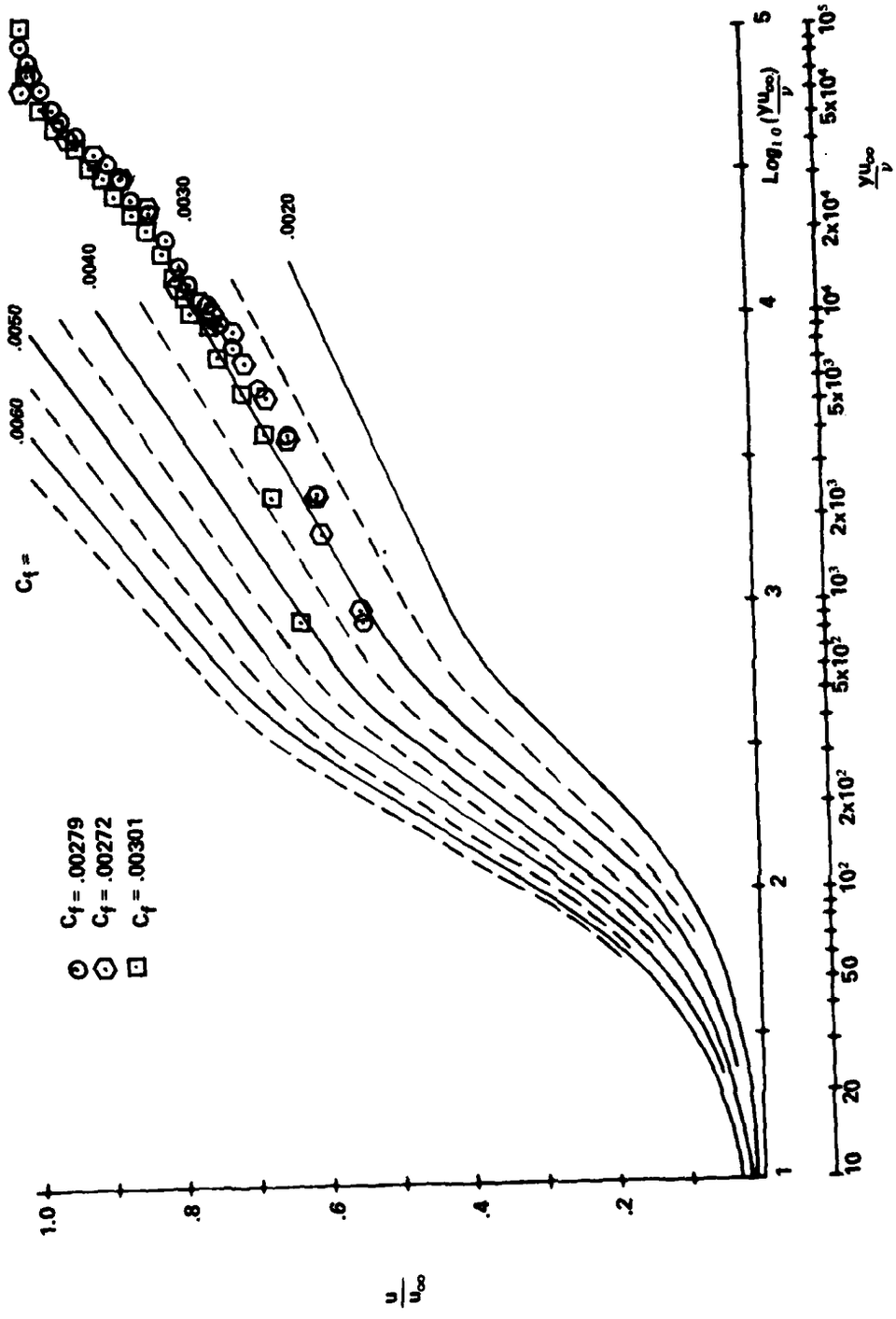

d. STATION 7 (THREE RUNS)

Figure 9. Continued

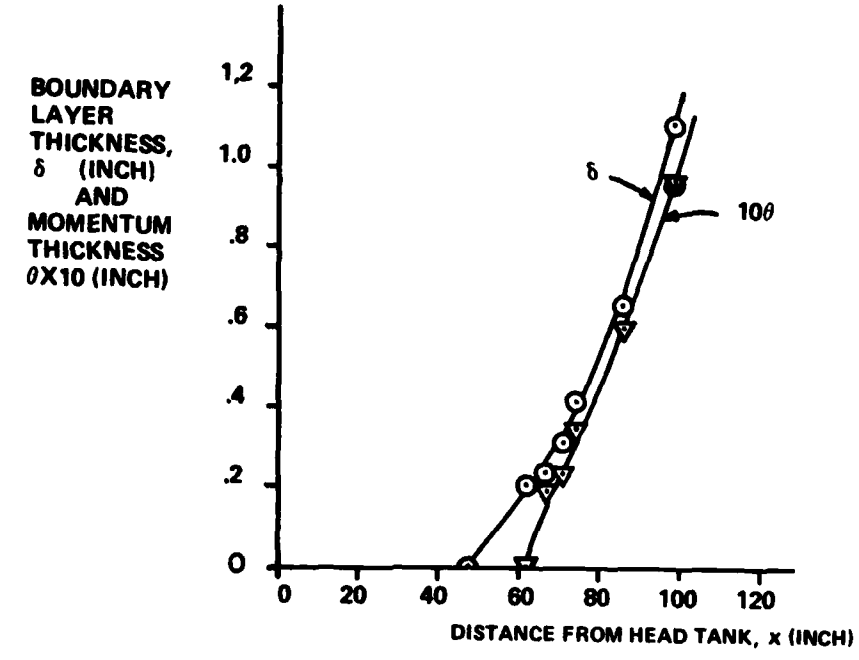

Figure 10. Boundary Layer and Momentum Thickness Versus Distance

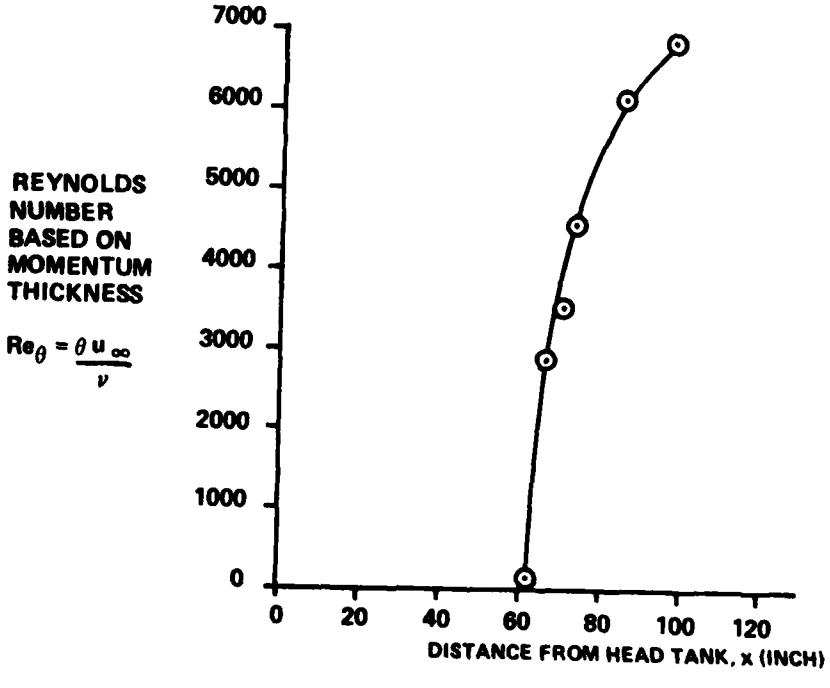

Figure 11. Reynolds Number Versus Distance

Figure 11 shows the increase in the Reynolds number, Re_θ, based on the momentum thickness and the local velocity. It is very small at station 2 but grows rapidly as the momentum thickness grows, even though the local velocity decreases down to half after station 4.

3. Skin Friction Coefficient

Figure 12 shows the skin friction coefficient determined from the boundary layer profiles. It is plotted versus the Reynolds number based on the momentum thickness. This is the curve used in the data reduction for the Preston tubes. Deviations from the line are due mainly to data accuracy. The maximum probability error in C_f varies from 18% at station 2 and 4.2% at station 3 to 2.5% at station 7.

With these skin friction coefficients, the boundary layer profile could be converted to the universal profile based on u/u_τ. A typical result (for station 7) is shown in Figure 13. The universal profile of Eqns (1) is presented for comparison. Except very close to the wall, there is very good agreement between the experimental and theoretical profiles. Only at station 2 is the agreement poor, but this is expected from Figure 9a.

C. Preston Tube Calibration

There were seven different Preston tube designs tested. The variables were the Pitot tube outer diameter, Pitot tube length, the spacing between the Pitot tube and the static port, and the location on the plug which held the Preston tube. The various combinations tested are shown in Table 1.

Table 1

PRESTON TUBE DESIGNS TESTED

Probe Number	Pitot Tube		Spacing Between Pitot Tube and Static Pressure Port (Ratioed) To Pitot Tube Outer Diameter)
	Outer Diameter Inches	Length Inches	
1	.032	$\frac{3}{4}$	7.0D
2	.032	$\frac{3}{4}$	3.9D
3	.032	2	4.9D
4	.0483	$\frac{3}{4}$	3.4D
5	.0483	2	5.6D
6	.0483	2	3.0D
7	.0483	$\frac{3}{4}$ (aft location)	2.8D

Originally, more designs were to be tested; but, since none of the variables affected the results significantly, the number tested was reduced. Figure 4b shows probe 1.

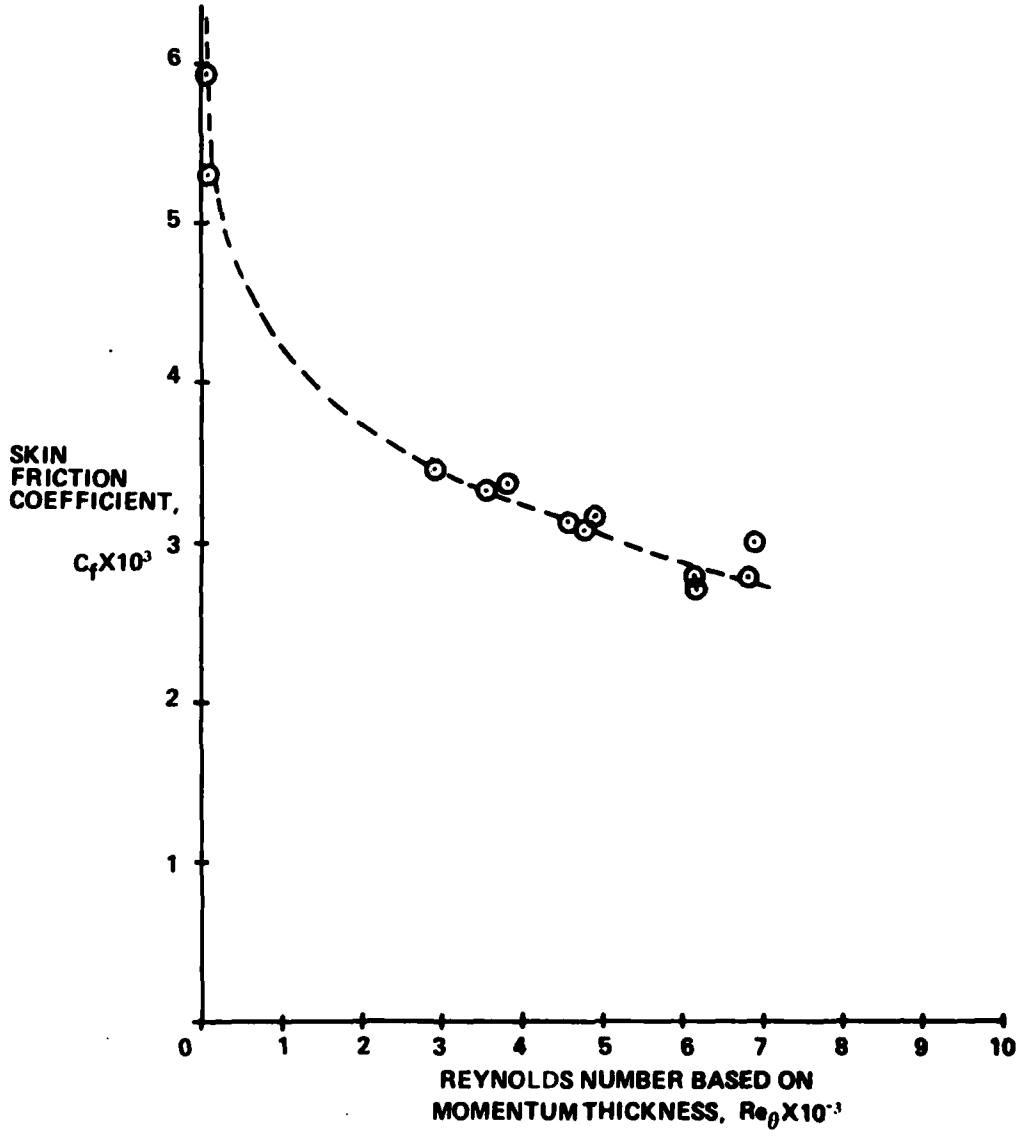

Figure 12. Skin Friction Coefficient Versus Reynolds Number

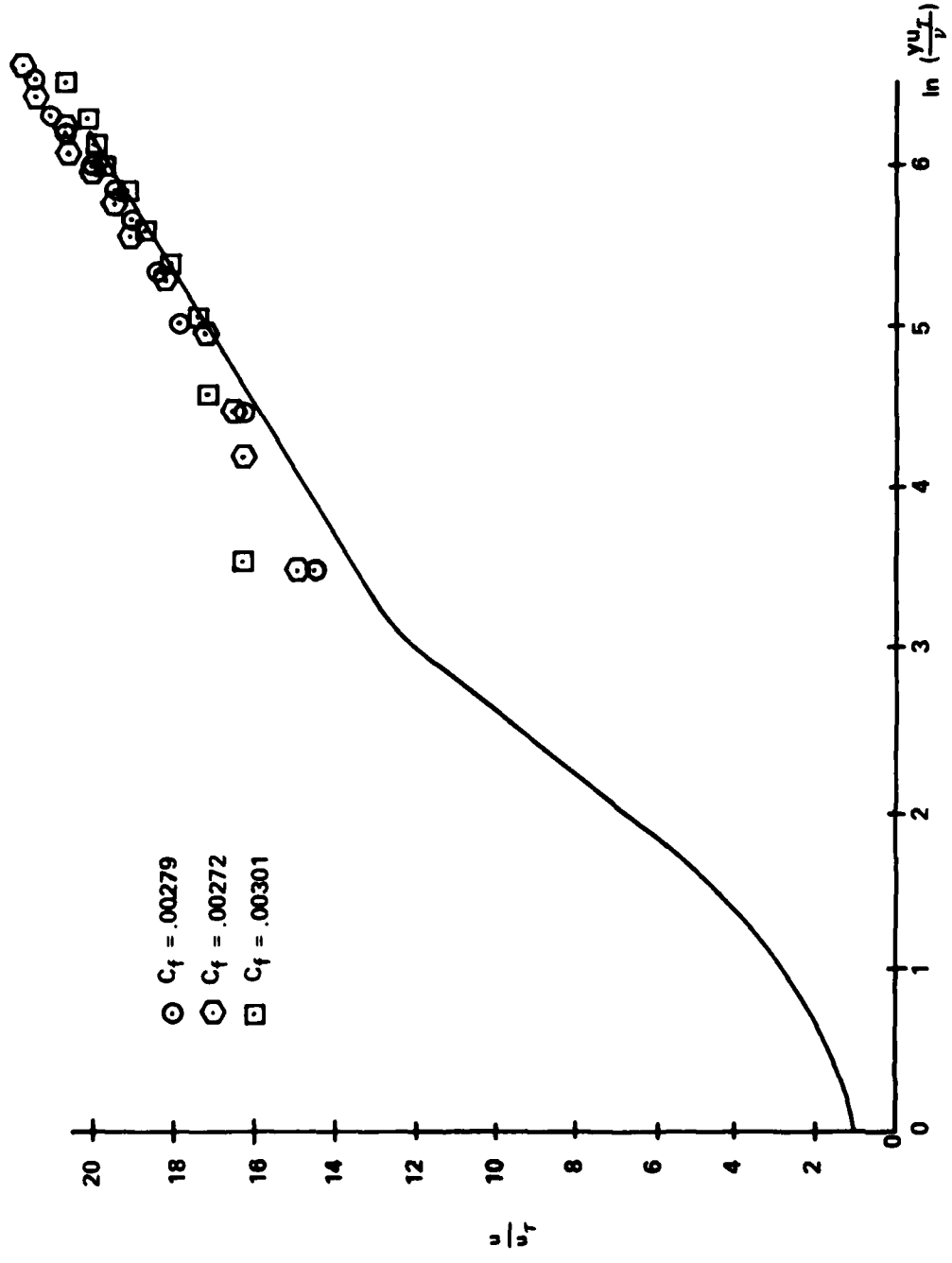

Figure 13. Velocity Data at Station 7 Compared to the Inner Solution

Probe 7 is similar to probe 4 except it was moved aft on the plug by 1.25 inches to test if a surface discontinuity directly ahead of the probe would affect the results. This discontinuity did not seem to have any effect either.

Figures 14a - f show the results of these tests. The solid line is the curve fit of Patel, given by Eqn (7b). The deviation of the data from Patel's curve fit directly correlates to the pressure gradient as indicated in Table 2. (Note that except at station 2, the uncertainty in C_f cannot explain the deviation.) At stations 2 and 3, there is a favorable pressure gradient and the data points for these tests consistently fall below the results of Patel's tests, i.e., y^*, τ_w, or C_f are less than their values determined by Patel for the same x^*. Similarly, at stations 5A, 6, and 7, where there is an adverse pressure gradient, the data points for these tests consistently fall above Patel's results. Station 4 was located just after the transition from a favorable to an adverse pressure gradient as shown in Figure 8b. There, the data usually fall very close to the line. However, as mentioned earlier, the non-dimensional pressure gradient, Δ, never exceeds Patel's 3% error limits. The other limit, on $\frac{u_\tau d}{\nu}$, is exceeded at stations 2 through 5A for the bigger diameter Preston tubes and at station 2 for the smaller diameter tube. The combined values of Δ and $\frac{u_\tau d}{\nu}$ never exceed the 1% error limit of Brown and Joubert. The different fluids used (air versus water) could be the cause of the deviations, but this cannot be confirmed with the available data.

Table 2

COMPARISON OF DATA FROM EXPERIMENT TO THAT OF PATEL

Station Number	Δ	C_f/C_f Patel	
		Mean Value	Standard Deviation
2	-.00203	.815	.050
3	-.00041	.719	.046
4	+.00188	.933	.047
5A	+.00226	1.091	.030
6	+.00184	1.223	.039
7	+.00118	1.123	.040

VI. Conclusions

The measurement of boundary layer skin friction can be determined by various means. The velocity profile methods give very reliable data when the boundary layer is large enough to obtain a sufficient number of data points to get a logarithmic region. A pressure gradient that is not too strong, i.e., within Patel's limits, has little effect on the profile shape and the calculation of the skin friction coefficient.

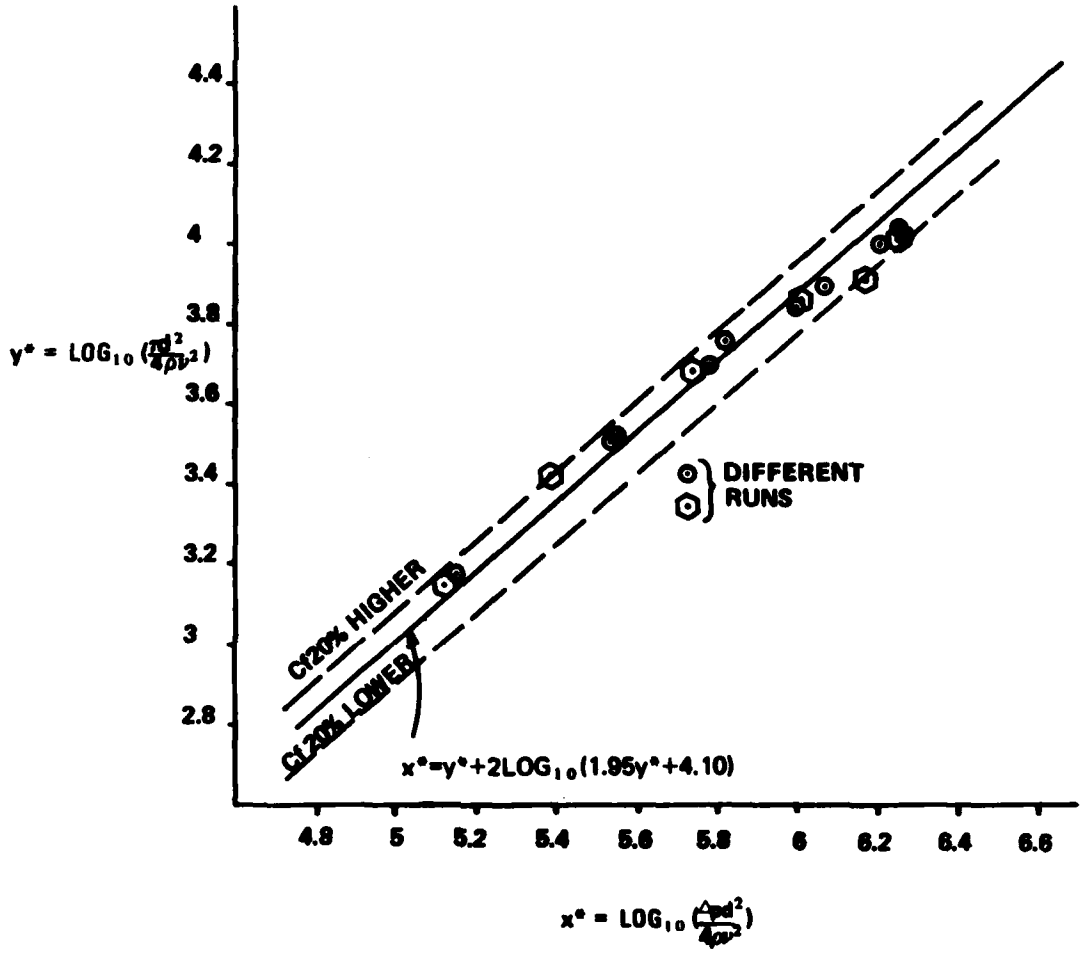

a. PROBE 1

Figure 14. Preston Tube Calibration

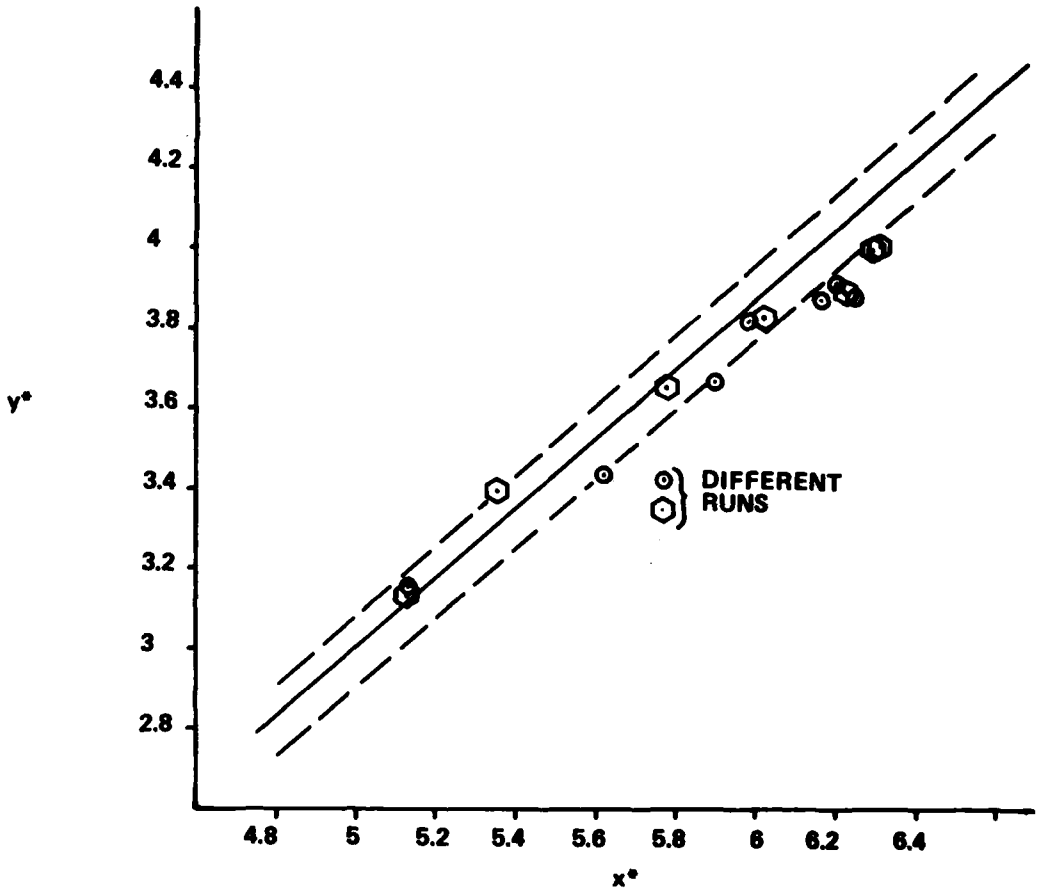

b. PROBE 2

FIGURE 14 (CONT.)

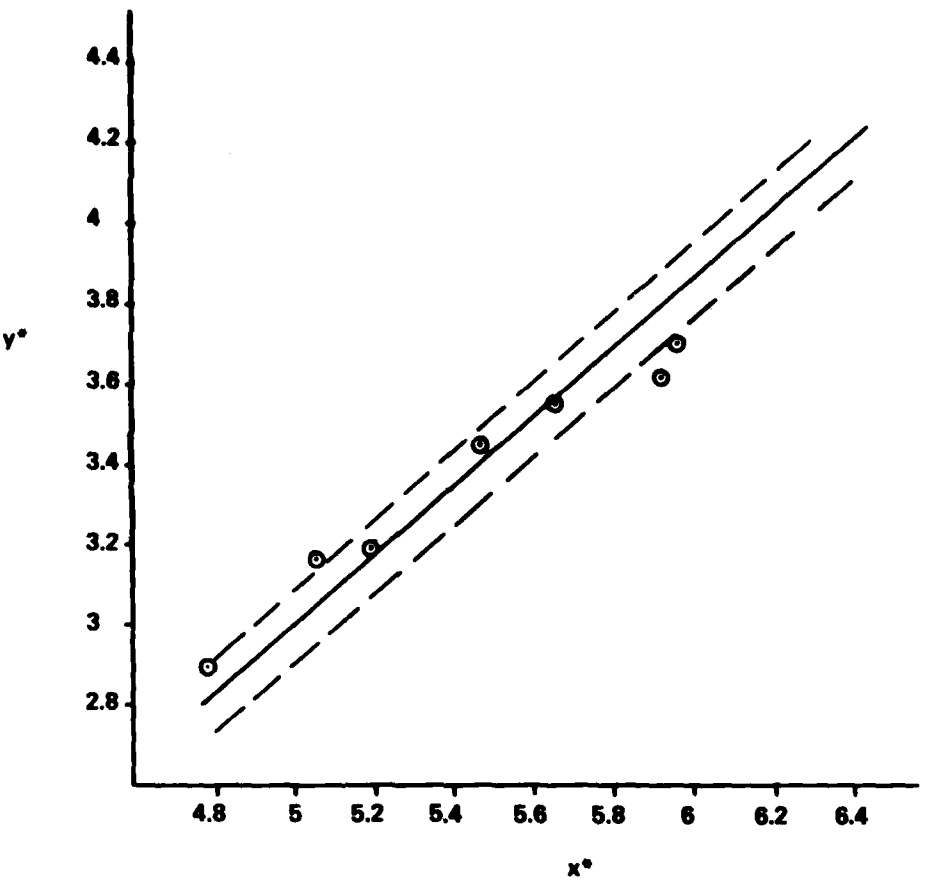

c. PROBE 3

FIGURE 14 (CONT.)

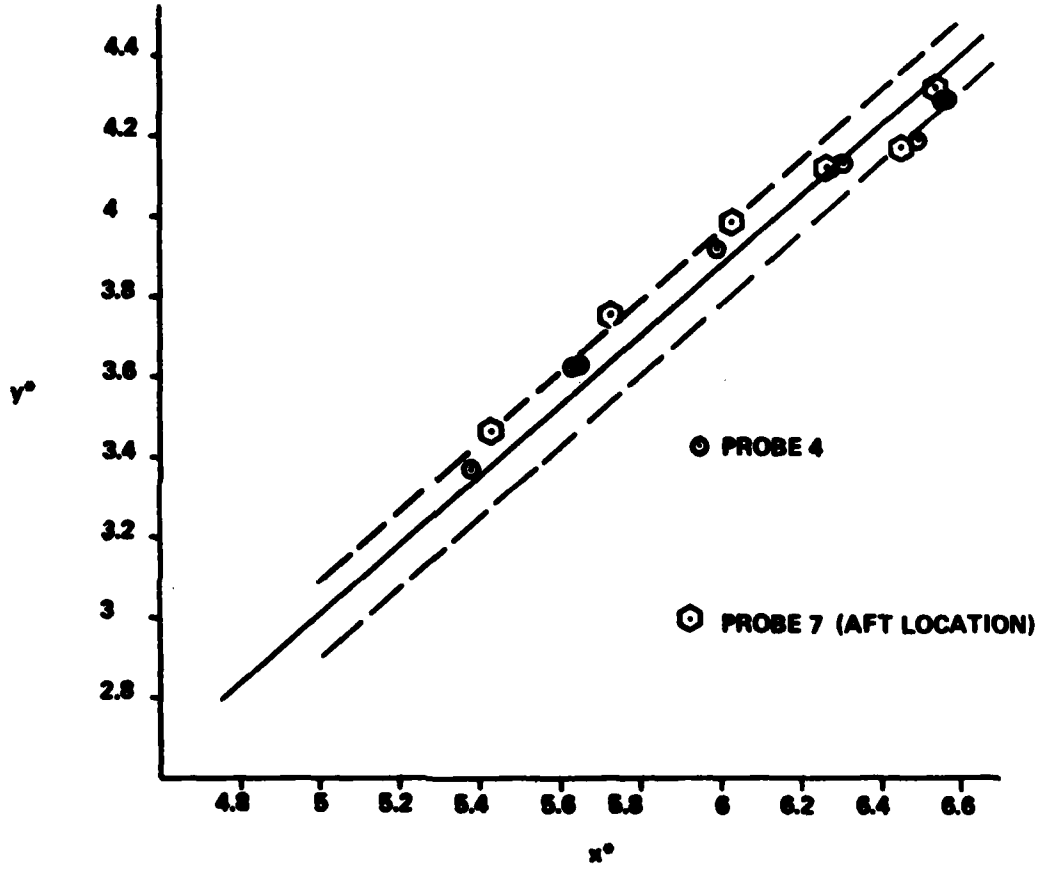

d. PROBES 4 AND 7

FIGURE 14 (CONT.)

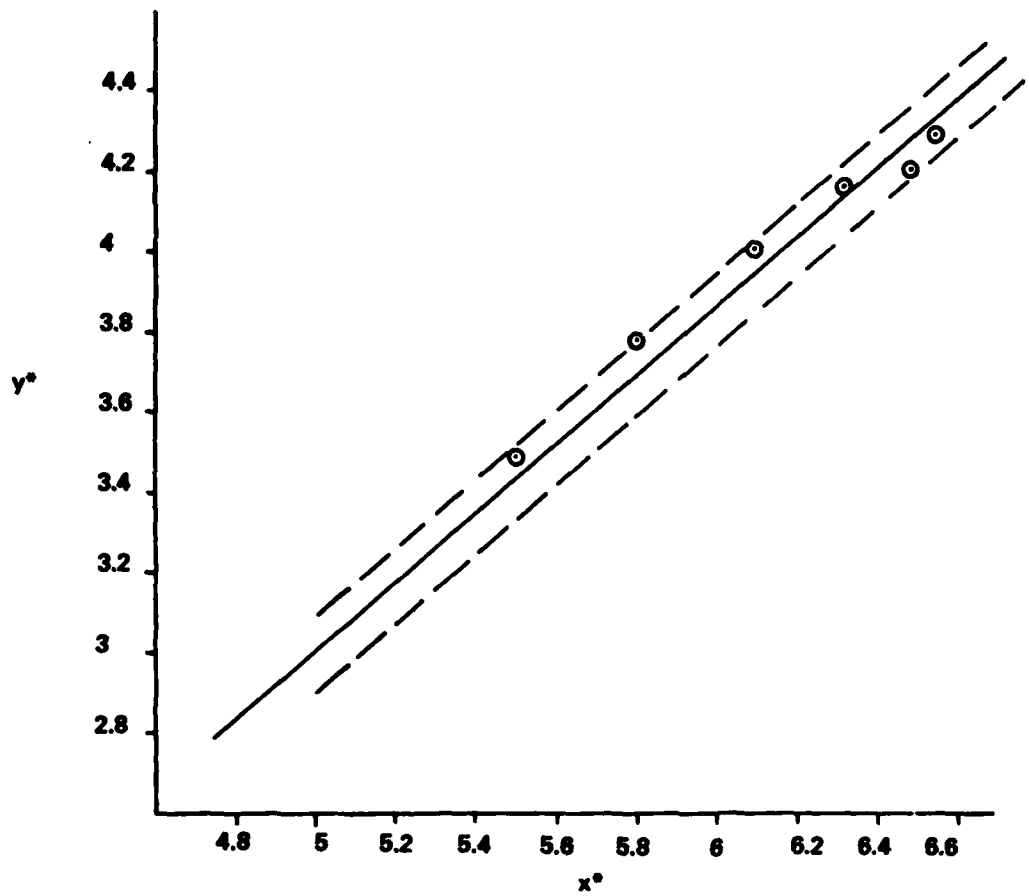

e. PROBE 5

FIGURE 14 (CONT.)

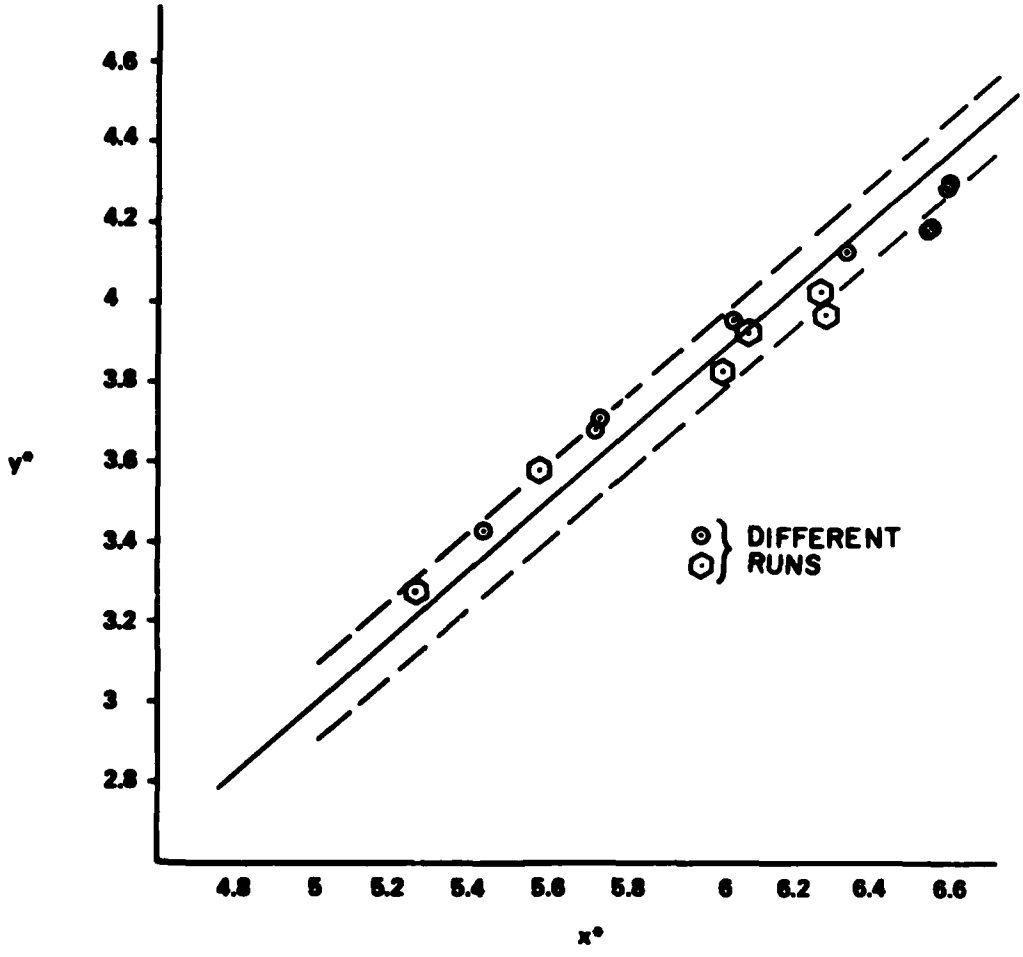

f. PROBE 6

FIGURE 14 (CONT.)

The use of Preston tubes adds more uncertainty to the measurement of the skin friction coefficient. The effect of pressure gradient seems to be more important in this experiment than in previous experiments. The direction of the deviation from previous experiments is related to sign of the pressure gradient, i.e., whether it is favorable or unfavorable; however, the magnitude of the deviation is not related to the magnitude of the pressure gradient (or at least the magnitude of the non-dimensional pressure gradient).

Acknowledgements

The author would like to thank Dr. G. David Huffman, who suggested the project and did some of the initial design; Mr. Fred Jayne, who constructed the water channel; and Mr. Don Puterbaugh, who constructed the Preston tubes. Some of the data and analysis of the profile data were performed by Cadets Knowlton, Moore, and Quinn as part of an Aero 450 project.

References

1. Winter, K. G. "An Outline of the Techniques Available for the Measurement of Skin Friction in Turbulent Boundary Layers." In Progress in Aerospace Science. Vol. 18, 1-57. Edited by J. A. Bagley and P. J. Finley. Oxford: Pergamon Press, 1977.

2. Brown, K. C. and P. N. Joubert. "Measurement of Skin Friction in Turbulent Boundary Layers with Adverse Pressure Gradients." Journal of Fluid Mechanics, Vol. 35, Part 4 (10 Mar 1969), 737-757.

3. Preston, J. H. "The Determination of Turbulent Skin Friction by Means of Pitot Tubes." Journal of the Royal Aeronautical Society, Vol. 58 (February 1954), 109-121.

4. Patel, V. C. "Calibration of the Preston Tube and Limitations on its Use in Pressure Gradients." Journal of Fluid Mechanics, Vol. 23, Part 1 (September 1965), 185-208.

5. Clauser, Francis H. "Turbulent Boundary Layers in Adverse Pressure Gradients." Journal of the Aeronautical Sciences, Vol. 21 (February 1954), 91-108.

6. Bradshaw, P. An Introduction to Turbulence and its Measurements. Oxford: Pergamon Press, 1971.

7. Huffman, G. David, C. D. Jones, and R. S. Bradley. "Optimization of Turbulence Models by Means of a Logical Search Algorithm." Applied Scientific Research (The Hague), Vol. 27 (April 1973), 321-334.

8. Thompson, B. G. J. A New Two Parameter Family of Mean Velocity Profiles for Incompressible Boundary Layers on Smooth Walls. ARC R&M 3463, 1965.

9. Galbraith, R. A. McD. and M. R. Mead. "Eddy Viscosity and Mixing Length from Measured Boundary Layer Developments." Aeronautical Quarterly, Vol. 26 (May 1975), 133-154.

CALIBRATION OF TRI-AXIAL HOT WIRE PROBES USING A NUMERICAL SEARCH ALGORITHM

G. David Huffman*

Abstract

Calibration of tri-axial hot wire probes is both a tedious and a time-consuming task. Five calibration constants per wire, i.e., fifteen constants per probe, must be determined. Three constants are related to the wire aerothermodynamics and two, to the velocity direction. An automated calibration procedure has been developed which employs two data sets - one at variable velocity and fixed angle and a second at fixed velocity and variable angle - and a numerical search algorithm. This technique yields precise calibrations and a one-to-two order of magnitude reduction in calibration times.

I. Introduction

Many naturally occurring and man-made flowfields are three-dimensional. Studies of atmospheric turbulence and measurements within turbomachines both exhibit three-dimensional characteristics. Three-dimensional velocity measurements are far from routine but have been carried out with hot wire anemometers, various flow direction probes using pressure sensors, and, to a lesser extent, laser Doppler velocimeters. Utilization and/or calibration of these devices is both a complex and time-consuming process. An innovative calibration technique for tri-axial hot wire and/or hot film probes has been developed and is described in the ensuing paper. The calibration procedures are fully automated and reduce the time required in the calibration process by one-to-two orders of magnitude.

II. Tri-axial Hot Wire Probe

The calibration procedures described herein were developed in conjunction with a study of atmospheric ozone transport mechanisms (Ref. 1). Three-dimensional velocity measurements were carried out using both stationary towers and aircraft. A commercially available probe, DISA Model 55P91, satisfied the measurement requirements and was used throughout the test program. The probe itself (see Figures 1 and 2) uses three hot wires, each orthogonal to one another. The wire length is 3.4 mm with an active length of 1.25 mm. The wire diameter is 5 μm, yielding a sensor ℓ/d of 250. The active wire portions are contained within a sphere of 3 mm diameter. At least one wire length separates the sensors, and according to Jerome, et al. (Ref. 2), this separation should preclude interaction of the heated wake of one wire with its neighbors.

III. Probe Geometric Considerations

The calibration of a tri-axial probe or the measurement of an unknown three-dimensional flow field is predicated upon eventually linking the measured flow field to

*Professor of Applied Mathematics and Director, Fluid Dynamics Laboratory, Purdue University, IN. Formerly Distinguished Visiting Professor, USAF Academy, CO.

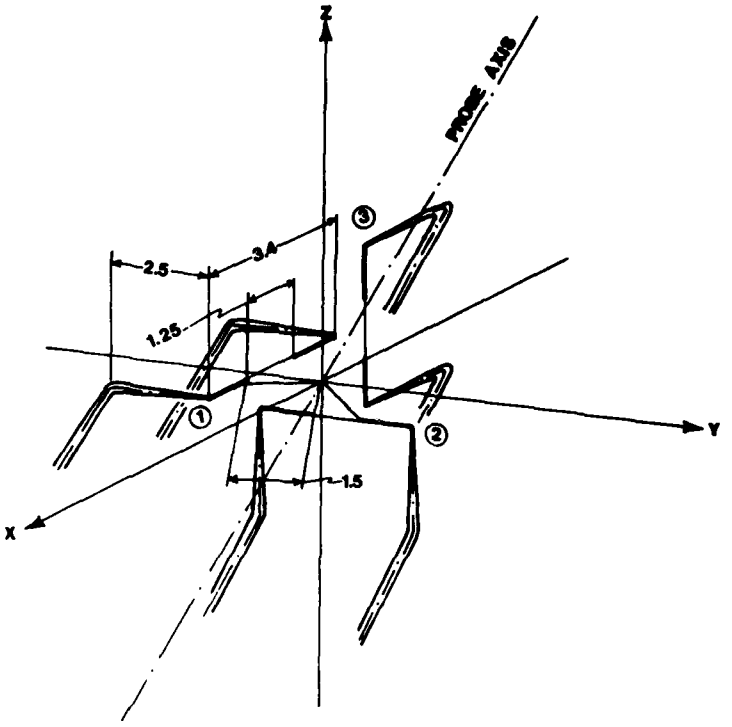

Figure 1. Schematic Diagram of the Tri-axial Hot Wire Probe (All Dimensions in mm)

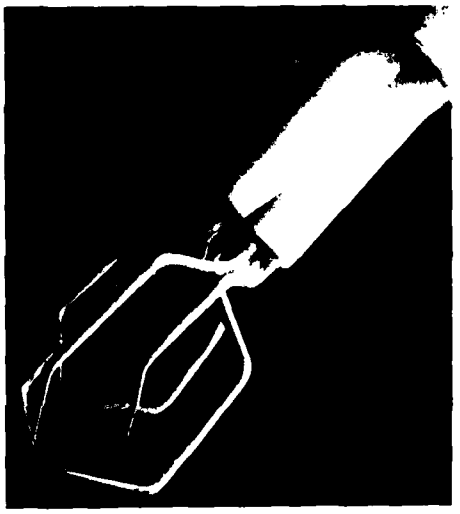

Figure 2. The Tri-axial Hot Wire Probe Installed in the Calibration Mechanism

Figure 3. Photograph of the Probe Calibration System Showing the Attack and Side-Slip Angles

velocity components which are normal and tangential to the wires themselves. In the calibration mode, we can write a known velocity field, W_j, in terms of a velocity field referenced to the probe axis, U_k, by means of

$$U_\ell = c_{kj} W_j \quad , \tag{1}$$

where c_{kj} denotes a transformation matrix,

$$c_{kj} = \begin{Bmatrix} \cos\alpha & 0 & -\sin\alpha \\ -\sin\alpha\sin\beta & \cos\beta & -\cos\alpha\sin\beta \\ \sin\alpha\cos\beta & \sin\beta & \cos\alpha\cos\beta \end{Bmatrix} \quad , \tag{2}$$

with a repeated subscript indicating a summation and α and β denoting the pitching and yawing or attack and side-slip angles as referenced to the calibration nozzle axis, Figure 3.

The wires themselves are rotated relative to the probe axis with the locations shown in Figure 4. Since the wires respond to normal and tangential velocities, the velocity field referenced to the probe axis, i.e., U_k, must be further redefined in terms of sensor components and

$$U_k = d_{kj} V_j \quad , \tag{3}$$

where V_j denotes the velocities in a wire-based coordinate system and

$$d_{kj} = \begin{Bmatrix} \cos45^\circ & 0 & -\sin45^\circ \\ -\sin35.3^\circ\sin45^\circ & \cos35.3^\circ & -\sin35.3^\circ\cos45^\circ \\ \cos35.3^\circ\sin45^\circ & \sin35.3^\circ & \cos35.3^\circ\sin45^\circ \end{Bmatrix} \quad . \tag{4}$$

Eqn (3) can be inverted, yielding V_j in terms of U_k.

The wires do not respond in a like manner to both normal and tangential velocities, e.g., see Champagne, et al. (Ref. 3), Tutu and Chevray (Ref. 4), and Moussa and Eskinazi (Ref. 5). As a result, an effective wire coolant velocity must be defined and

$$V_{e_1}^2 = q_1^2 V_x^2 + V_y^2 + r_1^2 V_z^2 \quad , \tag{5}$$

where the subscript 1 denotes wire number 1 of Figure 1. For this wire, V_x denotes the velocity component parallel or tangential to the wire; V_y, the component normal to the wire in the plane of the prongs; and V_z, the component normal both to the wire and to the prongs. The coefficients q_1 and r_1 are the angularity coefficients, with q expected to be fairly small and r of order one. Jorgensen (Ref. 6) has determined values for these quantities for two wire probes. We can generalize Eqn (5) as

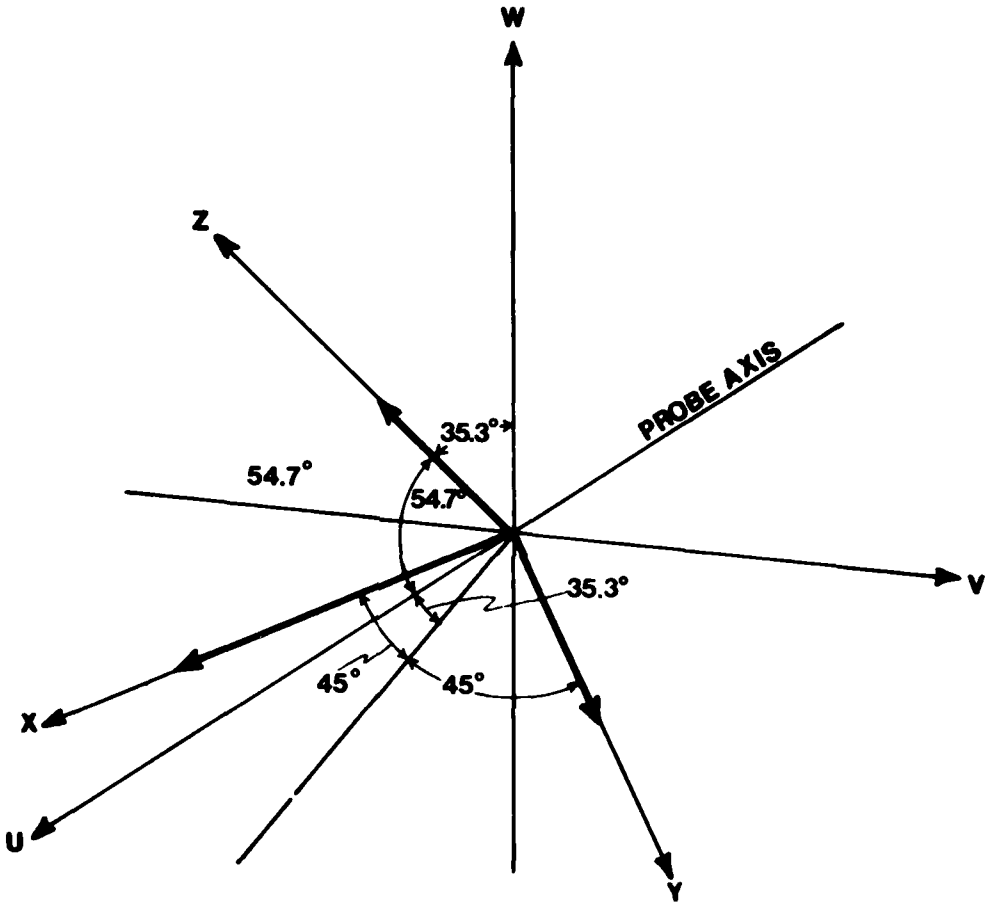

Figure 4. Wire and Probe-Axis Coordinate System

$$V_{e_i}^2 = e_{ij} V_j^2 \quad , \tag{6}$$

with

$$e_{ij} = \begin{Bmatrix} q_1^2 & 1 & r_1^2 \\ r_2^2 & q_2^2 & 1 \\ 1 & r_3^2 & q_3^2 \end{Bmatrix} \quad , \tag{7}$$

and q_i^2 and r_i^2 must be determined in the calibration process. Note that the wires respond to V_{e_i}; thus, this is the velocity actually sensed by the wires. In the calibration process, the known velocity, W_k, must be related to V_{e_i}, and in the measurement process, V_{e_i} must be related to U_j.

IV. Wire Aerothermodynamics

Collis and Williams (Ref. 7) have shown that the wire heat transfer can be related to the gas temperature and velocity via

$$Nu = \left(\frac{T_m}{T_a}\right)^{0.17} (A+BRe^n) \quad , \tag{8}$$

where Nu denotes the Nusselt number, $h_f/[\pi k_m \ell (T_w - T_a)]$; Re the Reynolds number, $V_e d_w \rho_m / M_m$; T_m the mean temperature, $1/2(T_w + T_a)$; and k_m, ρ_m, and μ_m the fluid thermal conductivity, density, and viscosity, respectively, all evaluated at T_m. Dimensions d and ℓ denote the wire diameter and length, with the subscript, w, denoting the wire and a, the ambient condition.

A series of ensuing authors, e.g., Koch and Gartshore (Ref. 8), Bradbury and Castro (Ref. 9), and Davis and Davies (Ref. 10), have suggested minor changes in Eqn (8), with perhaps the most meaningful generalization offered by Koch and Gartshore, i.e.,

$$Nu = \left(\frac{T_m}{T_a}\right)^m (A+BRe^n) \quad , \tag{9}$$

with the exponent, m, shown to be a function of the wire ℓ/d.

The wire will respond to temperature, velocity, and density variations. For flows without substantial temperature changes, we can adopt m directly from previous authors and we can assume A, B, and n to be independent of temperature. Since the tri-axial probe contains three wires, we can write Eqn (9) as

$$Nu_i = \left(\frac{T_m}{T_a}\right)^m \left(A_i + B_i Re_i^{n_i}\right) \quad , \tag{10}$$

where nine separate calibration constants must be determined, i.e., A_i, B_i, and n_i, with $i = 1$, 2, and 3.

V. Calibration Procedures

The calibration constants consist of the three coefficients of the Nusselt number - Reynolds number relationship and the two angularity coefficients of Eqn (5). Since these constants must be determined for each wire, a grand total of 15 coefficients must be specified, i.e., A_i, B_i, n_i, q_i, and r_i, for $i = 1$, 2, and 3. This is a formidable task which Huffman et al. (Ref. 11) have undertaken, using a logical search algorithm.

An optimization function is defined as

$$er_i^2 = \sum_{j=1}^{J} \left\{ \left(\frac{T_{m_i}}{T_a}\right)^m \left[A_i + B_i (Re_i)_j^{n_i}\right] - (Nu_i)_j \right\}^2 \Big/ \left[(Nu_i)_j\right]^2 \quad , \tag{11}$$

where the subscript, i, denotes the wire number and j, the data point. Note that, in the calibration process, T_a, T_{m_i}, Re_i and Nu_i are known, provided q_i and r_i are specified. Coefficients q_i and r_i enter the determination of V_{e_i}, which is used in computing Re_i. The averaged error between the calibration equation and the measured point is

$$er_i = \sqrt{er_i^2}/J = \phi(A_i, B_i, n_i, q_i, r_i) \quad , \tag{12}$$

which is a function of the calibration constants.

The calibration constants are divided into two groups: A_i, B_i, and n_i, and q_i and r_i. A series of variable velocity, constant angle (i.e., $\alpha = \beta = 0$) calibrations are carried out and the error is defined as

$$er_{v_i} = \phi_v(A_i, B_i, n_i) \tag{13}$$

with q_i and r_i specified. Constants A_i, B_i, and n_i are computed using the logical search algorithm, so that $er_{v_i} \to 0$. Following this computation, a second series of calibration values is generated with constant velocity and variable values of α and β. The error is now defined as

$$er_{\alpha_i} = \phi_\alpha(q_i, r_i) \quad , \tag{14}$$

with A_i, B_i, and n_i determined from Eqn (13). Again employing the logical search algorithm, we can compute q_i and r_i such that $er_{\alpha_i} \rightarrow 0$. With q_i and r_i known, we can repeat the optimization process of Eqn (14) and determine a new series of A_i, B_i, n_i values. Coefficients q_i and r_i are computed in a like manner and the process continued until successive coefficient values agree to an acceptable level of accuracy.

VI. Calibration Results

The calibration results appear in Table 1 and in Figures 5 through 10. A review of these indicates that the angular results - as manifest by the er_α and er_v values - show considerably more scatter than the variable velocity calibrations. This is due to a number of potential causes, three of which are

(1) Resolution of the α values to $\pm$ 0.1° and the β values of $\pm$ 0.5°.

(2) Impact of wire misalignment on q_i and r_i rather than A_i, B_i, and n_i.

(3) Greater uncertainty in Eqns (6) and (7) than in Eqn (10).

Even though er_α exceeds er_v, both values are small, with er_v about 0.6% and er_α values of around 2%.

As a note in passing, the calibration procedure is fully automated with velocities determined from pressure measurements which are digitized and transferred directly to computer buffer storage. The flow angles α and β are dealt with in the same manner. The anemometer outputs are likewise digitized and the data sets converted to Nusselt and Reynolds numbers. The data base is then used to generate the calibration coefficients as previously described.

VII. Conclusions

A calibration procedure for tri-axial hot wire probes has been developed which employs a numerical search algorithm. This technique yields extremely precise calibrations with a one-to-two order of magnitude reduction in calibration times.

VIII. Acknowledgement

The work reported herein was partially supported by DISA Electronics and the Environmental Activities Staff of the General Motors Corporation.

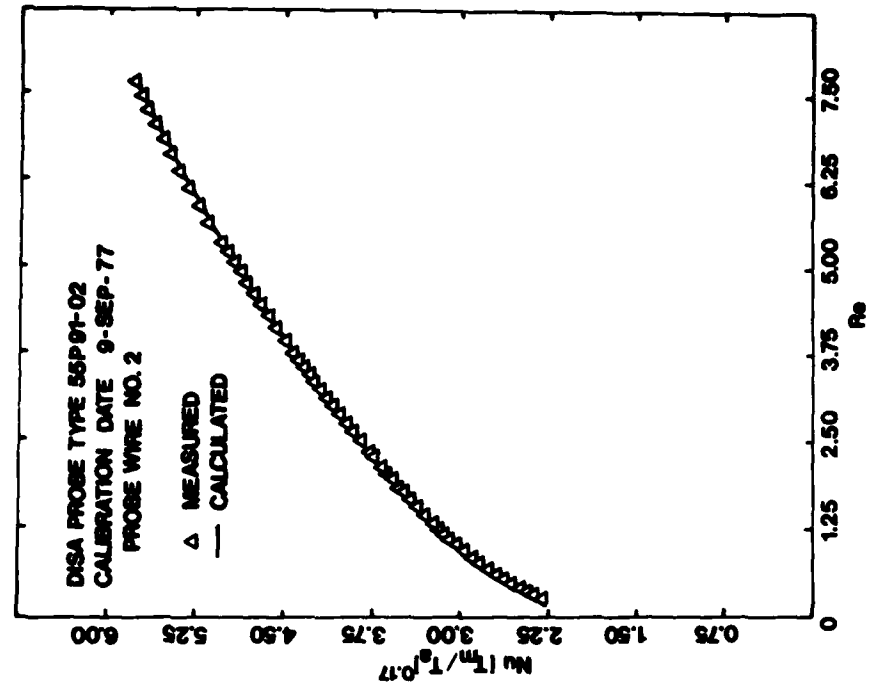

Figure 6. Calibration Results for Wire 2 ($\alpha = \beta = 0$)

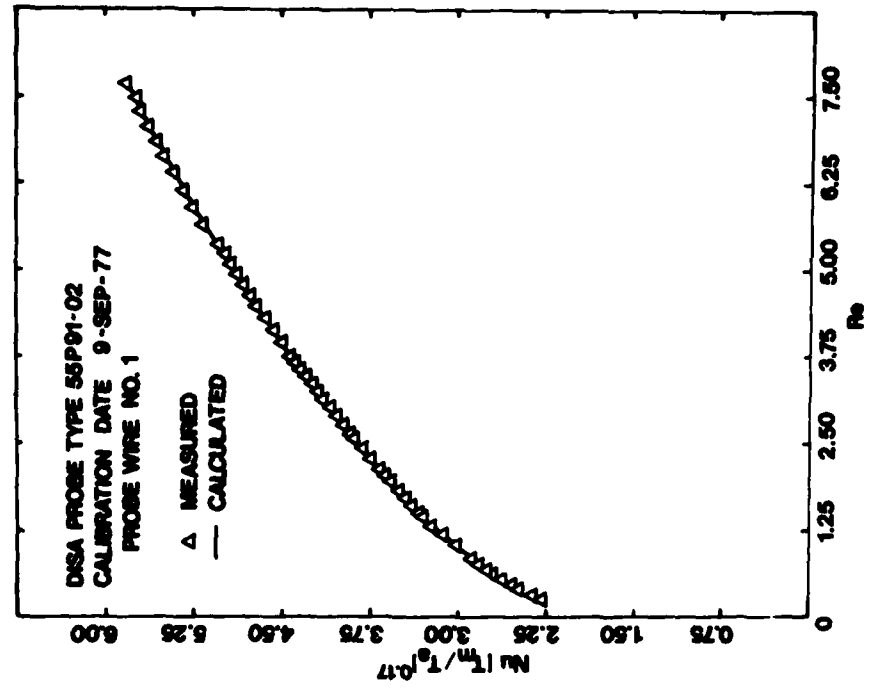

Figure 5. Calibration Results for Wire 1 ($\alpha = \beta = 0$)

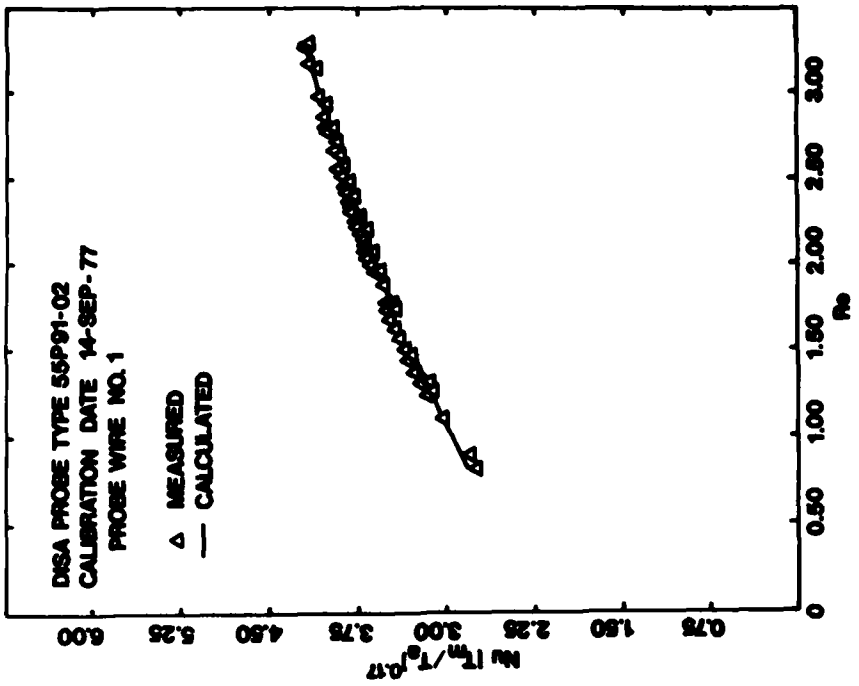

Figure 8. Calibration Results for Wire 1

(N_1 = constant; $-45^\circ \leq \alpha \geq +45^\circ$; $0^\circ \leq \beta \geq 45^\circ$)

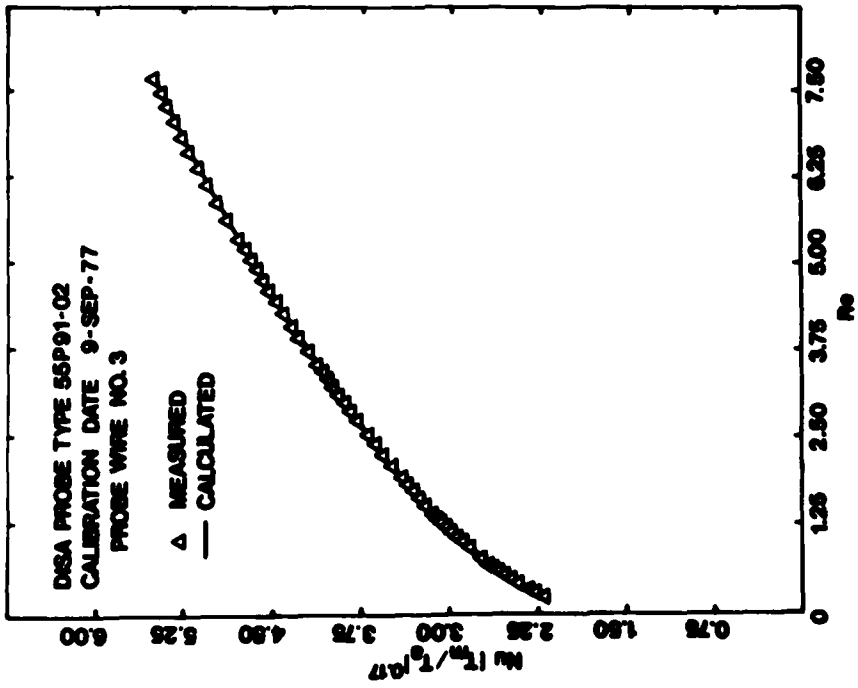

Figure 7. Calibration Results for Wire 3 ($\alpha = \beta = 0$)

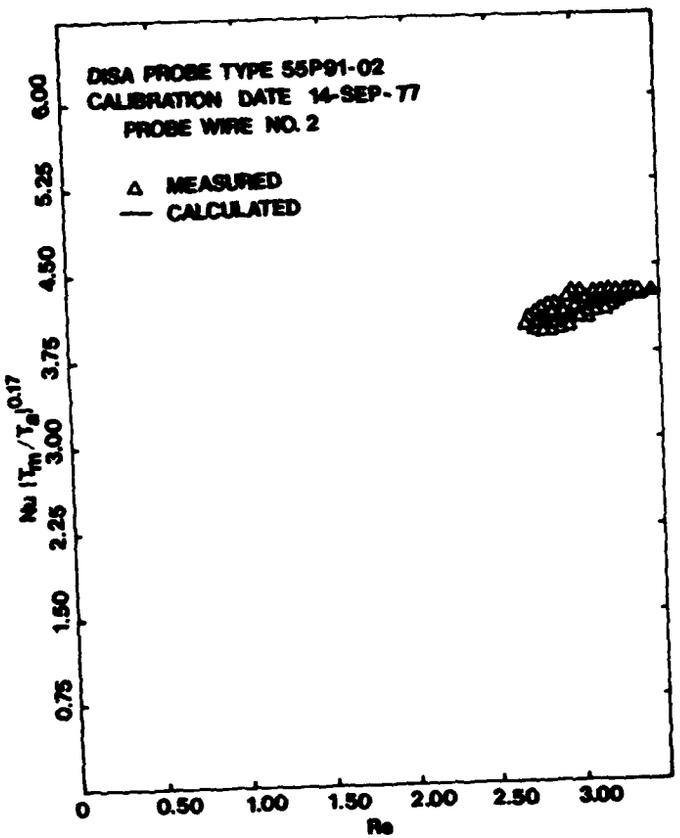

Figure 9. Calibration Results for Wire 2

(W_1 = constant; $-45^\circ \leq \alpha \geq +45^\circ$; $0^\circ \leq \beta \geq 45^\circ$)

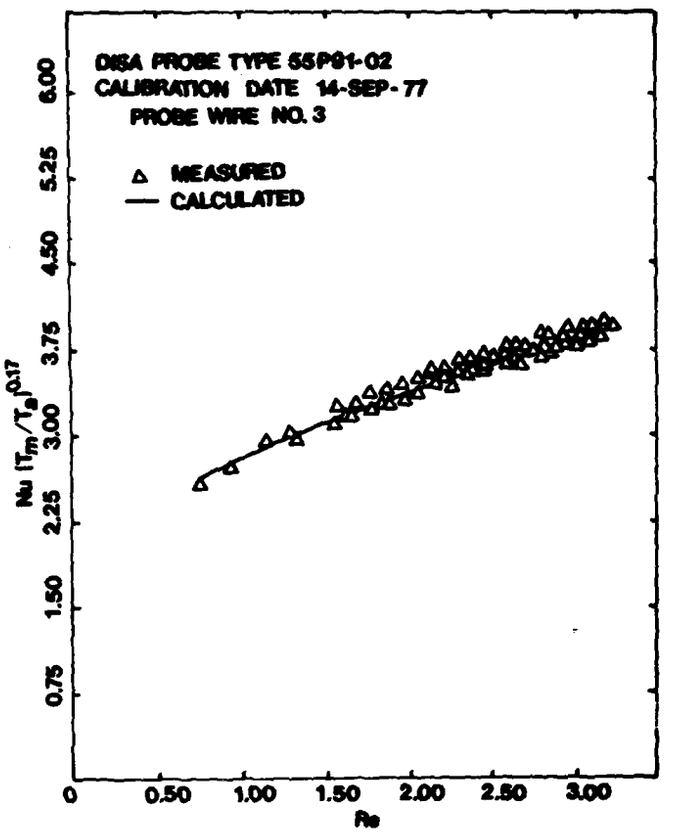

Figure 10. Calibration Results for Wire 3

(W_1 = constant; $-45^\circ \leq \alpha \geq +45^\circ$; $0^\circ \leq \beta \geq 45^\circ$)

Table 1

CALIBRATION COEFFICIENTS FOR HOT WIRE PROBES

Probe Designation	DISA Probe 55P91-01		
Wire Number	1	2	3
A	1.42	2.09	2.11
B	1.10	1.54	1.56
n	0.60	0.57	0.57
q	0.34	0	0
r	1.15	1.00	1.02
er_v, %	0.5	0.5	0.5
er_α, %	3.5	1.7	0.8
Probe Designation	**DISA Probe 55P91-02**		
Wire Number	1	2	3
A	1.64	1.70	1.74
B	1.18	1.27	1.25
n	0.58	0.58	0.58
q	0.19	0.20	0.56
r	1.36	1.12	1.18
er_v, %	0.3	0.3	0.4
er_α, %	5.0	1.0	1.7
Probe Designation	**DISA Probe 55P91-03**		
Wire Number	1	2	33
A	1.52	1.34	1.61
B	1.23	1.03	1.16
n	0.55	0.56	0.59
q	0.10	0.04	0.19
r	1.23	1.14	1.16
er_v, %	0.9	0.9	1.2
er_α, %	2.3	1.3	1.6

References

1. Huffman, G. D. "Ozone Transport Mechanisms as Determined from Real-Time Velocity, Temperature and Ozone Measurements." Paper in preparation, 1979.

2. Jerome, F. E., et al. "Experimental Study of the Thermal Wake Interference Between Closely Spaced Wires of an X-Type Hot Wire Probe." Aero Quarterly, Vol. 22 (1971), 119-126.

3. Champagne, F. H., et al. "Turbulence Measurements with Inclined Hot Wires." Journal of Fluid Mechanics, Vol. 28, Part 1 (1967), 153-175.

4. Tutu, N. K. and Rene Chevray. "Cross-wire Anemometry in High Intensity Turbulence." Journal of Fluid Mechanics, Vol. 71 (1975), 785-800.

5. Moussa, Z. M. and S. Eskinazi. "Directional Mean Flow Measurements Using a Single Inclined Hot Wire." Physics of Fluids, Vol. 18 (1975), 298-305.

6. Jorgensen, F. E. "Directional Sensitivity of Wire and Fiber-film Probes." DISA Information, No. 11 (1971), 31-37.

7. Collis, D. C. and M. J. Williams. "Two-Dimensional Convection from Heated Wires at Low Reynolds Numbers." Journal of Fluid Mechanics, Vol. 6 (1959), 357-384.

8. Koch, F. A. and I. S. Gartshore. "Temperature Effects on Hot Wire Anemometer Calibrations." Journal of Physics E (Scientific Instrumentation), Vol. 5 (1972), 77-86.

9. Bradbury, L. J. S. and I. P. Castro. "Some Comments on Heat Transfer Laws for Fine Wires." Journal of Fluid Mechanics, Vol. 51 (1972), 487-495.

10. Davis, M. R. and P.O.A.L. Davies. "Factors Influencing the Heat Transfer from Cylindrical Anemometer Probes." International Journal of Heat and Mass Transfer, Vol. 15 (1972), 1659-1677.

11. Huffman, G. D., et al. "Optimization of Turbulence Models by Means of a Logical Search Algorithm." Applied Scientific Research, Vol. 27 (1973), 321-334.

FLOW QUALITY IMPROVEMENTS IN THE USAFA TRISONIC TUNNEL

M. W. Davis*, S. E. Icardi**, R. W. Gallington***, and J. A. Wright****

Abstract

This paper discusses a modification of the inlet valve and diffuser section of the USAF Academy Supersonic Wind Tunnel accomplished to reduce large scale pressure fluctuations. We examine here the rationale and design considerations as well as an evaluation of the effectiveness of the modifications. Pressure oscillations in the stilling chamber and test section are presented both prior to and after the modification. These pressure fluctuations are presented both in RMS and Power Spectral Density plots so that overall levels and specific frequencies of the fluctuations may be examined. The effect of the modification has been to reduce the overall pressure fluctuations by a factor of approximately three.

I. Introduction

A. Tunnel Description

The US Air Force Academy Trisonic Wind Tunnel is a blow-down facility exhausting to atmosphere with a one-foot square test section. Fixed interchangeable nozzle blocks establish the Mach number in increments between M = 1.44 and M = 4.38. For Mach numbers between 0.14 and 1.33 a pair of convergent nozzle blocks is used with a porous-walled transonic test section, the flow being controlled by a second throat located downstream of the test section. Convergent-divergent nozzle block pairs are used with the porous-walled test section to achieve M = 1.44 and M = 1.67.

With these mechanical arrangements and considering the static and total pressure limitations the tunnel operating range is roughly $0.14 \leq M \leq 4.38$ and $6 \times 10^6 \leq R_e/ft \leq 30 \times 10^6$. The total temperature is maintained near room temperature by a heat sink in one of six high-pressure air storage tanks.

The transonic test section has variable porosity walls on all four sides. The side wall angle is also variable. The porosity is adjustable between 0% and 7.32% by the sliding action of two similarly drilled plates. The circular holes are at an angle of 30 degrees to the plate surface. Pressure fluctuations, to be discussed later, are

---

*Engineer, Sverdrup/ARO, Inc.
**Engineer, Westinghouse Electric Corp., formerly Major, USAF, Assistant Professor of Aeronautics, DFAN
***Lt Col, USAF, Tenure Associate Professor of Aeronautics, DFAN
****Major, USAF, Assistant Professor of Aeronautics, DFAN

Editor's Note: Presented at the 51st meeting of the Supersonic Tunnel Association at Lockheed Aircraft Corp., Burbank, CA, 10-11 April 1979.

especially pronounced around M = 1 and are partially due to edge tones from these holes. The pressure in the cabin around the transonic test section is established by the flow through the porous walls and into the downstream diffuser which has an adjustable inlet area - generally equal to or greater than the test section exit area. A rough description of the major features is given in Figure 1.

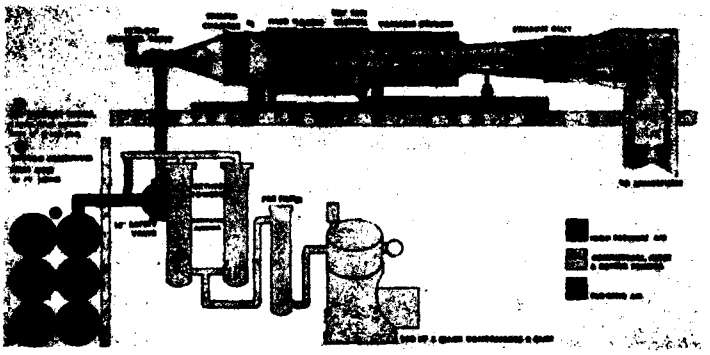

Figure 1. Schematic of USAF Academy Trisonic Wind Tunnel Less Transonic Test Section

A control valve is located in a right-angle turn at the entrance to the wide angle diffuser. The valve was extensively modified to achieve the improvements in the flow quality reported here.

The wide-angle diffuser - with a half angle of 18 degrees - was the designer's initial choice and has required a number of improvements over the years. The first fix was a conical "core breaker" installed to prevent destruction of the stilling chamber screens by the jet issuing from the control valve. The second major flow improvement modification, described herein, was undertaken as a joint effort with the Arnold Engineering Development Center and their operating contractor Sverdrup/ARO, Inc.

B. Flow Disturbances

Although this tunnel had always been noisy in operation and there had always been some low-frequency oscillation in the force data, we did not become acutely aware of the seriousness of the disturbances until a test was made on a series of different bluff-body missile nose shapes over a large range of Mach numbers. During this test we observed fluctuating side forces of sufficient magnitude to seriously influence drag measurements through the small balance interaction terms. In fact, it was impossible to see the differences in drag due to nose shape on this series. The problem existed from the lowest (M = .14) through the highest (M = 4.38) Mach numbers although it was worst around M = 1. The axi-symmetric model was rotated 90 degrees to check for symmetry, verifying that the problem was side-to-side fluctuations in the tunnel and not

model construction. There was some concern that the angle-of-attack mechanism controlling the sting was mechanically loose and it was completely rebuilt with no effect. On these particular models the side force fluctuations indicated flow angle fluctuations of 2-4 degrees.

The next experiment was a wedge with a pressure transducer connected between holes on opposite surfaces. The apparent fluctuations in the horizontal plane were found to be considerably larger than those in the vertical plane.

All these experiments convinced us that something had to be done to improve the flow quality in the trisonic tunnel. As a bench mark to assess future improvements we recorded the RMS of the pressure fluctuations as a function of valve position at M = .97. The valve position is a logical independent variable because it is the only geometry change during a run. The four pressures selected were (1) total pressure in the stilling chamber; (2) pitot pressure in the test section; (3) static pressure at the front of the test section; and (4) static pressure at the rear of the test section. Figures 2 through 4 show these RMS pressure fluctuations and the resulting pressure coefficients. Before the tunnel modification the RMS of the fluctuations in pressure coefficient were about 7.9% maximum or about four times that in comparable tunnels (see Figure 5).

II. Modification Rationale and Design

A. Valve Modifications

The original valve for this tunnel was a sleeve control valve supplied by Hammel Dahl and is described by them as a "series 7000 Balanced Holo Plug" with a 6-inch stroke. From the cross-sectional view (Figure 6), one can see that the moving hollow cylinder control element (12.25" OD & 8.00" ID) requires a small actuator force for control movement since the pressure on the downstream force is vented to the upstream edge through the control rod spider. The geometry of the valve as originally supplied is illustrated in the upper left of Figure 6. From this geometry, we reasoned that the supersonic expansion zone after the conical sonic throat was very abrupt and consequently the terminal shock configuration would not only be highly oscillatory in nature but there could exist a bi-stable characteristic for a given valve pressure ratio. The amount of supersonic flow turning after the sonic surface would, of course, depend upon the ambient pressure inside the cylinder which could only adjust itself through "organ-pipe" reverberations from the back of the inner-cylinder cavity which would tend to amplify further any terminal shock oscillation. Also, a 0.8-inch rearward facing step at the valve exit followed by a 1/8-inch forward facing step at the diffuser entrance was not co.ducive to boundary layer stability for the terminal shock interaction zone, possibly leading to further pressure fluctuations. To counteract these valve terminal shock instabilities and diffuser entrance pressure fluctuations, we developed the

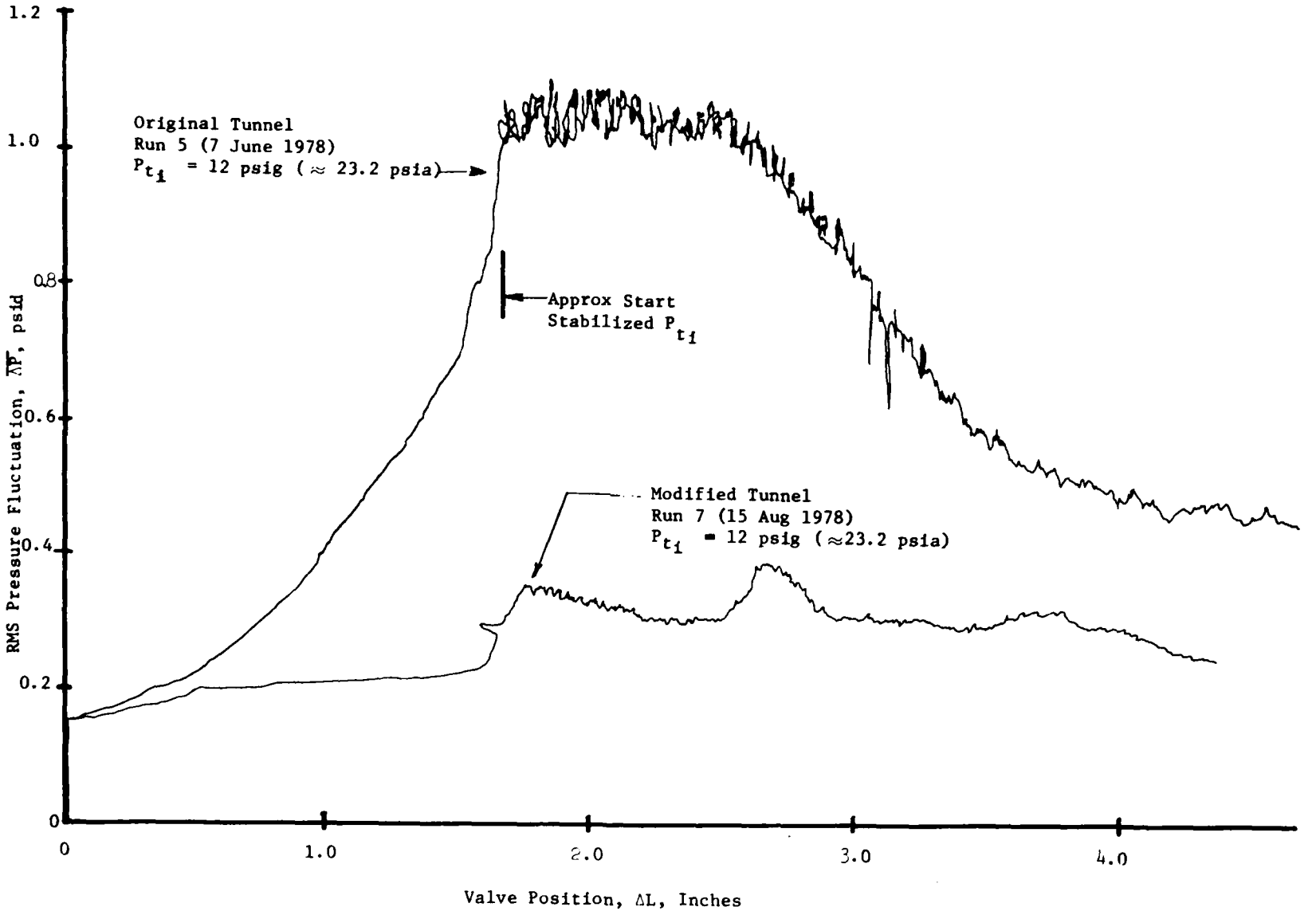

Figure 2. Typical Test Section Pitot Pressure Fluctuations for Full-Tank Run M ≅ 0.97, Before and After Modifications

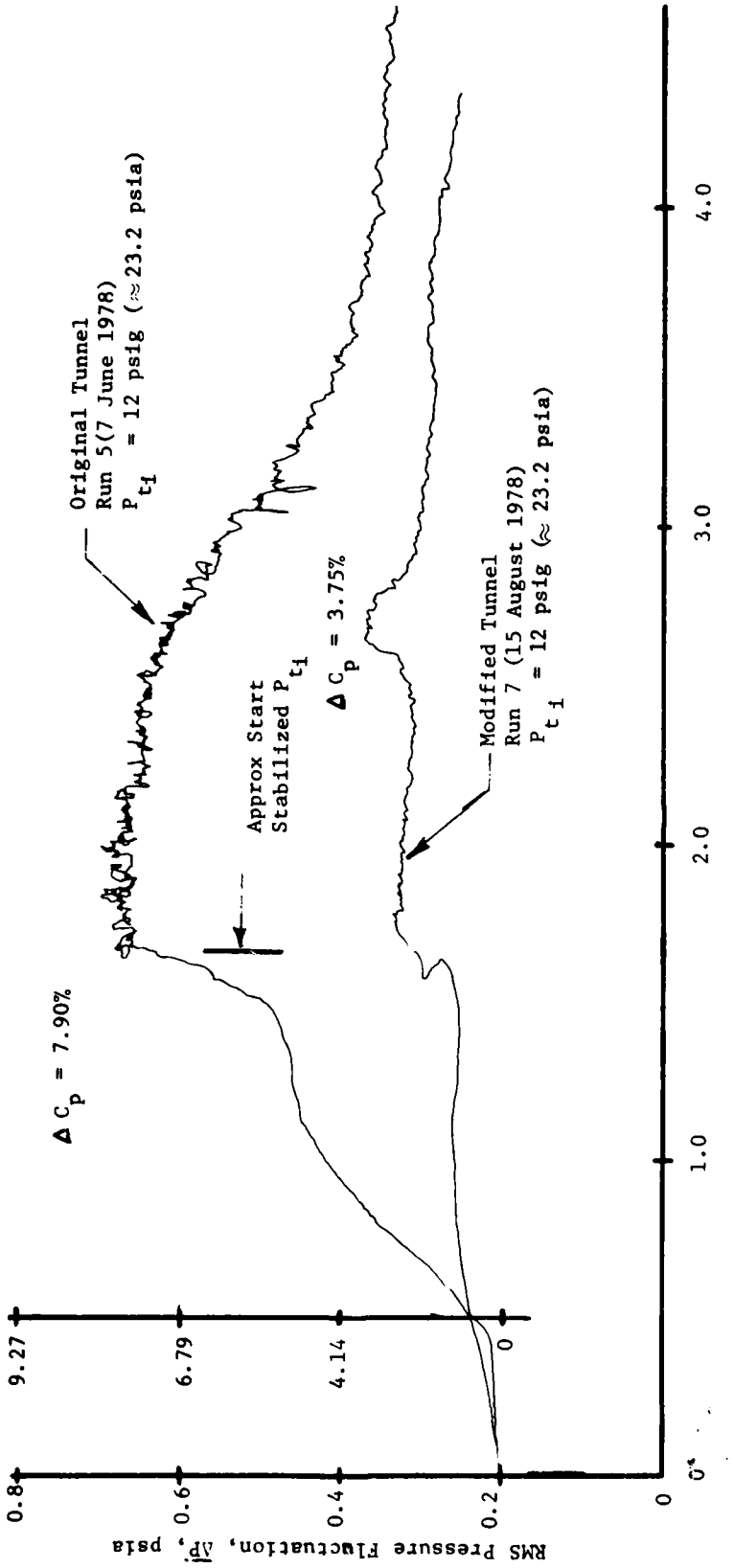

Figure 3. Typical Test Section Wall Static Pressure (Forward) Fluctuations for Full-Tank Run M ≅ 0.97, Before and After Modifications

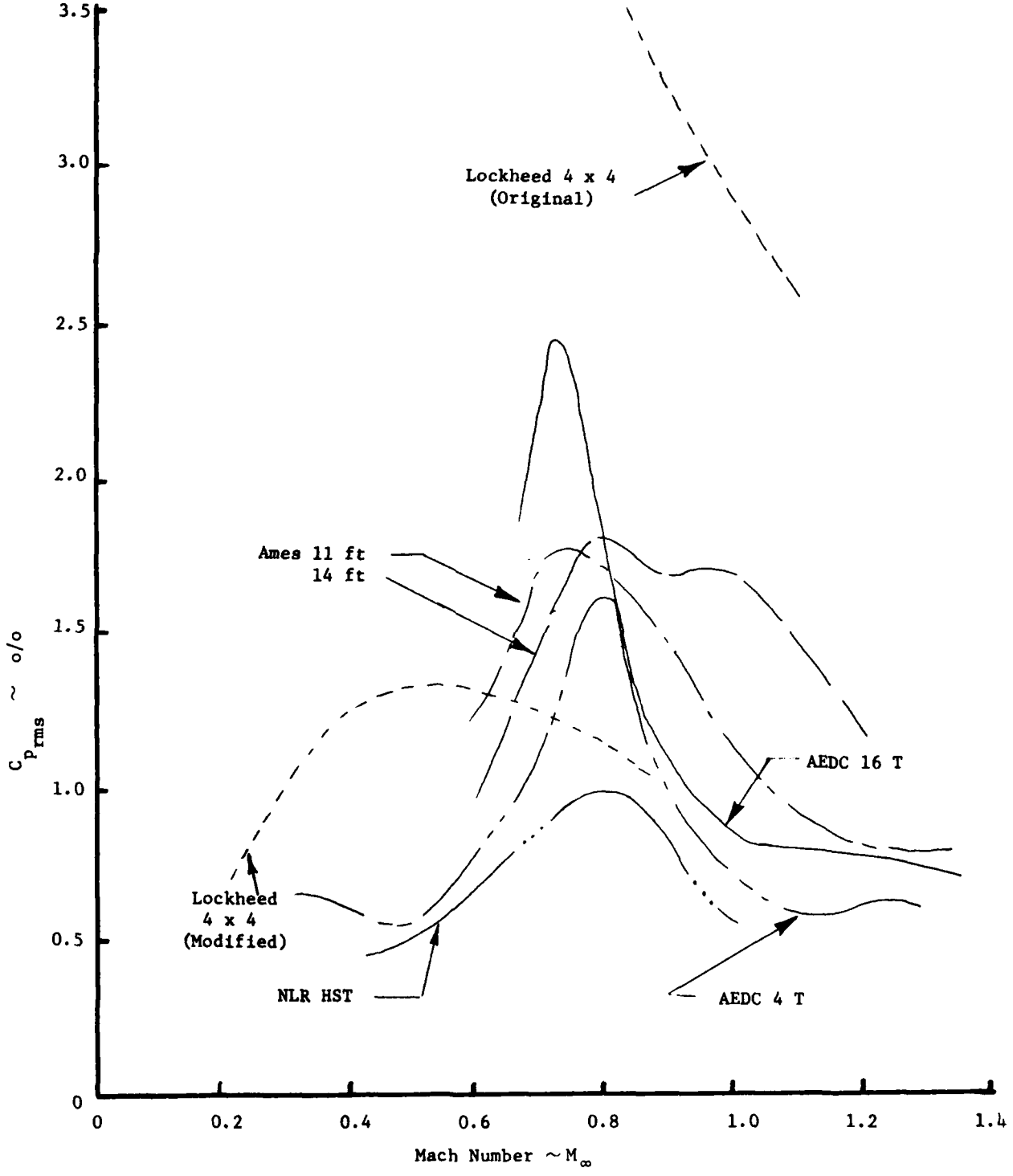

Figure 4. Comparison of Broadband Noise Levels in Several Tunnels

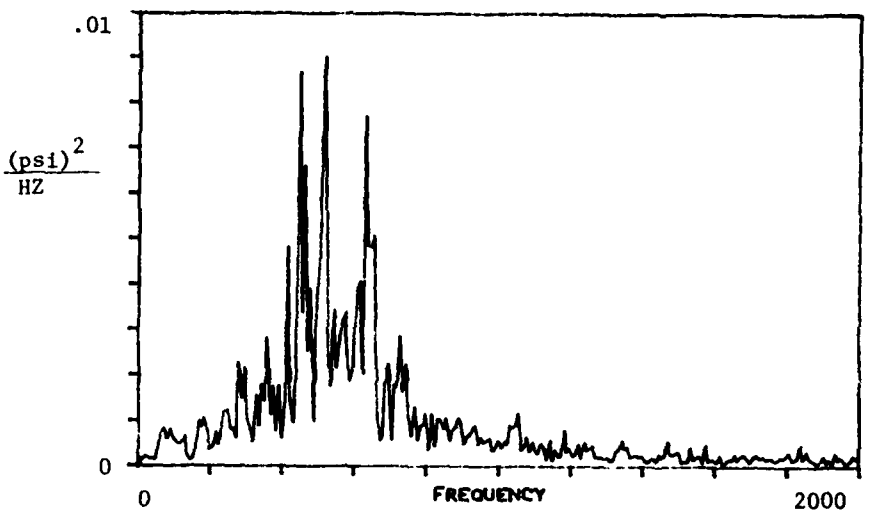

Pre-Modification Valve at 2.2 in.

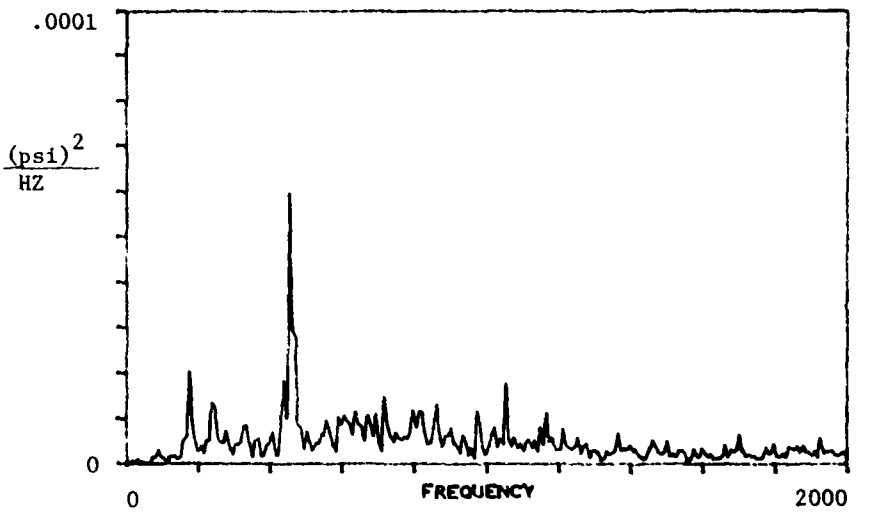

Post-Modification Valve at 2.2 in.

Figure 5. Power Spectral Density Analysis of Stilling Chamber Pressure Fluctuations

contoured plug shown in the lower left of Figure 6. The contour was calculated to keep the flow area approximately constant for the valve open case. The small cone at the end of the plug was added to provide a stable conical shock zone at the valve centerline and to start the flow into the desired expanding direction into the diffuser entrance. The successful use of a similar fixed cone and cruciform struts in the NAE 5-foot Tunnel (Ref. 1) also influenced this decision. The contour steps at the valve exit were faired over with the insert shown in the lower quarter-section of Figure 6, in the hope of providing further stabilizing influence on terminal shock oscillation or diffuser entrance pressure fluctuations.

One concern with the contoured plug valve modification was that a large unbalanced force could be developed that would overpower the existing actuator. After some study, a radius of 3.80 inches was selected as the location for eight 1/2-inch vent holes. The virtue of this decision was verified during shakedown by measuring the hydraulic pressure on each side of the actuator. From the indicated hydraulic pressures the net force on the actuator was calculated for several representative runs as shown in Figure 7. The initial plug vent location appears almost ideal, producing a small valve-closing force for most of the stroke in the event of hydraulic system failure.

Also of some concern in contouring the valve plug was that the effective flow area (or flow coefficient) might be significantly reduced. As previously mentioned, the plug contour was calculated to give constant flow area at the valve open position. The success of this process can be judged by examination of the valve stroke time history for near identical conditions (Figure 8) where a maximum run-time penalty of about 4.7 percent can be charged to the modifications. Also, by close examination of the valve position traces in Figure 4, one observes that the modified-valve trace has less high-frequency oscillation. This result, though not as conclusive as having a velocity pick-up on the actuator, indicates a significant reduction in the oscillatory forces acting on the valve control element.

B. Diffuser Modifications

An examination of the geometry of the existing "core-breaker" grid in the wide angle diffuser (upper right of Figure 6) as compared to the classical screened diffuser work of Schubauer and Spangenburg (Ref. 2), also led us to recommend extensive modifications to the wide angle diffuser. As illustrated in the lower right of Figure 6, the existing grid was removed and replaced with three spherical dished heads with inside diameters of 18, 30 and 42 inches. We chose the porosities of these heads by using the recommended pressure loss area relationship in Ref. 2 and the grid pressure drop relations defined by Hoerner (Ref. 3). Somewhat similar to the diffusers for the Sandia tunnel (Ref. 4) and the LTV Tunnel (Ref. 5), the first grid should be near choking for most operating conditions; however, no measurements have been made to date

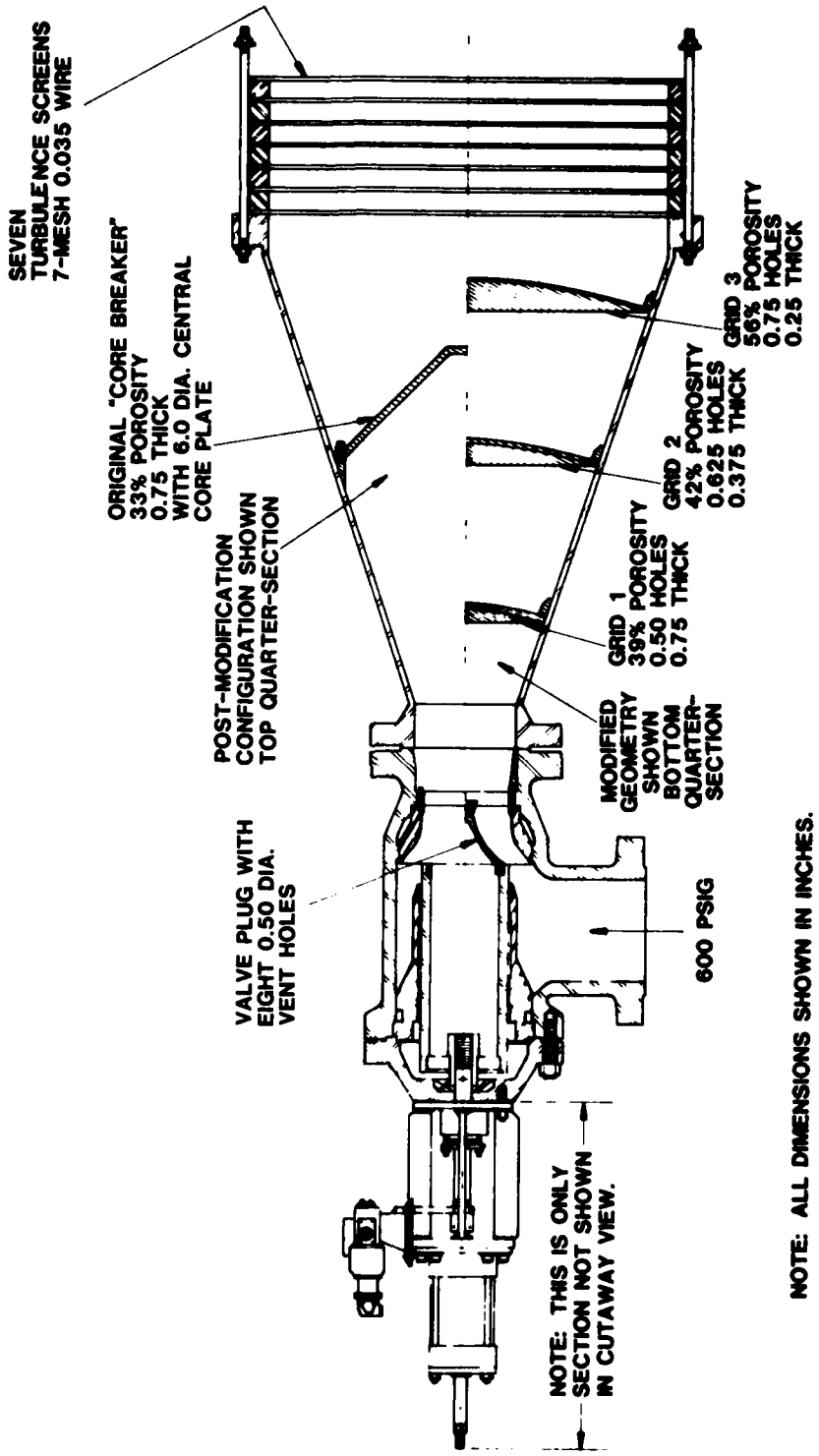

Figure 6. Cross Sections Through Valve and Wide-Angle Diffuser Showing Geometric Details Before and After Modifications

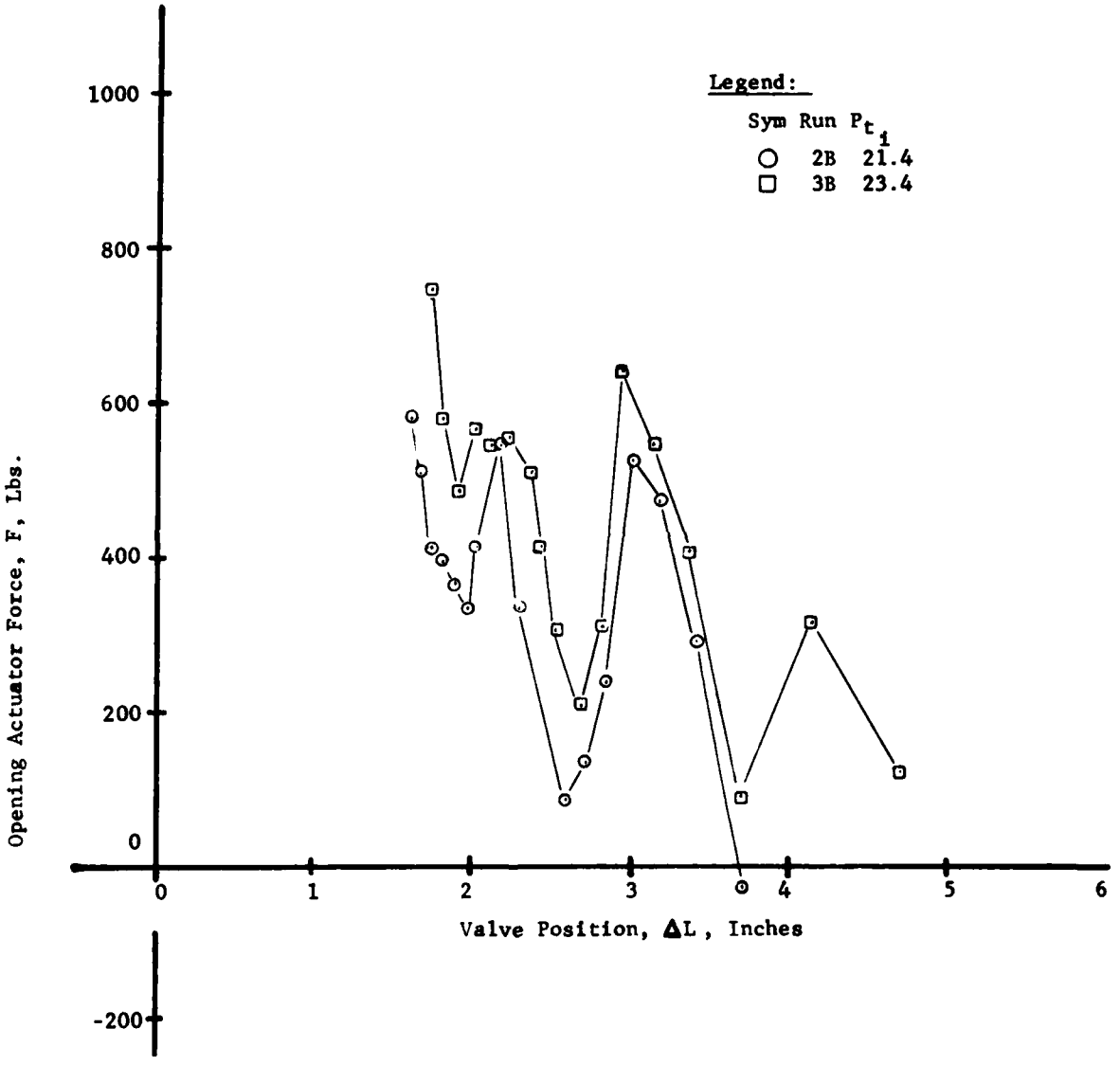

Figure 7. Control Valve Actuator Force for Full-Tank Run M ≅ 0.97 With Plug Installed

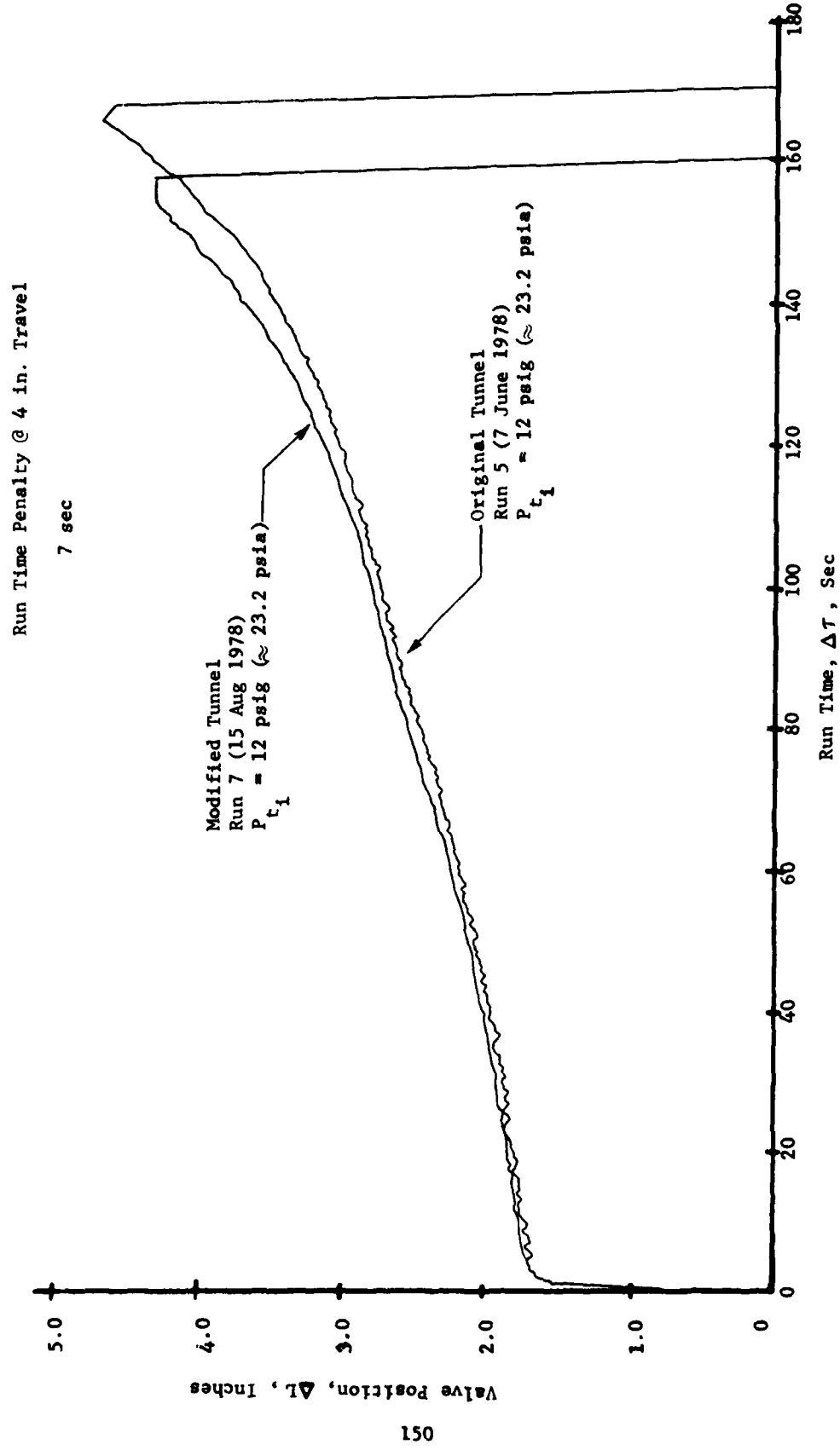

Figure 8. Effect of Modifications on Maximum Run Time for Full-Tank Run M ≈ 0.97

to confirm this. To keep the grid to diffuser wall interface as aerodynamically clean as practical, we elected to weld the dished grids into place with 12 back-up gussets. Because of the significant history of fatigue failures with such units in blowdown tunnels, we instigated rigid quality control of the full-penetration welds. Table 1 shows the results of stress analysis of the units by Al Simmons and Jim Majors,* who noted minimum material steady-state safety factors based on a 36 ksi yield strength.

Table 1

STRESS ANALYSIS RESULTS

Grid	Porosity (%)	Thickness (In.)	Design ΔP (psid)	Safety Factor
1	39	0.75	141.0	4.2
2	42	0.375	19.4	8.1
3	56	0.250	2.25	21.4

Because of these high safety factors and the unavailability of dynamic forcing function characteristics, we have undertaken no check of dynamic stresses. As a precaution, a removable-flange port was provided downstream of grid No. 1 to facilitate periodic visual Borescope inspections for fatigue cracks.

III. Instrumentation and Measurements

A series of four Kulite Transducers, Model XB-093-5, were used to measure pressure in the tunnel. These transducers have a natural frequency of 175 KH_Z and exhibit a flat response to approximately 25% of the natural frequency. The sensitivity and rated pressure are 11.1 mv/psi and 5 psid respectively, with a temperature effect on sensitivity of $< \pm$ 5%/100°F. The analog electrical signals from the four transducers were recorded on magnetic tape using a Philips multi-channel tape recorder, model ANS-LOG 7. The recorder can record in two modes, direct recording using suitable amplification and an FM mode. For this series of tests the FM mode was incorporated. All data were recorded at a tape speed of 15 ips which allowed a useful frequency response of 0 to 5 KH_Z.

Power Spectral Density (PSD) plots were generated using a Time/Data Fourier Analyzing System with a PDP 11/45 central processing unit. A frequency band of 0 - 2 KH_Z was selected to accommodate the above-mentioned tape recorder limits and due to the fact that the power was concentrated in the first 2 KH_Z of the spectrum.

*Engineers at Sverdrup/ARO

IV. Test Procedure

A. Calibration

The four Kulite differential pressure transducers were calibrated by applying a known positive, zero, and negative pressure to the reference chambers. The output voltages were noted, then recorded on tape. The tape was then played back and the voltage levels plotted. This procedure allowed us to calibrate the entire pressure sensing system including not only the transducers but all the amplifiers and the tape recorder.

B. Test Procedure

Once all the transducers were calibrated, the tape recorder was turned on followed by tunnel start. For all tests the storage tank pressure was initially 550 psig. In each test run the tank pressure was allowed to decrease to approximately 50-100 psig, thus allowing nearly full valve travel and maximum run time. We were thus able to observe pressure within the tunnel as a direct function of valve position by plotting the pressure fluctuations recorded on tape versus the valve position which was also recorded.

V. Flow Quality Results

It would have been enlightening to have evaluated the flow improvement effect of the value and diffuser modifications separately. The cost of modifying the valve twice ruled out this separation of variables and we had to be content with an evaluation of the net effect. Since the primary objective for the modifications was to reduce the pressure/acoustic fluctuations as much as possible and to make the resultant disturbance independent of valve position, a succinct presentation devised by Major Steve Icardi was to record broad-band (0 to about 2000 HZ) Kulite transducer information on a magnetic tape along with valve position and storage tank pressure. The resulting information with appropriate scaling was then played back with valve position as the argument on a computer-controlled plotter system. The before and after modification root-mean-square pressure fluctuations (RMS-ΔP) for the stilling chamber stagnation pressure appear in Figure 9. Similar data for test section pitot and forward wall static pressure were given in Figures 2 and 3. As previously noted, these "bench-mark" data were taken with a test section Mach number of 0.97 and a nominal stilling chamber pressure of 23.2 psia with valve position controlled by a tunnel operator. An apparent amplification of the absolute RMS-ΔP in stagnation pressure through the contraction is observed by comparing Figures 9 and 2. This is not an uncommon result as reported in Ref. 4 for the Sandia 12-inch Tunnel. For the cited test condition, the modifications have made the three RMS-ΔP measurements nearly independent of valve position with a curious bump at a valve opening of 2.7 inches. (See Figures 2, 3, and 9.) The usual decrease when the valve approaches subcritical operation toward the end of the run (3.75 in.) was less pronounced for the modified configuration.

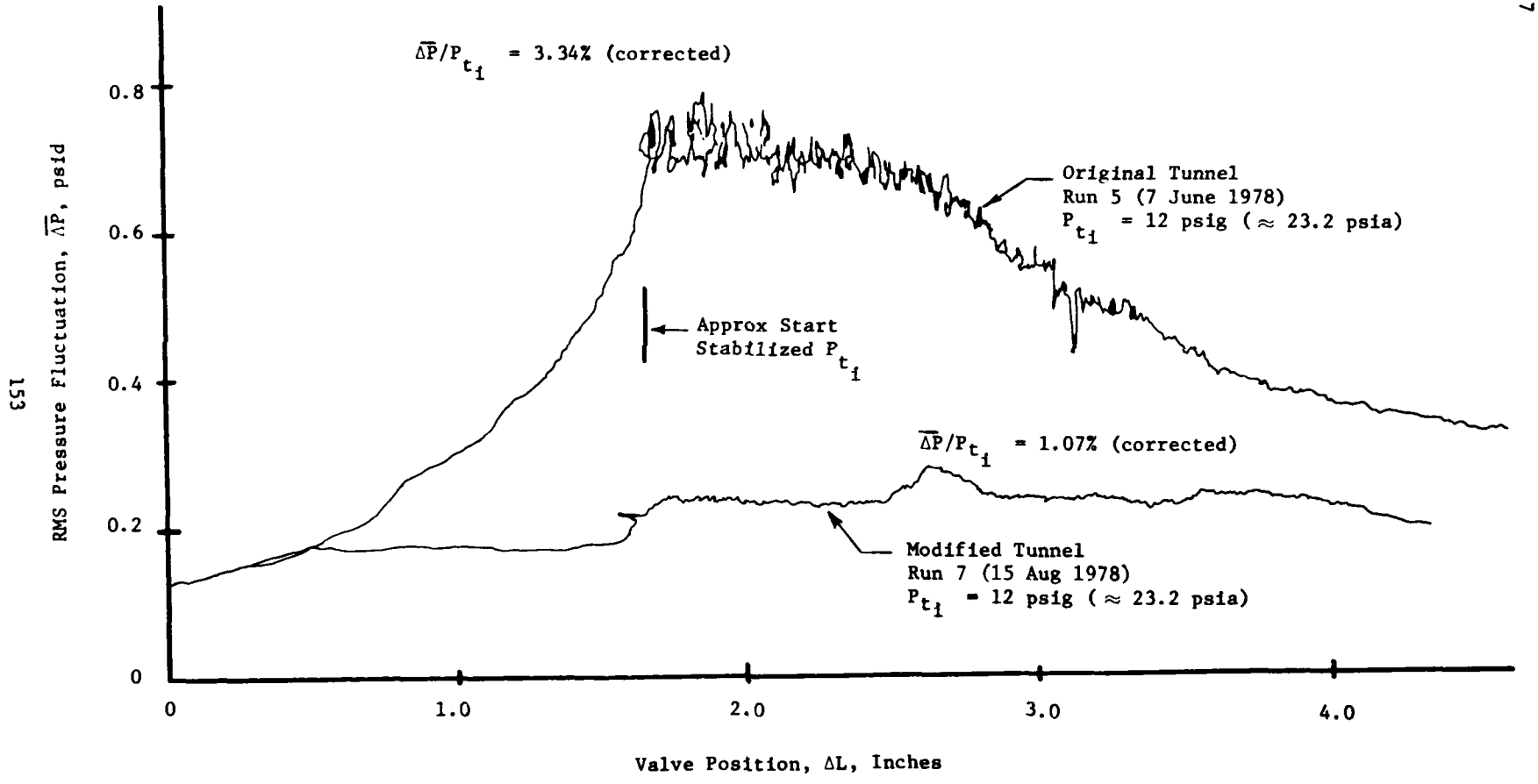

Figure 9. Typical Stilling Chamber Pitot Pressure Fluctuations for Full-Tank Run M ≅ 0.97 Before and After Modification

Since rms voltmeters are in effect mean effective integrators of the power-spectral-density (PSD) plots up to some cut-off frequency, they quite often have a wind-off residual from electronic system noise. This appears to be the case in these data. To rigorously correct for this spurious off-set, we squared the rms signal at a wind-on condition diminished by the square of the wind-off residual and the square root of the resulting difference taken. Making this correction, we note from Figure 9 that the maximum rms pressure fluctuation for the original tunnel of about 3.34 percent of the stagnation pressure has been diminished by the modification to a maximum rms fluctuation of about 1.07 percent for a reduction of 68 percent. These final-tunnel fluctuations are quite comparable to the Sandia Tunnel results (Ref. 4). The corresponding change in the maximum test section pitot pressure fluctuation (Figure 6) is 4.74 percent to 1.56 percent. In both instances the contraction amplification on the absolute fluctuation is about 44 percent, somewhat larger than the approximate 11 percent reported in Ref. 4.

To further compare the broad-band pressure/acoustic fluctuations in the Academy Trisonic to other tunnels, the more popular wall-static measurement was examined (see Figure 3). Making the wind-off correction that was previously described and normalizing by test section dynamic pressure, we obtained the conventional coefficient, ΔCp. For this parameter a 52.5 percent reduction in the maxima has been effected by the modification. Comparing this measurement to other wind tunnels (Figure 4 from Ref. 6), we find that the 3.75 percent value is above the boundary of the graph.

One can obtain further insight into the complex nature of the problem by a brief examination of the PSD functions for the stilling chamber fluctuations at typical valve positions of 2.2 and 2.7 in Figures 5 and 10, respectively. The almost pure tone at 450 HZ at a valve position of 2.2 in. suggests that a narrow-band stilling-chamber acoustic wall liner might be very effective for further reduction. The appearance of other narrow-band peaks at about 10 other frequencies when the valve is 2.7 inches open (Figure 10) suggests that a more broad-band attenuation device like a paneled silencer would be more effective; however, the 450 HZ tone is still predominant.

To further examine the result of the modification, we repeated the fluctuating flow-angle wedge experiment. The large horizontal plane fluctuations have been reduced by an order of magnitude and the remaining oscillations are about equal to the vertical-plane values. This is a pleasant resolution of a paradoxical result that at first glance indicated that some contraction modifications might need to be made.

VI. Conclusions

The modifications made to the USAF Academy Trisonic Tunnel seem to have been very successful. The overall pressure fluctuations have been reduced by a factor of approximately three. These fluctuations have been changed from predominantly lateral

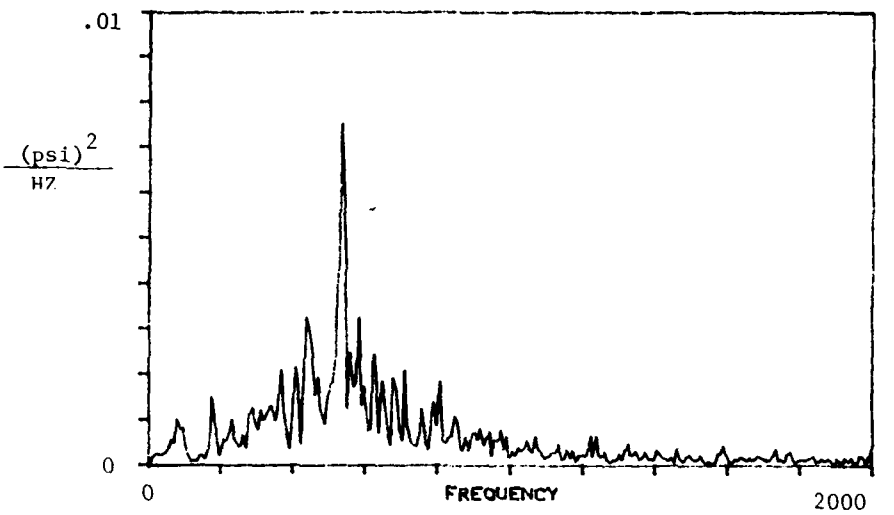

Pre-Modification, Valve at 2.7 in.

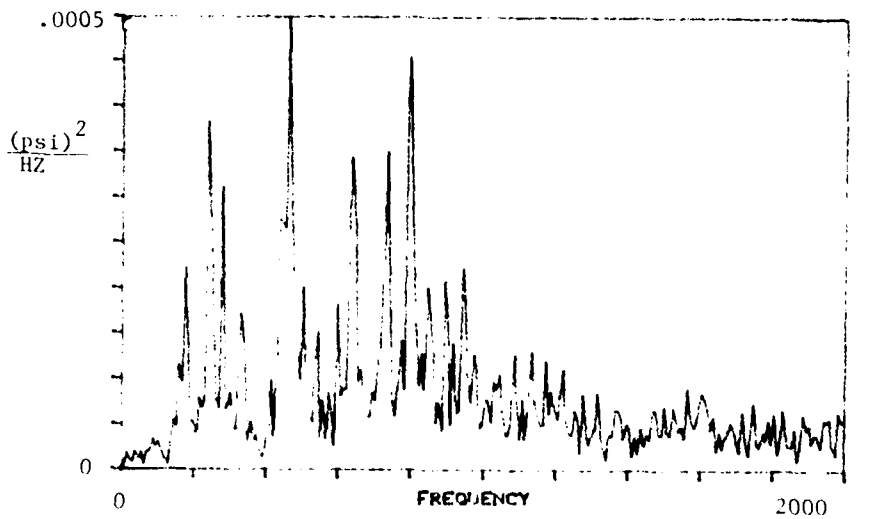

Post-Modification, Valve at 2.7 in.

Figure 10. Power Spectral Density Analysis of Stilling Chamber Pressure Fluctuations

or side-to-side , to oscillations of approximately equal magnitude in all planes. No detrimental effects have been noted in the valve actuator forces, and in fact there now exists a small closing force which provides a safety factor should the hydraulic actuator fail. Finally the remaining pressure fluctuations are predominantly at 450 HZ. which seems to indicate a characteristic Helmholtz frequency of the stilling chamber. In summary, our recent try at reducing the pressure fluctuations has been highly successful.

References

1. Brown, D. "Improvement Following Changes in the Flow-Restricting Plates and Replacement of Flow Smoothing Screens in the NAE 5 x 5 Ft. Blowdown Wind Tunnel." STA Paper, presented at the Supersonic Tunnel Association's 49th Meeting, 17-18 April 1978.

2. Schubauer, G. B. and W. G. Spangenberg. Effect of Screens in Wide-Angle Diffusers. NACA TR-949, 1949.

3. Hoerner, S. F. "Pressure Losses Across Screens and Grids." USAF TR-6289, November 1950.

4. Davis, M. W. "Turbulence Considerations in the Design of the Sandia Corporation 12-Inch Transonic Wind Tunnel." STA Paper, presented at the Supersonic Tunnel Association's 6th Meeting, Aberdeen, 11 October 1956.

5. Cooksey, J. M. and J. W. Arnold. "The Development of an Improved Flow Conditioning System for a Blowdown Wind Tunnel." STA Paper, presented at the Supersonic Tunnel Association's 35th Meeting, Dallas, TX, 8-9 March 1971.

6. Whitfield, E. L. "Noise and Flow Management in Blowdown Wind Tunnels." Lockheed-California, AGARD-CP-174, October 1975.

SECTION V

ENGINEERING EDUCATION

AN EXCURSION AWAY FROM THE TECHNICAL AXIS

Michael M. Tower

Abstract

Traditionally, college-level scientific courses have been presented to the student from a purely technical point of view without much attention paid to the historical and political issues that molded the development of that particular field. This paper argues against this tradition and gives examples of how history and issues can shape scientific thought. An extensive historical-background example in the field of aeronautics is given from the compiled papers of Wilbur and Orville Wright.

1. Introduction

Let me start with an assumption that "most" university professors in basic and applied science present their students with voluminous equations and technical concepts in almost total disregard of philosophical, historical, or political issues that shaped the development of the equation and concepts that embody their particular field. By stating this as an assumption I, of course, avoid the burden of proof, even though many of us are all too familiar with just this sort of character.

Taking this assumption as a promise, I propose that these professors should depart from the straight-lined approach of addressing only technical topics and make excursions into the three-dimensional space that comprises all human awareness. To produce this volumetric space, we can use a three-dimensional axis-system to describe the components of the driving force that advances technology. Figure 1 illustrates the three mutually dependent axes that describe this space (Ref. 1).

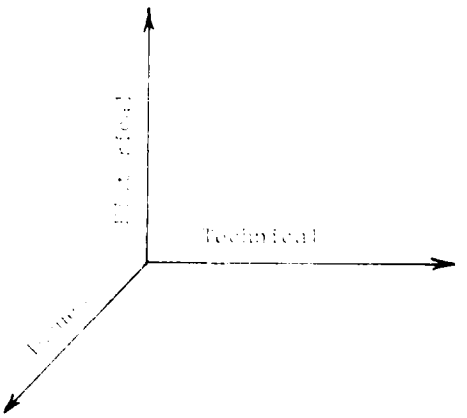

Figure 1. Three-Dimensional Development of a Scientific Discipline **

*Captain, USAF, Associate Professor of Aeronautics, DFAN

**Thanks to Lt. Gen (Ret) B. P. Thomas, Former Head, DFAN

No technical development can occur without being impacted by its current political issues and historical background. As an illustration of technical concepts that were significantly molded by political issues or historical events, I present the following examples.

A. Political Issues

In the sixteenth century the field of astronomy was in a state of upheaval. The conservative-thinking astronomers believed that the earth was the center of the universe, with the sun, planets, and stars revolving around it. This geocentric system was first advanced by the Greeks, refined by Cladius Ptolemy (A.D. 200) and adopted as truth by the Church in Western Europe (Ref. 2). This earth-centered system was staunchly supported until the sixteenth century when Nicolaus Copernicus began to develop a different line of thought. Copernicus believed that the earth and other planets revolved around the sun in a heliocentric system and published his hypothesis in the year of his death, 1543. Copernicus was diplomatic with regard to the Church's dogma and stated that he was just "postulating and theorizing, not necessarily speaking the absolute truth." It is clear that Copernicus believed what he hypothesized, and his banner was taken up by another astronomer, Giordano Bruno, who was not so diplomatic and was burned at the stake in 1600 for heresy. About this same time Galileo was also placed under house arrest for his belief in a heliocentric universe.

It was not until the first of the seventeenth century that the Church acquiesced to the heliocentric concept when detailed scientific observations by Tycho Brahe using a telescope proved the theory.

B. Historical Influence

Extending over twenty-three hundred years, one man's influence on the development of scientific knowledge finds no parallel in history (Ref. 3); Aristotle (384-322 BC) created an intense scientific curiosity which led to the emergence of the sciences. He formulated many basic laws of nature in the area of mechanics and fluidmechanics.

As mankind was emerging from medieval times, at the beginning of the Renaissance, the scientific community placed great faith in Aristotle's axioms and conclusions on the laws of nature. The scientific community's faith in Aristotle led them to criticize and publicly harass early Renaissance thinkers who questioned, or disputed Aristotle. One particular aspect of Aristotle's writings that negatively affected scientific thought was his rejection of the concept of a vacuum. He believed nature abhors a vacuum.

As a consequence of Aristotle's writings on the lack of "nothingness" Augustin J. Fresnel (1788-1827) assumed that light was a wave motion transmitted through an "ether" (Ref. 4). He derived formulas for the intensity ratios for the reflected and the

transmitted light resulting from a light beam incident on the interface between two media. Although these formulas were consistent with experimental observation, they were based on an incorrect "ether" hypothesis which can be historically traced to Aristotle.

Another example of Aristotle's negative influence resulted from his statement (Ref. 5), "since every body in the universe has a 'heaviness,' it must, and does, tend to move (to fall) towards its 'natural place,' therefore, the lower layers of matter, for example, of water and of the atmosphere, must be more dense than the upper layers," which is an accurate hypothesis, but he drew a false conclusion when he asserted that "if a weight falls from a given height in a given time, twice that weight will fall from the same height in half the time." It was nineteen hundred years later that Galileo showed experimentally that Aristotle was wrong, and that, in actuality, bodies of all weights fall from the same height in the same time. He was initially criticized by members of the Aristotelian School in Italy for his assault on principles historically drawn from Aristotle's writings.

II. A Historical Excursion

I would not do justice to the Aeronautics Digest if I did not include in this paper a historical example in the field of aeronautics. The following example was used as anecdotes included in 42 lesson plans for Fundamentals of Aeronautics during the 1979 Fall semester. The purpose of the anecdotes was to give the instructors, in a small way, an appreciation for the traditions and heritage of the Aeronautical Engineering profession, so that they might in some way pass on this appreciation to their students.

The anecdotes were taken from the compiled papers of Wilbur and Orville Wright as edited by Marvin W. McFarland (Ref. 6). The anecdotes begin with the first letter on the subject of aviation written by Wilbur Wright in 1899 up to the date of the Brothers' first successful powered flight, December 17, 1903, with a telegram sent to their father.

Letter from Wilbur Wright to the Smithsonian Institution, Dayton, Ohio, May 30, 1899:

> I have been interested in the problem of mechanical and human flight ever since as a boy I constructed a number of bats of various sizes after the style of Cayley's and Penaud's machines. My observations since have only convinced me more firmly that human flight is possible and practicable.

Letter from Wilbur Wright to Octave Chanute, Dayton, May 13, 1900:

> For some years I have been afflicted with the belief that flight is possible to man. My disease has increased in severity and I feel that it will soon cost me an increased amount of money if not my life. It is possible to fly without motors, but not without knowledge and skill.
>
> I also conceive Lilienthal's apparatus to be inadequate not only from the fact that he failed, but my observations of the flight of birds convince me that birds use more positive and energetic methods of regaining equilibrium than that of shifting the center of gravity.

I make no secret of my plans for the reason that I believe no financial profit will accrue to the inventor of the first flying machine and that only those who are willing to give as well as to receive suggestions can hope to link their names with the honor of its discovery. The problem is too great for one man alone and unaided to solve in secret.

My business requires that my experimental work be confined to the months between September and January and I would be particularly thankful for advice as to a suitable locality where I could depend on winds of about fifteen miles per hour without rain or too inclement weather.

Letter from Wilbur Wright to Bishop Milton Wright, Kitty Hawk, September 23, 1900:

I am constructing my machine to sustain about five times my weight and am testing every piece. I think there is no possible chance of its breaking while in the air. If it is broken it will be by awkward landing. My machine will be trussed like a bridge and will be much stronger than that of Lilienthal, which, by the way, was upset through the failure of a movable tail and not by breakage of the machine.

Wilbur Wright Notebook A, Kitty Hawk, September - October, 1900:

The buzzard which used the dihedral angle finds greater difficulty to maintain equilibrium in strong winds than eagles and hawks which hold their wings level.

The hen hawk can rise faster than the buzzard and its motion is steadier. It displays less effort in maintaining its balance.

A pigeon moving directly from the observer oscillates very rapidly laterally, especially when moving slowly just before lighting.

Letter from Wilbur Wright to Octave Chanute, Dayton, November 16, 1900:

In October my brother and myself spent a vacation of several weeks at Kitty Hawk, NC, experimenting with a soaring machine. The machine we used was a double-decker with surfaces 17 feet by 5 feet.

We spent quite a large portion of our time in testing the lift and drift of the machine in winds of different velocities and with various loads. ...we found the drift of the surfaces under full load was greater than the Lilienthal tables would indicate...

...just before returning we went down to the big hill which was about three miles from our camp and spent a day in gliding. Our plan of operation was for the aeronaut to lie down on the lower plane while two assistants grasped the ends of the machine and ran forward till the machine was supported on the air. The distance glided was between three and four hundred feet at an angle of one in six and the speed at landing was more than double that of starting.

Letter from Wilbur Wright to Octave Chanute, Dayton, March 19, 1901:

Can you give us any advice in regard to anemometers for field use?

Letter from Octave Chanute to Wilbur Wright, San Diego, March 26, 1901:

The best is made by Richard in Paris. I have one of them... I will lend it to you when you are ready to experiment.

Letter from Wilbur Wright to Octave Chanute, Dayton, May 12, 1901:

> Our plans call for a trip of about six or eight weeks in September and October at the same locality we visited last year on the North Carolina coast. We will erect a frame building to house the machine in. The glider itself will be built on exactly the same general plan as our last year's machine, but will be larger and of improved construction in its details.

Letter from Wilbur Wright to Octave Chanute, Dayton, May 17, 1901:

> We have your letter of 15th and are very much pleased to know that there is a possibility that you may pass through Dayton on your trip East. During the months of March, April, May and June our time is very closely occupied as our business requires our attention from twelve to fourteen hours daily. After July 4th the tension is considerably relaxed and after September 1st we are almost free for four months.

Letter from Wilbur Wright to Octave Chanute, Dayton, June 19, 1901:

> Your article is the most accurate and sensible brief statement of the flying problem that has appeared for some time. I only regret that so few investigators seem to be actively at work trying to gain the knowledge and skill necessary to manage aeroplanes in the air. There is really no other way of solving the problem. Balloons will not do.

Wilbur Wright, "Angle of Incidence," The Aeronautical Journal, July 1901:

> The angle of incidence is fixed by area, weight, and speed alone. It varies directly as the weight and inversely as the area and speed though not in exact ratio.

Letter from Octave Chanute to Wilbur Wright, Chicago, July 4, 1901:

> I found the clinometer I was looking for, which is most applicable to the lengths of flight I hope you will make, and sent it. The maker calls it an altimeter.

Letter from Orville Wright to Katharine Wright, Kill Devil Hills, July 28, 1901:

> Our first experiments were rather disappointing. The machine refused to act like our machine last year and at times seemed to be entirely beyond control. On one occasion it began gliding off higher and higher (Will doing the gliding) until it finally came almost at a stop at a height variously estimated by Mr. Spratt and Huffaker at from 18 feet to 40 feet. This wound up in the most encouraging performance of the whole afternoon. This was the very fix Lilienthal got into when he was killed. His machine dropped head first to the ground and his neck was broken. Our machine made a flat descent to the ground with no injury to either operator or machine.

Letter from Octave Chanute to Wilbur Wright, Chicago, August 19, 1901:

> It has occurred to me that you would get still flatter glides by making sure that the center of gravity coincides exactly with the center of pressure, and possibly by decreasing the angle of your rudder to 4°.
>
> Please take plenty of snapshots. You will want them to illustrate whatever you write.

Letter from Wilbur Wright to Octave Chanute, Dayton, August 29, 1901:

> Glide no. 5, August 8th, p.m., 1901, was made under the following conditions: Length of glide 366 feet, of which 125 feet was at an angle of 14° and the remaining 240 feet at an angle of 7°. By following the surface of the ground closely I raised the speed to about 33 miles per hour at point A, from which place I glided to B at an angle of about 8° with no loss of speed, and then ran out on the flat to C by using up this speed. I do not think it possible with this machine to glide permanently at less angle than 8° in still air.

Letter from Katharine Wright to Bishop Milton Wright, Dayton, September 3, 1901:

> Through Mr. Chanute, Will has an invitation to make a speech before the Western Society of Civil Engineers, which has a meeting in Chicago in a couple of weeks. Will is to perform on the 18th. His subject is his gliding experiments. Will was about to refuse but I nagged him into going. He will get acquainted with some scientific men and it may do him a lot of good. We don't hear anything but flying machine and engine from morning till night.

Letter from Katharine Wright to Milton Wright, Dayton, September 11, 1901:

> The boys are still working in the machine shop. A week from today is Will's speech at Chicago. We asked him whether it was to be witty or scientific and he said he thought it would be pathetic before he got through with it!

Wilbur Wright's lecture on "Some Aeronautical Experiments" to the Western Society of Civil Engineers, Chicago, September 18, 1901:

> The difficulties which obstruct the pathway to success in flying machine construction are of three general classes: (1) Those which relate to the construction of the sustaining wings. (2) Those which relate to the generation and application of the power required to drive the machine through the air. (3) Those relating to the balancing and steering of the machine after it is actually in flight. Of these difficulties two are already to a certain extent solved.
>
> Herr Otto Lilienthal seems to have been the first man who really comprehended that balancing was the first instead of the last of the great problems in connection with human flight.
>
> The balancing of a gliding or flying machine is very simple in theory. It merely consists in causing the center of pressure to coincide with the center of gravity. But in actual practice there seems to be an almost boundless incompatibility of temper which prevents their remaining peaceably together for a single instant, so that the operator, who in this case acts as peacemaker, often suffers injury to himself while attempting to bring them together.
>
> We figured that Lilienthal in five years of time had spent only about five hours in actual gliding through the air. The wonder was not that he had done so little, but that he had accomplished so much. It would not be considered at all safe for a bicycle rider to attempt to ride through a crowded city street after only five hours practice, spread out in bits of ten seconds each over a period of five years; yet Lilienthal with this brief practice was remarkably successful in meeting the fluctuations and eddies of wind gusts.

Our system of twisting the surfaces to regulate the lateral balance was tried and found to be much more effective than shifting the operator's body.

Letter from Octave Chanute to Wilbur Wright, Chicago, October 12, 1901:

I have been endeavoring to account for the discrepancy of your results with those of Lilienthal, and I think I have found one possible explanation. You will note that those made in 'natural wind,' from which he derived his coefficients, are greatly in excess of those made with the same surfaces with a whirling apparatus, and that your own recent experiments belong to the latter class, i.e., surfaces driven against still air.

It seems to me that there may be a difference in the result whether the air is impinged upon by a moving body, or whether the wind impinges upon the same body at rest. In the latter case each molecule, being driven from behind, tends to transfer more of its energy to the body than in the former case when the body meets each molecule successively before it has time to react on its neighbors.

Letter from Octave Chanute to Wilbur Wright, Chicago, October 20, 1901:

I am very much pleased that you have undertaken these experiments, and I will be glad to contribute to the expense if you will let me do so.

Letter from Wilbur Wright to Octave Chanute, Dayton, October 24, 1901:

We very much feel the generosity and kindly spirit which has prompted your offers of financial assistance in our experiments. For the present we would prefer not to accept it for the reason that if we did not feel that the time spent in this work was a dead loss in a financial sense, we would be unable to resist the temptation to devote more time than our business will stand.

Letter from Octave Chanute to Wilbur Wright, Chicago, November 18, 1901:

It is perfectly marvelous to me how quickly you get results with your testing machine. You are evidently better equipped to test the endless variety of curved surfaces than anybody has ever been.

Letter from Wilbur Wright to Octave Chanute, Dayton, November 22, 1901:

[the last paragraph of a five-page letter] Please excuse the inordinate length of several of my letters. I sometimes fail to consider that your time is more valuable than my own.

Letter from Octave Chanute to Wilbur Wright, Chicago, November 27, 1901:

I am amused with your apology for writing long letters, as I find them always too brief.

Letter from Wilbur Wright to Octave Chanute, Dayton, December 15, 1901:

We stopped experimenting about two weeks ago and shall probably not be able to resume them till next fall as our busy season is about here.

Letter from Octave Chanute to Wilbur Wright, Chicago, December 19, 1901:

> I very much regret in the interest of science that you have reached a stopping place, for further experimenting on your part promises important results, yet my judgment cannot but approve of your decision, for I see as yet no money return for the pursuit, save from possible exhibition. If, however, some rich man should give you $10,000 a year to go on, to connect his name with progress, would you do so? I happen to know Carnegie. Would you like for me to write to him?

Letter from Wilbur Wright to Octave Chanute, Dayton, December 23, 1901:

> As to your suggestion in regard to Mr. Carnegie, of course nothing would give me greater pleasure than to devote my entire time to scientific investigations; and a salary of ten or twenty thousand a year would be no insuperable objection, but I think it possible that Andrew is too hard-headed a Scotchman to become interested in such a visionary pursuit as flying. But to discuss the matter more seriously, I will say that several times in the years that are past I have had thoughts of a scientific career, but the lack of a suitable opening, and the knowledge that I had no special preparation in any particular line, kept me from entertaining the idea very seriously. I do not think it would be wise for me to accept help in carrying our present investigation further.

Letter from Wilbur Wright to Octave Chanute, Dayton, February 7, 1902:

> The newspapers are full of accounts of flying machines which have been building in cellars, garrets, stables and other secret places, each one of which will undoubtedly carry off the hundred thousand dollars prize at the St. Louis Exhibition. They all have the problem "completely solved," but usually there is some insignificant detail yet to be decided, such as whether to use steam, electricity, or a water motor to drive it. Mule power might give greater ascensional force if properly applied, but I fear would be too dangerous unless the mule wore pneumatic shoes. Some of these reports would disgust one, if they were not so irresistibly ludicrous.

Letter from Octave Chanute to Wilbur Wright, Chicago, May 30, 1902:

> I suggest that you take out a patent or caveat on those principles of your machines as are important, not that money is to be made by it, but to save unpleasant disputes as to priority.

Orville Wright's Diary, September 20, 1902:

> In the afternoon we continued the gliding, Will making one glide of 11 seconds covering a distance a little over 200 feet in which the machine began to gradually glide to the side of the right wing, which was the lower one. The wind getting under the left wing from the side, on account of the flight being made a little to the right of the direction of the wind, raised it higher and higher, when he suddenly by mistake, while attempting to alter the wing tips, turned the front rudder down at the rear, causing the machine to 'pierce the ethereal' to all appearances at an angle of over 45°.

Letter from Wilbur Wright to Octave Chanute, Kill Devil Hills, September 23, 1902:

> Today made probably 75 glides in a wind blowing 9 to 11 meters. The distances were not measured accurately except in a few cases. The usual length was 150 to 225 feet. The times were about 10 to 12 seconds for the most part, though we measured but few.

Letter from Orville Wright to Katharine Wright, Kill Devil Hills, October 23, 1902:

> The largest machine we handled in any kind of weather, made the longest distance glide (American), the longest time in the air, the smallest angle of descent, and the highest wind! (622 feet and 26 sec)

Letter from Wright Cycle Co. to the Daimler Mfg Co., Dayton, December 3, 1902:

> The possibility of obtaining on the market a gasoline engine which would develop 8 to 9 brake H.P., would weigh no more than 180 lbs or an average of 20 lbs per H.P., and would be free from vibrations is desired.

Letter from Wilbur Wright to George Spratt, Dayton, February 28, 1903:

> We recently built a four-cylinder gasoline engine with 4" piston and 4" stroke, to see how powerful it would be, and what it would weigh. At 670 revolutions per minute it developed 8½ horsepower, brake test. By speeding it up to 1,000 rev. we will easily get 11 horsepower and possibly a little more at still higher speed, though the increase is not in exact proportion to the increase in number of revolutions. The weight including the 30 pound flywheel is 140 lbs.

Letter from Octave Chanute to Wilbur Wright, Paris, April 4, 1903:

> Your experiments are attracting a good deal of attention in Paris. I have had to give several talks, and to promise to write something for publications on you and your brother's work.

Letter from Orville Wright to George Spratt, Dayton, June 7, 1903:

> We have also made some experiments on the best shapes for the uprights of our machine, and again found out that everybody but ourselves are very badly mistaken!
>
> Mr. Chanute thinks the dirigible balloon is fast losing favor in France, and that the French are getting worked over gliding, and that before long a number of them will be engaged in experimenting.
>
> Please do not mention the fact of our building a power machine to anybody. The newspapers would take great delight in following us in order to record our troubles.

Letter from Wilbur Wright to Octave Chanute, Dayton, July 24, 1903:

> The vertical tail is operated by wires leading to the wires which connect with the wing tips. Thus the movement of the wing tips operates the rudder. This statement is not for publication, but merely to correct the misapprehension in your own mind. As the laws of France and Germany provide that patents will be held invalid if the matter claimed has been publicly printed we prefer to exercise reasonable caution about the details of our machine until the question of patents is settled.

Letter from Octave Chanute to Wilbur Wright, Chicago, September 12, 1903:

> I am really sorry for Langley. He has had more than his share of mishaps, and the pesky reporters are giving him the reputation of a bungler.

Letter from Wilbur Wright to Octave Chanute, Kill Devil Hills, October 1, 1903:

> We did some practicing at soaring and found it easier than we expected. Once we succeeded in remaining almost in one spot for 26 seconds and finally landed 50 feet from the starting point. With a little more practice I think we can soar on the north slope of the Big Hill whenever the wind has a velocity of 9 meters or more.

Letter from Wilbur Wright to Octave Chanute, Kill Devil Hills, October 16, 1903:

> I see that Langley has had his fling, and failed. It seems to be our turn to throw now, and I wonder what our luck will be.

Orville Wright's Diary, Kill Devil Hills, October 21, 1903:

> Just before 5 o'clock we returned to the point near top of hill and made 8 or 10 glides, each increasing in time and making new records. The best flight was 450 feet with an endurance of 1 minute and 11 seconds.

Orville Wright's Diary, Kill Devil Hills, November 8, 1903:

> Sat up to 11 o'clock talking over with Mr. Chanute plans for next year, should machine make a successful flight.

Letter from Orville Wright to father and sister, Kill Devil Hills, November 15, 1903:

> The weight of our machine complete with man will be a little over 700 pounds and we are now quite in doubt as to whether the engine will be able to pull it at all with the present gears, as we will not be able to use more than 3/4 of our power in getting started.

Letter from Wilbur Wright to father and sister, Kill Devil Hills, December 14, 1903:

> We took to the hill and after tossing for first whack, which I won, got ready for the start. The wind was a little to one side and the track was not exactly straight downhill which caused the start to be more difficult than it would otherwise have been. However, the real trouble was an error in judgment, in turning up too suddenly after leaving the track, and as the machine had barely speed enough for support already, this slowed it down so much that before I could correct the error, the machine began to come down, though turned up at a big angle. Toward the end it began to speed up again but it was too late, and it struck the ground while moving a little to the side, due to wind and a rather bad start. A few sticks in the front rudder were broken, which will take a day or two to repair probably.

Orville Wright's Diary, Kill Devil Hills, December 17, 1903:

> I got on the machine at 10:35 for the first trial. The wind, according to our anemometers at this time, was blowing a little over 20 miles. On slipping the rope the machine started off increasing in speed to probably 7 or 8 miles. The machine lifted from the truck just as it was entering the fourth rail. Mr. Daniels took a picture just as it left the tracks.

Telegram from Orville Wright to Bishop Milton Wright, Kitty Hawk, December 17, 1903:

> Success four flight Thursday morning all against twenty-one mile wind started from level with engine power alone average speed through air 31 miles longest 57 seconds inform press home Christmas.

References

1. Daley, D. H. Introductory Remarks at the DFAN Faculty Summer Workshop, US Air Force Academy, CO, July 1979.

2. Anderson, J. D., Jr. Introduction to Flight. New York: McGraw-Hill Book Company, 1978.

3. Tokaty, G. A. A History and Philosophy of Fluidmechanics, Henley-on-Thames, Oxfordshire, England: G. T. Foulis and Co., Ltd., 1971.

4. Gartenhaus, Solomon. Physics Basic Principles. New York: Holt, Rinehart, and Winston, 1977.

5. Aristotle. On the Heavens. Trans. W. K. Guthrie. London: William Heinemann, Ltd., 1936.

6. McFarland, M. W., ed. The Papers of Wilbur and Orville Wright. Vol. 1. New York: McGraw-Hill Book Company, 1953.

MILITARY AVIATION: THE NEXT TWENTY-FIVE YEARS

Clarence L. "Kelly" Johnson

Editor's Note

The paper that follows is the text of a talk given to the Department of Aeronautics by Mr. Johnson on the occasion of his visit to the Air Force Academy on 6 September 1979.

I would like to speak to you today about my personal thoughts on some factors which will affect our military air forces in the next 20 years. This is a very brave venture for me because my experience with such long-range projections over the past 50 years of my career in aviation prove quite conclusively that we are very lucky in the aircraft business to be able to project five years accurately, to say nothing of a 20-year period. I don't know anyone who, in 1974, predicted that jet fuel costs would rise from 23 cents/gallon to as much as 84 cents. Or that in such a short period, aircraft first costs would double. Or that long-range commercial transports would fly non-stop stages over 6,000 miles in length. Or that the time required to get a heavy aluminum forging would exceed a year and a half!

Having gained your confidence, then, with these factual examples from the recent past, I will, therefore, launch into a discussion of what I believe to be coming in the period between now and the year 2000. These are obviously not in any special order or priority of ranking, but just subjects for you to consider.

New Aircraft Types

We can see many factors which tell us that we will have very few new types of military aircraft being produced during the time period under consideration. One must review factors such as these, which are pertinent.

A. What kind of war or wars are we likely to be engaged in?

Our concept of successful low-altitude penetration by manned aircraft has been rudely shaken by the development and use of very effective ground-to-air missiles, new guns and radar. We started into Viet Nam operating at altitudes under 1,000' for many missions. By the end of that war, "low altitude" meant down to 11,000'. In the last Sinai engagements "low altitude" was 21,000' from the best information I can gather. Our B-1 bomber was cancelled partly because of its great vulnerability during its design mission use of low-altitude penetration.

Obviously, use of unmanned cruise missiles will play a major role in determining what new types of military aircraft we need.

B. Are aircraft truly cost effective against hordes of tanks likely to be used in a NATO conflict?

Sending a $10,000,000 fighter carrying a $1,000,000 man to shoot $2,000,000 tanks requires an exchange ratio of six to one for the airplane. This may be hard to achieve. Will we reach the point where one man on the ground with a simple I-R or electro-optical missile can do a more effective and much cheaper job so the airplane can be spared from anti-tank missions?

C. What can we do about the high loss rate of aircraft in the initial days of a war?

Israeli losses of fighters in the last Sinai war reached a level of over 35 aircraft per day. In a European conflict, I believe we could expect similar or higher losses. That would mean that in 20 days, all the F-16's now being built in Europe would be used up, assuming they were all made operational.

In such a short period it is difficult to replenish such losses. They must come from forces in being and none of the NATO nations to my knowledge has stand-by aircraft numbers in impressive quantities. One doesn't have time to start up production lines such as we had in World War II producing up to 50 fighters per day. Our reserves are F-104's, F-4's and Panavia Tornados which would be in existence when a NATO conflict might begin.

I do not believe another war will see anything like the numbers of aircraft involved that we had in World War II. A figure I find very impressive is that the top 30 aces (from both sides) in that war shot down a total of over 3,200 airplanes. Obviously we will have fewer, more capable, more expensive aircraft in use.

If I might quote my good friend Norm Augustine, once Undersecretary of the Army, and now vice president of Martin-Marietta, he states (after projecting cost and budget growth), "By the year 2054, the cost of a single aircraft will equal the entire national defense budget which would require the Air Force to have its use 3½ days a week and the Navy the other 3½ days." President Coolidge would, therefore, be proven correct in making his statement about aircraft procurement in the 1920's!

D. What problems do we have in command, communication and control of our forces?

Many of my friends who flew in South East Asia told me."We flew in a sea of electrons, not air!!" I would like to show you an Air Force chart on "Interoperability" which shows actual and some projected systems for control of the air battle in NATO.

One of my General friends, upon seeing this, said, "I think I can fight a better war from inside a telephone booth - even a French one - without all this help."

Obviously we have a major job to do to develop and protect whatever systems we finally use. We must provide complete all-weather operational systems including blind

takeoff and landing means for all our military aircraft and helicopters. Our Lockheed L-1011 transport is demonstrating daily the feasibility of such a system in practically zero-zero conditions.

We cannot have another situation develop as we did in the World War II Battle of the Bulge where we had to keep our Air Forces on the ground for a nine-day period during which our ground forces were almost over-run.

E. What is the role of air transport to be in our review period?

Because of high cost, long development periods required and lack of any very important technological breakthroughs, I believe our military transports to be used in the next 20 years are already here today. They are the C-141's, C-130's, C-5's, 747's, DC-10's and KC-135's. Our larger aircraft have been designed or redesigned to have service lives of over 30 years. Air-to-air refueling greatly extends their useful range with good payloads.

F. What types of fuel will be used for our aircraft in the period being considered?

It is my considered opinion that airplanes will use petroleum or coal-based fuel long after we have electric automobiles, solar and wind power generating plants and reliable nuclear power stations.

I do not believe we will see liquid hydrogen powered aircraft very soon, not because we can't build them, but because of the terrible logistic problems of distributing the material and the high cost in energy to make it. Currently used processes, for instance, require four to eleven times as much power input to make liquid hydrogen as we obtain back when the fuel is burned. In 1957, we at Lockheed were far into the design and construction of liquid hydrogen powered aircraft designed to cruise supersonically about 100,000' altitude. Fortunately, a realistic study of the logistic problems provided us the answer--"go back to petroleum fuels," which we did on the SR-71 family of aircraft.

I am, likewise, not a believer in the use of nuclear power in manned aircraft during the next several decades in spite of spending seven years of my life after World War II trying to design a nuclear bomber known as System 1251. With the high power levels required for flight at high altitude, the crew shielding problem was ridiculous. The cockpit section for the crew weighed over 40,000 pounds which included four-inch thick glass for the windshield. We could never derive an operating plan for the aircraft which was safe for the people on the ground in case of a crash. Nuclear fallout and melt down was totally unacceptable. Most of these factors have not changed appreciably in the last 20 years to my knowledge. Use of lower power level and turbo props alleviate the intensity of the problem but I'm not greatly attracted to this solution to only a part of the problem.

G. What will develop in terms of aircraft weapons?

There will continue to be slow progress in gun development, but the major effects will be seen in our smart missiles. I would like to close this question with a statement by my friend Ben Rich who now runs my old "Skunk Works." Ben says, "We have enough MISSILES! What we need is a new brand of HITTLES." I agree with him completely.

With that safe advice, I will now close. Let me express again my sincere pleasure for the opportunity of speaking to you once again. You must forgive my presumption for trying to peer four times as far into the future as I have ever done successfully before. But I've had fun doing it and I hope you have with me - Good day.

SECTION VI

AERONAUTICAL HISTORY

In beginning a new section on Aeronautical History, we thought the following reprint from US War Department records would make an appropriate first entry.

FIRST UNITED STATES MILITARY AIRCRAFT ACCIDENT

17 SEPTEMBER 1908

MR. ORVILLE WRIGHT AND LT. THOMAS E. SELFRIDGE

WAR DEPARTMENT

OFFICE OF THE CHIEF SIGNAL OFFICER

WASHINGTON

AERONAUTICAL DIVISION

February 19, 1909

The Chief Signal Officer, U. S. Army

Sir:

I have the honor to submit the following detailed report of the accident to the Wright Aeroplane at Ft. Myer, Virginia, on September 17, 1908.

The Aeronautical Board of the Signal Corps, composed of Major C. McK. Saltzman, S. C., Captain Chas. S. Wallace, S. C. and Lieut. Frank P. Lahm, S. C., assisted by Lieut. Sweet, of the Navy, and Lieut. Creecy, of the Marine Corps, also Mr. Octave Chanute and Professor Albert Zahm, made a thorough examination on the morning of September 18, the day after the accident, of the aeroplane and the ground, and carefully examined witnesses of the accident. The following is their report:

"That the accident which occurred in an unofficial flight made at Ft. Myer, Va., at about 5:18 p.m., on September 17th, 1908, was due to the accidental breaking of a propeller blade and a consequent unavoidable loss of control which resulted in the machine falling to the ground from a height of about seventy-five (75) feet.

The Board finds that First Lieutenant Thomas E. Selfridge, First Field Artillery, (attached to the Signal Corps of War Department orders and assigned to aeronautical duty), accompanied Mr. Wright, by authority, on the aeroplane, for the purpose of officially receiving instruction, and received injuries by the falling of the machine which resulted in his death."

The detailed examination of witnesses referred to in the above paragraph is given herewith.

Sergeant Daley, Battery "D", 3d Field Artillery, was on the artillery guard house porch at the time of the accident and testified that he saw the rear rudder collapse and fall to the front and to the right, then after the machine had advanced about 60 feet, the broken propeller blade fell to the ground. Sergeant Daley gave the impression of being a reliable witness.

Private Allen, Troop "F", 13th Cavalry, was the mounted sentinel stationed in front of the lower cemetery gate. He was about 30 yards from where the aeroplane struck the

ground. He testified that he heard a loud noise, saw the propeller blade fly, and saw the machine start down, then saw it drop rapidly head first. While the machine was falling, he was occupied trying to get out of the way with his horse. He said the men in the machine tried to talk while falling; that when he went up to the machine after it was on the ground, Mr. Wright's head was hanging down between two wires which crossed on his chest. His right arm was extended under Lieut. Selfridge as though to hold him up. He exclaimed, "Oh, my arm." He said that the front ends of the skids struck the ground first.

Corporal Forrester, Battery "D", 3d Field Artillery, was the noncommissioned officer of the guard on duty around the field. He was mounted and was just in the rear of the aeroplane shed. He heard the propeller snap, then saw nothing until the machine was on the ground. Corporal Forrester and Private Allen demonstrated to the Board the position in which Lieut. Selfridge and Mr. Wright were found.

Private Mincey, Battery "D", 3d Field Artillery, was stationed as a mounted sentinel in front of the south end of Battery "E's" gun shed. He testified that he heard a pop, looked up and saw the machine advance a certain distance, then drop straight down.

Mr. Chanute was 15 feet south of the press tent and 560 feet west of the point where the machine struck, that is on the opposite side of the aeroplane shed. Mr. Chanute testified that the machine was perhaps 60 feet up and circling the field to the left. He went 40 or 50 feet to the south so as not to be behind the tents between himself and the aeroplane shed. When the machine was 300 feet from him, the propeller flaked off or snapped, and the piece fluttered down to the ground; the aeroplane maintained its level for 60 or 100 feet, then oscillated and pitched down with the left side depressed and disappeared from his view behind the bushes. He did not see it strike. When he examined the broken propeller blade, Mr. Chanute testified that the wood was brittle and over seasoned, or kiln dried. A few days later Mr. Chanute informed me that he thought the propeller blade had struck the upper guy wire of the rear rudder and had torn the end of the wire from its attachment to the rudder.

Dr. George A. Spratt, of Dayton, Ohio, a friend of Mr. Wright's, was at the upper end of the field near the starting point at the time of the accident. His written statement of his observations of the accident is attached hereto marked "A".

Sergeant Sweeney, post ordnance sergeant at Ft. Myer, was at the battery guard house at the time of the accident. Mr. Charles Taylor, a mechanician employed by Mr. Wright, was also examined. Their testimony was not particularly pertinent.

On October 31, 1908, I talked with Mr. Wright at the hospital at Ft. Myer, and learned from him the following facts:

He said he heard a clicking behind him about the time he crossed the aeroplane shed: He decided to land at once but as there was scarcely time to do it before reaching the cemetery wall, he decided to complete the turn and head toward the upper end of field. He thought he was about 100 feet high at the time the propeller broke and that he descended more or less gradually about 40 feet, then the machine dropped vertically. He shut off the engine almost as soon as the clicking began, then corrected a tendency to turn which the machine seemed to have. All this time the machine was coming down pretty rapidly. He pulled the lever governing the front rudder as hard as possible, but the machine still tipped down in front, so he pushed the lever forward and pulled it back again hard, thinking it might have caught or stuck. At the time of our conversation, October 31st, he said he thought that the rear rudder had fallen sideways and the upward pressure of the air on it probably threw the rear of the machine up and the front down, and that this accounted for its failure to respond more readily to the front rudder. He stated that at a height of about 60 feet, the front end of the machine turned nearly straight down and then it fell. About 15 feet from the ground it again seemed to respond to the front rudder and the front end came up somewhat, so that it struck the ground at an angle of about 45 degrees.

The following is a list of witnesses in addition to those whose testimony is given above:

Mr. Magoon, Superintendent of Arlington Cemetery, was half way between the two gates of the cemetery and just inside the wall.

The following reporters were at the balloon tent:

Mr. Heiss, of the New York World.
Mr. Dugan, of the United Press.
Mr. Smith, of the Baltimore Sun.
Mr. McMahan, of the Washington Herald

The following witnesses were near the new artillery stable, west of the point where the accident occurred:

Mr. Robert F. Crowley, Arlington, Va.
Mr. H. C. Ball, Clarendon, Va.
Mr. E. E. Speer, Ballston, Va.
Mr. R. Tall, Ballston, Va.

I examined most of the witnesses whose testimony is given above, immediately after the accident, on the field I was present when the Aeronautical Board made its examination on the following day, September 18th, and talked at various times with Mr. Wright, Mr. Chanute, Professor Zahm, and others relative to the accident. At the time of the accident I was holding my horse and watching the machine from the upper end of the field near the starting point. When the machine struck, I galloped at once to the spot.

On September 17th, Mr. Wright was almost ready to begin his official trails [sic] so he put on a set of new and longer propellers that day for the purpose of tuning up the speed of his machine preparatory to making his official speed trial. These propellers were probably 9 feet in diameter; the ones in use up to that time were probably 8 feet 8 inches in diameter.

Lt. Selfridge was to leave for Saint Joseph, Missouri, for duty in connection with Dirigible No. 1, on September 19th, and was very anxious to make a flight before leaving, so Mr. Wright, at my suggestion, had said a few days before that he would take him up at the first opportunity. On September 15th and 16th, high winds prevented his making a flight. On September 17th, the instruments at the aeroplane shed recorded a north-east wind of four miles an hour. At 4:46 p.m. the aeroplane was taken from the shed, moved to the upper end of the field and set on the starting track. Mr. Wright and Lieut. Selfridge took their places in the machine, and it started at 5:14, circling the field to the left as usual. It had been in the air four minutes and 18 seconds, had circled the field 4 ½ times and had just crossed the aeroplane shed at the lower end

of the field when I heard a report then saw a section of the propeller blade flutter to the ground. I judge the machine at the time was at a height of about 150 feet. It appeared to glide down for perhaps 75 feet, advancing in the meantime about 200 feet. At this point it seemed to me to stop, turn so as to head up the field toward the hospital, rock like a ship in rough water, then drop straight to the ground the remaining 75 feet. I had measurements taken and located the position where the machine struck, 304 feet from the lower cemetery gate and 462 feet from the northeast corner of the aeroplane shed. The pieces of propeller blade was [sic] picked up at a point 200 feet west of where the aeroplane struck. It was 2 ½ feet long, was a part of the right propeller, and from the marks on it had apparently come in contact with the upper guy wire running to the rear rudder. This wire, when examined afterward, had marks of aluminum paint on it such as covered the propeller. The left propeller had a large dent, and the broken piece of the right propeller had a smaller dent indicating that the broken piece flew across and struck the other propeller. The upper right had [sic: hand] guy wire of the rear rudder was torn out of the metal eye which connected it to the rear rudder. I am of the opinion that due to excessive vibration in the machine, this guy wire and the right hand propeller came in contact. The clicking which Mr. Wright referred to being due to the propeller blade striking the wire lightly several times, then the vibrations increasing, it struck it hard enough to pull it out of its socket and at the same time to break the propeller. The rear rudder then fell to the side and the air striking this from beneath, as the machine started to glide down, gave an upward tendency to the rear of the machine, which increased until the equilibrium was entirely lost. Then the aeroplane pitched forward and fell straight down, the left wings striking before the right. It landed on the front end of the skids, and they as well as the front rudder were crushed. Both Mr. Wright and Lieut. Selfridge were on their seats when the machine struck the ground, held there by wire braces which cross immediately in front of the two seats. It is probable that their feet struck the ground first, and as the machine dropped nearly head first, they were supported by these wire braces across their bodies. When I reached the machine, the mounted sentinels at the lower end of the field were entering at the

left hand end between the two main surfaces, which were now standing on their front edges. I found Mr. Wright lying across the wires mentioned above, trying to raise himself, but unable to do so. He was conscious and able to speak, but appeared very badly dazed. He was cut about the head where he had struck the wires,and possible [sic] the ground. Lieut. Selfridge was lying stretched out on the wires, face downward, with his head supported by one of these wires. He died at 8:10 that evening of a fracture of the skull over the eye, which was undoubtedly caused by his head striking one of the wooden supports or possibly one of the wires. He was not conscious at any time. With the assistance of a couple of enlisted men I removed Mr. Wright from the machine and placed him on the ground where he was immediately taken charge of by Army surgeons, among them Major Ireland, who were among the spectators at the time of the accident. Lieut. Selfridge was carried out immediately afterward and similarly cared for. At least two civilian surgeons among the spectators, whose names are not known, assisted in caring for both of them. Within ten minutes they were carried to the post hospital on litters by hospital corps men and were placed on the operating table. Captain Bailey, Medical Corps, USA Army, was in charge of the hospital at the time. He was assisted in the operating room by the surgeons mentioned above. In the meantime the mounted sentinels had been placed around the aeroplane to keep back the crowd, a very difficult matter at that time. Mr. Wright was found to have two or three ribs broken, a cut over the eye, also on the lip, and the left thigh broken between the hip and knee. He was in the hospital at Ft. Myer for six weeks under the care of Major Francis A. Winter, and at the end of that time went to his home at Dayton, Ohio. Lieut. Selfridge was buried with full military honors at Arlington Cemetery on September 25th.

The wings on the right side of the machine were not badly damaged, those on the left side which struck the ground first were crushed and broken. Apparently the front rudder, skids, and left wings received most of the force of the fall. The rear rudder as shown on the accompanying photographs, exhibits "C", "D", and "E", was thrown down on the rear end to the skids and on the main body of the machine, probably due to the shock on striking the ground. The gasoline tank was damaged sufficiently to allow the

gasoline to leak out. The water cooler of the engine was somewhat twisted: the engine itself was not badly damaged, and could probably be very easily put in running order again. I had the aeroplane taken to pieces and removed to the aeroplane shed the evening of the accident. It was afterward shipped to Dayton, Ohio, by Mr. Wright's direction.

Very Respectfully,
(Signed) Frank P. Lahm
1st Lieut. Signal Corps

Exhibit "C". Mr. Wright has been removed and is in the group at the right. Lt. Thomas E. Selfridge is being taken out. September 17, 1908*.

*Only the photograph from Exhibit "C" was available.

Gentlemen:

The machine was completing the last quarter of the turn when the portion of the blade was thrown off. It was apparently the blade toward the center of the circle being described by the course of the machine, that was broken. The machine completed the circle and was headed toward the starting derrick, the engine running and the flight apparently undisturbed. It proceeded about 200 feet and started to descend assuming a negative angle (i.e. the chord of the surfaces became directed toward the earth).

Its elevation was probably 65 feet when the descent began. At about 25 feet above the ground its angle of incidence became positive (i.e. the chord of the surfaces directed skyward). It did not gain sufficient horizontal velocity by the downward and forward pitch for support. It again took a negative angle of incidence and struck the ground. The forward framing struck first the side to the left of the aviators slightly in advance of the side to the right. The angle at which the surfaces struck seemed to be about 40°.

The stability of the machine considered sideways was disturbed and unsteady. The motor was topped during the first pitch forward.

The course of the descent may be shown diagrammatically, as it appeared to me, by the following dotted lines. The accompanying straight lines show the angle of incidence at the point in the course at which they are placed. The cross indicates the point of accident to the propeller.

Submitted by,
Geo. A. Spratt

PROCEEDINGS OF THE AERONAUTICAL BOARD OF THE SIGNAL CORPS WHICH CONVENED AT FORT MYER AT 10:15 a.m., SEPTEMBER 18, 1908, FOR THE PURPOSE OF INVESTIGATING AND REPORTING UPON THE CAUSE OF THE ACCIDENT TO THE WRIGHT AEROPLANE WHICH RESULTED IN THE DEATH OF FIRST LIEUTENANT THOMAS E. SELFRIDGE, FIRST FIELD ARTILLERY.

Present: Major C. McK. Saltzman, Captain Charles S. Wallace and Lieutenant F. P. Lahm.

Absent: Major George O. Squier and Lieutenant Benjamin D. Foulois.

There were also present Lieutenant George C. Sweet, U.S.N. and Lieutenant Richard B. Creecy, U.S.M.C., Officers officially detailed for purpose of observing and reporting upon aeronautical work of the signal corps.

With the exception of Lieutenant Foulois, all members of the Board and Lieutenants Sweet and Creecy were present at the time of the accident.

The Board visited the scene of the accident, questioned witnesses very carefully and examined the machine.

Mr. Octave Chanute and Professor Albert F. Zahm were present by courtesy during the entire investigation and were consulted by the Board.

Mr. Wright's condition was such as to prohibit the Board consulting or questioning him relative to the accident.

After due deliberation, from the evidence obtainable from all available sources, the Board finds-------

That the accident which occurred in an unofficial flight made at Fort Myer, Va., at about 5:18 p.m., on September 17, 1908, was due to the accidental breaking of a propeller blade and a consequent unavoidable loss of control which resulted in the machine falling to the ground from a height of about seventy-five (75) feet.

The Board finds that First Lieutenant Thomas E. Selfridge, First Field Artillery, (attached to the Signal Corps by War Department orders and assigned to aeronautical duty), accompanied by [sic] Mr. Wright, by authority, on the aeroplane, for the purpose of officially receiving instruction, and received injuries by the falling of the machine which resulted in his death.

(Signed) C. McK. Saltzman
Major, Signal Corps, U.S.A.
President

(Signed) Charles S. Wallace
Captain, Signal Corps, U.S.A.
Member

(Signed) Frank P. Lahm
1st Lieut, Signal Corps, U.S.A.
Recorder

APPROVED:

(Signed) George O. Squier
Major, Signal Corps, U. S. Army,
Acting Chief Signal Officer

SECTION VII

STYLE PAPER

SAMPLE STYLE PAPER FOR THE AIR FORCE ACADEMY AERONAUTICS DIGEST

E. J. Jumper,* M. M. Tower,* and F. Guggisberg**

Abstract

This paper discusses (through description and example) the style required in papers submitted to the Air Force Academy Aeronautics Digest. As illustrated here, authors should provide a single-spaced abstract of the content of their papers. Our sample style sheet gives guidance on format, style, illustrations, tables, equations, symbols, and references and appendices.

I. Introduction

Since formats for papers are so varied, we thought a sample paper would serve as a useful style guide for submissions to the Air Force Academy Aeronautics Digest. As such, this paper will both discuss the desired style as well as illustrate how to handle major headings, subheadings, figures, and references. The writer need not feel restricted by this general overview. For example, the major heading of "Introduction" need not appear; perhaps one would rather start with the heading of "Background" or whatever seems appropriate. Although the abstract is required, no other headings are prescribed.

In the sections that follow, we hope to address many of the questions on style which potential authors may have. Where we do not address a specific question, the author is free to follow whatever convention he is accustomed to using.

II. Stylistic Considerations

Authors should employ clear, understandable prose in presenting ideas. Obviously, the purpose of any publication is to share information; communication occurs only when the reader understands what the author is trying to convey. It fails when an author's thinking is fuzzy, the word choice is inexact, the grammar is garbled, and the sentence construction is awkward or obtuse. Consequently, for their readers' sakes, writers should consciously guard against these possible causes of miscommunication. The chief offender in this regard is the passive voice.

A. Improper Use of Passive Voice

A prime source of inexactness is overuse of the passive voice. In using passive voice, an author risks obscuring the message or distracting the reader's train

*Captain, USAF, Assistant Professor of Aeronautics, DFAN
**Captain, USAF, Instructor of English, DFENG

AD-A085 770 AIR FORCE ACADEMY CO F/G 20/4
AIR FORCE ACADEMY AERONAUTICS DIGEST - FALL 1979.(U)
APR 80 E J JUMPER, M M TOWER, F GUGGISBERG
UNCLASSIFIED USAFA-TR-80-7 NL

END
DATE FILMED
7 80
DTIC

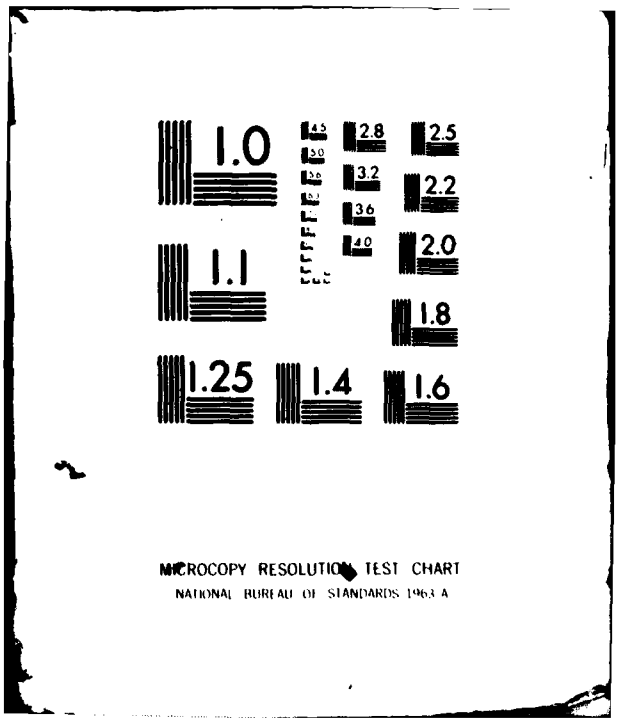
1.0
1.1
1.25
1.4
1.6
2.8
3.2
3.6
4.0
2.5
2.2
2.0
1.8
MICROCOPY RESOLUTION TEST CHART
NATIONAL BUREAU OF STANDARDS 1963 A

of thought. By contrast, the active voice communicates more directly; it is the natural order of most speech and thought. Therefore, we encourage our authors to write in the active voice. Abuse of passive voice has been a problem (probably the problem) in governmental and scientific writing in the past, and we must do our part to get rid of it.

Is passive voice a grammatical error? No. Overuse, however, makes for deadening prose and dull writing. We want readers to find our writing crisp and concise; passive voice merely adds dead wood--excess words not necessary to convey meaning. As such, it yields unprofitable prose. Consider the following:

> Now that a formula has been derived whereby the boundary layer thickness can be predicted, some predictions about how the boundary layer is affected when the free stream velocity is changed can be made. From Eqn (10) it can be seen that as the velocity is increased, the boundary layer thickness at the same location is decreased.

How about that? Did you have as much trouble plowing through that sentence as we did? Consider this version:

> Now that we have a formula for predicting the boundary layer thickness, we can make some predictions about what happens to the boundary layer as we change the free stream velocity. From Eqn (10) we can see that as the velocity increases, the boundary layer thickness at the same location decreases.

By activating the passage, we have considerably reduced the fog count and increased the readability of this passage.

How do you recognize passive constructions? It's as easy as 1-2-3.

1. Normal order is reversed.

   Instead of

   > Adam ate the apple (which is active construction), you have
   >
   > The apple was eaten by Adam.

   The true actor (Adam) has changed places with the object of the action (the apple). In many cases, the true actor leaves the stage entirely:

   > The apple was eaten.

2. The sentence employs a form of the verb "to be" and the past participle form of the main verb of action, usually ending in -ed or -en. For example:

was eaten, am constructed, is added, are increased,
were accomplished; will be eaten, is being constructed,
have been accomplished, etc.

3. The sentence employs the preposition "by" to indicate the actor, or implies an action caused by someone or something unstated:

"... by Adam" tells us that Adam did the acting. "The apple was eaten" implies "by person or persons unknown or unstated."

B. Legitimate Uses of the Passive Voice (Beware! Use Sparingly)

Sometimes you may have a legitimate reason for using the passive voice. If so, go right ahead. Use the following criteria to determine if your intended use is justified:

1. Is the object of the action or the action itself more important than the actor (such that placing the object in the subject position emphasizes this importance)?

Dinglebert Hooper was elected the next president of the Lodge.

2. Is the actor obvious, unimportant, or unknown?

America was discovered in 1492.
At precisely 0042 on the morning of May 14, the bank was robbed.

If either of the above criteria applies, you may use the passive voice. Remember, though, that limiting your use of this construction improves your paper's readability, so exercise restraint in applying the criteria. Use the passive voice only occasionally--in all other instances, join the active generation!

III. Illustrations

A. Philosophy

Authors may want to use figures to re-enforce ideas discussed in the text of the paper itself. Figures should be functional rather than ornamental; in other words, they should provide information that is pertinent to an article. Eliminate all unnecessary illustrations and photographs.

B. Acceptable Types of Illustrations

1. Graphs
2. Schematics
3. Photographs
4. Drawings

C. Guidelines for Using Illustrations

Refer to all figures in the text of your paper (e.g., see Figure 1). Place illustrations in numerical sequence either in the paper near the point of reference, or at the end. You may gather a sequence of related illustrations, such as plots of test data, in an appendix. Number figures consecutively with Arabic numerals and give all figures a title. Place the title to the right of the figure number, underneath the illustration (see Figure 1). Center second and subsequent lines of the title as illustrated. Capitalize all important words of the title.

D. Format

1. Graph paper--use the type most suited to your need.

a. Rectilinear

b. Polar

c. Log - log

d. Semi - log

2. Ink

Use only black pencil or ink. Colored pencils and ink will not reproduce on Ozalid, thermofax, or Xerox.

3. Symbols

Use different symbols (i.e., ○, △, □) or coded lines of dots and dashes to distinguish between plots. Use closed symbols (circles, triangles, squares, etc.) to show experimental points. Identify each symbol with the associated test conditions within the boundaries of the figure. Natural laws and theory may be represented by lines without points.

4. Titles

Figure titles should be descriptive and brief. Indicate the source of the data in the title either in a short statement, a parenthetical expression, or as a reference. When appropriate, note the date of the data collection.

5. Scale

Select a scale which uses as much of the paper as possible, <u>but</u> leave room for labeling the axes, title, and page number.

6. Placement

Place the axes, along with their scales and labels, away from the edges of the paper in order to maintain the margins.

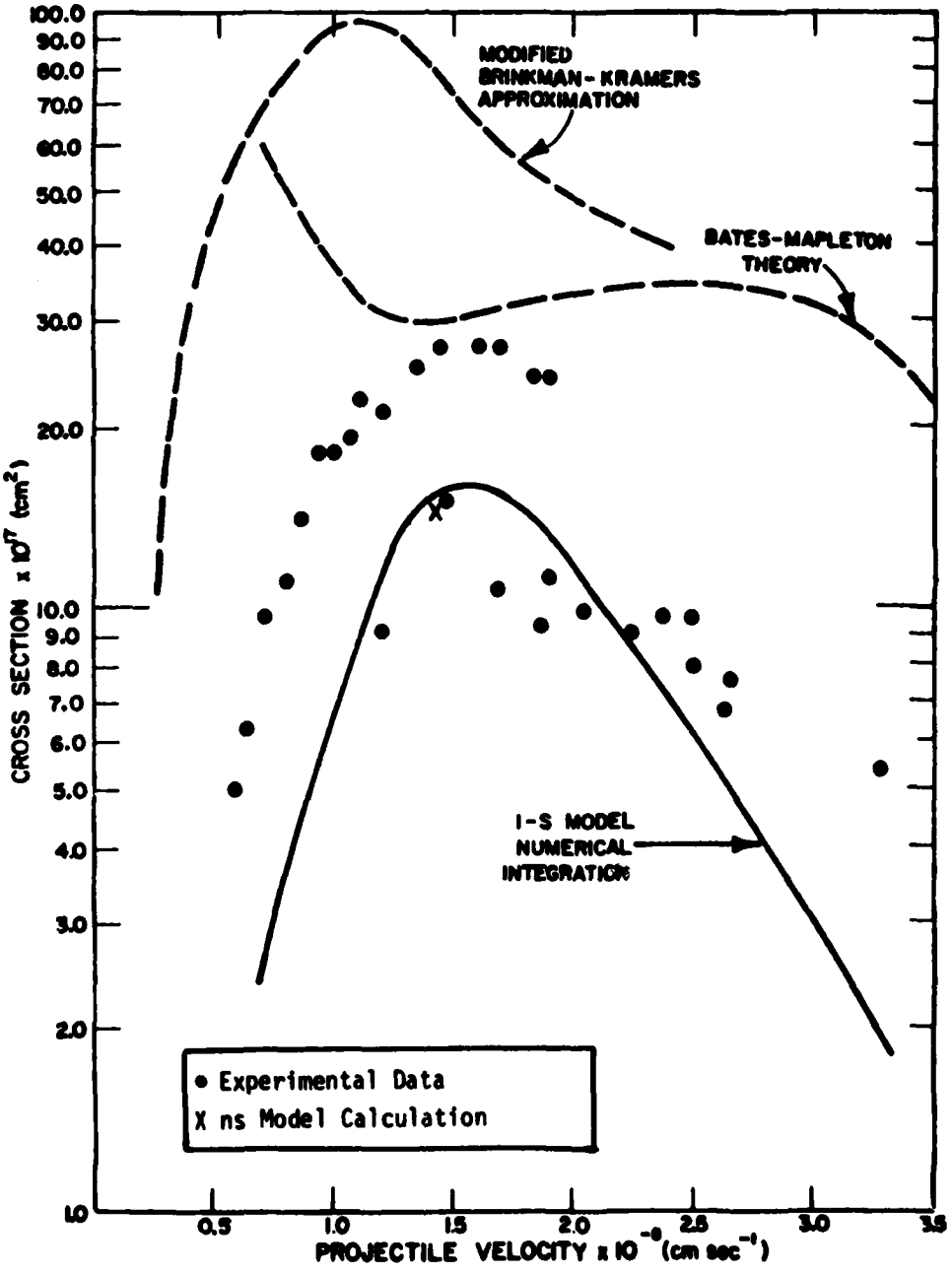

Figure 1. Charge Exchange Cross Sections for Al^+ + Ar in Various Approximations

Enclose the entire graph with solid boundary lines where possible. When using lined graph paper, cut away the excess graph paper along the boundary of the graph or figure and rubber cement the graph or figure to white bond to allow for crisp, uncluttered reproduction. Horizontal or vertical figures are acceptable.

IV. Tabular Material

Information that is readily grouped into classes or categories is usually best presented in a table. Tables present in a concise and orderly manner information that cannot be presented in any other way. Keep tabular material as simple as possible so that the reader can easily grasp the meaning of the data. Table 1 defines the printer's terms for the types of tables that most frequently appear in technical papers.

Table 1

DEFINITION OF TERMS RELATING TO TABULAR MATTER

Stub Column Head	Boxhead	Run-up Box-head	Spannerhead		Remarks
			Boxhead*	Boxhead	
Stub entry	Read column	---	Read	Read	May be left blank as desired.
Stub entry	Read column	---	Read	---	---
Stub entry	Read column	---	---	Read	---

*This is a footnote to the table.

Number tables consecutively using Arabic numerals, and give each table a title using all capital letters. Place each table after the first reference to it in the text. If a paper contains only a few pages of text and a large number of tables, then place the tables in numerical sequence at the end of the paper.

We encourage authors to use abbreviations and unit symbols in tabular matter, especially in boxheads and stub entries, as an aid to fitting copy in the space allotted in the table and in fitting the table to the page. If possible, include unit symbols in the boxhead rather than repeat them in the read columns.

Authors who require a table of more than one page may set one up by repeating the boxheads from page to page.

V. Equations

Display important equations by setting them off from the text and numbering them in parentheses (see Eqn (1)). Align a series of equations on the equal signs or center

equations on the page. Keep derivations concise; if they are lengthy, you may wish to place them in an appendix. Define symbols in one of two ways, either immediately before or after the equation in which they first appear, or in a list of symbols at the end of the text, just before the References.

Equations and symbols must be typed or printed clearly. Placement of subscripts and superscripts must be readily apparent. Number equations sequentially, using Arabic numerals in parentheses at the right hand margin of the page, including equations contained in appendices. A sample equation appears below.

$$\frac{T - T_\infty}{T_o - T_\infty} = \exp \left\{ - \left(\frac{hA}{\rho CV} \right) \tau \right\} \qquad (1)$$

Note that Eqn (1) shows how exponentials should be expressed and how all quotients should be displayed (i.e., use horizontal lines, not a slash (/)).

Symbols*

A	surface area
C	specific heat
h	heat transfer coefficient
T	temperature
V	volume
ρ	density
τ	time
Subscripts	
o	initial condition
∞	free stream

References

The purpose of the References section is to document (cite) the sources of the information you as author have used in your article. This section also helps your reader to go directly to your sources; consequently, make your sources as complete and as accurate as possible. Please use the outlined system below.

*Authors may place a list of symbols at the end of the text, if such is needed.

In place of footnotes and a bibliography, the Digest uses an integrated system of References, to save space. This Reference listing will be numerical, not alphabetical. Here's how to set it up. Number sequentially (1, 2, 3, etc.) in your text the items you need to document, and set up the References following this order. Ref. 1 will thus refer to the first entry in the References listing; Ref. 8, to the eighth, and so on. See AFP 13-2, Atch 2, pp. 204-205 for the format to use in arranging the information in your entries. We print below some examples from a previous Digest to give you an idea of how your entries at the end of your text should read. For more examples, consult the Digest-Spring 1979 issue (Ref. 13).

1. Rayleigh, J. W. S. The Theory of Sound. Vol. 2. London: Macmillan, 1896, p. 412.
(*Simple book entry, one author. Delete volume reference if there is only one volume.*)

2. Squire, H. B. "Note on the Motion Inside a Region of Recirculation (Cavity Flow)." Journal of the Royal Aeronautical Society, Vol. 60 (March 1956), 203-205.
(*Simple journal entry--give specific page, or inclusive pages if citing whole article.*)

3. Pan, F. and A. Acrivos. "Steady Flows in Rectangular Cavities." Journal of Fluid Mechanics, Vol. 28, Part 4 (June 1967), 643-655.
(*Two-author entry. Note the Part or Issue of a journal only if separately paginated.*)

4. Roshko, A. Some Measurements of Flow in a Rectangular Cutout. NACA TN-3488, August 1955.
(*Technical publication. Underline title and give series and number and any other necessary identifying information.*)

5. Reference Data for Radio Engineers. 5th ed. Indianapolis, IN: Howard W. Sams & Co., Inc., 1968.
(*An edition, other than the first, of a book.*)

6. Buell, D. A. "Airloads Near the Open Port of a One-Meter Airborne Telescope." AIAA Paper 75-71, presented at the AIAA Aerodynamic Acoustic Conference, San Diego, California, January 1975.
(*Conference paper. Include paper number, conference presented at, place, and date.*)

7. Lindsay, C. L. "An Investigation of the Flow Through Perforated Spoilers." Aeronautics Department 499 Report, USAF Academy, Colorado, December 1975.
(*Student paper.*)

8. Tower, M. M. Flow Visualization in Square and Circular Cavities Behind a Porous Spoiler. USAFA-DFAN-TN-1. USAF Academy, Colorado, Aeronautics Department, December 1976.
(*USAFA departmental publication.*)

9. Meyers, Philip F. Tethered Balloon Handbook. Cambridge, MA: Goodyear Aerospace Corp., Project No. AF-6665, AD685183, 31 December 1968.
(Civilian contract project. Give civilian corporation, project identifying numbers, and date.)

10. Stefan, Karl. "Performance Theory for Hot Air Balloons." Unpublished paper, National Center for Atmospheric Research, Boulder, Colorado, April 1971.
(Unpublished paper. Treat unpublished dissertations the same way: Thesis, Ohio State University, 1975.)

11. Jumper, Eric. Private communication. Aeronautics Department, USAF Academy, Colorado 80840.
(Tell where the individual can be currently located.)

12. Noyes, W. A., Jr. "The Contributions of R. G. W. Norrish to Photochemistry." In Photochemistry and Reaction Kinetics, pp. 234-256. Edited by P. G. Ashmore, T. M. Sugden, and F. S. Dainton. London: Cambridge University Press, 1967.
(Article contained in an edited collection (book)).

13. Jumper, E. J. and M. M. Tower, eds. Aeronautics Digest - Spring 1979. USAFA-TR-79-7, USAF Academy, Colorado, July 1979.
(A reference to the editors of a compilation if their efforts are what you are citing.)

Appendix

A DISCUSSION OF AN APPENDIX

Appendices may be used for material related to or additional to the paper. The title of the appendix should identify its content. If more than one appendix appears in the paper, use a capital letter (Appendix A, etc.) to designate each appendix. Number figures and tables in each appendix with the appropriate letter (Figure A1, Table C2, etc.).

★ U. S. GOVERNMENT PRINTING OFFICE 1980 - 678-177/367 Reg. 8

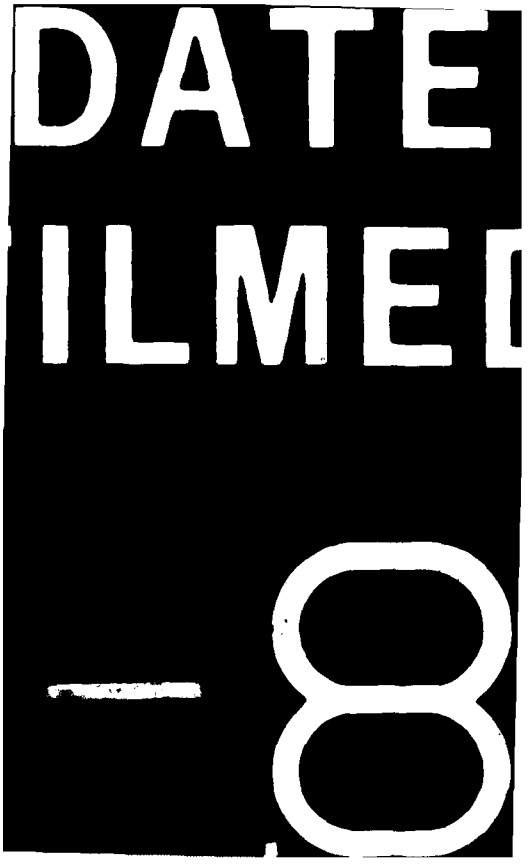
DATE
ILME
8